Pertanika Journal of

SCIENCE & TECHNOLOGY

JST

VOLUME 16 NO. 2 • JULY 2008

A scientific journal published by Universiti Putra Malaysia Press

About the Journal

Pertanika is an international peer-reviewed journal devoted to the publication of original papers, and it serves as a forum for practical approaches to improving quality in issues pertaining to tropical agriculture and its related fields. Pertanika Journal of Tropical Agricultural Science began publication in 1978. In 1992, a decision was made to streamline Pertanika into three journals to meet the need for specialised journals in areas of study aligned with the interdisciplinary strengths of the university. The revamped, Pertanika Journal of Science and Technology (JST) is now focusing on research in science and engineering, and its related fields. Other Pertanika series include Pertanika Journal of Tropical Agricultural Science (JTAS); and Pertanika Journal of Social Sciences and Humanities (JSSH).

JST is published in English and it is open to authors around the world regardless of the nationality. It is currently published two times a year i.e. in **January** and **July**.

Goal of Pertanika

Our goal is to bring the highest quality research to the widest possible audience.

Quality

We aim for excellence, sustained by a responsible and professional approach to journal publishing.

Future vision

We are continuously improving access to our journal archives, content, and research services. We have the drive to realise exciting new horizons that will benefit not only the academic community, but society itself.

We also have views on the future of our journals. The emergence of the online medium as the predominant vehicle for the 'consumption' and distribution of much academic research will be the ultimate instrument in the dissemination of the research news to our scientists and readers.

Aims and scope

Pertanika Journal of Science and Technology aims to provide a forum for high quality research related to science and engineering research. Areas relevant to the scope of the journal include: *bioinformatics, bioscience, biotechnology and bio-molecular sciences, chemistry, computer science, ecology, engineering, engineering design, environmental control and management, mathematics and statistics, medicine and health sciences, nanotechnology, physics, safety and emergency management,* and related fields of study.

JST accepts submission of mainly four types: original articles, short communications, reviews, and proposals for special issues.

Editorial Statement

Pertanika is the official journal of Universiti Putra Malaysia. The abbreviation for Pertanika Journal of Science & Technology is *Pertanika J. Sci. Technol.*

Editorial Office

Pertanika, Research Management Centre (RMC), 4th Floor, Administration Building
Universiti Putra Malaysia, 43400 Serdang, Selangor, Malaysia
Tel: +603 8946 6185, 8946 6192 • Fax: +603 8947 2075
E-mail: ndeeps@admin.upm.edu.my
www.rmc.upm.edu.my/pertanika

Publisher

The UPM Press
Universiti Putra Malaysia
43400 UPM, Serdang, Selangor, Malaysia
Tel: +603 8946 8855, 8946 8854 • Fax: +603 8941 6172
penerbit@putra.upm.edu.my
URL : http://penerbit.upm.edu.my

Pertanika Journal of Science & Technology
Vol. 16 (2) Jul. 2008

Regular Articles

Selected Papers from the World Engineering Congress 2007
Guest Editors: *(Siti Mazlina Mustapa Kamal, Farah Saleena Taip and Siti Aslina Hussain)*

Selected Papers from the Science Seminar 2007
Guest Editorial Board: *(W. Mahmood Mat Yunus, Nor' Aini Mohd Fadzillah, Abdul Halim Abdullah, Hishamuddin Zainuddin, Mahendran a/I Shitan and Shamarina Shohaimi)*

ISSN: 0128-7680
Pertanika J. Sci. & Technol. **16 (2)**: 83 - 95 (2008)

Parallel Weibull Regression Model

Jayanthi Arasan
Department of Mathematics, Faculty of Science,
Universiti Putra Malaysia, 43400 UPM,
Serdang, Selangor, Malaysia
E-mail: jayanthi@fsas.upm.edu.my

ABSTRACT

This paper focuses on the lifetime analysis of parallel systems consisting of Weibull components with independent failures and covariates. The performance of the parameter estimates of two and three-component parallel systems at different values of the shape parameter, σ, are compared and some confidence interval procedures are analyzed via a coverage probability study for m = 2, using simulated data.

Keywords: Wald, censoring, covariates

THE WEIBULL AND THE EXTREME VALUE DISTRIBUTION

There are numerous studies involving parallel systems in reliability. Many multivariate models have been developed, in particular, for the life testing of multi-component systems. Unfortunately, they may not be compatible with the lifetime analysis of medical data, which often involves other factors that affect survival times, more popularly known as covariates or concomitant variables. The estimation of the parameters of multivariate models is also usually very difficult and complicated, especially if it involves the estimation of a high number of parameters. More details on parallel systems can be found in Høyland and Rausand (1994), Kececioglu (1991) and in most books on reliability analysis.

Early work on parallel system models in the biomedical field was done by Gross *et al.* (1972), but this model does not include covariates and censored lifetimes. The same model was also discussed by Høyland and Rausand (1994) to study the reliability and mean time to failure of standby units in a parallel system. Elandt-Johnson and Johnson (1980) described another parallel system using the multi-hit models of Carcinogenesis via the Weibull distribution. Baklizi (1997) analyzed the likelihood inference in a parallel system regression model involving both censored and uncensored data. Arasan and Daud (2004) extended his work to analyze the efficiency of the parameter estimates of the same model with multiple covariates.

The Weibull distribution accommodates increasing, decreasing and also constant hazard rates as it reduces to the exponential as a special case. It is well known for modeling lifetimes and for its equivalence to extreme value distribution. The Weibull distribution can also be extended to include covariates by allowing its scale parameter, λ or shape parameter δ to depend on these variables, where $\lambda > 0$ and $\delta > 0$. The density and survivor functions of the Weibull are,

$$f(t) = \lambda\delta(\lambda t)^{\delta-1} exp\left[-\lambda t^{\delta}\right], t > 0 \quad (1)$$

Received : 8 January 2007
Accepted :14 April 2008

$$S(t) = exp[-(\lambda t)^{\delta}], \quad t > 0. \tag{2}$$

We know that if the lifetime, T has a Weibull distribution, then $Y = \log T$ has the extreme minimum value distribution, whose parameters could easily be modified to obtain the parameters of its Weibull counterpart. If Θ has extreme minimum value distribution, denoted as G(0,1), its density and survivor functions are,

$$f(\theta) = e^{(\theta - \exp(\theta))}, \; -\infty < \theta < \infty, \tag{3}$$

$$S(\theta) = e^{-\exp(\theta)}, \; -\infty < \theta < \infty \tag{4}$$

Suppose $x' = (x_0, x_1, ..., x_p)$ is the vector of covariate values, where $x_0 = 1$ and $\beta' = (\beta_0, \beta_1, ... , \beta_p,$ are unknown parameters. If $\lambda = e^{-\beta' x}$, then the log lifetime, can be written as $Y = \beta' x + \sigma\Theta$, where $\sigma = \frac{1}{\delta}$. Since $\dfrac{Y - \beta' x}{\sigma}$ is equal to Θ, its distribution is extreme minimum value with the following distribution function,

$$F(y, \beta, x) = 1 - e^{-exp(\frac{y-\beta' x}{\sigma})}, \; -\infty < y < \infty \tag{5}$$

If the shape parameter of the Weibull distribution σ equals 1, then the Weibull is reduced to an exponential distribution. Having exponential lifetime means that the components of the parallel system would have constant failure rates and not strictly monotonic ones as in the Weibull case.

PARALLEL WEIBULL SYSTEM WITH COVARIATES

A parallel system can function as long as at least one of its components is still functioning. If the unit failures in a parallel system are assumed to be independent, then, this simply means that failure in one component will not affect the hazard rate of the remaining components. Although, this assumption may seem unrealistic, especially in the biomedical area, it can be very useful in making an initial interpretation of the data because the statistical analysis is much simpler and faster.

For a parallel system consisting of m identical and independent components, the probability of survival is equivalent to the probability of at least one component still operating. If t_k is the survival time of component k, where $k = 1, 2, ... m$, the time to failure of the system t is then,

$$t = \max \{t_1, t_2, ..., t_m\}.$$

It follows that the survival function of the entire system is,

$$S_T(t) = P(T > t) = 1 - \prod_{k=1}^{m} P(t_k \le t) = 1 - \left[F(t)\right]^m \tag{6}$$

For the i^{th} observation, if $y_i = \log t_i$ and $x'_i = (x_{i0}, x_{i1}, ..., x_{ip})$, the density and survival functions of the system are,

$$f(y_i) = \frac{m}{\sigma}\left\{e^{\frac{y_i - \beta' x_i}{\sigma} - \exp\left(\frac{y_i - \beta' x_i}{\sigma}\right)}\right\}\left\{1 - e^{-\exp\left(\frac{y_i - \beta' x_i}{\sigma}\right)}\right\}^{m-1}, \quad -\infty < y_i < \infty \tag{7}$$

$$S(y_i) = 1 - \left\{1 - e^{-exp\left(\frac{y_i - \beta' x_i}{\sigma}\right)}\right\}^m, \quad -\infty < y_i < \infty \tag{8}$$

LIKELIHOOD EQUATIONS AND ESTIMATION

Suppose we have both censored and uncensored lifetimes for $i + 1, 2, ..., n$ observations, accompanied by the information on p covariates. Let us say the following indicator variables were used to identify whether the data was censored or otherwise,

$$s_i = \begin{cases} 1 \ for \ t_i \text{ uncensored,} \\ 0 \ for \ t_i \text{ censored.} \end{cases} \tag{9}$$

The log-likelihood function of the full sample of a system consisting of m identical and independent Weibull components and p covariates is,

$$L(\beta, \sigma) = \sum_{i=1}^{n} \{s_i \log f(y_i) + (1 - s_i) \log S(y_i)\}.$$

It follows that if $Z_i = \frac{y_i - \beta' x_i}{\sigma}$

$$L(\beta, \sigma) = \sum_{i=1}^{n} s_i \left\{\log \tfrac{m}{\sigma} + z_i - e^{z_i} + (m-1)\log(1 - e^{-exp(z_i)})\right\} + (1 - s_i)\log\left\{1 - (1 - e^{-\exp(z_i)})^m\right\}. \tag{10}$$

The first and second derivatives of the log-likelihood function would be as follows,

$$\frac{\partial L(\beta,\sigma)}{\partial \beta_j} = \sum_{i=1}^{n} x_{ij}\left(-\tfrac{s_i}{\sigma} A_i + (1 - s_i)h_i\right),$$

$$A_i = 1 - e^{zi} + \frac{(m-1)e^{zi - \exp(zi)}}{1 - e^{-\exp(zi)}},$$

$$h_i = \frac{f(z_i)}{S(z_i)} = \frac{\frac{m}{\sigma}(e^{z_i - \exp(z_i)})\,(1 - e^{-\exp(z_i)})^{m-1}}{1 - (-1 - e^{-\exp(z_i)})^m},$$

$j = 0, 1 \ldots, p.$

$$\frac{\partial L(\beta,\sigma)}{\partial \sigma} = \sum_{i=1}^{n} \tfrac{-s_i}{\sigma} B_i + (1 - s_i) z_i h_i,$$

$$B_i = 1 - z_i + z_i e^{z_i} + \frac{(m-1)\, z_i - \exp(z_i)}{1 - e^{-\exp(z_i)}}.$$

$$\frac{\partial^2 L(\beta,\sigma)}{\partial \beta_j \partial \beta_k} = \sum_{i=1}^{n} x_{ij} x_{ik}\left\{\tfrac{-s_i}{\sigma^2} D_i - (1 - s_i)\left(\tfrac{A_i h_i}{\sigma} + h_i^2\right)\right\},$$

$$D_i = e^{zi} + \frac{(m-1)(e^{zi} - \exp(zi))\,(-1 + e^{zi} + e^{-\exp(zi)})}{(1 - e^{-\exp(zi)})^2},$$

$j, k = 0, 1 \ldots, p.$

$$\frac{\partial^2 L(\beta,\sigma)}{\partial \beta_j \partial \sigma} = \sum_{i=1}^{n} x_{ij}\left\{-\tfrac{s_i}{\sigma^2}(-A_i + z_i D_i) - (1 - s_i)\left(\tfrac{1}{\sigma} B_i h_i + z_i h_i^2\right)\right\}$$

$j = 0, 1 \ldots, p.$

$$\frac{\partial^2 L(\beta,\sigma)}{\partial\sigma^2} = \sum_{i=1}^{n} -\frac{-s_i}{\sigma^2}\left\{-B_i + z_i\left((-1+e^{zi}+z_i e^{zi})+(m-1)E_i\right)\right\}$$
$$-(1-s_i)z_i\left(\frac{-h_i}{\sigma}-\frac{B_i h_i}{\sigma}-z_i h_i^2\right),$$
$$E_i = \frac{e^{z_i-\exp(z_i)}(-1+e^{-\exp(z_i)-z_i+z_{ie}-\exp(z_i)+z_{ie}z_i})}{(1-e^{-\exp(z_i)})^2}.$$

The inverse of the observed information matrix, which can be obtained from the second partial derivatives of the log-likelihood function evaluated at $\hat{\beta}$ and $\hat{\sigma}$ provides us with the estimators for the variance and covariance,

$$\widehat{var}(\hat{\beta},\hat{\sigma}) = [i(\hat{\beta},\hat{\sigma})]^{-1} \tag{11}$$

Simulation Study

Study Design

A simulation study was conducted to see how well the estimation procedure works with the parallel Weibull regression model with two components and two covariates at different values of sigma. In addition, we were also interested in investigating how the proportion of censoring in the data affected the parameter estimates. The study was conducted by using 1000 simulations, each with sample size of 100. The survival times were obtained by drawing 100 random numbers from the uniform distribution between 0 and 1, $U(0,1)$. These numbers were later used to produce the log survival time, y_i. For the i^{th} observation,

$$y_i = \beta' x_i + (\log(-\log(1-u^{\frac{1}{m}})))\sigma. \tag{12}$$

The value of 1 was used as the parameters of β_0, β_1 and β_2. As the parameter of σ, three different values of 0.5, 0.8 and 1.15 were used to enable a comparative study. We know that δ is the shape parameter of the Weibull distribution and its value determines whether the distribution has an increasing, constant or decreasing failure rate. Since, $\sigma = \frac{1}{\delta}$ a value of σ less than 1 would indicate an increasing hazard rate while value of more than 1 would indicate otherwise.

In addition, a simulation study for a three-component system with two covariates was carried out for σ = 0.5 to see how the bias, standard error and root mean square error (rmse) changes with increase in the number of components. The two covariates used in the model were simulated from the Bernoulli and standard normal distribution. Six different values of approximate censoring proportions (cp), between 0 and 0.5 were used to investigate the relationship between censoring proportion and efficiency of the parameter estimates. A value of cp=0.3 means that approximately 30% of the survival times were censored before the actual failure times.

The censoring time for the i^{th} observation, $c_i \sim \exp(\mu)$, is where the value of μ would be adjusted to obtain the desired approximate censoring proportion in our data. If t_i =exp(y_i) then t_i will be censored at c_i according to the following,

$$s_i = \begin{cases} 1 & if\ t_i \le c_i, \\ 0 & if\ t_i \le c_i. \end{cases} \tag{13}$$

Parameter Estimation and Calculations

The estimates of β and σ can be obtained by solving the likelihood equations using any iterative procedure for solving non linear equations. In this research, the maximum likelihood estimators of all the parameters were computed using the Newton Raphson iterative method, which was implemented using the FORTRAN programming language. In this section the true parameter values were used as the starting values for all the estimates.

Simulation Results and Conclusion

The results of the simulation study are given in the following section. Both bias and standard error contribute to the average error size of an estimator, thus the rmse, $\sqrt{s.e^2 + bias^2}$ is used to measure the average overall error of the parameter estimates. Tables 1-3 display the bias and standard error of the estimates at different values of σ.

The values of the rmse are illustrated in *Figs. 1-2*. It is clear that both standard error and rmse of all parameter estimates increase with the increase in censoring proportion. This was expected because increase in censoring proportion means less data with complete failure times and thus the likelihood contribution would depend more on the survival function and censored times instead of the density function and the exact failure times.

As for the bias, although it seems to increase with the increase in censoring proportion, the trend is not very clear, probably because of the increasing standard error values. It should be borne in mind that a low value of bias at higher levels of censoring proportion does not imply that the resulting estimates are better than the ones at lower censoring proportion. This is because the increasing standard error values at higher censoring proportion suggest that the estimates are still typically far from the real value even though the average is close to the parameter value.

However, none of the bias values were significant at the 5% level. In addition, the rmse and standard error also appear to be higher at higher values of σ. The reason for this can be explained as follows. In the original Weibull distribution the events will be sparse for smaller δ so the parameters will be estimated less efficiently when δ is smaller. Similarly, with the parallel Weibull model the parameters will be estimated less efficiently when σ is larger, because $\sigma = \frac{1}{\delta}$.

TABLE 1
Bias and standard error when σ = 0.5

	Bias				Std. Error			
cp	$\hat{\beta}_0$	$\hat{\beta}_1$	$\hat{\beta}_2$	$\hat{\sigma}$	$\hat{\beta}_0$	$\hat{\beta}_1$	$\hat{\beta}_2$	$\hat{\sigma}$
0.0	0.000581	0.000075	0.001155	-0.007104	0.057150	0.074871	0.038976	0.038511
0.1	0.001473	-0.002033	0.000003	-0.007816	0.058883	0.079985	0.041491	0.039747
0.2	0.000442	-0.000598	0.001274	-0.007355	0.060513	0.083162	0.043113	0.040508
0.3	-0.000347	-0.001084	0.000610	-0.008624	0.062857	0.087451	0.047459	0.041316
04	0.003094	-0.001318	0.001884	-0.009578	0.065999	0.100208	0.054448	0.042908
0.5	0.002043	-0.002524	0.002759	-0.011823	0.070825	0.107113	0.063674	0.044408

TABLE 2
Bias and standard error when $\sigma = 0.80$

	Bias				Std. Error			
cp	$\hat{\beta}_0$	$\hat{\beta}_1$	$\hat{\beta}_2$	$\hat{\sigma}$	$\hat{\beta}_0$	$\hat{\beta}_1$	$\hat{\beta}_2$	$\hat{\sigma}$
0.0	0.000772	0.001110	0.001402	-0.011430	0.091543	0.119754	0.062798	0.061781
0.1	0.001261	-0.003418	0.002256	-0.012283	0.093123	0.126553	0.065503	0.063672
0.2	-0.000451	-0.003492	0.000325	-0.015526	0.098181	0.130567	0.070673	0.063754
0.3	0.000202	-0.000566	0.002043	-0.002524	0.100325	0.137630	0.077110	0.065856
04	0.005657	-0.002862	0.003901	-0.028687	0.106841	0.149999	0.084543	0.068156
0.5	0.002043	-0.005297	0.007270	-0.030128	0.108170	0.169781	0.091523	0.071096

TABLE 3
Bias and standard error when $\sigma = 1.15$

	Bias				Std. Error			
cp	$\hat{\beta}_0$	$\hat{\beta}_1$	$\hat{\beta}_2$	$\hat{\sigma}$	$\hat{\beta}_0$	$\hat{\beta}_1$	$\hat{\beta}_2$	$\hat{\sigma}$
0.0	0.000662	0.000578	0.003038	-0.015808	0.131393	0.173225	0.089642	0.087425
10.0	0.001260	-0.002929	0.001837	-0.019161	0.134265	0.185366	0.096405	0.087970
20.0	0.008061	-0.005796	-0.001241	-0.023398	0.139283	0.196294	0.098891	0.0888667
30.0	0.003024	0.002277	0.013622	-0.022709	0.139601	0.206300	0.110511	0.090894
40.0	0.001900	0.008285	0.016151	-0.024623	0.151129	0.229006	0.126382	0.099512
50.0	0.000750	0.017021	0.017841	-0.021945	0.156191	0.245132	0.131873	0.132947

There were no serious problems encountered in the estimation process although there were a few samples with convergence problems when the censoring proportion in the data was high, usually when cp=0.5. Since efficiency of an estimator depends on both precision and accuracy, based on the rmse measures obtained, we conclude that the estimation procedure is most efficient when the censoring proportion in the data and the value of σ are both low.

Table 4 compares the bias, standard error and rmse rmse of the parameter estimates when m = 3, where m is the number of components in the system. It appears that the bias values increase whereas the standard error values decrease with an increase in the number of components in the system. The rmse, which is the total error, seems to decrease with the increase in number of components in the system. However, at high censoring proportions some of the rmse values for m = 3 are higher than m = 2.

CONFIDENCE INTERVAL ESTIMATES

It is rather common to resort to confidence interval estimates based on the asymptotic normality of maximum likelihood estimates when it is impossible to compute the exact confidence intervals of the parameters of a model. This is also known as basing the intervals on the Wald statistic or simply Wald intervals. Other popular interval estimates are those based on the likelihood ratio test and the score test. In this section, we will be focusing on intervals based on the Wald statistics and recommend suggestions on how to improve these estimates using parameterizations. The method will be assessed by conducting a coverage probability study.

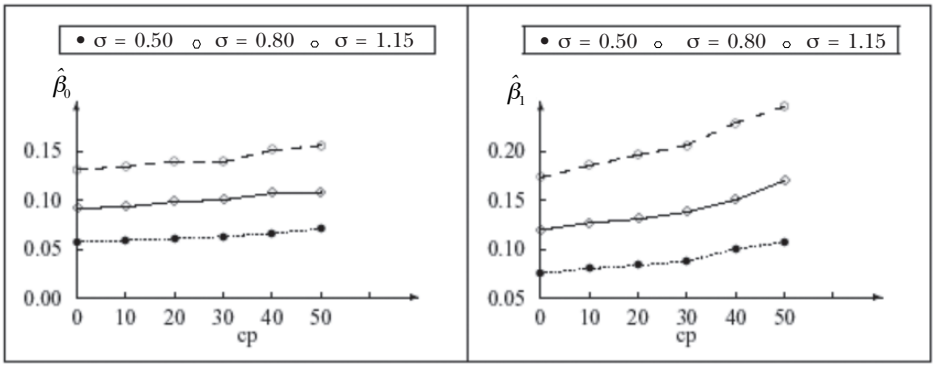

Fig. 1: Values of rmse for $\hat{\beta}_0$ *and* $\hat{\beta}_1$ *vs. cp*

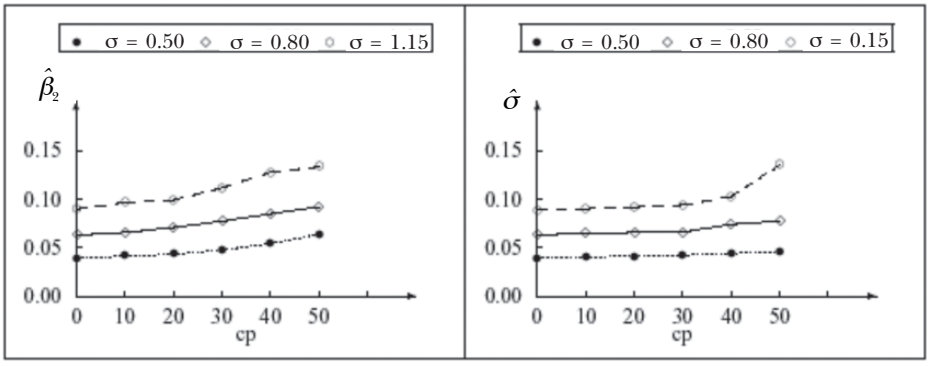

Fig. 2: Values of rmse for $\hat{\beta}_2$ *and* $\hat{\sigma}$ *vs. cp*

TABLE 4
Comparison between different number of component models

		m =2			*m* = 3		
Est.	cp	Bias	Std.err	rmse	Bias	Std.err	rmse
$\hat{\beta}_0$	0.0	0.000581	0.057150	-0.057153	0.002730	0.050849	0.050922
	0.2	-0.000442	0.060513	-0.0060515	0.016328	0.055214	0.057578
	0.4	-0.003094	-0.065999	-0.066071	0.033482	0.057741	0.066746
$\hat{\beta}_1$	0.0	0.000075	0.074871	0.074871	0.000326	0.063108	0.063109
	0.2	-0.000598	0.083162	0.083164	0.010462	0.071568	0.072329
	0.4	-0.001318	0.100208	0.100217	0.019873	0.085562	0.087839
$\hat{\beta}_2$	0.0	0.001155	0.038976	0.038993	0.001009	0.032872	0.032887
	0.2	0.001274	0.043113	0.043132	0.009371	0.038748	0.039865
	0.4	0.001884	0.054448	0.054480	0.018654	0.049361	0.052768
$\hat{\sigma}$	0.0	-0.007104	0.038511	0.039161	-0.007110	0.037757	0.038421
	0.2	-0.007355	0.040508	0.041170	-0.019685	0.038561	0.043295
	0.4	-0.009578	0.042908	0.043964	-0.027013	0.039846	0.048139

Wald Confidence Intervals

Let $\hat{\theta}$ be the maximum likelihood estimator for parameter θ and $l(\theta)$ the log-likelihood function of θ. Under mild regularity conditions, $\hat{\theta}$ is asymptotically normally distributed with mean θ and covariance matrix, $I^{-1}(\theta)$ where $I(\theta)$ is the Fisher information matrix evaluated at the true value of the parameter, θ (Cox and Hinkley, 1979). The matrix,$I(\theta)$ which is not available can be replaced by the observed information matrix, $i(\hat{\theta})$ whose $(j, k)^{th}$ element can be obtained from the second partial derivatives of the log-likelihood function evaluated at $\hat{\theta}$ as given below,

$$i(\hat{\theta})_{jk} = \left(-\frac{\partial^2 l(\hat{\theta})}{\partial \hat{\theta}_j \partial \hat{\theta}_k} \right), \quad j, k = 0, 1 \ldots, p. \tag{14}$$

The estimate of var$(\hat{\theta}_j)$is then given by the $(j, j)^{th}$ element of $i^{-1}(\hat{\theta})$ If $z_1 - \frac{\alpha}{2}$ is the $(1 - \frac{\alpha}{2})$ quartile of the standard normal distribution, then the $100(1- \alpha)\%$ confidence interval for θ_j is given by the following,

$$\hat{\theta}_j - z_{1-\frac{\alpha}{2}} \sqrt{i^{-1}(\hat{\theta})_{jj}} < \theta_j < \hat{\theta}_j + z_{1-\frac{\alpha}{2}} \sqrt{i^{-1}(\hat{\theta})_{jj}}\,. \tag{15}$$

Application of the Wald Intervals

The parallel system model with two covariates discussed in the previous section has a total of 4 parameters to be estimated, β_0, β_1, β_2 and σ. Estimates of var$(\hat{\beta}_j)$ and var$(\hat{\sigma})$ can be obtained from $[\mathrm{i}(\hat{\beta}, \hat{\sigma})]^{-1}$. The $100(1 - \alpha)$ % confidence interval for β_j and σ where $j = 0, 1, 2$ are,

$$\hat{\beta}_j - z_{1-\frac{\alpha}{2}} \sqrt{\widehat{var}(\hat{\beta}_j)} < \beta_j < \hat{\beta}_j + z_{1-\frac{\alpha}{2}} \sqrt{\widehat{var}(\hat{\beta}_j)}, \tag{16}$$

$$\hat{\sigma} - z_{1-\frac{\alpha}{2}} \sqrt{\widehat{var}(\hat{\sigma})} < \sigma < \hat{\sigma} + z_{1-\frac{\alpha}{2}} \sqrt{\widehat{var}(\hat{\sigma})}. \tag{17}$$

It is expected that Wald intervals work rather well for the covariate parameters but not so well for σ, the shape parameter. The Wald interval for σ will most probably be highly asymmetrical and will not have desirable statistical properties due to a sharp boundary in the parameter space. This is usually the case with other similarly bounded parameters, such as the odds ratio, as reported by Hosmer and Lemeshow (1999).

By applying a suitable parameterization such as $1/\sigma$ or log σ, it is expected that the confidence interval estimates will have better symmetry in its left and right estimated error probabilities because the parameterization will help in achieving more symmetry in the log-likelihood function. The following part deals with a suitable parameterization for σ and intervals based on these transformations.

Parameterization for σ

The usual procedure for applying any parameterization is rather straightforward. If a transformation $\varsigma = \varsigma(\sigma)$ is chosen, then $\hat{\sigma}$, the maximum likelihood estimator for σ must

be obtained and transformed to the ς scale, $\hat{\varsigma} = \varsigma(\hat{\sigma})$. Then calculate $i(\hat{\varsigma})$ which is the observed information matrix evaluated at $\hat{\varsigma}$,

$$i(\hat{\varsigma}) = \frac{i(\hat{\sigma})}{[\varsigma'(\hat{\sigma})]^2}. \tag{18}$$

where $\varsigma'(\hat{\sigma})$ is the first derivative of ς with respect to σ. The $100(1-\alpha)\%$ confidence interval for ς is,

$$\hat{\varsigma} - z_{1-\frac{\alpha}{2}}\sqrt{\widehat{var}(\hat{\varsigma})} < \varsigma < \hat{\varsigma} + z_{1-\frac{\alpha}{2}}\sqrt{\widehat{var}(\hat{\varsigma})}. \tag{19}$$

where $\widehat{var}(\hat{\varsigma})$ can be obtained from the inverse of the observed information matrix, $[i(\hat{\varsigma})]^{-1}$ The equivalent confidence interval for σ can be obtained by transforming the confidence interval for ς back to the original scale. For example, if $\varsigma = \log \sigma$ then the transformation back is $\sigma = \exp(\varsigma)$.

Simulation Study

Study Design

A simulation study was conducted using 2000 samples of size n=100, 150, 200 and 250 to evaluate the performance of the confidence intervals based on the Wald statistics. Since there are 4 parameters to be estimated in this model and data is censored, a larger sample size is required in order to have any meaningful results. Samples were generated from the parallel Weibull regression model with two components and two covariates when $\sigma = 0.5$. The samples were produced and censored using methods similar to the ones described in section (2.2.2). Two levels of approximate censoring proportions, cp=0.10 and cp=0.30 were used to see how the level of censoring affected the interval estimates. The values of cp=0.10 and cp=0.30 were chosen to represent both low and high levels of censoring proportions respectively.

These samples were then used to obtain the maximum likelihood estimators of the parameter and the estimators of their variances to carry out the coverage probability study. The coverage probability is the probability that an interval contains the true parameter value. For parameters, β_0, β_1 and β_2 only the coverage probability was analyzed using the untransformed Wald interval estimates. For the parameter σ the coverage probability study was conducted using both the untransformed and two transformed Wald interval estimates. The first parameterization is using $\varsigma = \log \sigma$ and the other is using $\varsigma = \frac{1}{\sigma}$.

Parameter Estimation and Calculations

The parameter estimation process is similar to that described in section (2.2.2). The coverage probability study was conducted by calculating the left and right estimated error probabilities for each of the parameter estimates. The estimated left(right) error probability is calculated by adding the number of times the left(right) endpoint was more(less) than the true parameter value divided by the total number of samples, *N*.

For the covariate parameters β_j, where j = 0, 1, 2, the left and right error probabilities are,

$$\text{Left} = \frac{\#\left\{\hat{\beta}_j - z_{1-\frac{\alpha}{2}}\sqrt{\widehat{var}(\hat{\beta}_j)} > \beta_j\right\}}{2000},$$

$$\text{Right} = \frac{\#\left\{\hat{\beta}_j + z_{1-\frac{\alpha}{2}}\sqrt{\widehat{var}(\hat{\beta}_j)} < \beta_j\right\}}{2000}.$$

For the untransformed σ

$$\text{Left} = \frac{\#\left\{\hat{\sigma} - z_{1-\frac{\alpha}{2}}\sqrt{\widehat{var}(\hat{\sigma})} > \sigma\right\}}{2000},$$

$$\text{Right} = \frac{\#\left\{\hat{\sigma} + z_{1-\frac{\alpha}{2}}\sqrt{\widehat{var}(\hat{\sigma})} < \sigma\right\}}{2000}.$$

For the transformed $\varsigma = \varsigma(\sigma)$,

$$\text{Left} = \frac{\#\left\{\hat{\varsigma} - z_{1-\frac{\alpha}{2}}\sqrt{\widehat{var}(\hat{\varsigma})} > \varsigma\right\}}{2000},$$

$$\text{Right} = \frac{\#\left\{\hat{\varsigma} + z_{1-\frac{\alpha}{2}}\sqrt{\widehat{var}(\hat{\varsigma})} < \varsigma\right\}}{2000}.$$

When the nominal error probability α is 0.05(0.1), the ideal left and right error probabilities should be equal to $\frac{\alpha}{2} = 0.025(0.05)$. Similarly, the ideal total error probabilities should be equal to $\alpha = 0.05(0.1)$. Following Doganaksoy and Schmee (1993), if α was the nominal error probability, then the standard error of the estimated error probability $\hat{\alpha}$ assuming that the observed and nominal error are close, is approximately, $\sqrt{\frac{\alpha(1-\alpha)}{N}}$.

Using a normal approximation, a 99.75% confidence interval for α would be $\hat{\alpha} \pm 2.58\ s.e(\hat{\alpha})$. So, if this interval contains α, then the total error probability, $\hat{\alpha}$ is considered to have actually converged to the nominal error probability, $\overline{\alpha}$. If the total error probability is greater than $\alpha + 2.58\ s.e(\hat{\alpha})$ then the method is termed anticonservative and if it is lower than $\alpha - 2.58\ s.e(\hat{\alpha})$, the method is termed conservative. The estimated error probabilities are called symmetric when the larger error probability is less than 1.5 times the smaller one.

The overall performance of the different methods will be judged based on their total number of anticonservative, conservative and asymmetrical intervals. When an interval is conservative (anticonservative), it means that it generates coverage probability that is greater (smaller) than $(1 - \alpha)$. So, a conservative (anticonservative) confidence interval procedure leads to confidence intervals, which are generally wider (shorter) than they need to be. Thus, a conservative interval is still considered valid and a higher penalty is attached to an anticonservative interval. In addition, methods that are robust in handling censored data and behave well at different nominal levels are also of interest.

Simulation Results and Conclusion

Tables 5-8 give the results of the simulation study at different levels of censoring proportion and two levels of α when $\sigma = 0.5$. The Wald procedure seems to work rather well for parameters β_0, β_1 and β_2. When α is 0.05, all total error probabilities of the

parameters seem to be close to the nominal level except in a few cases when the sample size is low, n = 100, where there were two anticonservative intervals even at low censoring proportion, as shown in Table 5.

Unexpectedly, there are fewer anticonservative and asymmetrical intervals when the censoring proportion is high and n is low compared to when censoring proportion is low. This is probably caused by the combined effect of both censoring and small sample size on the estimated parameters and its standard errors. The small sample size and high censoring proportion cause the intervals to be much wider (due to larger standard errors of the parameter estimates).

In addition, the high level of censoring in the data generated estimates that were very biased resulting in intervals that sometimes accidentally included the true parameter value. The coverage probabilities were also better at higher nominal levels, α. When censoring proportion and were high, there were no anticonservative, conservative or asymmetrical intervals.

For the parameter, σ , as expected the untransformed Wald procedure generated intervals that were highly asymmetrical. This method also generated more anticonservative intervals compared to the transformed methods. From the two different parameterizations of σ the transformation $\varsigma = \frac{1}{\sigma}$ produced more symmetrical intervals than the transformation $\varsigma = \log \sigma$.

The transformation $\varsigma = \frac{1}{\sigma}$ worked very well especially when α = 0.05 because in addition to being more symmetrical, it also did not generate any conservative or anticonservative intervals. However, it generated some conservative and asymmetrical intervals when both α and censoring proportion were high as shown in Table 8. The untransformed Wald method generated many anticonservative intervals whereas the transformation $\varsigma = \log \sigma$ produced many conservative intervals. Both the untransformed Wald and the transformation method $\varsigma = \log \sigma$ failed to generate a single symmetrical interval.

TABLE 5
Estimated error probabilities of β at α = 0.05, A = "Anticonservative"

θ	n	cp = 0.10			cp = 0.03		
		Left Error	Right Error	Total Error	Left Error	Right Error	Total Error
β_0	100	0.0330	0.0240	0.0570	0.0285	0.0300	0.0585
	150	0.0265	0.0225	0.0490	0.0265	0.0195	0.0460
	200	0.0285	0.0265	0.0550	0.0225	0.0260	0.0485
	250	0.0275	0.0280	0.0555	0.0245	0.0240	0.0485
β_1	100	0.0380	0.0285	0.0665^A	0.0325	0.0330	0.0655^A
	150	0.0325	0.0280	0.0605	0.0295	0.0295	0.0590
	200	0.0345	0.0250	0.0595	0.0250	0.0255	0.0505
	250	0.0315	0.0250	0.0565	0.0275	0.0235	0.0510
β_2	100	0.0300	0.0330	0.0630^A	0.0250	0.0305	0.0555
	150	0.0290	0.0315	0.0605	0.0255	0.0290	0.0545
	200	0.0220	0.0355	0.0575	0.0235	0.0350	0.0585
	250	0.0255	0.0320	0.0575	0.0275	0.0290	0.0565

TABLE 6
Estimated error probabilities of β at α = 0.10, A = "Anticonservative"

θ	n	cp = 0.10			cp = 0.03		
		Left Error	Right Error	Total Error	Left Error	Right Error	Total Error
β_0	100	0.0620	0.0435	0.1055	0.0555	0.0505	0.1060
	150	0.0570	0.0420	0.0990	0.0520	0.01445	0.0965
	200	0.0570	0.0475	0.1045	0.0455	0.0500	0.0955
	250	0.0515	0.0515	0.1030	0.0465	0.0480	0.0945
β_1	100	0.0635	0.0580	0.0665[A]	0.0575	0.0595	0.1170
	150	0.0555	0.0515	0.1070	0.0510	0.0505	0.1015
	200	0.0625	0.0495	0.1120	0.0555	0.0465	0.1020
	250	0.0530	0.0420	0.0950	0.0570	0.0425	0.0995
β_2	100	0.0555	0.0605	0.1160	0.0480	0.0570	0.1050
	150	0.0560	0.0620	0.1180[A]	0.0515	0.0585	0.1100
	200	0.0575	0.0585	0.1160	0.0455	0.0620	0.1075
	250	0.0485	0.0610	0.1095	0.0485	0.0605	0.1090

TABLE 7
Estimated error probabilities of σ at α = 0.05, A = "Anticonservative" C="Conservative"

cp	n	$\varsigma = \sigma$			$\varsigma = \log \sigma$			$\varsigma = \frac{1}{\sigma}$		
		Left Error	Right Error	Total Error	Left Error	Right Error	Total Error	Left Error	Right Error	Total Error
	100	0.0065	0.0570	0.0635[A]	0.0120	0.0420	0.0540	0.0190	0.0265	0.0455
	150	0.0080	0.0430	0.0510	0.0105	0.0355	0.0460	0.0165	0.0290	0.0455
0.1	200	0.0110	0.0535	0.0645[A]	0.0155	0.0430	0.0585	0.0220	0.0305	0.0525
	250	0.0120	0.0490	0.0490	0.0610	0.0170	0.0400	0.0570	0.0210	0.0555
	100	0.0025	0.0390	0.0415	0.0085	0.0280	0.0365[C]	0.0190	0.0265	0.0455
	150	0.0035	0.0410	0.0445	0.0070	0.0290	0.0360[C]	0.0165	0.0290	0.0455
0.3	200	0.0050	0.0380	0.0430	0.0105	0.0280	0.0385	0.0220	0.0305	0.0525
	250	0.0060	0.0415	0.0475	0.0070	0.0305	0.0375	0.0210	0.0345	0.0555

In fact, on average, the untransformed Wald method was almost five times more asymmetrical than the same method using $\varsigma = \frac{1}{\sigma}$, when σ was low. The confidence intervals for the $\varsigma = \log \sigma$ transformation were almost twice as asymmetrical as those for $\varsigma = \frac{1}{\sigma}$. The transformation, $\varsigma = \frac{1}{\sigma}$, should be preferred because the other two transformations gave very asymmetrical intervals. Thus, $\varsigma = \frac{1}{\sigma}$, in the original Weibull distribution works best.

The transformation, $\varsigma = \frac{1}{\sigma}$, worked very well especially when α =0.05 because in addition to being more symmetrical, it also did not generate any conservative or anticonservative intervals. However, it generated some conservative and asymmetrical intervals when both α and censoring proportion were high as shown in Table 8. The

TABLE 8
Estimated error probabilities of σ at α = 0.10, A = "Anticonservative" C="Conservative"

		$\varsigma = \sigma$			$\varsigma = \log \sigma$			$\varsigma = \frac{1}{\sigma}$		
cp	n	Left Error	Right Error	Total Error	Left Error	Right Error	Total Error	Left Error	Right Error	Total Error
	100	0.0215	0.0980	0.1195[A]	0.0245	0.0820	0.1065	0.0305	0.0660	0.0965
	150	0.0215	0.0815	0.1030	0.0260	0.0665	0.0925	0.0335	0.0530	0.0865
0.1	200	0.0295	0.0815	0.1110	0.0340	0.0735	0.1075	0.0380	0.0650	0.1030
	250	0.0310	0.0820	0.1130	0.0345	0.0745	0.1090	0.0400	0.0650	0.1050
	100	0.0150	0.0695	0.0845	0.0220	0.0550	0.0770[C]	0.0270	0.0400	0.0670[C]
	150	0.0130	0.0715	0.0845	0.0190	0.0610	0.0800[C]	0.0255	0.0485	0.0740[C]
0.3	200	0.0185	0.0670	0.0855	0.0230	0.0575	0.0805[C]	0.0290	0.0450	0.0740[C]
	250	0.0210	0.0695	0.0905	0.0240	0.0615	0.0855	0.0315	0.0535	0.0850

untransformed Wald method generated many anticonservative intervals whereas the transformation $\varsigma = \log \sigma$ produced many conservative intervals. Both the untransformed Wald and the transformation method $\varsigma = \log \sigma$ failed to generate a single symmetrical interval.

In fact, on average, the untransformed Wald method was almost five times more asymmetrical than the same method using $\varsigma = \frac{1}{\sigma}$ when α was low. The confidence intervals for the $\varsigma = \log \sigma$ transformation were almost twice as asymmetrical as those for $\varsigma = \frac{1}{\sigma}$. Thus, the transformation, $\varsigma = \frac{1}{\sigma}$, should be preferred because the other two transformations gave very asymmetrical intervals. So, basically $\varsigma = \frac{1}{\sigma}$ in the original Weibull distribution works best.

REFERENCES

ARASAN, J. and DAUD, I. (2004). Parallel system using the log-linear exponential model with censored data and two covariates. *Pertanika J. of Sci. and Technol., 12*(2), 265-275.

BAKLIZI, A.S.M. (1997). Likelihood inference in parallel systems regression models with censored data (PhD thesis, University Putra Malaysia, Department of Statistics, 1997).

COX, D.R. and HINKLEY, D.V. (1979). *Theoretical Statistics*. New York: Chapman and Hall.

DOGANAKSOY, N. and SCHMEE, J. (1993). Comparison of approximate confidence intervals for distributions used in life-data analysis. *Technometrics, 35*(2), 175-184.

ELANDT-JOHNSON, R.C. and JOHNSON, N.L. (1980). *Survival Models and Data Analysis*. New

York: Wiley.

HØYLAND, A. and RAUSAND, M. (1994). *System Reliability Theory*. New York: Wiley.

HOSMER, D.W. and LEMESHOW, S. (1999). *Applied Survival Analysis*. New York: Wiley.

KECECIOGLU, D. (1991). *Reliability Engineering Handbook* (Volume 1). New York. Prentice Hall.

ISSN: 0128-7680
Pertanika J. Sci. & Technol. **16 (2)**: 97 - 105 (2008)

Development of a Camera-Vision Guided Automatic Sprayer

Wan Ishak, W.I., Hazlina H. and Awal M.A.[1*]
Faculty of Engineering, Universiti Putra Malaysia,
43400 UPM, Serdang, Selangor, Malaysia
[1]*Bangladesh Agricultural University, Mymensingh, Bangladesh*
*E-mails: wiwi@putra.upm.edu.com or *mawal69@yahoo.com*

ABSTRACT

This study describes the design and development of a camera-vision guided unmanned mover sprayer for the purpose of automatic weed control. The sprayer system was mounted on the mover. Modifications were carried out for both sprayer and mover systems, so that it can be operated remotely. The automated system was developed using the electromechanical system and controllers. It is capable of directing the mover sprayer to the target location given by the user. The electromechanical system was developed to control the ignition, the accelerator and the spraying systems. The controllers consist of an I/O module (ICPCON I-87057) and also a pair of radio modems (SST-2400) for data transmission. The graphical user interface (GUI) software to control the automatic system was developed by using Visual Basic Programming. The GUI has features which enable the user to perform desired tasks using the computer instead of going directly to the sprayer/mover. The combination of the multi controllers and developed control software in the development of the camera-vision-guided unmanned mover sprayer can reduce drudgery and increase safety.

Keywords: Automation, sprayer and camera vision

INTRODUCTION

In the early days of plantation development virtually all work was done manually with the aid of only hand tools. At that early period economics of cost was possibly the greatest incentive because labour was plentiful and relatively inexpensive. However, with labour becoming more expensive and scarce, and also with the gradual introduction of various forms of machines, it is becoming more essential to introduce as many new techniques as possible. The use of machines in agricultural production has been one of the most outstanding developments in Malaysian agriculture in the past decades. The burden and drudgery of farm work has been reduced, and output per worker has greatly increased. Equipping a modern agricultural plantation for field operations involves more than merely shopping for functionally adequate machinery. Mechanization has been suggested as a method to improve productivity and making the task more acceptable to workers in the plantation. The production of plantation crops could be increased with improved agronomy and increased mechanized operations. There is a need to mechanize all activities in spraying operations. Modern and efficient methods of spraying systems need to be introduced in plantations. This could be achieved by integrating all activities in spraying with an integrated mechanized system.

Received : 8 January 2007
Accepted : 20 June 2007
* Corresponding Author

Automation contributes to the expansion of the industrial and agricultural sector. It reduces the needs for unskilled labour, renders obsolete some existing skills, and demands a high level of technical culture (Thomas, 1969). Many different types of technologies such as machine vision, radio frequency, laser and GPS have been attempted for use in navigation of agricultural vehicles (Noguchi *et al.,* 2002; Zuydam *et al.,* 1994; and Choi *et al.,* 1990). These automated technologies can work with any field operation, including planting, cultivating and harvesting. Since modern agricultural machinery is equipped with many controls, operator fatigue is a serious concern (Noh and Erach, 1993; and Tillet, 1991). Automatic guidance can reduce operator fatigue and improve machinery performance by reducing overlapping or skipping during field operations such as tillage and chemical application (Tillet, 1991; Klassen *et al.,* 1993).

In this project, two components were modified namely; the ignition system and accelerator system. The ignition system was modified in such a way that the mover can be remotely started within a certain range (maximum range 5km square) without disabling the manual ignition system. A mechanical relay was used for this purpose. To enable automatic ignition or automatic shut off, a radio modem and ICP I/O module (I-87057) was used to energize the relay coil. The 12V voltage from the tractor battery will flow through the Common pole and Normally Open pole to the ignition coil or shut off coil to start or off the mover engine. This connection completes the automatic ignition system (*Fig. 1*).

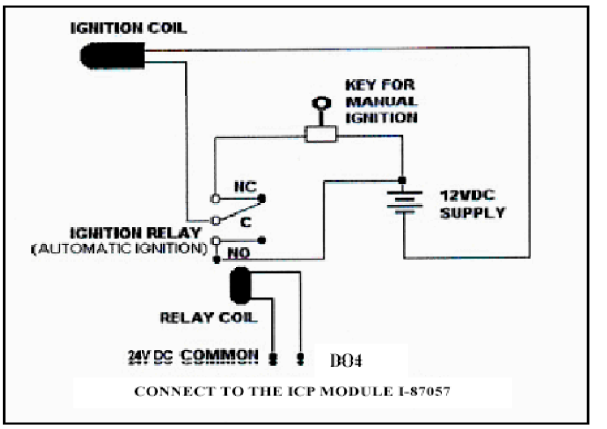

Fig. 1: Schematic diagram output signal of the ignition system

The Accelerator system will determine the speed of the mover, forward and reverse action. Two mechanical relays were used to accelerate the mover autonomously. The first relay was connected to the mover's forward electric motor and the other was connected to the reverse electric motor (*Fig. 2*). These two relays will only operate when the ICP modules receive signals either to forward or reverse the mover (Saufi, 2002). The accelerator system of the existing unmanned tractor was connected to the camera vision system. The purpose was to control the speed of the unmanned tractor based on the rate of spraying a weedicide. The rate of spraying depends on the intensity of weeds.

Vision system is a new field in the agricultural sector. In agricultural application, especially for fruit handling, we cannot detect fruit quality just by its shape or pattern. One type of fruit with variations in shape and pattern may have similar quality. The

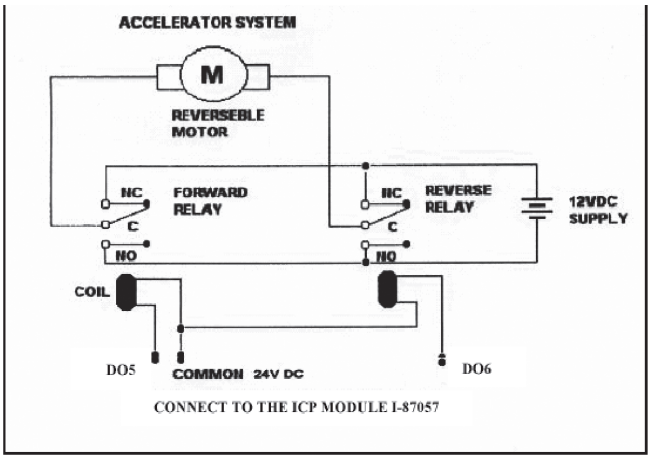

Fig. 2: Schematic diagram output signal of the accelerator system

difficulties encountered with vision for agriculture is to control the environment or the objects to be manipulated. The variations in lighting intensity from time to time and place to place cause difficulty in developing a complete vision system in terms of automatic recognition of an object's color. The use of cameras has failed to obtain sufficient information about fruits, mainly in unconstrained environments, where many factors affect the scene such as weather conditions, color of leaves and their position in relation to the fruit and light contrast (Kondo and Ting, 1998). Thus a method was devised to capture the initial image of weeds and analyze the weeds for color and saved as the reference color of the weeds to be sprayed.

In Malaysia most farm production tasks are not fully automated whereby man power is still needed in certain tasks. Therefore, the autonomous sprayer will be part of advanced agriculture production systems in Malaysia. The main purpose of this study was to design and develop an automatic sprayer, which can be controlled remotely. To achieve this objective a preliminary study was conducted to improve the system by designing the automatic sprayer. Image processing algorithm was developed to enable decision-making concerning the presence of weeds.

METHODOLOGY

The project activities were divided into three major sections. The first section consisted reconfiguration of a previous unmanned tractor system (Saufi, 2002), the second was to design and develop a camera-vision-guided sprayer, and the third was to attach the camera-vision-guided sprayer to an unmanned tractor. Minor modifications were carried out on the previous unmanned tractor system to enable computer control to replace human control. The development of the camera vision guided sprayer was divided into three main categories: (1) Planning and design of the spraying system, (2) Fabrication of the spraying system and (3) Development of the computer control software by using VB program.

In the design stage, the length and the size of the galvanized pipes and hoses were first determined. Hoses and fittings to handle the water at selected operating pressure and quantity were selected. Half inch galvanized pipe was used as the main line for liquid

flow. Galvanized pipe was chosen because of its high resistance characteristics to high pressure and also because it can hold more weight when other heavy components such as solenoid valves and nozzles were attached to it. The nozzle is the critical part of the sprayer. Nozzles determine the rate of water distribution at particular pressure, forward speed and nozzle spacing. A 5.0 mm narrow nozzle was selected for this purpose.

Solenoid valves are popularly used in control and automation application. Generally, solenoid operators and valves were devices which control the flow of liquids, gases, steam and other media. When electrically energized they either open, shut off or direct the flow of media. Two types of solenoid valves were used for this project. One was a Normally Open (NO) solenoid valve and the other one was a Normally Close (NC) solenoid valve. NO solenoid valve was mounted at the bottom of the tank for flow by-pass purposes. It was also used to avoid high pressure in the galvanized pipe and hose when the nozzles were not operated, while the NC solenoid valve was mounted at the nozzles for the purpose of ON/OFF of the nozzles. It will turn ON the nozzle when the camera detects the existence of weeds and turn it OFF when the camera does not detect weeds. This kind of ON/OFF function will help to reduce the amount of volume sprayed and therefore help reduce production cost.

Controller Development

Modules from ICPCON I-87K and radio modem (SST-2400) were selected for data acquisition and control. SST-2400 radio modem is the 'heart' of the PC-based control system. They provide digital input/output and other functions. They handle the signal transfer from the computer to the mover. The radio modem communicates with the computer by using the RS-232 serial port. The radio modem receiver receives the signals and transfers it to the ICP Modules (I-87057) via RS-485 bus. The radio modem needs to be configured before it can be used.

In this project, only 7 channels from the ICPCON I-87057 were used. DO0 from the ICPCON I-87057 was connected to the NO solenoid valve for flow by-pass action. When the output signal is activated, the relay will be energized and cause electrical supply to the NO solenoid valve and automatically close the valve. DO1, DO2 and DO3 from the ICPCON I-87057 were connected to the NC solenoid valve for nozzles 1, 2 and 3 respectively. When the output signal is activated, the relay energizes and cause electrical flow to the NC solenoid valve and automatically opens the valve to operate the nozzle. *Fig. 1* shows the schematic diagram of the automatic ignition system. DO4 from the ICPCON I-87057 was connected to the ignition relay. When the output signal is activated, the relay will energize and cause electrical supply to flow to the ignition coil and automatically start the mover's engine. Output signals DO5 and DO6 from the ICPCON I-87057 were used to energize the relay for forward and reverse movement of the mover. *Fig. 2* shows the schematic diagram of the accelerator system.

Software Development

In this project, Microsoft Visual Basic 6.0 was used to develop the GUI to monitor the parameters that control the autonomous sprayer operations. *Fig. 3* shows the GUI to control the whole system of the autonomous sprayer. With this program, users can give instructions to the autonomous sprayer to perform a specified task. *Fig. 4* shows the screen of the monitor being divided into 3 frames captured by one camera. The three frames were for 3 units of spray nozzles. The spray system consists of 2 cameras located

on the left and right side of the tractor. The weeds captured by the camera in each frame were analyzed to activate the respective nozzles either to open or close. All features that appear in the GUI contained special codes, which were written in Visual Basic. *Fig. 5* shows the flowchart of the program. The camera snaps the image and analyzes the red, green, blue (RGB) value in terms of computer pixel. The sprayer nozzle will turn on or off depending on the percentage or intensity of green color value of weeds.

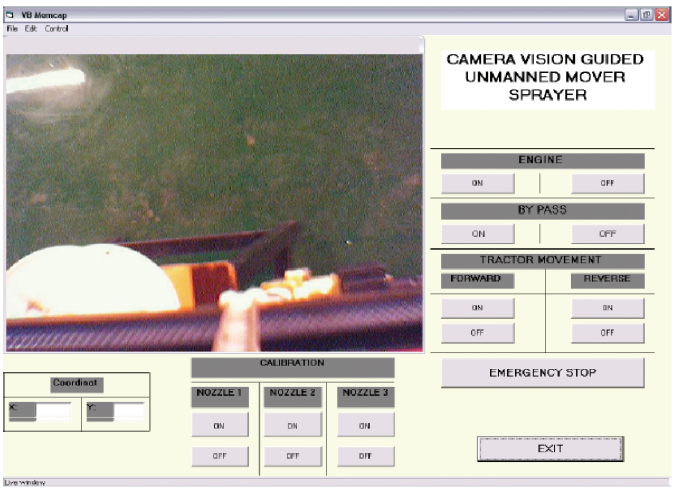

Fig. 3: GUI for controlling the camera vision guided unmanned mover sprayer

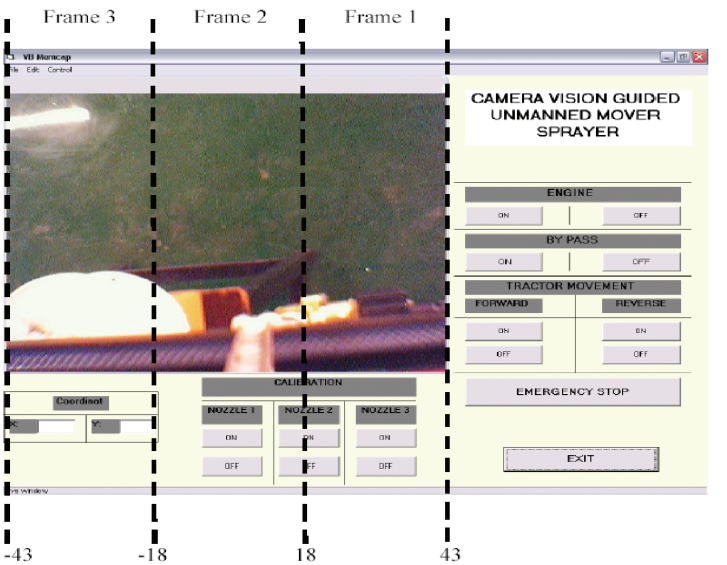

Fig. 4: Boundaries of image frames in GUI

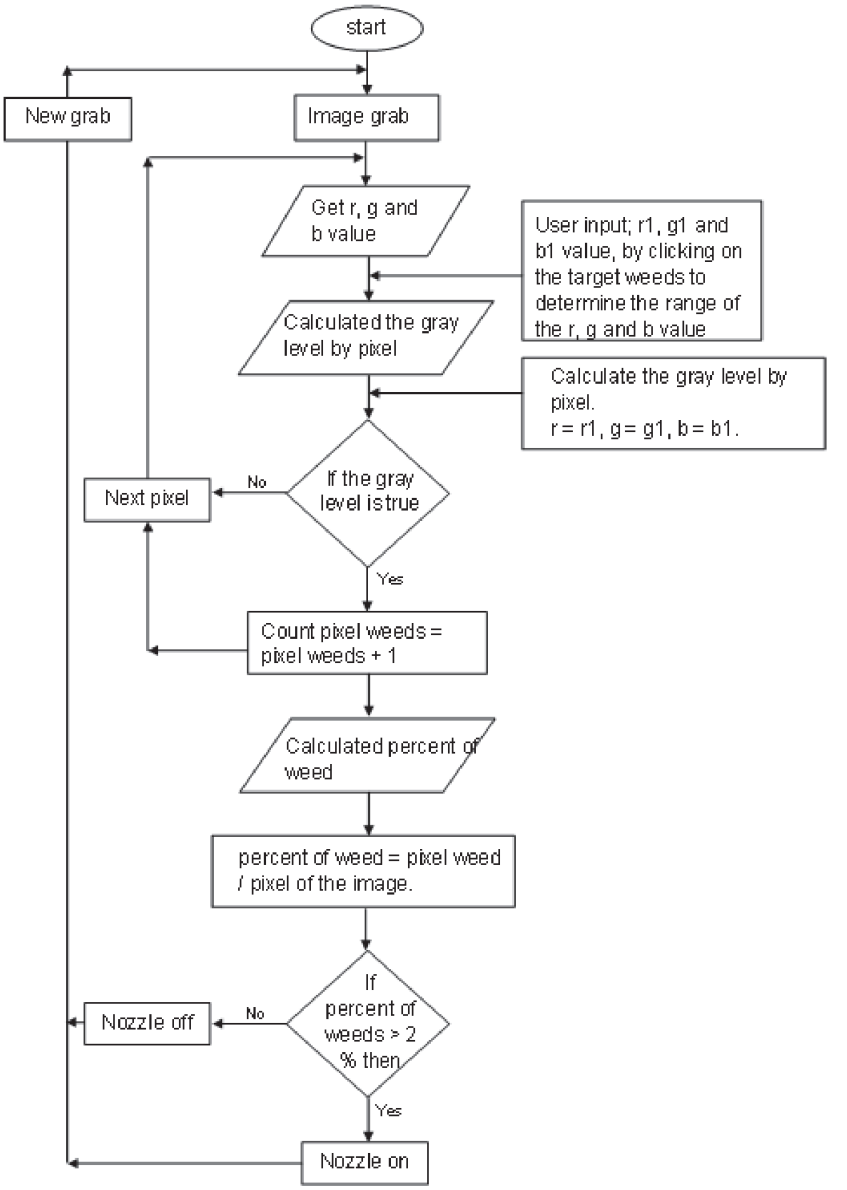

Fig. 5: Flowchart of the weed detection algorithm

Information in Table 1 is useful in determining the task for each output channel of the ICPCON I-87057. The software packages used for ICPCON I-7000/8000/87K series module were I-7000/8000 Utility and NAP 7000X. Table 1 shows the output signals assigned for the ICPCON I-87057. The source codes were written by referring to the information in Table 1. It also helps in the troubleshooting process when problems occur.

TABLE 1
Output assigning of the ICPCON I-87057

Module	Channel	Description
I-87057	DO0	Bypass
	DO1	Nozzle1
	DO2	Nozzle2
	DO3	Nozzle3
	DO4	Engine (Ignition)
	DO5	Motor (Forward)
	DO6	Motor (Reverse)

RESULTS AND DISCUSSION

The autonomous sprayer was successfully designed and fabricated. The electrical power from the tractor's battery was used as a power source, and ICPCON modules were used to control the operation of the autonomous sprayer. Tests were carried out for the whole system including the ignition, accelerator and the spraying systems. The GUI was tested to make sure that it works according to the autonomous sprayer system working process.

The accelerator system of the tractor was operated by using a reversible electrical motor. The user can increase tractor speed by pressing the key for forward (DO5) or reverse (DO6) direction. The Spraying system was tested to make sure that all the components were in good working condition. Nozzles calibration was done through a command button on the GUI. Besides using the command button, it can be done manually to operate the nozzle. Each nozzle (nozzle 1, nozzle 2 and nozzle 3) can be operated individually in their respective area of spray. Images that were captured were divided into three frames. The first nozzle can only operate in frame 1, the second nozzle in frame 2 and the third nozzle in frame 3. The boundaries of each frame were determined by the different values of x-axis as shown in *Fig. 4*. When the user clicks in the region of frame 1, nozzle 1 will be turned ON while the other nozzles will be turned OFF. The NC solenoid valves mounted at the nozzle carry out these functions. Therefore, the user can select the area to be sprayed from the image. Each application of ON operation will take 2 seconds before it turns OFF again. If there is nothing to be sprayed, the NO solenoid valves mounted at the tank will open to by pass the liquid back to the tank. This was used to avoid high-pressure build up in the main sprayer line. The GUI was designed to have an emergency stop button if the user needs to immediately stop the autonomous sprayer.

The visual basic programming languages used the basic API pixel routine. The pixel value will extract RGB colour pixels ranging from 0 to 255. The green colour of the weed was selected and was set at the range of plus and minus 10 from the RGB selected pixel values. The green weeds to be sprayed were calculated based on the percentage of intensity of weeds and percentage of green pixels of the weeds. The sprayer pump and the nozzles will be ON at 21 to 100% intensity of weeds and 0.4 to 100% of pixels percent of green weeds.

In this project, the performance of the autonomous sprayer was tested. The characteristics monitored included spraying triggering time, the width of spraying and the overlapping width of spraying. The spraying triggering time was monitored as an

important aspect in the automatic control system. It determines the relationship between the command given in the GUI and the time taken by the sprayer to operate. The width of spraying was measured in order to determine the coverage area being sprayed in one weed spot per nozzle. Besides that, the overlapping width of spraying was also measured. It represents wastage during spraying.

From the results, it was shown that there were different pressure build ups in the distribution system (nozzle). The nearer the nozzle to the pump, the higher was the pressure build up in the nozzle with an increase in the spraying width. The triggering time was instantaneous to the nozzle operations. In this project, spraying duration was set at 2 seconds for one application. The mover speed was set at 7 km/h. The sprayer motor operates once the mover moves. The spraying was measured to cover up to 3m width of weed spot per spraying. Therefore, the coverage area was 2467.8 m^2 per hour of spraying. With 7km/hr speed and 3 m spray width, it was found that 26.26% of the coverage area was overlapping spraying. This means that wastage will be higher compared to the wastage which occurs by using only one nozzle at a time.

CONCLUSIONS

Automation is one of the important components in mechanization. In this project, the automated control system for the camera vision guided unmanned mover sprayer was successfully designed and developed. The control system developed combined the technologies of computerized control system, sensor system, control software, wireless data communication, image processing and web-based control system. The user-friendly object oriented VB software was easy to understand which ensures that the autonomous sprayer can be easily operated. The wireless communication unit, SST-2400 radio modem, was easy to configure for several types of communication modes. The ICP modules were able to control the mover and its implement (sprayer). The modules series can acquire most of the needed data to control the mover.

Generally, the automated control system for weeding activities was successfully developed and introduced to optimize the use of weedicide application. This autonomous sprayer has the limitation that it is only suitable for use in plant-free areas.

REFERENCES

Choi, C.H., Choi, D.C., Erbach and Smith, R.J. (1990). Navigational tractor guidance system. *Trans. ASAE, 33*(3), 699–706.

Kondo, N. and Ting, K.C. (1998). Robotics for bioproduction systems. ASAE, St Joseph Michigan, USA.

Noguchi, N., Kise, M., Ishii, K. and Terao, H. (2002). Field automation using robot tractor. *ASAE Paper No. 701P0502, Conference Publication* (pp. 239–245), July 26–27.

Noh, K.M. and Erbach, D.C. (1993). Self-tuning controller for farm tractor guidance. *Trans. ASAE, 36*(6), 1583–1594.

Saufi, M. K. (2002). Design and development of automated system for agricultural tractor (A Masters Thesis, Intelligent System and Robotic Laboratory, Institute of Advance Technology, University Putra Malaysia, 2002).

TILLET, N.D. (1991). Automatic guidance sensors for agricultural field machines: A review. *J. Agric. Eng. Res., 50*(3), 167–187.

ZUYDAM, R., VAN, P. and SONNEVELD, C. (1994). Test of an automatic precision guidance system for cultivation implements. *J. Agric. Eng. Res., 59*(4), 239–243.

ISSN: 0128-7680
Pertanika J. Sci. & Technol. **16 (2)**: 107 - 117 (2008)

Evaluation of a New Estimator

Ng Set Foong[1*], Low Heng Chin[2] and Quah Soon Hoe[3]
[1]Department of Information Technology and Quantitative Sciences, Universiti Teknologi MARA, Jalan Permatang Pauh, 13500 Permatang Pauh, Penang, Malaysia
[2,3]School of Mathematical Sciences, Universiti Sains Malaysia, 11800 Minden, Penang, Malaysia
*E-mails: [1]*setfoong@yahoo.com, [2]hclow@cs.usm.my, [3]shquah@gmail.com*

ABSTRACT

An estimator is used to estimate the unknown parameter in a linear regression model. In this paper, a new estimator was derived from further modification of the Liu-type Estimator. The performance of the new estimator was evaluated by comparing its mean squared error with the mean squared errors of other estimators. It was found that there is a reduction in mean squared error in the new estimator under certain conditions.

Keywords: Estimator, mean squared error, regression

INTRODUCTION

A linear regression model is used to describe the relationship between a dependent variable and one or several independent variables. A linear regression model is generally written as $y = \beta_0 + \beta_1 x_1 + \beta_2 x_2 + ... + \beta_p x_p + \varepsilon$, where β_j, $j = 0, 1, 2, ..., p$, is a parameter and ε is the error term. The parameter β_j in the linear regression model is unknown and is to be estimated from data. There are many existing estimators in regression analysis such as the Ordinary Least Squares Estimator, the Shrunken Estimator (Stein, 1960; cited by Hocking *et al.*, 1976), the Ordinary Ridge Regression Estimator (Hoerl and Kennard, 1970), the $r - k$ Class Estimator (Baye and Parker, 1984), the Liu Estimator (Liu, 1993), the $r - d$ Class Estimator (Kaciranlar and Sakallioglu, 2001) and the Liu-type Estimator (Liu, 2003; Liu, 2004).

In this paper, a new estimator is developed to improve the accuracy of parameter estimates in regression analysis. The new estimator is developed by modification of the Liu-type Estimator. Its performance is evaluated by comparing it with other estimators. The Ordinary Ridge Regression Estimator and the Liu Estimator obtained much interest from the researchers as many studies have been done on these estimators (Baye and Parker, 1984; Pliskin, 1987; Sarkar, 1996; Kaciranlar *et al.*, 1998; Kaciranlar *et al.*, 1999; Sakallioglu *et al.*, 2001; Kaciranlar and Sakallioglu, 2001). In this paper, the performance of the new estimator is evaluated by comparing its mean squared error with the mean squared errors of the Ordinary Ridge Regression Estimator and the Liu Estimator.

A NEW ESTIMATOR

Suppose a linear regression model with standardized variables can be written in the matrix form (Akdeniz and Erol, 2003)

Received : 24 May 2007
Accepted : 17 October 2007
* Corresponding Author

$$Y = Z\gamma + \varepsilon, \qquad [2.1]$$

where Y is a vector of standardized dependent variables, Z is a matrix of standardized independent variables, γ is a vector of parameters, and ε is a vector of errors such that $\varepsilon \sim N(0, \sigma^2 I)$.

Then, the linear regression model, $Y = Z\gamma + \varepsilon$, can be transformed into a canonical form (Akdeniz and Erol, 2003)

$$Y = X\beta + \varepsilon \qquad [2.2]$$

where $X = ZT$, $\beta = T'\gamma$ is a vector of parameters, r is a vector of parameters in the regression model $Y = Z\gamma + \varepsilon$, $X'X = \lambda$, T is an orthonormal matrix consisting of the eigenvectors of $Z'Z$ and λ is $= \text{diag}(\lambda_1, \lambda_2, ..., \lambda_p)$ a diagonal matrix whose diagonal elements are the eigenvalues of $Z'Z$.

In this paper, a new estimator is introduced from further modification of the Liu-type Estimator. Here, a special case of Liu-type Estimator (Liu, 2003) is considered:

$$\hat{\beta}_c = (X'X + d)^{-1} (X'Y + \hat{\beta})$$

$$= [I - (\lambda + d)^{-1} (c-1)\ \hat{\beta} \qquad [2.3]$$

where c is the biasing parameter that is added to the diagonal of matrix X'X, $c > 1$, and $\hat{\beta} = (X'X)^{-1}X'Y$ is the Ordinary Least Squares Estimator of parameter β.

The bias and the mean squared error of $\hat{\beta}_c$ are given by Equations [2.4] and [2.5], respectively.

$$\text{bias}(\hat{\beta}_c) = -(\lambda + d)^{-1} (c - 1)\beta \qquad [2.4]$$

$$\text{mse}(\hat{\beta}_c) = \sum_{j=1}^{p} \left[\frac{(\lambda_j + 1)^2 \sigma^2}{\lambda_j (\lambda_j + c)^2} + \frac{(c-1)^2 \beta_j^2}{(\lambda_j + c)^2} \right] \qquad [2.5]$$

The estimator, $\hat{\beta}_c$, is a biased estimator since there is a certain amount of bias in the estimator. A new estimator is introduced by reducing the bias in $\hat{\beta}_c$. Let $\text{bias}(\hat{\beta}_c)$ be the bias of $\hat{\beta}$ with the unknown β replaced by $\hat{\beta}$. Thus, $\text{bias}(\hat{\beta}_c)$ is given by

$$\text{bias}(\hat{\beta}) = -(\lambda + d)^{-1} (c - 1)\ (c - 1)\hat{\beta} \qquad [2.6]$$

Hence, the new estimator, $\tilde{\beta}_c$, is given by

$$\tilde{\beta}_c = \hat{\beta} - \text{bias}\ (\hat{\beta}_c)$$
$$= \hat{\beta} - [-(\lambda + d)^{-1} (c - 1)\hat{\beta}]$$
$$= \hat{\beta} + (\lambda + d)^{-1} (c - 1)\hat{\beta}_c$$

$$= [I + (\lambda + d)^{-1} (c - 1)] \hat{\beta}_c$$
$$= [I + (\lambda + d)^{-1} (c - 1)][I - (\lambda + d)^{-1})(c - 1) \hat{\beta}_c$$
$$= [I + (\lambda + d)^{-2})(c - 1)^2] \hat{\beta}_c \quad [2.7]$$

where $c > 1$.

The bias, variance-covariance matrix and mean squared error of the new estimator are given by Equations [2.8], [2.9] and [2.10], respectively.

$$\text{bias}(\tilde{\beta}_c) = E(\tilde{\beta}_c) - \beta$$
$$= [I - (\lambda + d)^{-2} (c - 1)^2] E(\hat{\beta}) - \beta$$
$$= [I - (\lambda + d)^{-2} (c - 1)^2] \beta - \beta$$
$$= - (\lambda + d)^{-2} (c - 1)^2 \beta \quad [2.8]$$

$$\text{Var } (\tilde{\beta}_c) = \text{Var } ([I - (\lambda + d)^{-2} (c - 1)^2] \hat{\beta})$$
$$= [I - (\lambda + d)^{-2} (c - 1)^2]^2 \text{ Var}(\hat{\beta})$$
$$= [I - (\lambda + d)^{-2} (c - 1)^2]^2 \sigma^2 \lambda^{-1}$$
$$= \sigma^2 [I - (\lambda + d)^{-2} (c - 1)^2]^2 \quad [2.9]$$

$$\text{mse}(\hat{\beta}_c) = \text{Var}(\hat{\beta}_c) + [\text{bias}(\hat{\beta}_c)]^2$$
$$= \sum_{j=1}^{p} \left\{ \left[1 - \left(\frac{c-1}{\lambda_j + c} \right)^2 \right]^2 \frac{\sigma^2}{\lambda_j} \right\} + \sum_{j=1}^{p} \left[- \left(\frac{c-1}{\lambda_j + c} \right)^2 \beta_j \right]^2$$
$$= \sum_{j=1}^{p} \left\{ \left[1 - \left(\frac{c-1}{\lambda_j + c} \right)^2 \right]^2 \frac{\sigma^2}{\lambda_j} + \left(\frac{c-1}{\lambda_j + c} \right)^4 \beta_j^2 \right\} \quad [2.10]$$

It is found that the new estimator, $\tilde{\beta}_c$, has a reduction in bias compared to the special case of Liu-type Estimator, $\hat{\beta}_c$. This can be seen by considering the difference of the bias between these two estimators in terms of their individual magnitude:

$$\left|\text{bias}((\tilde{\beta}_c)_j)\right| - \left|\text{bias}((\hat{\beta}_c)_j)\right| = \left| - \left(\frac{c-1}{\lambda_j + c} \right)^2 \beta_j \right| - \left| - \left(\frac{c-1}{\lambda_j + c} \right) \beta_j \right|$$
$$= \left(\frac{c-1}{\lambda_j + c} \right)^2 |\beta_j| - \left(\frac{c-1}{\lambda_j + c} \right) |\beta_j|$$
$$= \left(\frac{c-1}{\lambda_j + c} - 1 \right) \left(\frac{c-1}{\lambda_j + c} \right) |\beta_j|$$
$$= - \left(\frac{\lambda_j + 1}{\lambda_j + c} \right) \left(\frac{c-1}{\lambda_j + c} \right) |\beta_j| \quad [2.11]$$

$j = 1, 2, \ldots, p$.

Since $c > 1$, thus $\left|\text{bias}((\tilde{\beta}_c)_j)\right| - \left|\text{bias}((\tilde{\beta}_r)_j)\right| < 0$. This implies that the magnitude of the bias of $\tilde{\beta}_c$ is less than magnitude of the bias of $\tilde{\beta}_r$.

MEAN SQUARED ERROR AS AN EVALUATION TOOL FOR ESTIMATORS

The performance of the new estimator is further evaluated by comparing its mean squared error with other estimators. In general, the mean squared error of an estimator is used as a measure of the goodness of the estimator. Let $\text{mse}(\tilde{\beta})$ denote the mean squared error of an estimator, $\tilde{\beta}$. Then, the $\text{mse}(\tilde{\beta})$ is given by

$$\text{mse}(\tilde{\beta}) = E\left[(\tilde{\beta}-\beta)'(\tilde{\beta}-\beta)\right]. \qquad [3.1]$$

Suppose $\tilde{\beta}_1$ and $\tilde{\beta}_2$ are two estimators of the parameter β. The estimator $\tilde{\beta}_2$ is superior to the estimator $\tilde{\beta}_1$ if the mean squared error of $\tilde{\beta}_2$ is smaller than the mean squared error of $\tilde{\beta}_1$, that is, Suppose the estimator, $\tilde{\beta}_1$, can be represented as a product of a matrix A_1 and the vector of standardized dependent variables, Y, that is, $\tilde{\beta}_1 = A_1 Y$. Suppose also that the estimator, $\tilde{\beta}_2$, can be represented as a product of a matrix A_2 and the vector of standardized dependent variables, Y, that is, $\tilde{\beta}_2 = A_2 Y$. Let $\text{bias}(\tilde{\beta}_1)$ and $\text{bias}(\tilde{\beta}_2)$ denote the bias of the estimators, $\tilde{\beta}_1$ and $\tilde{\beta}_2$ respectively. Then, the condition for $\text{mse}(\tilde{\beta}_1) > \text{mse}(\tilde{\beta}_2)$is given by Theorem 3.1.

Theorem 3.1. The conditions for $\text{mse}(\tilde{\beta}_1) > \text{mse}(\tilde{\beta}_2)$ are:

(a) $A_1A_1' - A_2A_2'$ is a positive definite matrix, and

(b) $\left[\text{bias}(\tilde{\beta}_2)\right]\left(A_1A_1' - A_2A_2'\right)^{-1}\left[\text{bias}(\tilde{\beta}_2)\right] < \sigma^2$.

Proof. Let $M(\tilde{\beta}_1)$ and $M(\tilde{\beta}_2)$ denote the mean squared error matrices of the estimators, $\tilde{\beta}_1$ and $\tilde{\beta}_2$, respectively. Let $\text{Var}(\tilde{\beta}_1)$ and $\text{Var}(\tilde{\beta}_2)$ denote the variance-covariance matrices of the estimators, $\tilde{\beta}_1$ and $\tilde{\beta}_2$, respectively. The mean squared error of an estimator is equal to the variance of the estimator plus the square of its bias. Hence, the mean squared error matrices, $M(\tilde{\beta}_1)$ and $M(\tilde{\beta}_2)$, are given by Equations [3.2] and [3.3], respectively.

$$\begin{aligned} M(\tilde{\beta}_1) &= \text{Var}(\tilde{\beta}_1) + \left[\text{bias}(\tilde{\beta}_1)\right]\left[\text{bias}(\tilde{\beta}_1)\right]' \\ &= \text{Var}(A_1 Y) + \left[\text{bias}(\tilde{\beta}_1)\right]\left[\text{bias}(\tilde{\beta}_1)\right]' \\ &= \sigma^2 A_1A_2' + \left[\text{bias}(\tilde{\beta}_1)\right]\left[\text{bias}(\tilde{\beta}_1)\right]' \end{aligned} \qquad [3.2]$$

$$M(\tilde{\beta}_2) = \sigma^2 A_2A_2'\left[\text{bias}(\tilde{\beta}_2)\right]\left[\text{bias}(\tilde{\beta}_2)\right]' \qquad [3.3]$$

Thus, $M(\tilde{\beta}_1) - M(\tilde{\beta}_2)$ is given by

$$\begin{aligned} &M(\tilde{\beta}_1) - M(\tilde{\beta}_2) \\ &= \left\{\sigma^2\left(A_1A_1' - A_2A_2'\right) - \left[\text{bias}(\tilde{\beta}_2)\right]\left[\text{bias}(\tilde{\beta}_2)\right]\right\} + \left[\text{bias}(\tilde{\beta}_1)\right]\left[\text{bias}(\tilde{\beta}_1)\right]. \end{aligned} \qquad [3.4]$$

Note that $[\text{bias}(\tilde{\beta}_1)][\text{bias}(\tilde{\beta}_1)]'$ is positive definite. Therefore, $M(\tilde{\beta}_1) - M(\tilde{\beta}_2)$ is positive definite if $\sigma_2 (A_1A_1' - A_2A_2') - [\text{bias}(\tilde{\beta}_2)][\text{bias}(\tilde{\beta}_2)]'$ is also positive definite.

Applying the theorem from Farebrother (1976): Let Q be a $p \times p$ positive definite matrix, ψ a nonzero $p \times 1$ vector and ς a positive scalar, then $\varsigma Q - \psi\psi'$ is positive definite if and only if $\psi' Q^{-1} \psi < \varsigma$. Thus, the conditions for $\sigma_2 (A_1A_1' - A_2A_2') - [\text{bias}(\tilde{\beta}_2)][\text{bias}(\tilde{\beta}_2)]'$ to be positive definite are:

(a) $A_1A_1' - A_2A_2'$ is a positive definite matrix and

(b) $[\text{bias}(\tilde{\beta}_2)] (A_1A_1' - A_2A_2')^{-1} [\text{bias}(\tilde{\beta}_2)] < \sigma^2$.

On the other hand, Theobald (1974) considered a weighted sum of the coefficient mean squared error as another measure of the goodness of an estimator. The weighted sum of the coefficient mean squared error is known as the generalized mean squared error (Sakallioglu *et al.*, 2001). The generalized mean squared error of an estimator, $\tilde{\beta}$, is given by

$$\text{gmse}(\tilde{\beta}) = E[(\tilde{\beta}-\beta)'(\tilde{\beta}-\beta)], \qquad [3.5]$$

where B is a nonnegative definite matrix.

Theobald (1974) established a relationship between the generalized mean squared error and the mean squared error matrix of an estimator: Suppose there are two estimators, namely, $\tilde{\beta}_1$ and $\tilde{\beta}_2$, the following conditions are equivalent:

(a) $M(\tilde{\beta}_1) - M(\tilde{\beta}_2)$ is positive definite, and

(b) $\text{gmse}(\tilde{\beta}_1) > \text{gmse}(\tilde{\beta}_2)$ for all positive definite matrix B.

Note that $\text{gmse}(\tilde{\beta})$ is equal to $\text{msegmse}(\tilde{\beta})$ when the matrix B in Equation [3.5] is equal to an identity matrix I. From this, we see that the condition for $M(\tilde{\beta}_1) - M(\tilde{\beta}_2)$ is positive definite is equivalent to the condition for $\text{mse}(\tilde{\beta}_1) - \text{mse}(\tilde{\beta}_2)$.
Thus, the conditions for $\text{mse}(\tilde{\beta}_1) - \text{mse}(\tilde{\beta}_2)$ are:

(a) $A_1A_1' - A_2A_2'$ is a positive definite matrix and

(b) $[\text{bias}(\tilde{\beta}_2)]' (A_1A_1' - A_2A_2')^{-1} [\text{bias}(\tilde{\beta}_2)] < \sigma^2$.

Hence, the proof for Theorem 3.1 is completed. ❑

The comparison between the new estimator and other estimators is performed by applying the concept of Theorem 3.1.

THE EVALUATION OF THE NEW ESTIMATOR

The Ordinary Ridge Regression Estimator and the Liu Estimator are two biased estimators. The new estimator is compared with these two estimators in terms of mean squared error.

The Ordinary Ridge Regression Estimator is given by (Hoerl and Kennard, 1970)

$$\hat{\beta}_k = (X'X + kI)^{-1} X'Y$$
$$= A_k Y, \qquad [4.1]$$

where $A_k = (X'X + kI)^{-1} X'$, $k > 0$.
Hence, $A_k A_k'$ is given by (Hoerl and Kennard, 1970)

$$A_k A_k' = (\pi + kI)^{-2}\lambda . \quad [4.2]$$

The bias and the mean squared error of $\hat{\beta}_k$ are given by Equations [4.3] and [4.4], respectively (Hoerl and Kennard, 1970).

$$\text{bias}(\hat{\beta}_k) = -(X'X + kI)^{-1} k\beta \quad [4.3]$$

$$\text{mse}(\hat{\beta}_k) = \sum_{j=1}^{p}\left[\frac{\lambda_j\sigma^2}{(\lambda_j+k)^2} + \frac{k^2\beta_j^2}{(\lambda_j+k)^2}\right] \quad [4.4]$$

The Liu Estimator is given by (Liu, 1993)

$$\begin{aligned}\hat{\beta}_d &= (X'X + I)^{-1} (X'X + dI)(X'X)^{-1} X'Y \\ &= A_d Y,\end{aligned} \quad [4.5]$$

where $A_d = (X'X + I)^{-1} (X'X + dI)(X'X)^{-1} X'$, $0 < d < 1$.
Hence, $A_d A_d'$ is given by (Liu, 1993)

$$A_d A_d' = (\lambda + I)^{-2} (\lambda + dI)^2 \lambda^{-1} \quad [4.6]$$

The bias and the mean squared error of $\hat{\beta}_d$ are given by Equations [4.7] and [4.8], respectively (Liu, 1993).

$$\text{bias}(\hat{\beta}_d) = -(X'X + I)^{-1}(1 - d)\beta \quad [4.7]$$

$$\text{mse}(\hat{\beta}_d) = \sum_{j=1}^{p}\left[\frac{(\lambda_j+d)^2\sigma^2}{\lambda_j(\lambda_j+1)^2} + \frac{(1-d)^2\beta_j^2}{(\lambda_j+1)^2}\right] \quad [4.8]$$

The new estimator, $(\tilde{\beta}_c)$, can also be written as

$$\begin{aligned}(\tilde{\beta}_c) &= \left[I - (\lambda + d)^{-2} (c - 1)^2\right]\hat{\beta} \\ &= \left[I - (\lambda + d)^{-2} (c-1)^2\right]\lambda^{-1}X'Y \\ &= A_c Y,\end{aligned} \quad [4.9]$$

where $A_c = \left[I - (\lambda + d)^{-2}(c-1)^2\right] \lambda^{-1}X'$, $c > 1$.
Hence, $A_c A_c'$, is given by

$$A_c A_c' = [I - (\lambda + d)^{-2} (c-1)^2]^2 \lambda^{-1}. \quad [4.10]$$

Theorem 4.1 shows the comparison between $\tilde{\beta}_c$ and $\hat{\beta}_k$ while Theorem 4.2 shows the comparison between $\tilde{\beta}_c$ and $\hat{\beta}_d$.

Theorem 4.1. Let c in $\tilde{\beta}_c$ be fixed and $c > 1$.

(a) If $[\text{bias}(\tilde{\beta}_c)]' (A_kA_k' - A_cA_c')^{-1}[\text{bias}(\tilde{\beta}_c) < \sigma^2$, then $\text{mse}(\hat{\beta}_k) > \text{mse}(\tilde{\beta}_c)$ for $0 < k < \min\{(b_1)_j\}$, and

(b) If $[\text{bias}(\tilde{\beta}_k)]' (A_cA_c' - A_kA_k')^{-1}[\text{bias}(\hat{\beta}_k) < \sigma^2$, then $\text{mse}(\tilde{\beta}_c) > \text{mse}(\hat{\beta}_k)$ for $0 < \max\{(b_1)_j\} < k$,

where $(b_1)_j = \dfrac{\lambda_j(c-1)^2}{\lambda_j^2 + 2c\lambda_j + 2c - 1}$, $j = 1, 2, \ldots, p$.

Proof.

(a) From Theorem 3.1, the conditions for $\text{mse}(\hat{\beta}_k) > \text{mse}(\tilde{\beta}_c)$ are:

(i) $A_kA_k' - A_cA_c'$ is a positive definite matrix, and

(ii) $\left[\text{bias}(\tilde{\beta}_c)\right]' (A_kA_k' - A_cA_c')^{-1}\left[\text{bias}(\tilde{\beta}_c)\right] < \sigma^2$.

Using $A_kA_k' = (\lambda + kI)^{-2}\lambda$ (Equation [4.2]), and $A_cA_c' = \left[I - (\lambda + d)^{-2}(c-1)^2\right]^2 \lambda^{-1}$ (Equation [4.10]), the matrix $A_kA_k' - A_cA_c'$ is a $p \times p$ diagonal matrix with diagonal elements $\dfrac{\lambda_j}{(\lambda_j + k)^2} - \dfrac{1}{\lambda_j}\left[1 - \dfrac{(c-1)^2}{(\lambda_j + c)^2}\right]^2$, $j = 1, 2, \ldots, p$. Hence, $A_kA_k' - A_cA_c'$ is a positive definite matrix if and only if

$$\frac{\lambda_j}{(\lambda_j + k)^2} - \frac{1}{\lambda_j}\left[1 - \frac{(c-1)^2}{(\lambda_j + c)^2}\right]^2 > 0$$

$$\frac{\lambda_j}{(\lambda_j + k)^2} - \frac{1}{\lambda_j}\left[\frac{(\lambda_j + c)^2 - (c-1)^2}{(\lambda_j + c)^2}\right]^2 > 0$$

$$\frac{\lambda_j}{(\lambda_j + k)^2} - \frac{(\lambda_j + 2c - 1)^2(\lambda_j + 1)^2}{\lambda_j(\lambda_j + c)^4} > 0$$

$$\frac{\lambda_j^2(\lambda_j + c)^4 - (\lambda_j + k)^2(\lambda_j + 2c - 1)^2(\lambda_j + 1)^2}{\lambda_j(\lambda_j + k)^2(\lambda_j + c)^4} > 0$$

$$\lambda_j^2(\lambda_j + c)^4 - (\lambda_j + k)^2(\lambda_j + 2c - 1)^2(\lambda_j + 1)^2 > 0$$

$$\lambda_j(\lambda_j + c)^2 - (\lambda_j + k)(\lambda_j + 2c - 1)(\lambda_j + 1) > 0$$

$$\lambda_j(c-1)^2 - k(\lambda_j^2 + 2c\lambda_j + 2c - 1) > 0$$

$$k < \frac{\lambda_j(c-1)^2}{\lambda_j^2 + 2c\lambda_j + 2c - 1}.$$

Let $(b_1)_j = \dfrac{\lambda_j(c-1)^2}{\lambda_j^2+2c\lambda_j+2c-1}$, $j = 1, 2, ..., p$. Note that $(b_1) > 0$ and $c > 1$. Hence, $A_kA_k' - A_cA_c'$ is a positive definite matrix if and only if $0 < k < \min\{(b_1)_j\}$. From Theorem 3.1, the proof for Theorem 4.1(a) is completed.

(b) From Theorem 3.1, the conditions for $\text{mse}(\tilde{\beta}_c) > \text{mse}(\hat{\beta}_k)$ are:
   (i) $A_cA_c' - A_kA_k'$ is a positive definite matrix, and
   (ii) $[\text{bias}(\hat{\beta}_k)]' (A_cA_c' - A_kA_k')^{-1}[\text{bias}(\hat{\beta}_k)] < \sigma^2$.

Hence, $A_cA_c' - A_kA_k'$ is a positive definite matrix if and only if

$$\frac{1}{\lambda_j}\left[1-\frac{(c-1)^2}{(\lambda_j+c)^2}\right]^2 - \frac{\lambda_j}{(\lambda_j+k)^2} > 0$$

$$k > \frac{\lambda_j(c-1)^2}{\lambda_j^2+2c\lambda_j+2c-1}.$$

Let $(b_1)_j = \dfrac{\lambda_j(c-1)^2}{\lambda_j^2+2c\lambda_j+2c-1}$, $j = 1, 2, ..., P$. Hence, $A_cA_c' - A_kA_k'$ is a positive definite matrix if and only if $0 < \max\{(b_1)_j\} < k$. From Theorem 3.1, the proof for Theorem 4.1(b) is completed. ❑

Theorem 4.2. Let c in $\tilde{\beta}_c$ be fixed and $1 < c < \min\left\{\dfrac{2\lambda_j+1+(\lambda_j+1)^{\frac{3}{2}}}{\lambda_j}\right\}$.

(a) If $[\text{bias}(\tilde{\beta}_c)]' (A_dA_d' - A_cA_c')^{-1}[\text{bias}(\tilde{\beta}_c)] < \sigma^2$, then $\text{mse}(\hat{\beta}_d) > \text{mse}(\tilde{\beta}_c)$ for $0 < \max \max\{(b_2)_j\} < d < 1$, and

(b) If $[\text{bias}(\hat{\beta}_d)]' (A_cA_c' - A_dA_d')^{-1}[\text{bias}(\hat{\beta}_d)] < \sigma^2$, then $\text{mse}(\tilde{\beta}_c) > \text{mse}(\hat{\beta}_d)$ for $0 < d < \min\{(b_2)_j\} < 1$,

where $(b_2)_j = \dfrac{\lambda_j^2+4\lambda_jc-\lambda_j+2c-1-\lambda_jc^2}{(\lambda_j+c)^2}$, $j = 1, 2, ..., p$.

Proof.

(a) From Theorem 3.1, the conditions for $\text{mse}(\hat{\beta}_d) > \text{mse}(\hat{\beta}_c)$ are:
   (i) $A_dA_d' - A_cA_c'$ is a positive definite matrix, and
   (ii) $[\text{bias}(\tilde{\beta}_c)]' (A_dA_d' - A_cA_c')^{-1}[\text{bias}(\tilde{\beta}_c)] < \sigma^2$.

Using $A_dA_d' = (\lambda + I)^{-2} (\lambda + dI)^2 \lambda^{-1}$ (Equation [4.6]), and $A_cA_c' = [I - (\lambda + d)^{-2} (c-1)^2]^2) \lambda^{-1}$ (Equation [4.10]), the matrix $A_dA_d' - A_cA_c'$ is a $p \times p$ diagonal matrix with diagonal elements $\dfrac{(\lambda_j+d)^2}{\lambda_j(\lambda_j+1)^2} - \dfrac{1}{\lambda_j}\left[1-\dfrac{(c-1)^2}{(\lambda_j+c)^2}\right]^2$, $j = 1, 2, ..., p$. Hence, $A_dA_d' - A_cA_c'$ is a positive definite matrix if and only if

$$\frac{(\lambda_j+d)^2}{\lambda_j(\lambda_j+1)^2}-\frac{1}{\lambda_j}\left[1-\frac{(c-1)^2}{(\lambda_j+c)^2}\right]^2>0$$

$$\frac{(\lambda_j+d)^2}{\lambda_j(\lambda_j+1)^2}-\frac{1}{\lambda_j}\left[\frac{(\lambda_j+c)^2-(c-1)^2}{(\lambda_j+c)^2}\right]^2>0$$

$$\frac{(\lambda_j+d)^2}{\lambda_j(\lambda_j+1)^2}-\frac{(\lambda_j+2c-1)^2(\lambda_j+1)^2}{\lambda_j(\lambda_j+c)^4}>0$$

$$\frac{(\lambda_j+d)^2(\lambda_j+c)^4-(\lambda_j+1)^4(\lambda_j+2c-1)^2}{\lambda_j(\lambda_j+1)^2(\lambda_j+c)^4}>0$$

$$(\lambda_j+d)^2(\lambda_j+c)^4-(\lambda_j+1)^4(\lambda_j+2c-1)^2>0$$

$$(\lambda_j+d)(\lambda_j+c)^2-(\lambda_j+1)^2(\lambda_j+2c-1)>0$$

$$d(\lambda_j+c)^2-(\lambda_j^2+4\lambda_j c-\lambda_j+2c-1-\lambda_j c^2)>0$$

$$d>\frac{\lambda_j^2+4\lambda_j c-\lambda_j+2c-1-\lambda_j c^2}{(\lambda_j+c)^2}.$$

Let $(b_2)_j=\dfrac{\lambda_j^2+4\lambda_j c-\lambda_j+2c-1-\lambda_j c^2}{(\lambda_j+c)^2}$, $j = 1, 2, \ldots, p$. Note that d is the biasing factor of $(\hat{\beta}_d)$, where $0 < d < 1$. Thus, $0<(b_2)_j=\dfrac{\lambda_j^2+4\lambda_j c-\lambda_j+2c-1-\lambda_j c^2}{(\lambda_j+c)^2}<1$. Solving the inequality $0<\dfrac{\lambda_j^2+4\lambda_j c-\lambda_j+2c-1-\lambda_j c^2}{(\lambda_j+c)^2}<1$ for c we get $1<c<\dfrac{2\lambda_j+1+(\lambda_j+1)^{\frac{3}{2}}}{\lambda_j}$. Hence, by letting c in $\tilde{\beta}_c$ be fixed and $1 < c <$ min, $1<c<\min\left\{\dfrac{2\lambda_j+1+(\lambda_j+1)^{\frac{3}{2}}}{\lambda_j}\right\}$, $A_dA_d' - A_cA_c'$ is a positive definite matrix if and only if $0 < \max\{(b_2)_j\} < d < 1$. From Theorem 3.1, the proof for Theorem 4.2(a) is completed.

(b) From Theorem 3.1, the conditions for $\text{mse}(\tilde{\beta}_c) > \text{mse}(\hat{\beta}_d)$ are:

(i) $A_cA_c' - A_dA_d'$ is a positive definite matrix, and

(ii) $[\text{bias}(\hat{\beta}_d)]'\,(A_cA_c' - A_dA_d')^{-1}\,[\text{bias}(\hat{\beta}_d)] < \sigma^2$.

Hence, $A_cA_c' - A_dA_d'$ is a positive definite matrix if and only if

$$\frac{1}{\lambda_j}\left[1-\frac{(c-1)^2}{(\lambda_j+c)^2}\right]^2-\frac{(\lambda_j+d)^2}{\lambda_j(\lambda_j+1)^2}>0$$

$$d<\frac{\lambda_j^2+4\lambda_j c-\lambda_j+2c-1-\lambda_j c^2}{(\lambda_j+c)^2}.$$

Let $(b_2)_j = \dfrac{\lambda_j^2 + 4\lambda_j c - \lambda_j + 2c - 1 - \lambda_j c^2}{(\lambda_j + c)^2}$, $j = 1, 2, ..., p$. By letting c in $\hat{\beta}_c$ be fixed and $1 < c < \min\left\{\dfrac{2\lambda_j + 1 + (\lambda_j + 1)^{\frac{1}{2}}}{\lambda_j}\right\}$, $A_c A_c' - A_d A_d'$ is a positive definite matrix if and only if $0 < d < \min\{(b_2)_j\} < 1$. From Theorem 3.1, the proof for Theorem 4.2(b) is completed. ❑

CONCLUSIONS

A new estimator was introduced from further modification of the Liu-type Estimator. The new estimator, $\tilde{\beta}_c$, was compared with the Ordinary Ridge Regression Estimator, $\hat{\beta}_k$, and the Liu Estimator, $\hat{\beta}_d$, in terms of the mean squared error. The comparison results are presented in Theorem 4.1 and Theorem 4.2. It was found that the accuracy of the new estimator is higher compared to these two estimators because there is a reduction in the mean squared error of the new estimator under certain conditions, which are

(i) $\text{mse}(\hat{\beta}_k) > \text{mse}(\tilde{\beta}_c)$ for $0 < k < \min\{(b_1)_j\}$ and $c > 1$ if $[\text{bias}(\tilde{\beta}_c)]' (A_k A_k' - A_c A_c')^{-1} [\text{bias}(\tilde{\beta}_c)] < \sigma^2$, where $(b_1)_j = \dfrac{\lambda_j (c-1)^2}{\lambda_j^2 + 2c\lambda_j + 2c - 1}$, $j = 1, 2, ..., p$,

(ii) $\text{mse}(\hat{\beta}_d) > \text{mse}(\tilde{\beta}_c)$ for $0 < \max\{(b_2)_j\} < d < 1$ and $1 \le c \min \left\{\dfrac{2\lambda_j + 1 + (\lambda_j + 1)^{\frac{1}{2}}}{\lambda_j}\right\}$ if $[\text{bias}(\tilde{\beta}_c)] (A_d A_d' - A_c A_c')^{-1} [\text{bias}(\tilde{\beta}_c)] < \sigma^2$, where $(b_2)_j = \dfrac{\lambda_j^2 + 4\lambda_j c - \lambda_j + 2c - 1 - \lambda_j c^2}{(\lambda_j + c)^2}$, $j = 1, 2, ..., p$.

Therefore, this new estimator can be considered as an alternative to estimate the unknown parameter in linear regression models. This new estimator could be recommended to those working on applications involving regression analysis in any field of study such as econometrics, oceanography and geophysics, In directly, the results of the regression analysis could be improved.

This study focused on the estimator for the linear regression model. Extending from this study, future research could be done on exploring the estimators for the non-linear regression model.

ACKNOWLEDGEMENTS

This research was supported by the Fundamental Research Grant Scheme.

REFERENCES

Akdeniz, F. and Erol, H. (2003). Mean squared error matrix comparisons of some biased estimators in linear regression. *Communications in Statistics-Theory and Methods, 32*(12), 2389 – 2413.

Baye, M.R. and Parker, D.F. (1984). Combining ridge and principal component regression: A money demand illustration. *Communications in Statistics-Theory and Methods, 13*(2), 197 – 205.

FAREBROTHER, R.W. (1976). Further results on the mean square error of ridge regression. *Journal of the Royal Statistical Society, B*(38), 248 – 250.

HOCKING, R.R., SPEED, F.M. and LYNN, M.J. (1976). A class of biased estimators in linear regression. *Technometrics, 18,* 425 – 437.

HOERL, A.E. and KENNARD, R.W. (1970). Ridge regression: biased estimation for non-orthogonal problems. *Technometrics, 12,* 55 – 67.

KACIRANLAR, S. and SAKALLIOGLU, S. (2001). Combining the Liu estimator and the principal component regression estimator. *Communications in Statistics-Theory and Methods, 30*(12), 2699 – 2705.

KACIRANLAR, S., SAKALLIOGLU, S. and AKDENIZ, F. (1998). Mean squared error comparisons of the modified ridge regression estimator and the restricted ridge regression estimator. *Communications in Statistics, 27*(1): 131–138.

KACIRANLAR, S., SAKALLIOGLU, S., AKDENIZ, F., STYAN, G.P.H. and WERNER, H.J. (1999). A new biased estimator in linear regression and a detailed analysis of the widely-analysed dataset on Portland cement. *Sankhya: The Indian Journal of Statistics, 61*(B3), 443–459.

LIU, K. (1993). A new class of biased estimate in linear regression. *Communications in Statistics-Theory and Methods, 22*(2), 393–402.

LIU, K. (2003). Using Liu-type estimator to combat collinearity. *Communications in Statistics-Theory and Methods, 32*(5), 1009–1020.

LIU, K. (2004). More on Liu-type estimator in linear regression. *Communications in Statistics-Theory and Methods, 33*(11), 2723–2733.

PLISKIN, J.L. (1987). A ridge-type estimator and good prior means. *Communications in Statistics-Theory and Methods, 16*(12), 3429–3437.

SAKALLIOGLU, S., KACIRANLAR, S. and AKDENIZ, F. (2001). Mean squared error comparisons of some biased regression estimators. *Communications in Statistics-Theory and Methods, 30*(2), 347–361.

SARKAR, N. (1996). Mean square error matrix comparison of some estimators in linear regressions with multicollinearity. *Statistics & Probability Letters, 30*(2), 133–138.

STEIN, C.M. (1960). Multiple regression. In I. Olkin (Ed.), *Contributions to Probability and Statistics. Essays in Honor of Harold Hotelling* (pp. 424–443). Stanford University Press.

THEOBALD, C. M. (1974). Generalizations of mean square error applied to ridge regression. *Journal of the Royal Statistical Society, B*(36), 103–106.

ISSN: 0128-7680
Pertanika J. Sci. & Technol. **16 (2)**: 119 - 127 (2008)

Development of a Single-Phase PWM AC Controller

S.M. Bashi*, N.F. Mailah and W.B. Cheng
Department of Electrical and Electronic Engineering, Faculty of Engineering, Universiti Putra Malaysia, 43400 UPM, Serdang, Selangor, Malaysia
**E-mail: senan@eng.upm.edu.my*

ABSTRACT

An AC chopper controller with symmetrical Pulse-Width Modulation (PWM) is proposed to achieve better performance for a single-phase induction motor compared to phase-angle control line-commutated voltage controllers and integral-cycle control of thyristors. Forced commutated device IGBT controlled by a microcontroller was used in the AC chopper which has the advantages of simplicity, ability to control large amounts of power and low waveform distortion. In this paper the simulation and hardware models of a simple single phase IGBT An AC controller has been developed which showed good results.

Keywords: PWM, AC controller, AC choppers

ABBREVIATIONS

PWM	Pulse-Width Modulation
AC	Alternating Current
RMS	Root Mean Square
IGBT	Insulated Gate Bipolar Transistor
DC	Direct Current

INTRODUCTION

The AC voltage regulator is used as one of the power electronic systems to control AC voltage output for power ranges from a few watts up to fractions of megawatts, as in starting systems and speed control for large induction motors. Traditionally, phase-angle control line-commutated voltage controllers and integral-cycle control of thyristors have been used in these types of regulators. These techniques suffer from inherent disadvantages, such as retardation of the firing angle that causes a lagging power factor at the input side, and distorted waveforms in load and supply voltages and currents (Ahmed *et. al.* 1999).

Many researchers have investigated and studied these types of AC controllers. Kwon *et. al.* (1999) have proposed a novel topology of pulse-width modulated AC chopper for single-phase, and three-phase systems are proposed for buck, boost and buck-boost types. The advantages of their proposed topologies for AC choppers include increased power factor, low harmonic input current, fast dynamics, high efficiency and high reliability. They have compared their results with the phase-controlled AC controller using thyristors. Bodur *et. al.* (2000) have carried out research on universal motor speed control with current controlled PWM AC chopper using a microcontroller. The proposed method proved that the universal motor speed control system has stable control in a wide range

Received :5 July 2007
Accepted:13 February 2008
* Corresponding Author

of speeds, and also found that the motor shows good response to sudden load changes, which is suitable for many industrial control system applications.

Ryoo *et al.* (2003) has studied the series compensated AC voltage regulator using AC chopper with auxiliary. The proposed AC regulator has many advantages such as fast voltage control, high efficiency and simple control logic. Experimental results proved that it can be used very efficiently as step-down AC voltage regulators for power saving purposes.

Hongxiang *et. al.* (2004) has improved the PWM AC chopper for harmonic elimination. The modulation function is derived from the input voltage signal. Compared with previous constant duty cycle controls, it has the advantage of eliminating 11 low order harmonic voltages contained in AC mains without the need for processing harmonic frequency.

In this work, an AC chopper controller with a symmetrical pulse-width modulation (PMW) was modified to achieve a simple controller for a single-phase induction motor. Only two forced commutated devices IGBTs have been used as switching elements to construct the controller, while in the literature, at least three of these switching devices were reportedly used in the controller (Ahmed, *et al,* 1999).

Simulation of the system was developed using Matlab and the hardware system constructed. The results showed good agreement in the waveforms and harmonics content

Concept of AC Voltage Controller

The concept used in this motor control is to implement the power switching device to chop the input source voltage. This method will cause the pulse-width of the AC voltage waveform to change. So, this method of AC voltage controller is called symmetrical pulse-width modulation (PWM) AC chopper. *Fig. 1* shows the circuit diagram of an AC controller. The current in the inductive load always has a continuous path to flow regardless of its direction. To explain the operation of this circuit, three operating modes are proposed, namely active mode, freewheeling mode and dead time mode. The advantages of the AC chopper are simplicity, ability to control large amounts of power, low waveform distortion, high power factor and high response (Ahmed, 1994).

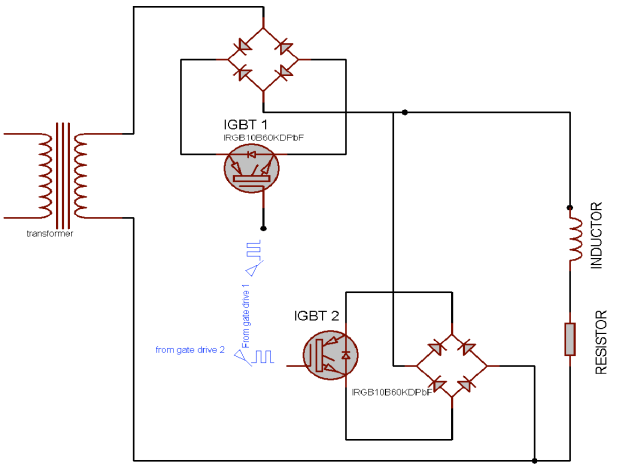

Fig. 1: Circuit diagram of symmetrical PWM AC chopper

A. Active Mode

The active mode occurs when switch 1 is closed and the current is flowing across the load as shown in *Fig. 2(a)*. During this stage switch 2 is opened. Power flows from the supply to the load.

B. Freewheeling Mode

As for the freewheeling mode, switch 1 is opened and the load is disconnected from the supply. Meanwhile switch 2 is closed. The load current freewheels and naturally decays through the freewheeling path according to the direction of the load current as shown in *Fig. 2(b)*. The current can flow until the energy in the inductor is fully depleted. The trapped energy in the inductor is dissipated in the resistances of the freewheeling path.

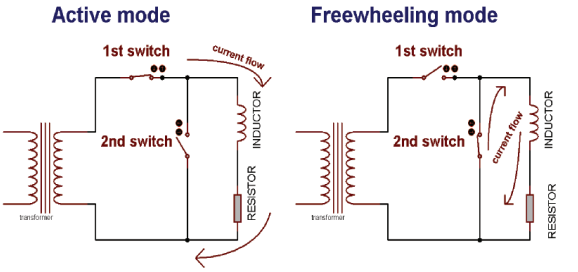

Fig. 2: AC controller operation modes

C. Dead Time Mode

In order to prevent short circuit of switches, a short dead time mode is inserted between the active mode and freewheeling mode. This is due to the characteristic of the switching device that owns rise time, t_r and fall time t_f. A typical time delay of 30 microseconds is introduced to make sure that the switching device 1 is completely opened before the switching device 2 is closed. The value of this delay depends on the specification of the switching devices.

High chopping frequency can be used, thereby reducing the output current harmonics. The root-mean-square (RMS) voltage is proportional to the duty cycle, *D*, which is defined by the ratio of the ON time, T_{on} to the total period, $T_s = T_{on} + T_{off} + 2T_{deadtime}$. Thus chopping frequency, $f = 1/ Ts$. Usually $T_{deadtime}$ is very small compared to T_{on} and T_{off}, then $Ts= T_{on}+T_{off}$.

Advantage of the AC Controller

AC chopper regulation has basic advantages over phase and integral cycle techniques which can be summarized as follows (Ahmed, 1994):

i. Does not require synchronization with the power source. Less switching device used. Only two switching devices are used compared to 4 in a H-bridge inverter.
ii. Faster response of voltage variation across the load. This occurs because a chopper can be turned ON or OFF at any instant in the AC cycle, whereas, in phase controlled circuits, once the power switches have been turned ON, it will go OFF only when the supply voltage polarity is reversed.

iii. The overall power factor in the chopper regulator is higher than other topologies.
iv. Although the output voltage is PWM modulated sinusoidal, the impact of the harmonics at high frequency is minimal. Output voltage can be smoothed by simple capacitive filter.

MATERIALS AND METHODS

Matlab software has been used to simulate the AC controller circuit, and a hardware model has been designed and constructed. The load and component ratings chosen for power circuit in this work were about 10A and 240V. The main components used are as follows:-

i. IGBT (insulated gate bipolar transistor)
The IGBT chosen is IRGB10B60KDPbF with V_{CES} = 600V and Ic = 12A. The rise time (29ns) and fall time (32ns) is also very fast, so it is excellent for fast switching operations.
ii. Rectifier
The bridge rectifier which consists of a power diode is implemented. The bridge rectifier provides the DC voltage to IGBT because current can only flow through IGBT in one direction.
iii. Microcontroller
The microcontroller chosen for this project was an 8-bit PIC16F873 microcontroller which has high speed technology, low power consumption, wide operating voltage range and fully static design.
iv. Gate Drive
To provide voltage isolation and floating points required to operate the IGBTs, single channel gate IR2117 drives have been used. There are a number of ways in which the gate to source, Vgs floating supply can be generated, one of these being the bootstrap method. The duty cycle and on-time are limited by the requirement to refresh the charge in the bootstrap capacitor (long on-times and high duty cycles require a charge pump circuit). This means that the output IR2117 has to be off for a short time enough to charge the bootstrap capacitor.
v. Freewheeling diode
A "freewheeling diode" is put into a circuit to protect the switching device from being damaged by the reverse current of an inductive load. Without the "freewheeling diode", the voltage can go high enough to damage the switching devices.

RESULTS AND DISCUSSION

To verify the performance of the proposed symmetrical PWM AC chopper, an experimental model was constructed, and a software simulation of the system developed using Matlab. *Fig. 3* shows the circuit used in Matlab simulation. The circuit consists of a transformer, diodes, IGBTs and pulse generator. Inductive load has been used to represent the induction motor at study state.

A microcontroller program has been written in C language which can provide required signals with variable duty cycles, as shown in *Fig. 4*. Both models have been tested with different types of load (resistive and inductive) and different values of duty cycle. In general close agreement has been found in the simulated and experimental results. Table 1 shows the simulation and practical measurements, and the variation of effective voltage V_{RMS} when the duty cycle changes.

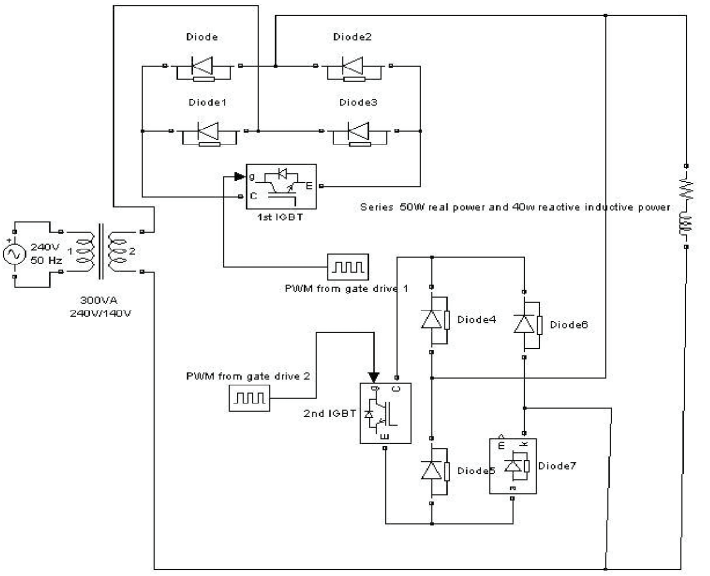

Fig. 3: Circuit arrangement for Matlab simulation for inductive load

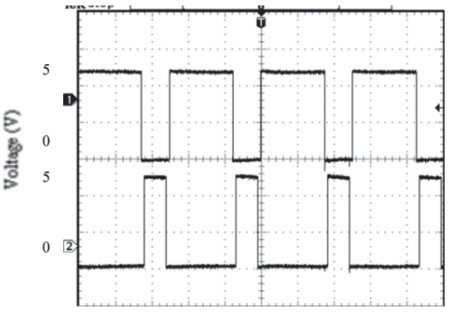

(a) 0.7 duty cycle

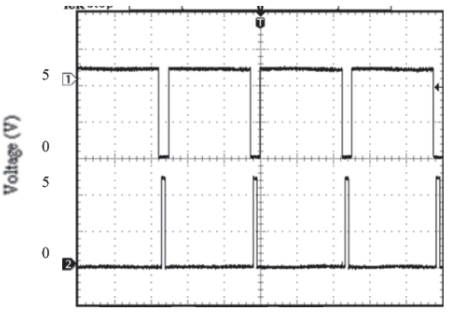

(a) 0.9 duty cycle

Fig. 4: Triggering signals with variable duty cycles

TABLE 1
Variation of V_{RMS} across the inductive load

Duty cycle	Simulation result (v)		Hardware result (v)	
	Vp	V_{RMS}	Vp	V_{RMS}
0.6	198	106.6	198	107
0.7	198	115	197	115
0.8	198	123	197	123
0.9	198	134.6	196	130
1.0	198	140	198	140

To show the effect of load types on the AC controller waveform and its effect on the harmonics content, simulation and experimental results of current and voltage waveforms of two types of load have been considered, which are resistive and inductive loads. The value of the duty cycle is 0.6 and the chopping frequency is 1 kHz, *Fig. 5* shows waveforms of the resistive load, it is clear that the current waveform has the same shape as voltage waveform, while *Fig. 6* shows the frequency spectrum for simulated and experimental current and voltage waveforms. The dominant harmonics are at the sum/difference of AC supply and the switching frequency.

Fig. 5: Comparison of simulation and experimental voltage and current waveforms for 0.6 duty cycle (Resistive load)

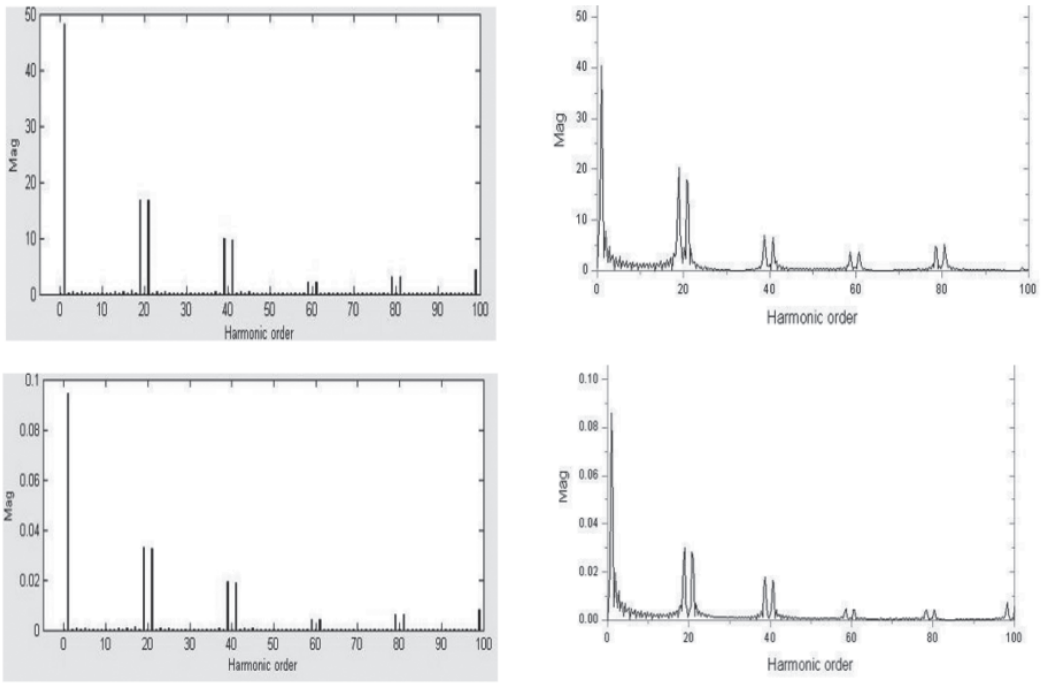

Simulation Experimental

Fig. 6: Comparison of simulation and experimental harmonic spectra for 0.6 duty cycle, voltage and current (Resistive load)

K= fc / fs , where fc is carrier frequency (1000Hz) and fs is the supply frequency (50 Hz).

The order of the high harmonic content can be found as:

Harmonic order = nK ±1, where, n=1,2,3,……

So, the high harmonic contents of the voltage and current can be found in order of 19, 21, 39, 40, 59 and 61. Also this can be proven by comparing with harmonic spectra as in *Fig. 7*. The Total Harmonic Distortion, THD of the simulated current waveform was found to be equal to 48% and the experimental was 51%, without any filter.

Similar measurements have been carried out for inductive loads represented by small motors. In *Fig. 8* and due to presence of inductance, the shape of the current and voltage waveforms are not the same. Further, there is a difference in the simulated and experimental current waveforms and this is due to the dynamic parameters of the motor. The harmonics analysis shows that the harmonic order are the same but the amplitude of the current harmonics are smaller due to presence of the inductance. It is clear that the THD of the current waveform has lower values compared with resistive loads which showed 17% for simulation and 21% for the experimental waveform.

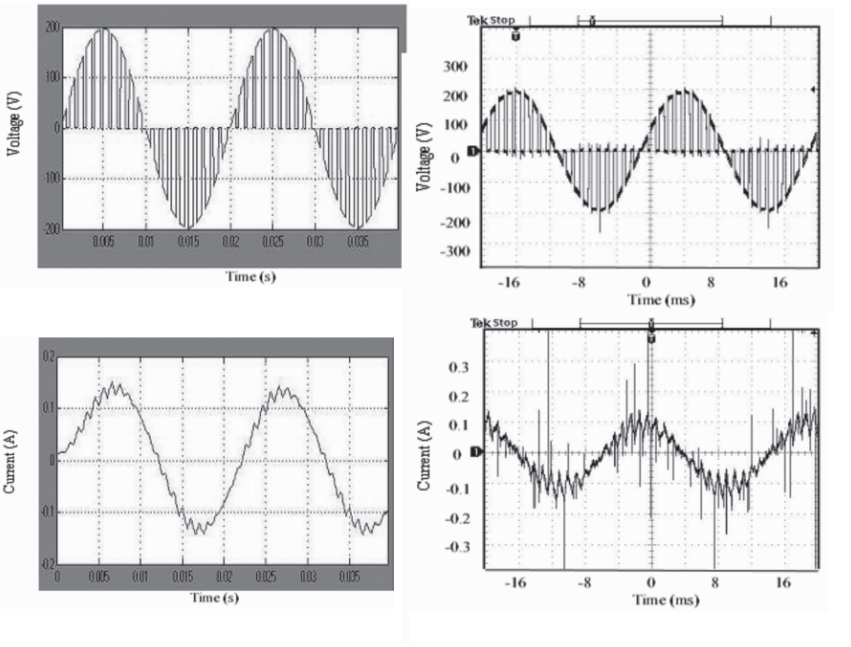

Fig. 7: Comparison of simulation and experimental voltage and current waveforms for 0.6 duty cycle (Induction motor)

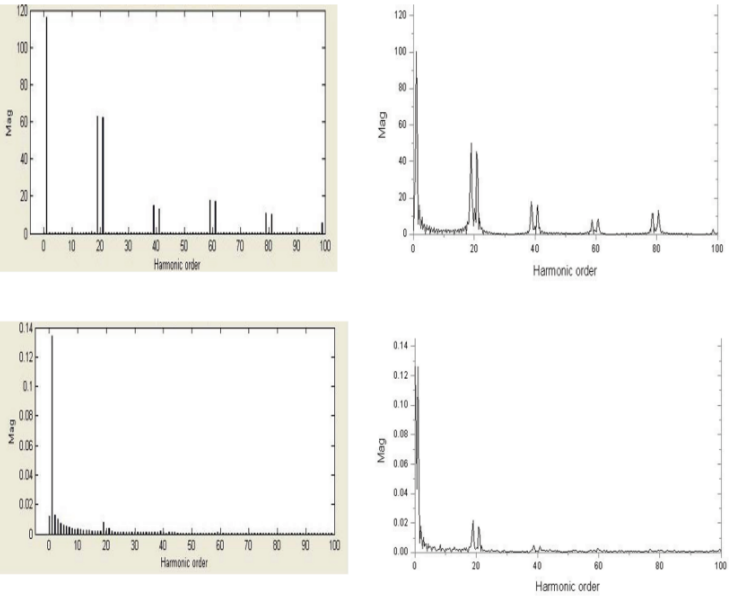

Fig. 8: Comparison of simulation and experimental harmonic spectra for 0.6 duty cycle, voltage and current (Induction motor)

CONCLUSIONS

A software simulation was developed for a simple AC controller and a hardware system constructed. Good agreement was achieved between the simulation and experimental results. The amount of voltage supply across the motor can be changed by varying the PWM signal of the symmetrical PWM AC chopper. This was done with the aid of a PIC16F873 microcontroller. In general, the performance of the symmetrical PWM AC chopper was good. The high order of harmonic content can be eliminated easily by a small LC passive filter. Therefore, this method can replace the convention phase-angle control line-commutated voltage controllers and integral-cycle control.

REFERENCES

AHMED F.I., ZAKI A.M. and ALI E. (1994). Terminal-impedance control for energy saving in induction motor at no and partial loads using microprocessor. *Power Electronics and Variable-Speed Drives, 5th International Conference* (pp. 336-341).

AHMED, N.A., AMEI, K. and SAKUI, M. (1999). A new configuration of single-phase symmetrical pwm ac chopper voltage controller. *IEEE Transactions on Industrial Electronics* (pp. 942 – 952).

BODUR, H., BAKAN, A. F. and SARUL, M. H. (2000). Universal motor speed control with current controlled pwm - ac chopper by using a microcontroller. *Proceedings of IEEE International Conference Industrial Technology* (pp. 394-398).

GUILLEMIN, P. (1996). Fuzzy logic applied to motor control. *IEEE Transactions Industry Applications* (pp. 51-56).

HONGXIANG Y., MIN L. and YANCHAO J. (2004). An advanced harmonic elimination PWM technique for AC choppers. *35th Annual IEEE Power Electronics Specialist Conference* (pp. 161-165).

KWON B.H., B. MIN D. and KIM J.H. (1999). Novel topologies of AC choppers. *IEE Proceedings Electrical Power Application* (pp. 323-330).

RYOO H. J., KIM J.S., RIM G.H. and KIM D.S. (2003). A study on the series compensated AC voltage regulator using AC chopper with auxiliary transformer. *Industrial Electronics Society, IECON '03, The 29th Annual Conference of the IEEE2003* (pp. 2628- 2633).

ISSN: 0128-7680
Pertanika J. Sci. & Technol. **16 (2)**: 129 - 139 (2008)

Agrobacterium-mediated Genetic Transformation of *Phalaenopsis bellina* Using GFP and GUS Reporter Genes

Mahmood Maziah* and Chew Yee Chern
Department of Biochemistry, Faculty of Biotechnology and Biomolecular Sciences, Universiti Putra Malaysia, 43400 UPM, Serdang, Selangor, Malaysia
**E-mail: maziahm@biotech.upm.edu.my*

ABSTRACT

Genetic transformation protocols of *Phalaenopsis bellina* protocorm-like bodies (PLBs) were established using *gfp* (green fluorescent protein) and *gus* (β-glucuronidase) genes as the reporter system. *Agrobacterium tumefaciens* strain, LBA 4404 containing the binary vector, pCAMBIA 1304, with the *hptII* gene as the selectable marker and *gfp* and gus-intron genes as the reporter genes. Horizontally dissected PLBs were immersed in *A. tumefaciens* suspensions with 200uM acetosyringone (AS) for 45 minutes. This was followed by co-cultivation until the growth of *A. tumefaciens* was observed surrounding the PLBs on the co-cultivation medium. GFP detection and GUS histochemical assay were carried out to investigate the transient expression of both GFP and GUS reporter genes. The selection of proliferating PLBs was carried out on 4 mg/L hygromycin and 100 mg/L cefotaxime. GFP could be used as the reporter system as it is an effective, rapid and non-destructive system to monitor the transformed tissues.

Keywords: ***Agrobacterium tumefaciens*, genetic transformation, *gfp*, *gus*, *Phalaenopsis bellina***

INTRODUCTION

Phalaenopsis bellina (*Fig. 1*) is a commercially important fragrant orchid species endemic to Borneo and Peninsular Malaysia. The attractive features of this orchid are that they flower freely all year round and produce strong sweet-flora fragrance. Genetic improvement of *P. bellina* through sexual hybridization is, however, restricted by a long growth period and limited genetic pool within the germplasm. Genetic engineering offers a promising approach in improving the orchid quality.

A protocol was developed to obtain transient expression of *P. bellina* via *Agrobacterium tumefaciens* (Strain LBA 4404 harboring vector pCAMBIA 1304). Prior to the genetic transformation study, hygromycin sensitivity of the PLBs was investigated to determine the minimal concentration required to sufficiently inhibit the growth of PLBs. Transient expression of *gfp* gene in PLBs was observed under the florescence microscope after co-cultivation period. The effect of inoculation time on transient GFP expression was also evaluated in this study. The putative transformants displayed distinguishingly strong fluorescence when observed under a GFP stereomicroscope using GFP2 filter.

Received : 2 August 2007
Accepted: 21 April 2008
* Corresponding Author

Fig. 1: The P. bellina *flower*

MATERIALS AND METHODS

Plant Materials

Induction and Establishment of PLBs

PLBs were induced using young leaf segments of approximately 1 x 1 cm 2 , excised from three-month old *in vitro* seedlings. The leaf segments were placed adaxial side up in orientation inside the culture tubes containing 1/2 strength MS medium (Murashige and Skoog) supplemented with 100 mg/L myo-inositol, 0.5 mg/L niacin, 0.5 mg/L pyridoxine-HCl, 0.1 mg/L thiamine-HCl, and 2.0 mg/L glycine (Tokura and Mii, 2003 and Cheng and Chang, 2004). Twenty g/L sucrose and 3 g/L gelrite was adjusted to pH 5.6 (Islam *et al.*, 2003) before autoclaving for 15 min at 121°C. Different auxins at different concentrations were investigated. The auxins used were 2,4-D, NAA, picloram and dicamba and the range of concentrations was 0.2, 0.4, 0.6, 0.8 and 1.0 µM. The number of explants forming PLBs was recorded after 12 weeks of culture. In addition, the size and quantity of the PLBs induced were also observed. The proliferated masses of PLBs were subcultured every four weeks for six months to obtain large quantities of PLBs for *Agrobacterium*-mediated transformation.

Determination of Minimal Inhibitory Concentration of Hygromycin

Single PLBs of 3 - 4 mm in size (measured from shoot tip to root tip) were aseptically excised using scalpel and subjected to different concentrations (1, 2, 3, 4, 5, 6, 7, 8, 9, 10, 15, 20, 25, 30, and 35 mg/L) of hygromycin treatments to determine their minimal hygromycin killing level. Hygromycin was added into the selection medium consisting 1/2 strength MS basal medium. The hygromycin-free 1/2 strength MS medium served as a control medium. Observations were conducted on a weekly basis and the percentages of surviving PLBs per replicate were recorded. Changes in the physical appearance of the cultured PLBs, from healthy greenish to black, whitish or brownish colour, were used as indicators for scoring the PLBs. Meanwhile unaffected PLBs should remain green and continue to proliferate. Each treatment consisted of three replications with 16 PLBs per replicate, culturing on 20 ml of solidified medium in a 50 mm diameter petri dish. This

experiment was repeated three times. Eventually, the specific concentration that was sufficient to completely inhibit growth of PLBs or kill the PLBs would be determined and later applied for screening of putative transformed PLBs in the genetic transformation study.

Preparation of *A. tumefaciens* Strain and Plasmid

A. tumefaciens strain LBA 4404 (pCAMBIA 1304) was used for the transformation study. The T-DNA region of the binary vector pCAMBIA 1304 contains the selectable marker *hptII* gene, encoding hygromycin phosphotransferase, the reporter *gfp*, and intron-*gus* genes. The β-glucuronidase gene was disrupted by an intron. This intron-gus reporter gene expresses GUS activity in plant cells but not in the cell of *A.tumefaciens*. Expression of *gfp*, *gus* and *hptII* genes are under the control of the cauliflower mosaic virus (CaMV) 35S promoter.

The Effect of Inoculation Time

The *A. tumefaciens* strain LBA 4404 was grown overnight at 28°C in liquid LB broth medium containing 100 mg/L kanamycin. The following day, 500 ul of the bacterial suspension was spread over the surface of LB agar solid medium, and incubated at 28°C for 2 days. *A. tumefaciens* cells were collected with a aseptic flame inoculums and suspended in 30 ml LB liquid medium containing 100 mg/L kanamycin and 200 uM AS to and OD600 at 0.7 - 1.0 and agitated (100 rpm) in a shaker, at 25°C for 30 min before inoculating. PLBs of *P. bellina* were cut into pieces, 3-4 mm in diameter. The PLBs were then immersed in the *A. tumefaciens* suspension for 15, 30, 45, 60, 75 and 90 min respectively, with 20 PLBs per treatment. These PLBs were blotted dry on sterile filter paper, and co-cultured on 1/2 MS medium containing 200 μM AS at 25°C in the dark for 3 days until *A. tumefaciens* growth was observed. This experiment was repeated 3 times.

GFP Monitoring

GFP-expressing cells were detected using a fluorescence microscope (Leica MZFL III) equipped with GFP2 filter (Excitation filter: 480/40 nm) to mask the red fluorescence of chlorophyll, thereby permitting the visualization of the green fluorescence GFP-expressing cells. The PLBs observed with green fluorescent sections (using magnification 25X) were considered GFP positive. An imaging system (Laica DC 200) was attached to the fluorescence microscope to capture the image in real time using the Leica DC Viewer software.

Selection of Putative Transformants

After 2-3 days of co-cultivation, the cultures were transferred to selective medium (1/2 MS medium containing 100 mg/L cefotaxime, 4 mg/L hygromycin) and incubated at 25°C under 16 photoperiod. Previous research indicated that 4 mg/L hygromycin was sufficient to inhibit the growth of non-transformed tissues of *P. bellina*. Tissues were subcultured in a new selective medium every month. Cefotaxime were omitted after two months of selection. After three months of being cultured on the hygromycin-containing medium, the surviving and growing cell clusters were picked out and cultured on 1/2 MS medium supplemented with 4 mg/L hygromycin but without phytohormones for plant regeneration.

GUS Histochemical Assay

GUS activity assays were performed on PLBs, hygromycin-resistent PLBs and then on leaves and roots of the regenerated transformants using the method of Jefferson et al., (1986). Tissues were immersed in X-gluc solution, (1 mM EDTA, 50 mM NaH_2PO_4 (pH 7.0), 10 mM -mercaptoethanol and 0.1% Triton X-100) and incubated overnight at 37°C. After staining, the materials were treated with 70% ethanol to remove chlorophyll before observation. Transient GUS expression of PLBs was examined after 2 days of co-cultivation.

RESULTS AND DISCUSSION

Protocorm-like Bodies (PLBs) Induction

There has been limited information on the utilization of leaf segments as explant source for PLBs induction. The appearance of nodular masses protruding from the wounded surfaces and epidermal layers of leaf explants could be observed as early as eight weeks after culture. The production of PLBs was greatest at week twelve. The highest frequency of PLB formation was 53% in media containing 0.8 μM 2,4-D (*Figs. 2* and *3*). This was followed by 0.6 μM 2,4-D (37%), 1.0 μM 2,4-D (23%), and 0.2 μM 2,4-D (10%). The frequency of PLBs production is low (5 - 12%) in treatments containing 0.6 μM NAA and 0.4 μM NAA, respectively (*Fig. 2*). Moreover, the NAA induced PLBs were small in size, low in quantity and did not proliferate readily (Table 1). No PLBs were formed in other treatments particularly in those containing picloram and dicamba, although the explants remain green for many months of culture (*Fig. 4*). The use of leaf segments to induce PLBs has recently been reported by Park *et al.* (2002) in different *Phalaenopsis* hybrids and Chen and Chang (2004) in *Oncidium* Gower Ramsey.

TABLE 1
Effect of different auxins (2,4-D and NAA) on quantity and size of induced *P. bellina* PLBs after 12 weeks of culture

PGR (auxin)	Concentration (μM)	[a]Quantity of induced PLBs Sizes (< 0.3 mm)	[a]Quantity of induced PLBs Sizes (> 0.3 mm)
2,4-D	0.0	0 a	0 a
	0.2	9.3 ± 1.5 a	4.3 ± 2.5 a
	0.4	12.3 ± 3.5 a,b	7.7 ± 3.8 a,b
	0.6	39.3 ± 11.0 c	21.0 ± 3.0 c
	0.8	82.3 ± 6.8 d	43.7 ± 4.0 d
	1.0	27.3 ± 6.7 c,d	13.7 ± 3.2 b,c
NAA	0.0	0 a	0 a
	0.2	0 a	0 a
	0.4	9.7 ± 4.7 b	0 a
	0.6	1.7 ± 1.5 a	1.0 ± 1.0 a
	0.8	0 a	0 a
	1.0	0 a	0 a

Different auxins (2,4-D and NAA) and auxin concentrations were supplemented to half strength MS basal medium as described in Section 3.3.2.

[a]The quantity of induced PLBs was calculated as the average quantity of three independent experiments and represent mean (± SD). Three replicates were used in each treatment.

The data were analysed by one-way ANOVA in a completely randomised design using auxin concentration as factor. Mean values were compared by Tukey's multiple range test at 5 % (p = 0.05) significance level

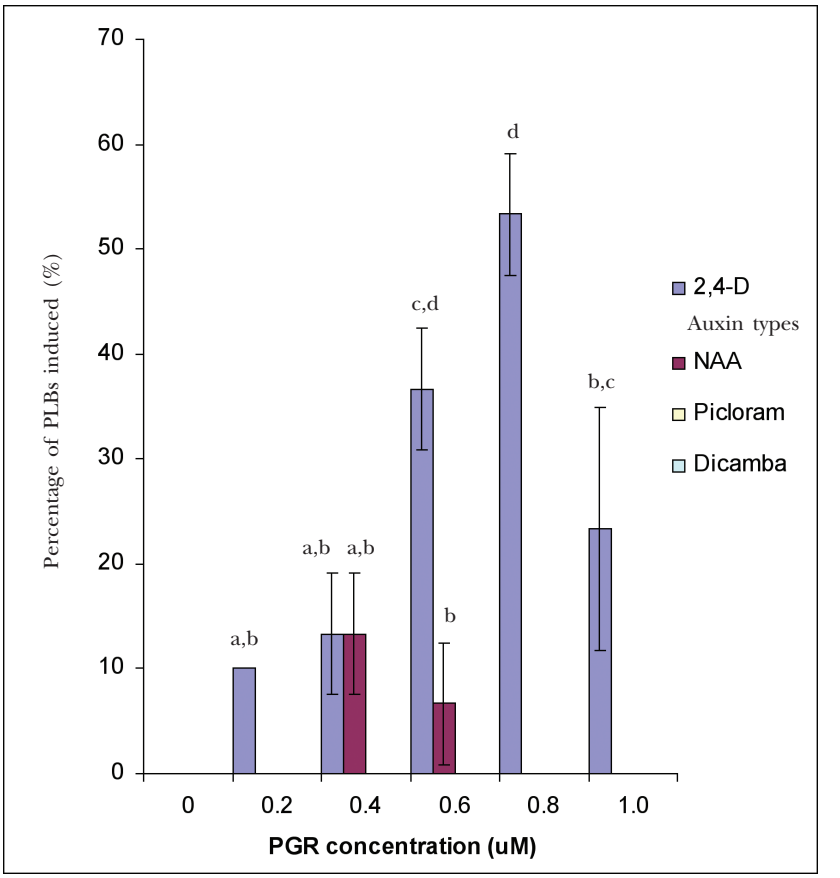

Fig. 2: Effect of different auxins concentrations on PLBs induction from leaf segments of P. bellina. *All results were scored after 12 weeks of culture. The results indicate the mean standard error (± SE) of 3 independent experiments with 10 replicates for each treatment concentration. The experiment was repeated thrice. The data were analysed by one-way ANOVA in a completely randomised design using auxin concentration as factor. Mean values were compared by Tukey's multiple range test at 5 % (p = 0.05) significance level*

Determination of Hygromycin Killing Curve

In this experiment, 16 two-month-old PLBs of *P. bellina* were placed on 1/2 strength MS basal medium containing various concentrations of hygromycin (0, 1, 2, 3, 4, 5, 6, 7, 8, 9, 10, 15, 20, 25, 30, and 35 mg/L) for five weeks, and the number of surviving PLBs was recorded weekly. Black, whitish or brownish colour was an indicator of dead PLBs. An early inhibitory effect of hygromycin at 10 mg/L on PLBs was initially observed during the first week of culture. Increased hygromycin concentration reduced the growth frequency from 100% at hygromycin 0 mg/L to 43% at hygromycin 1 mg/L, to 32% at hygromycin 2 mg/L, to 23% at hygromycin 3 mg/L and to 0% at hygromycin 4 - 35 mg/L (*Fig. 5*). All of the PLBs multiplied healthily and remained greenish on hygromycin-free medium, whereas, PLBs cultured on medium containing ≥ 4 mg/L hygromycin, for 5 weeks resulted in complete fatality, giving entirely black, brown or white necrotic PLBs

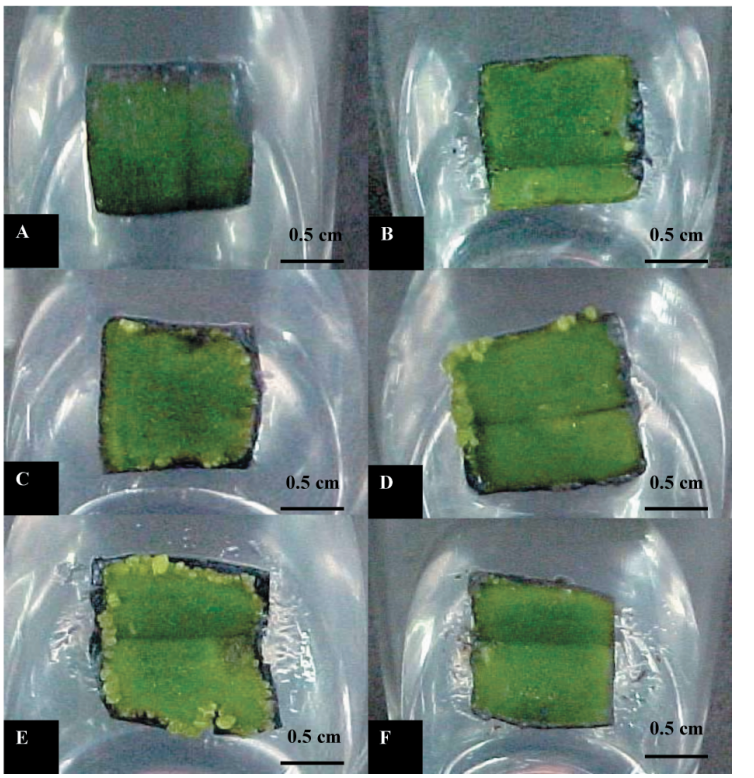

Fig. 3: Effect of different 2,4-D concentrations on P. bellina *PLBs induction after 12 weeks of culture. A Control treatment B-F PLBs induction on 1/2 strength MS basal medium supplemented with 0.2, 0.4, 0.6, 0.8, and 1.0 μM 2,4-D respectively*

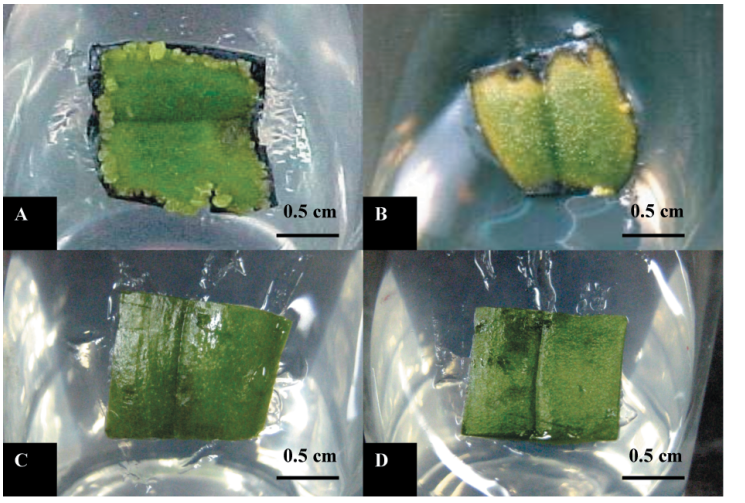

Fig. 4: Effect of different auxins on P. bellina *PLBs induction after 12 weeks of culture. A PLBs induction on medium containing 2,4-D (0.8 μM) B PLBs induction on medium containing NAA (0.4 μM) C-D Leaf treated with picloram and dicamba respectively*

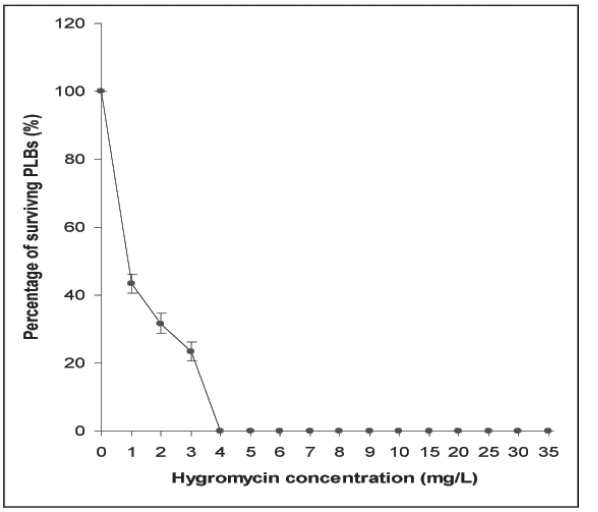

Fig. 5: The hygromycin killing curve for P. bellina *PLBs. Data were recorded based on percentage of surviving PLBs after 5 weeks of culture in selection medium containing different concentrations of hygromycin (0 - 35 mg/L). Black, whitish or brownish colour was the indictor of the dead PLBs. Each point represents the mean ± standard error (SE) for n = 3 replicates with 16 PLBs on each replicate. The experiment was repeated 3 times*

appearances (*Fig. 6*). It was clearly evident that *P. bellina* PLBs were very sensitive to hygromycin as most of the PLBs were killed at very low (4 mg/L) hygromycin concentration after five weeks. This experiment, therefore, revealed that 4 mg/L hygromycin was the lowest concentration required for *P. bellina* to discriminate between transformed and non-transformed PLBs. The hygromycin killing level observed from the present study was very similar to the findings reported by Chai *et al.* (2002), who also examined the hygromycin killing curves in four different *Phalaenopsis* lines, and found low hygromycin concentrations (1.5-3 mg/L) were suitable for putative transformed PLBs selection.

Effect of Inoculation Time

An inoculation period of 45 min to 90 min resulted in the highest percentage of transient expression compared to other inoculation periods (Table 2) as detected by the GFP reporter system (*Fig. 7 a - d*). The degree of transient expression is different with different hybrids (Tee *et al.*, 2004; Tee and Maziah, 2005). After eight weeks on selection medium, with hygromycin and cefotaxime antibiotics, green colour, hygromycin- resistant PLBs were observed. These hygromycin-resistant PLBs were then selected and subcultured in the cefotaxime-free medium. Putative transformed PLBs clumps were obtained after 2 months of culture.

Transient Expression Detection

Putative transformed PLBs can also be detected in GUS histochemical assay by showing GUS positive sections (sections that stained in blue colour) (*Fig. 7 e* and *f*). However,

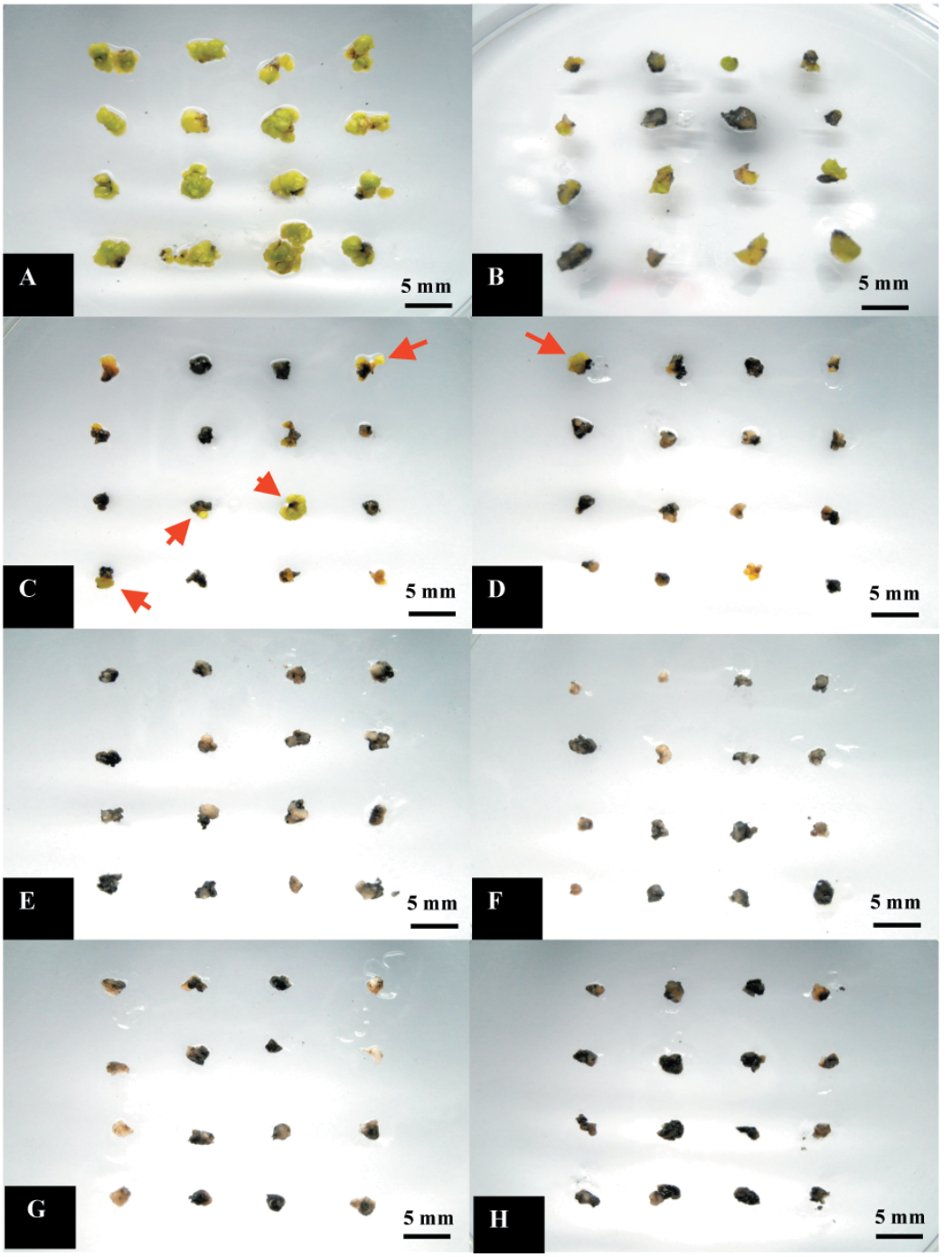
A
5 mm
B
5 mm
C
5 mm
D
5 mm
E
5 mm
F
5 mm
G
5 mm
H
5 mm

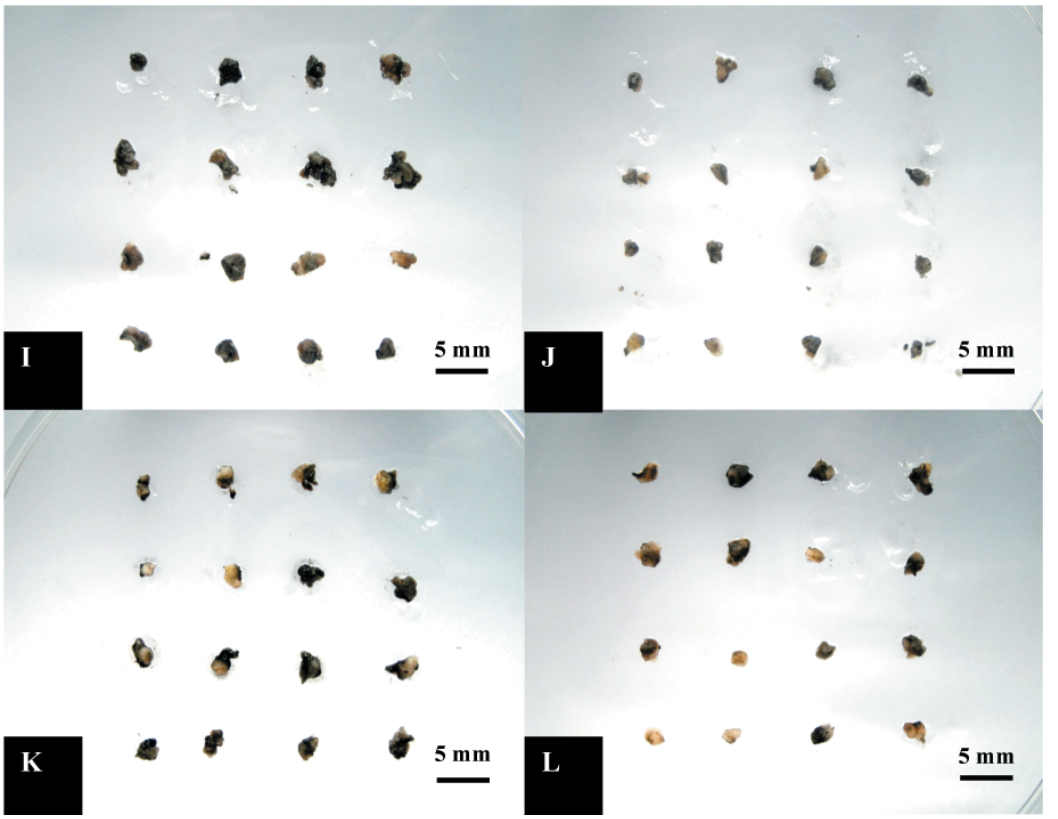

Fig. 6: Physical effects exhibited by PLBs after five weeks of culture on selection medium containing various concentrations of hygromycin. Black, whitish yellowish or brownish colour was the indictor of the dead PLBs. A All PLBs remained greenish and proliferating on hygromycin-free medium B 50% of the PLBs remained greenish and survived on media containing 1 mg/L hygromycin C-D Most of the PLBs were dead on media containing 2 mg/L and 3 mg/L hygromycin respectively E- L All PLBs were dead on medium containing 4, 5, 6, 7, 8, 9, 10 and 15 mg/L hygromycin respectively. Red arrows show the surviving PLBs cultured on hygromycin selection medium

TABLE 2
Effect of inoculation period on the percentage of GFP transient expression of *P. bellina*

Length of inoculation time (min)	Number of PLBs inoculated	Percentage of GFP transient expression (%)
15	40	2.8
30	40	2.8
45	40	5.6
60	40	5.6
75	40	5.6
90	40	5.6

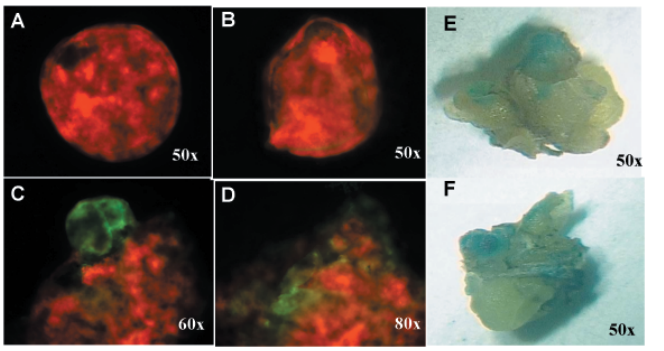

Fig. 7: GFP and GUS transient expression on P. bellina *PLBs. A Negative control B Positive control C-D GFP transient expression in PLBs E-F GUS transient expression in PLBs*

GUS assay for transient detection was not favorable throughout this study due to the irreversible destructive character to transient tissues or somehow, stable transformants (Schopke *et al.,* 1997).

CONCLUSIONS

In accessing the genetic transformation in this study, *GFP* was successfully used in *Agrobacterium*-mediated transformation of *P. bellina* PLBs. GFP has certainly proved its superior characteristics of being non-destructive, direct and rapid detection, non-cofactor or substrate required.

REFERENCES

Chai, M.L., Xu, C.J., Senthil, K.K., Kim, J.Y. and Kim, D.H. (2002). Stable transformation of protocorm-like bodies in *Phalaenopsis* orchid mediated by *Agrobacterium tumefaciens. Scientia Horticulturae, 96*, 213-224.

Chen, J.T. and Chang, W.C. (2004). Induction of repetitive embryogenesis from seed-derived protocorms of *Phalaenopsis amabilis* var. *formosa* Shimadzu. *In Vitro Cellular and Developmental Biology, 40,* 290-293.

Islam, M.O., Rahman, A.R.M.M., Matsui, S. and Prodhan, A.K.M.A. (2003). Effects of complex organic extracts on callus growth and PLB regeneration through embryogenesis in the *Doritaenopsis orchid. Japan Agricultural Research Quarterly, 37*(4), 229-235.

Jefferson, R.A., Burgess, S.M. and Hirsh, D. (1986). β-glucuronidase from Escherichia coli as a gene-fusion marker. *Proceedings of the National Academy of Sciences of the United States of America, 83,* 8447-8451.

Park, S.Y., Murthy, H.N. and Peak, K.Y. (2002). Rapid propagation of Phalaenopsis from floral stalk-derived leaves. *In Vitro Cellular and Developmental Biology, 38*, 168-172.

Schopke, C., Taylor, N.J., Carcamo, R., Beachy, R.N. and Fauquet, C. (1997). Optimization of parameters for particle bombardment of embryogenic suspension cultures of cassava (Manihot esculenta Crantz) using computer image analysis. *Plant Cell Reports, 16,* 526-530.

Tee, C.S., Maziah, M., Tan, C.S. and Abdullah, M.P. (2003). Evaluation of different promoters deriving the GFP reporter gene and selected target tissues for particle bombardment of *Dendrobium Sonia 17. Plant Cell Reports, 21,* 452-458.

Tee, C.S. and Maziah, M. (2005). Optimization of biolistic bombardment parameters for *Dendrobium* Sonia 17 callus using GFP and GUS as the reporter system. *Plant Cell, Tissue and Organ Culture, 80,* 77-89.

Tokuhara, K. and Mii, M. (2003). Highly-efficient somatic embryogenesis from cell suspension cultures of *Phalaenopsis* orchids by adjusting carbohydrate sources. *In Vitro Cellular and Developmental Biology, 39*, 635-639.

Pertanika J. Sci. & Technol. 16 (2): 141 - 156 (2008)
ISSN: 0128-7680

Phase Behavioural Study of Palm-Based Lauryl Alcohol Ethoxylates

Lim Hong Ngee[1*], Anuar Kassim[1], Huang Nay Ming[2], Dzulkefly Kuang Abdullah[1], Abdul Halim Abdullah[1], Mohd. Ambar Yarmo[3] and Yeong Shoot Kian[4]

[1]Chemistry Department, Faculty of Science, Universiti Putra Malaysia, 43400 UPM, Serdang, Selangor, Malaysia

[2]School of Applied Physics, Faculty of Science and Technology, Universiti Kebangsaan Malaysia, 43000 Bandar Baru Bangi, Selangor, Malaysia

[3]School of Chemical Sciences and Food Technology, Faculty of Science and Technology, Universiti Kebangsaan Malaysia, 43000 Bandar Baru Bangi, Selangor, Malaysia

[4]AOTD MPOB, Lot 9 & 11, Jalan P10/14, Seksyen 10, 43650 Bandar Baru Bangi, Selangor, Malaysia

**E-mail: janet_limhn@yahoo.com*

ABSTRACT

Palm-based lauryl alcohol ethoxylates were synthesized with different chain lengths of ethylene oxide using an ethoxylation reactor. The effect of changing the ethylene oxide chain length was investigated by reacting 3, 6 and 100 moles of ethylene oxide with palm-based lauryl alcohol. The samples were labeled as $C_{12}E_3$, $C_{12}E_6$ and $C_{12}E_{100}$. The 6 moles of ethylene oxide was approximately the same length as the palm-based lauryl alcohol. The chromatograms of $C_{12}E_x$ showed less retention peaks than the standard, Brij 40 (Tetraethylene glycol dodecyl ether - $C_{12}E_4$). Fourier Transformed Infrared Spectroscopy (FTIR) displayed a strong C-O stretch at 1120 cm^{-1} which was attributed to C-O single-bond stretching of the ether group. The ternary phase diagrams for a series of olive or olein oil/water/$C_{12}E_x$ systems were investigated at 25°C. The important features of the ternary phase systems are the emulsion and the concentrated emulsion phases. Optical microscopy revealed the difference in morphology between emulsion and concentrated emulsion. The particle size of the emulsions and the concentrated emulsions were in the range of 2.635 μm to 9.175 μm and 0.694 μm to 4.764 μm, respectively. The rheological flow curves measurement of the concentrated emulsion showed crossover of the ascendant and descendant curves which indicated structural build up of the sample instead of destruction.

Keywords: Palm-based lauryl alcohol ethoxylates, ethoxylation reactor, ternary phase diagram, emulsion, concentrated emulsion

ABBREVIATIONS

$C_{12}E_x$	Palm-based lauryl alcohol ethoxylates with x as the average number of moles of ethylene oxide
$C_{12}E_3$	Palm-based lauryl alcohol with an average number of 3 moles of ethylene oxide
$C_{12}E_6$	Palm-based lauryl alcohol with an average number of 6 moles of ethylene oxide

Received : 8 August 2007
Accepted : 30 May 2008
* Corresponding Author

$C_{12}E_{100}$ Palm-based lauryl alcohol with an average number of 100 moles of ethylene oxide

$C_{12}E_4$ Brij 30 (Tetraethylene glycol dodecyl ether)

INTRODUCTION

Emulsions form the basis of a wide variety of natural and manufactured materials, including foods, pharmaceuticals, biological fluids, agrochemicals, petrochemicals, cosmetics and explosives (Schramm, 1992; Semenzato *et al.* 1994, Hyuk *et al.* 2006). Emulsions are dispersions of at least two immiscible liquids stabilized by emulsifiers, which are often surfactants (Sjoblom, 1996). The droplets of one liquid are dispersed through a second, which is the continuous phase. Surfactants, which possess polar and non-polar regions, are absorbed into the phase interfaces thus, decreasing the interfacial free energy.

In recent years, concentrated emulsions are gaining interest among researchers (Kizling and Kronberg, 2001, Becu *et al.*, 2004). The internal phase volume fraction of the concentrated emulsion is in the range of 0.8 to 0.99. These concentrated emulsions are termed biliquid foams due to their foam-like structure where the internal phase consists of polyhedral compartments. Other terminologies include high internal phase ratio emulsions (HIP) (Williams, 1991) and gel-emulsions (Ravey *et al.*, 1994), which can be either water-in-oil (W/O) or oil-in-water (O/W) type emulsions. One advantage of the highly concentrated emulsions reported by Kizling *et al.*, (2006) is their long-term stability despite very low surfactant concentrations. The characteristic resemblance of emulsions to stiff gels is attributed to its internal structure being similar to that of foams with large air/liquid ratio.

The presence of surface active agent helps reduce the tension (interfacial free energy) at the interface, thus rendering some degree of stability to the resulting emulsion system. Since the hydrophile lipophile balance (HLB) of the polyoxyethylene surfactants used in this study are higher than 10, it is highly likely that O/W type emulsions are generated, and not W/O type. The HLB value is the balance of the size and strength of the hydrophilic and lipophilic moieties of a surfactant molecule (Niraula *et al.* 2004).

Functional oils play an essential role as marketing tools to attract consumers. Olive oil is rich in monounsaturates and has resistance to oxidative change because of the presence of nutrient and non-nutrient antioxidants (Paraskevopoulou, 2005). Olein oil has 44.2% palmitic acid (16:0), 39% oleic (18:1) and 10% linoleic (18:2) acids (Solomons and Orozco, 2003). Olein oil contains tocopherol and tocotrienol content which defines Vitamin E activity (Sundram *et al.*, 2003).

The aim of this study is to examine the phase behaviour of emulsions prepared using olive or olein oil/water/$C_{12}E_x$ systems. The emulsions were characterized using an optical microscope, a particle size analyzer and a rheometer.

MATERIALS AND METHODS

Materials

Distilled water was used throughout this study for the preparation of emulsion systems. Lauryl alcohol with a purity of 99% was obtained from Cognis (M) Oleochemicals Sdn Bhd. Ethylene oxide 100% was obtained from Fluka. Potassium hydroxide 85% and citric acid were obtained from Sigma-Aldrich. Olive oil with a purity of 100% was obtained from Bronson & Jacobs. Olein oil with a purity of 99% was obtained from Moi Foods Malaysia Sdn. Bhd. Brij 40 (Tetraethylene glycol dodecyl ether - $C_{12}EO_4$) was obtained from Fluka. All chemicals were of analytical grade and were used as received.

METHODS

Synthesis of Palm–Based Lauryl Alcohol Ethoxylates ($C_{12}E_x$)

Lauryl alcohol was ethoxylated with 3, 6 and 100 moles of ethylene oxide respectively using potassium hydroxide (1 w/w %) as catalyst for the reactions. Da Vinci reactor was used for the ethoxylation process. Each reaction was left to complete for three hours at 140°C, under atmospheric pressure and stirred at 100 rpm. The pH of the synthesized liquid samples was adjusted to pH 5.0-7.0 using citric acid. The resulting liquid samples were then centrifuged at 10 000 rpm for 20 minutes to remove salt that was formed during neutralization. While for sample in solid form, no pH adjustment was required as it would be more economical to use the as-synthesized solid sample as is. Finally, both the liquid and solid samples were vacuumed at 40°C for two days to remove water. The as-synthesized samples were labeled as $C_{12}E_x$ with x as the average number of moles of ethylene oxide.

Gas Chromatography (GC)

The $C_{12}E_x$ samples were diluted with chloroform (1:500) and analysed using a Hewlett Packard gas chromatograph (GC) installed with 30 m length fused silica capillary column (HP 5) having 0.32 mm i.d. and 0.25 µm thickness. The samples were detected by flame ionization detector (FID) working at $T_{injector}$ and $T_{detector}$ = 280°C. Column temperature program was set from 50°C for 3 minutes, and then heated up to 250°C at the rate of 10°C/minute. Helium gas was used as the mobile phase at the flow rate of 1 ml/minute.

Fourier Transformed Infrared Spectroscopy (FTIR)

A Perkin Elmer Model GX type FTIR was used to investigate the structural carbonyl groups of $C_{12}E_x$. The FTIR spectrum was recorded in wavenumbers range of 500 - 4000 cm^{-1} with a resolution of 1 cm^{-1}. Sample preparation was based on KBr disk technique.

Phase Behaviour Determination

Ternary phase diagram of each of the three $C_{12}E_x$ surfactants was studied. The three components of the phase diagrams were lauryl alcohol ethoxylate as the surfactant, water as the aqueous phase and olive or olein oil as the oil phase. Six diagrams were considered namely $C_{12}E_3$/water/olive oil, $C_{12}E_6$/water/olive oil, $C_{12}E_{100}$/water/olive oil, $C_{12}E_3$/water/olein oil, $C_{12}E_6$/water/olein oil and $C_{12}E_{100}$/water/olein oil. The regions in the phase diagram were determined by titrating the oil phase into water/surfactant (w/w) in 15 mm x 100 mm test tubes. The ratios of water/surfactant were in the range of 0.11 to 9.0. $C_{12}E_{100}$ is a solid type surfactant which has to be melted by heating prior to mixing. Results of the phase diagrams were plotted. An AND analytical balance was used to determine the weight of the materials. A Thermolyne vortex was used to homogenize the samples.

Macroscopy Analysis

Organoleptic characteristics and homogeneity of emulsions were observed to identify visible instability such as creaming, flocculation or coalescence. Centrifugation was carried out for visibly stable emulsions using Hettich Retafix 32 to affirm their stability. Each emulsion sample was submitted to a cycle of 2 min at 4000 rpm at room temperature. At the end of the cycle, a macroscopic evaluation was made to observe any possible phase separation.

Particle Size Analysis

Droplet size distributions of the emulsions were measured using a Mastersizer 2000S. This system measures droplet size with the help of the light scattering technique. Owing to their opaque nature, the light scattering technique required the parent emulsion samples to be diluted. The samples were diluted at the ratio of 1:1000 with distilled water in the equipment chamber and sonicated before analysis.

Microscopy Analysis

Droplet images (size and morphology) of the emulsions were analysed by an optical microscope at room temperature (25°C). A small drop of emulsion was placed onto the microscope slide and carefully covered. After equilibration for 1 min, photomicrographs (x100 magnification) were taken using the optical microscope (Nikon, Japan) equipped with a digital camera (XLi, USA). The size of the emulsion droplets was measured using an I-Solution Image Analyzer (IMT Inc., Canada).

Rheological Study

A Rheometer (PAAR Physica MCR 300), operated by a Rheoplus software, was used to evaluate steady–shear analysis of emulsion and concentrated emulsion. The analysis was carried out using a cone and plate geometry. The plate gap was set to 0.125 mm. Steady-state analysis was used for characterization of the emulsion and concentrated emulsion behaviour under shear. Measurements were carried out on emulsion samples to determine the role of shear in the eventual destruction of the emulsion. The controlled shear rate (CSR) procedure was selected for flow curve evaluation. Values of maximal and minimal apparent viscosity were used for characterization of the samples for flow analysis. The speed was varied to produce the two curves (ascendant and descendant). Flow index data and viscosity were obtained at different times during the test. All samples were tested at 25 ± 0.2°C.

RESULTS AND DISCUSSION

Gas Chromatography (GC)

Fig. 1 shows the chromatograms of lauryl alcohol, Brij 30 ($C_{12}E_4$), $C_{12}E_3$, $C_{12}E_6$ and $C_{12}E_{100}$. Chromatograms having less retention peaks imply higher purity samples. The chromatogram of lauryl alcohol displayed only one retention peak at 15 min (*Fig. 1* (a)). Brij 30 ($C_{12}E_4$) was used as a standard for the as-synthesized palm-based lauryl alcohol ethoxylates. The chromatogram of Brij 30 ($C_{12}EO_4$) consisted of eleven significant retention peaks which implied that the number of moles of ethylene oxide for the standard was taken as an average (*Fig. 1* (b)). The chromatogram also had a retention peak at 15 min which shows that the lauryl alcohol of the standard had not undergone a full conversion during the reaction. The chromatograms of $C_{12}E_3$ (*Fig. 1* (c)), $C_{12}E_6$ (*Fig. 1* (d)) and $C_{12}E_{100}$ (*Fig. 1* (e)) displayed less retention peaks than Brij 30 ($C_{12}E_4$) which shows that the as-synthesized samples had higher purity than the standard. Moreover, the lauryl alcohol of $C_{12}E_3$, $C_{12}E_6$ and $C_{12}E_{100}$ had been fully converted during reaction as there was no retention peak at 15 min.

Fourier Transformed Infrared Spectroscopy (FTIR)

In *Fig.* 2, the spectrum of lauryl alcohol was differentiated from the rest of the ethoxylated standard and as-synthesized samples by the medium stretch at 1050cm^{-1}

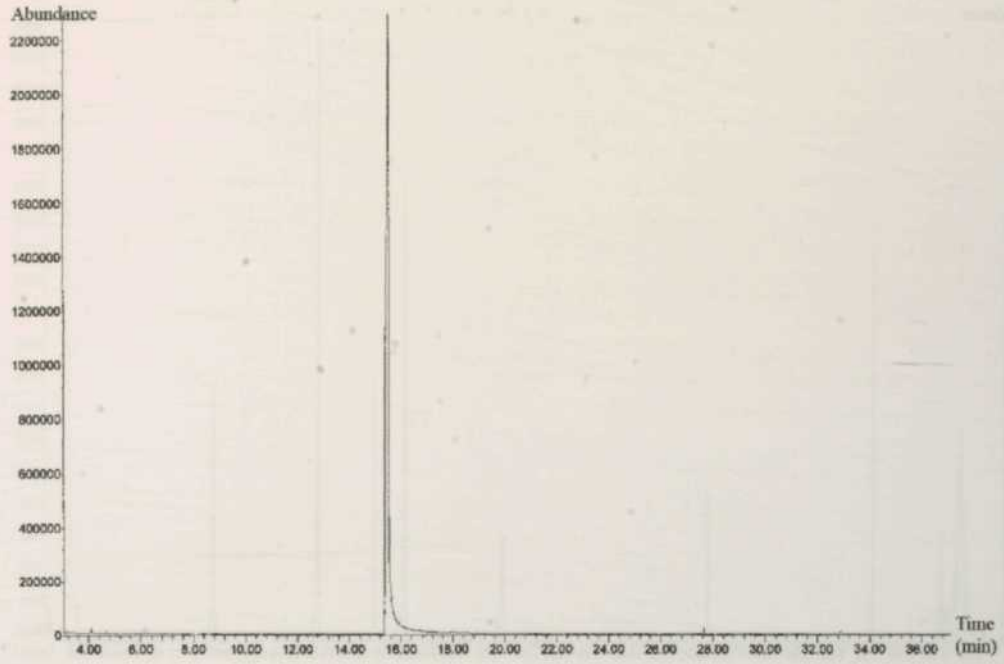
Abundance
2200000
2000000
1800000
1600000
1400000
1200000
1000000
800000
600000
400000
200000
0
4.00 6.00 8.00 10.00 12.00 14.00 16.00 18.00 20.00 22.00 24.00 26.00 28.00 30.00 32.00 34.00 36.00
Time (min)

Fig. 1 (a)

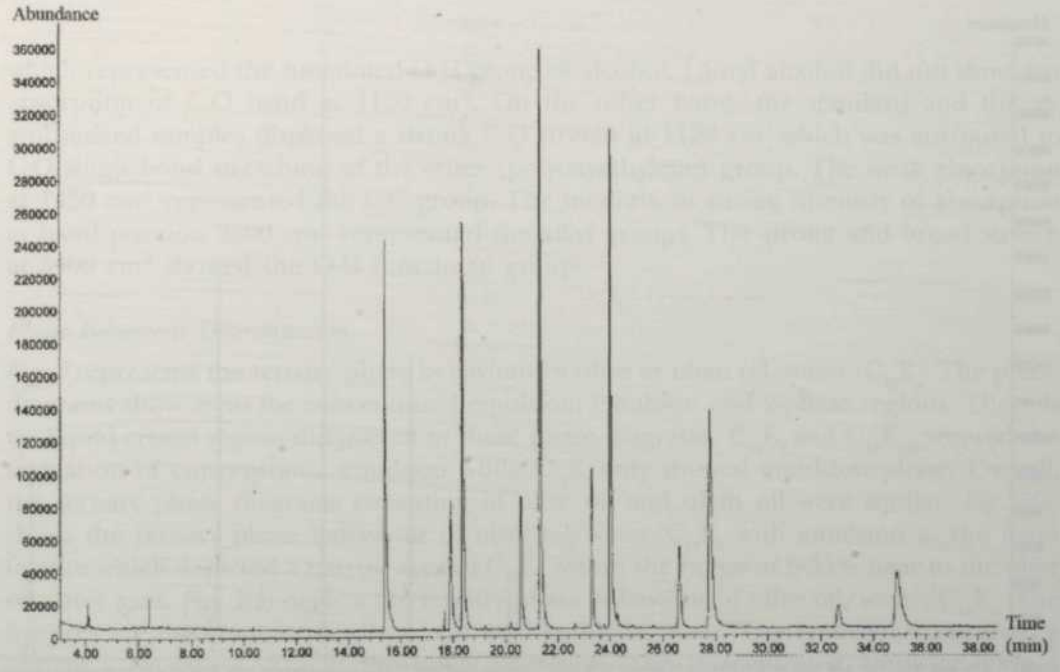
Abundance
360000
340000
320000
300000
280000
260000
240000
220000
200000
180000
160000
140000
120000
100000
80000
60000
40000
20000
0
4.00 6.00 8.00 10.00 12.00 14.00 16.00 18.00 20.00 22.00 24.00 26.00 28.00 30.00 32.00 34.00 36.00 38.00
Time (min)

Fig. 1 (b)

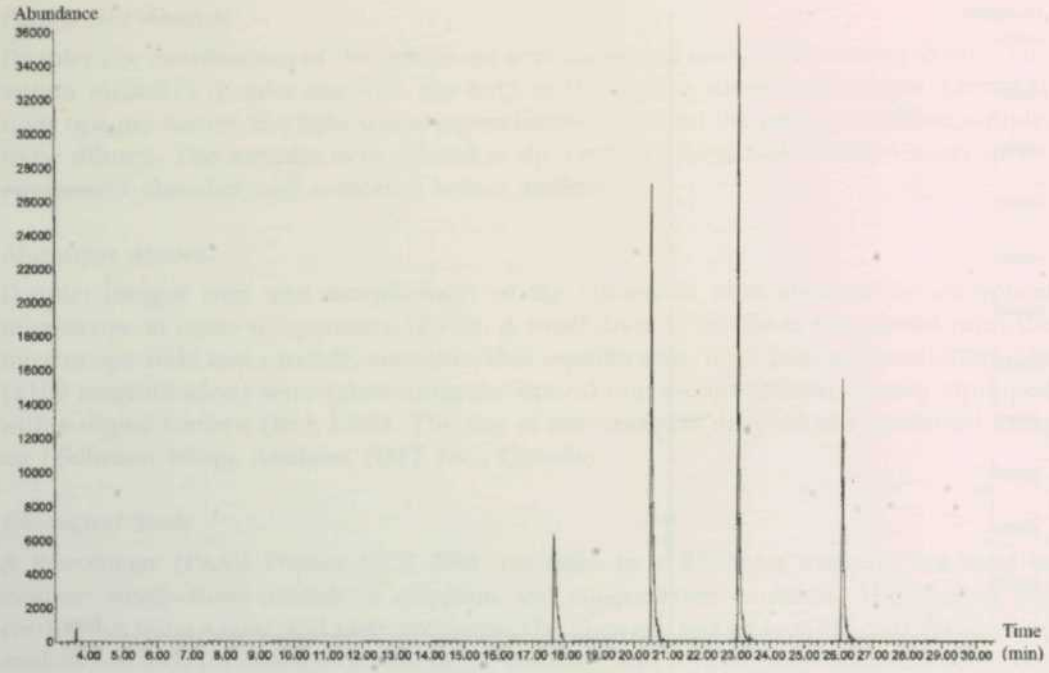
Abundance
36000
34000
32000
30000
28000
26000
24000
22000
20000
18000
16000
14000
12000
10000
8000
6000
4000
2000
0
4.00 5.00 6.00 7.00 8.00 9.00 10.00 11.00 12.00 13.00 14.00 15.00 16.00 17.00 18.00 19.00 20.00 21.00 22.00 23.00 24.00 25.00 26.00 27.00 28.00 29.00 30.00
Time
(min)

Fig. 1 (c)

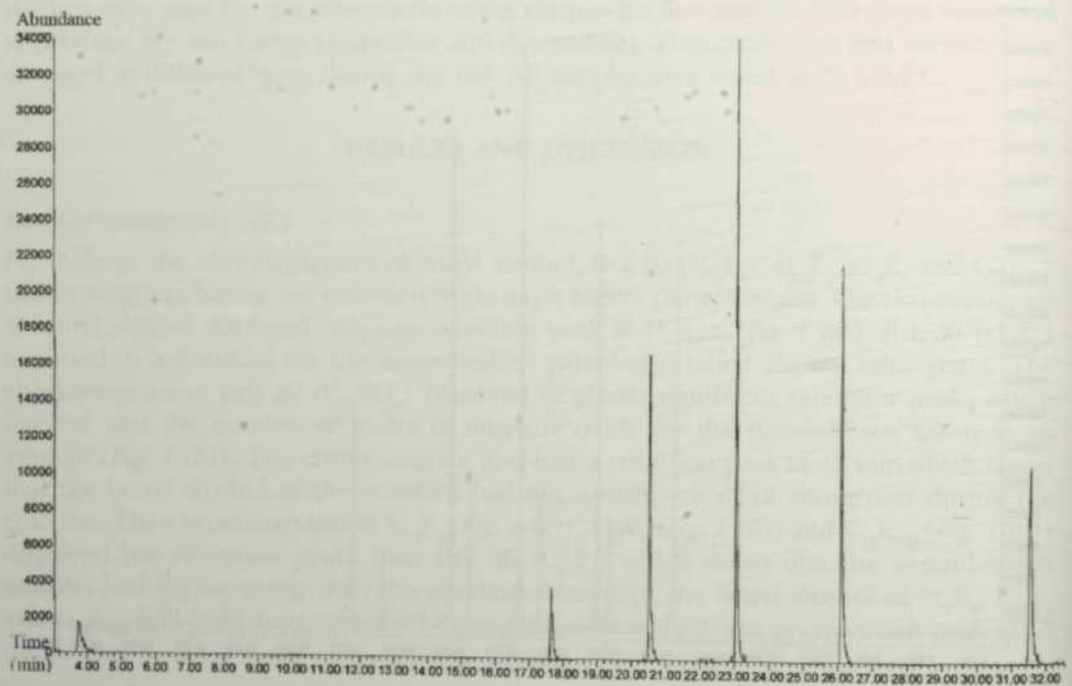
Abundance
34000
32000
30000
28000
26000
24000
22000
20000
18000
16000
14000
12000
10000
8000
6000
4000
2000
Time
(min)
4.00 5.00 6.00 7.00 8.00 9.00 10.00 11.00 12.00 13.00 14.00 15.00 16.00 17.00 18.00 19.00 20.00 21.00 22.00 23.00 24.00 25.00 26.00 27.00 28.00 29.00 30.00 31.00 32.00

Fig. 1 (d)

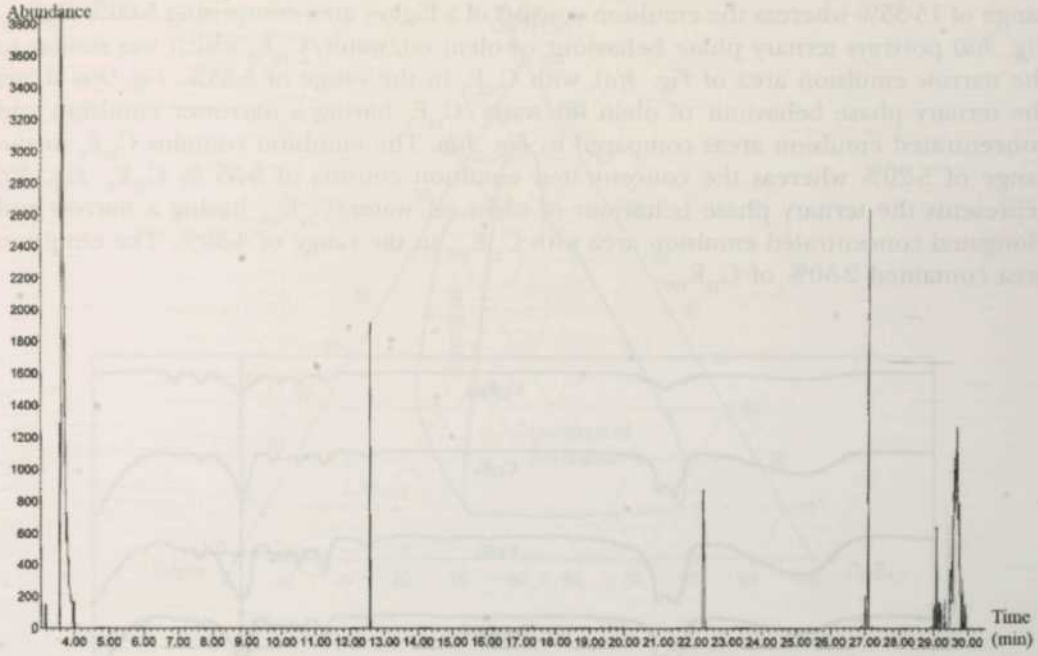

Fig. 1: Chromatograms of (a) lauryl alcohol, (b) standard, Brij 30 ($C_{12}E_4$), (c) $C_{12}EO_3$, (d) $C_{12}EO_6$ and (e) $C_{12}EO_{100}$

which represented the functional O-H group of alcohol. Lauryl alcohol did not show any absorption of C-O band at 1120 cm^{-1}. On the other hand, the standard and the as-synthesized samples displayed a strong C-O stretch at 1120 cm^{-1} which was attributed to C-O single-bond stretching of the ether (polyoxyethylene) group. The weak absorption at 1450 cm^{-1} represented the C-C group. The medium to strong intensity of absorption at band position 2800 cm^{-1} represented the alkyl groups. The strong and broad stretch at 3400 cm^{-1} showed the O-H functional group.

Phase Behaviour Determination

Fig. 3 represents the ternary phase behaviour of olive or olein oil/water/$C_{12}E_x$. The phase diagrams show areas for concentrated emulsion, emulsion and 2-phase regions. There is no liquid crystal region discovered in these phase diagrams. $C_{12}E_6$ and $C_{12}E_{100}$ showed the formation of concentrated emulsion while $C_{12}E_3$ only showed emulsion phase. Overall, the ternary phase diagrams consisting of olive oil and olein oil were similar. *Fig. 3(a)* shows the ternary phase behaviour of olive oil/water/$C_{12}E_3$ with emulsion as the main feature which depicted a narrow area of $C_{12}E_3$ within the range of 5-35% near to the olive oil-water axes. *Fig. 3(b)* depicts the ternary phase behaviour of olive oil/water/$C_{12}E_6$. The features are the emulsion and concentrated emulsion areas. The emulsion comprised a narrow area with $C_{12}EO_6$ in the range of 3-35%. The concentrated emulsion gave a smooth and stiff texture with $C_{12}E_6$ in the range of 8-70%. *Fig. 3(c)* represents the ternary phase behaviour of olive oil/water/$C_{12}E_{100}$ featuring the emulsion and concentrated emulsion areas. The concentrated emulsion covers only a small area with $C_{12}E_{100}$ in the

range of 15-35% whereas the emulsion consists of a bigger area comprising 5-60% $C_{12}E_{100}$. *Fig. 3(d)* portrays ternary phase behaviour of olein oil/water/$C_{12}E_3$ which was similar to the narrow emulsion area of *Fig. 3(a)*, with $C_{12}E_3$ in the range of 5-35%. *Fig. 3(e)* shows the ternary phase behaviour of olein oil/water/$C_{12}E_6$ having a narrower emulsion and concentrated emulsion areas compared to *Fig. 3(b)*. The emulsion contains $C_{12}E_6$ in the range of 5-20% whereas the concentrated emulsion consists of 5-35 % $C_{12}E_6$. *Fig. 3(f)* represents the ternary phase behaviour of olein oil/water/$C_{12}E_{100}$ having a narrow and elongated concentrated emulsion area with $C_{12}E_{100}$ in the range of 4-30%. The emulsion area contained 2-50% of $C_{12}E_{100}$.

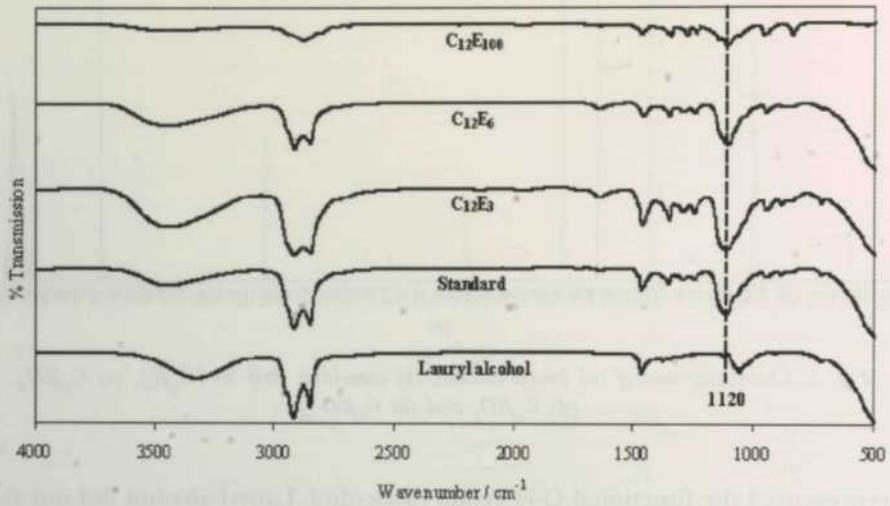

Fig. 2: FTIR spectrum of palm-based lauryl alcohol, Brij 40 ($C_{12}EO_4$) as a standard and as-synthesized samples of $C_{12}EO_3$, $C_{12}EO_6$ and $C_{12}EO_{100}$

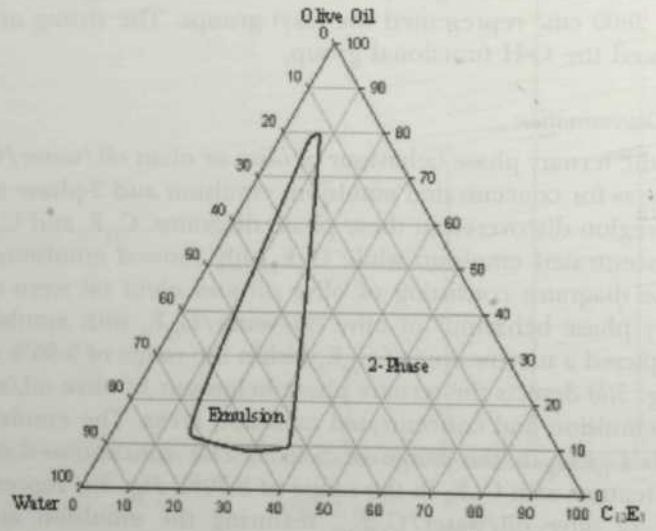

Fig. 3 (a)

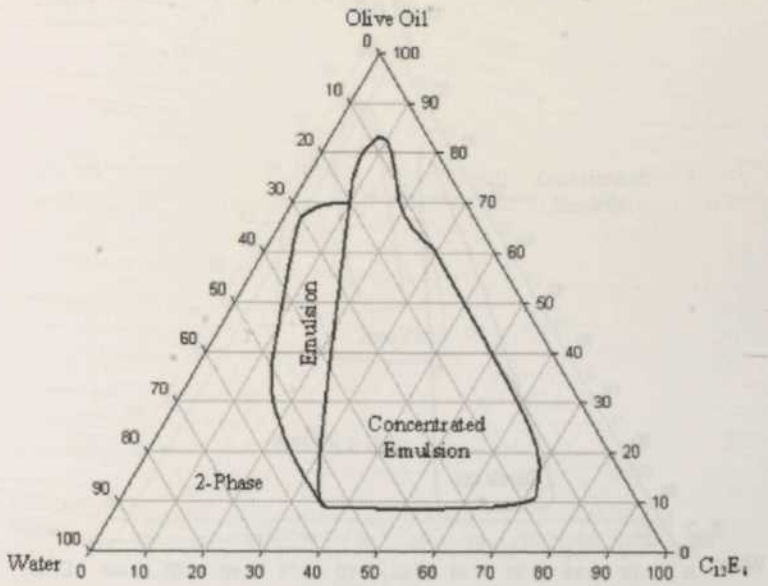
Olive Oil
Emulsion
Concentrated Emulsion
2-Phase
Water
$C_{12}E_4$

Fig. 3 (b)

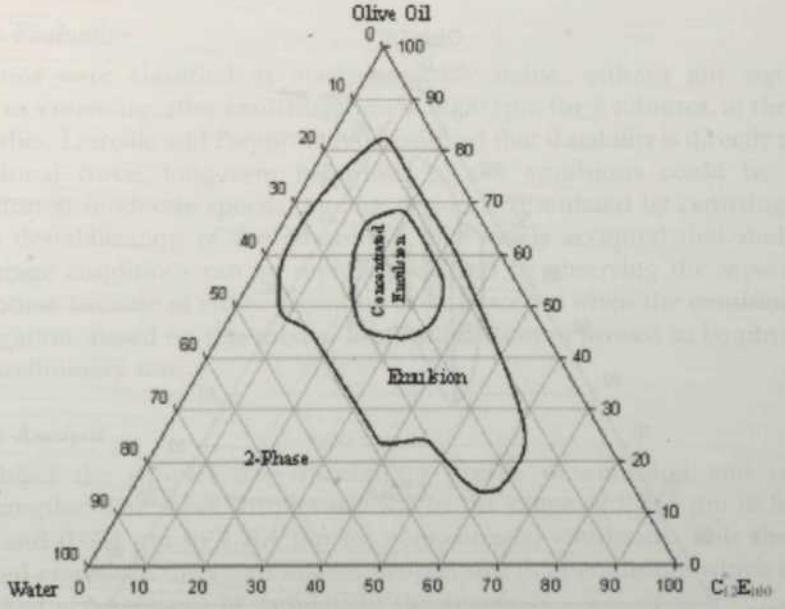
Olive Oil
Concentrated Emulsion
Emulsion
2-Phase
Water
$C_{12}E_{10}$

Fig. 3 (c)

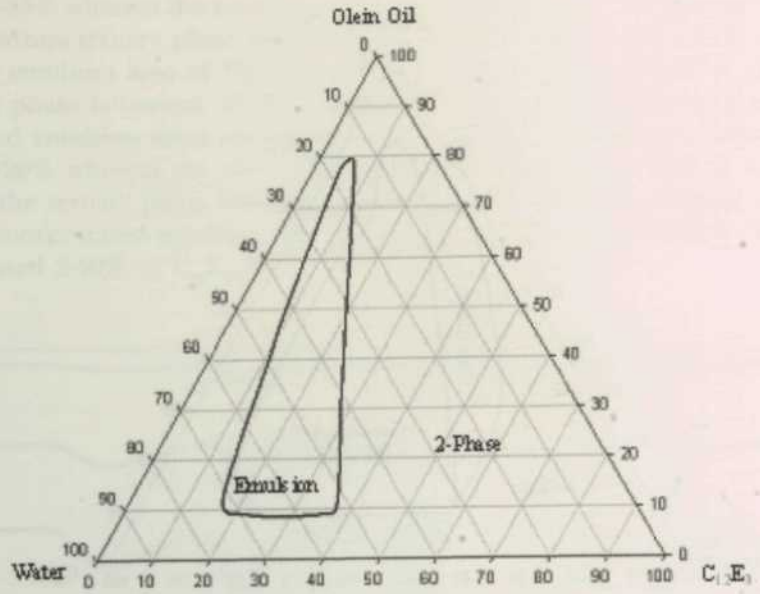
Olein Oil
Water
$C_{12}E_4$
Emulsion
2-Phase

Fig. 3 (d)

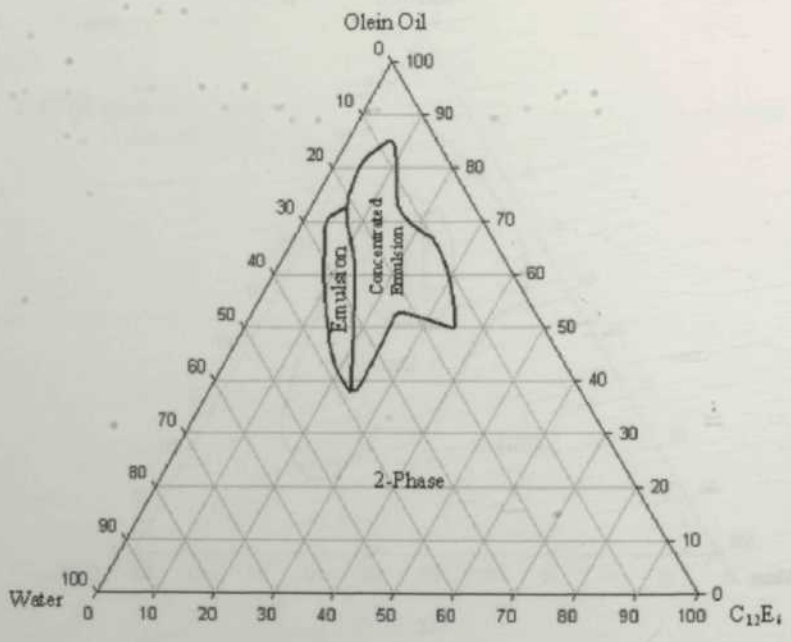
Olein Oil
Water
$C_{12}E_4$
Emulsion
Concentrated Emulsion
2-Phase

Fig. 3 (e)

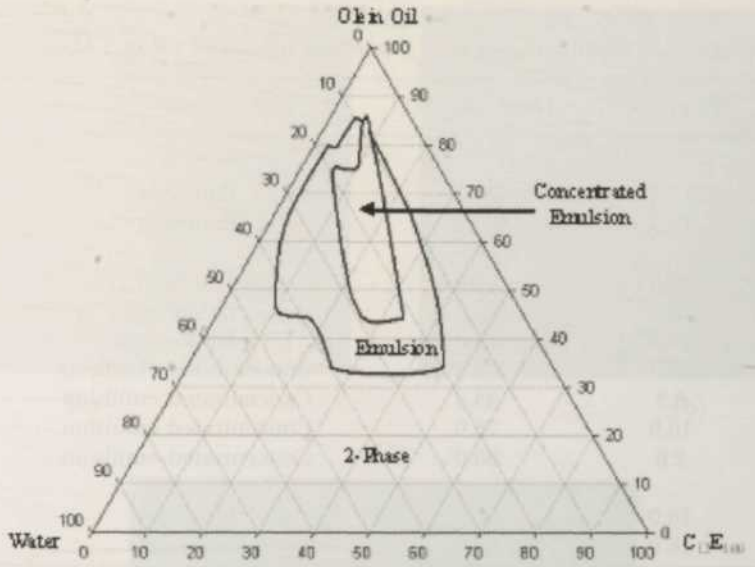

Fig. 3 (f)

Fig. 3: Ternary phase diagrams of (a) $C_{12}EO_3$/water/olive oil, (b) $C_{12}EO_6$/water/olive oil, (c) $C_{12}EO_{100}$/ water/olive oil, (d) $C_{12}E_3$/water/olein oil, (e) $C_{12}E_6$/water/olein oil and (f) $C_{12}E_{100}$/water/olein oil

Macroscopic Evaluation

All emulsions were classified as macroscopically stable, without any signs of phase separation or creaming, after centrifugation at 4000 rpm for 2 minutes, at the start of the stability studies. Latreille and Paquin (1990) assumed that if stability is directly proportional to gravitational force, long-term behaviour of the emulsions could be assessed by centrifugation at moderate speeds. Ageing period is stimulated by centrifugation which accelerates destabilization of the emulsions. It is widely accepted that shelf life under normal storage conditions can be rapidly predicted by observing the separation of the dispersed phase because of either creaming or coalescence when the emulsion is exposed to centrifugation. Based on this theory, the emulsions were proven to be physically stable after the preliminary test.

Particle Size Analysis

Table 1 shows the droplet size distribution profile of emulsion and concentrated emulsion samples. The mean droplet size was in the range of 2.635 μm to 9.175 μm for emulsions and 0.694 μm to 4.764 μm for concentrated emulsions. This shows that the concentrated emulsions displayed smaller droplet size than emulsions which is due to the closely packed arrangement of droplets in the system.

Microscopic Evaluation

Fig. 4(a) depicts the emulsion of the $C_{12}E_6$/water/olein oil (2.5%/22.5%/75.0%) system observed under an optical microscope. The average size of the emulsion oil droplets by counting at least 1000 droplets using image analysis software was 6.45 ± 1.39 μm, which

TABLE 1
Average droplet size distribution of $C_{12}E_x$/water/oil measured using a Mastersizer 2000S

$C_{12}E_x$ (%)	Water (%)	Olive Oil (%)	Type	Size (μm)
$C_{12}E_3$				
4.3	17.0	78.7	Emulsion	3.06
6.0	14.0	80.0	Emulsion	2.64
$C_{12}E_6$				
2.5	22.5	75.0	Emulsion	5.77
5.0	20.0	75.0	Emulsion	5.36
7.5	17.5	75.0	Emulsion	3.08
8.9	13.3	77.8	Concentrated emulsion	2.15
8.3	8.3	83.4	Concentrated emulsion	1.12
15.0	10.0	75.0	Concentrated emulsion	1.47
18.0	2.0	80.0	Concentrated emulsion	0.69
$C_{12}E_{100}$				
2.0	18.0	80.0	Emulsion	9.18
4.0	16.0	80.0	Emulsion	7.28
$C_{12}E_x$ (%)	Water (%)	Olein Oil (%)	Type	Size (μm)
$C_{12}E_3$				
5.0	20.0	75.0	Emulsion	3.33
6.0	14.0	80.0	Emulsion	2.76
$C_{12}E_6$				
2.5	22.5	75.0	Emulsion	5.99
5.0	20.0	75.0	Concentrated emulsion	4.76
4.8	11.3	83.9	Concentrated emulsion	2.69
5.7	8.6	85.7	Concentrated emulsion	1.34
$C_{12}E_{100}$				
2.0	18.0	80.0	Emulsion	7.82
4.0	16.0	80.0	Emulsion	6.58
4.3	10.0	85.7	Emulsion	5.27
5.7	8.6	85.7	Concentrated emulsion	3.65

was similar to the particle size measured by the light scattering method. *Fig. 4(b)* shows the droplets arrangement of concentrated emulsion of the $C_{12}EO_6$/water/olive oil (8.3%/8.3%/83.4%) system. The droplets were found to be closely arranged with the oil droplets dispersed in the continuous water phase. Oil droplets are confirmed as the dispersed phase through a simple microslide capillary test by diffusing water into the concentrated emulsion observed under an optical microscope. The droplets of oils were released into water as soon as it was diluted. *Fig. 4(c)* shows oil droplets dispersed in water when the concentrated emulsion was diluted by water using the capillary method. The average size of the oil droplets for the concentrated emulsion is 1.01 ± 0.17 μm, which is close to the particle size measured by the light scattering method.

Rheological Study

Flow experiment involves measuring the shear rate as a function of shear stress. Continuous shear experiments measure the ability of each system to resist structural

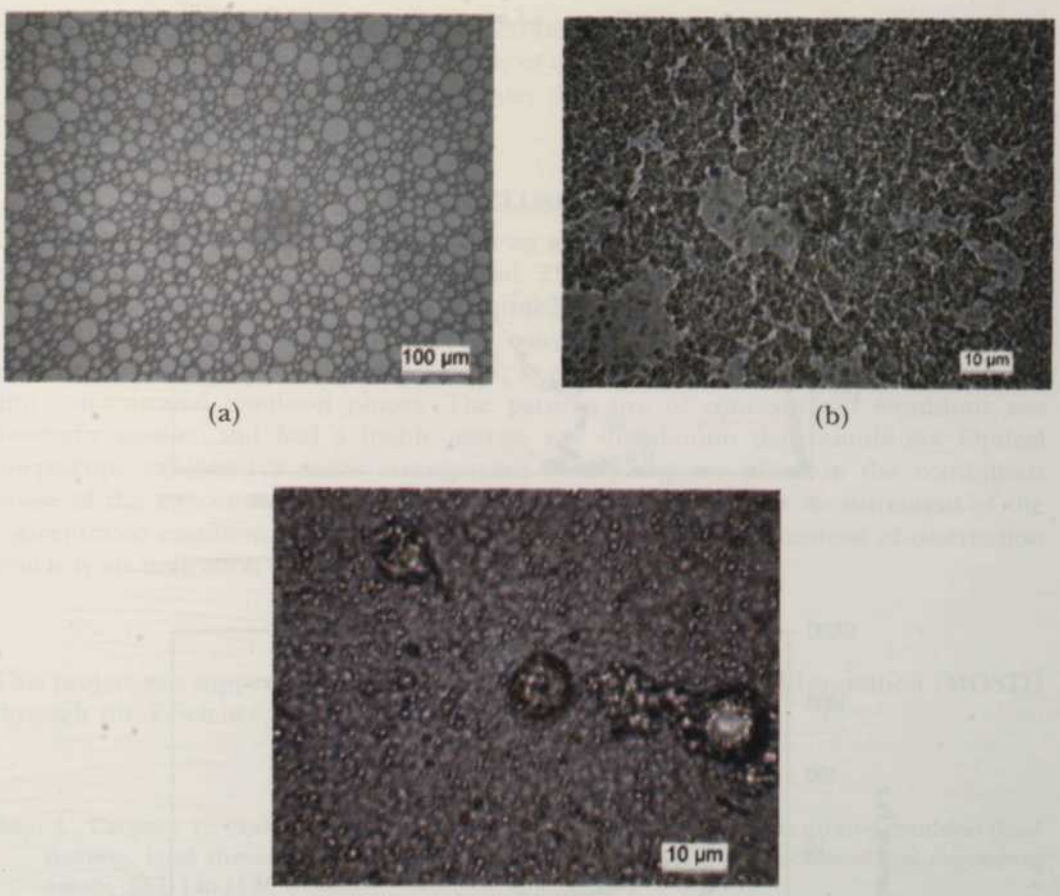

(a) (b)

(c)

Fig. 4: Morphologies of the (a) $C_{12}E_6$/water/olein oil emulsion, (b) $C_{12}E_6$/water/olive oil concentrated emulsion and (c) dilution of concentrated emulsion from (b) in water

breakdown during the standardized shearing procedure. The resulting rheogram shows three sections: the ascendant curve, the peak hold region and the descendant curve. Both the ascendant and descendant flow curves in *Fig. 5(a)* indicated shear thinning. The smooth flow curve (1) indicated a stable emulsion. In contrast, the concentrated emulsion indicated by flow curve (2) was complex and different from flow curve (1). The ascendant and descendant curves cross over implies that the shearing cycle itself might cause structural build-up, rather than destruction (Ribeiro *et al.*, 2003). If on a shear rate-shear stress plot for a material, the data are extrapolated to zero shear rate and the plot appears to cut the shear stress axis on the graph at a positive stress value, then the material is said to possess a yield stress. In practice, it means that a certain mild force must be applied before the system will flow (Strivens, 1987). A yield stress of approximately 25 Pa is observed in flow curve (2). The hysteresis loop can be interpreted as the stability of the droplets. The ascendant and descendant curves in flow curves (1) were almost the same. This means that the shear does not induce irreversible structural changes (Terrisse *et al.*, 1993).

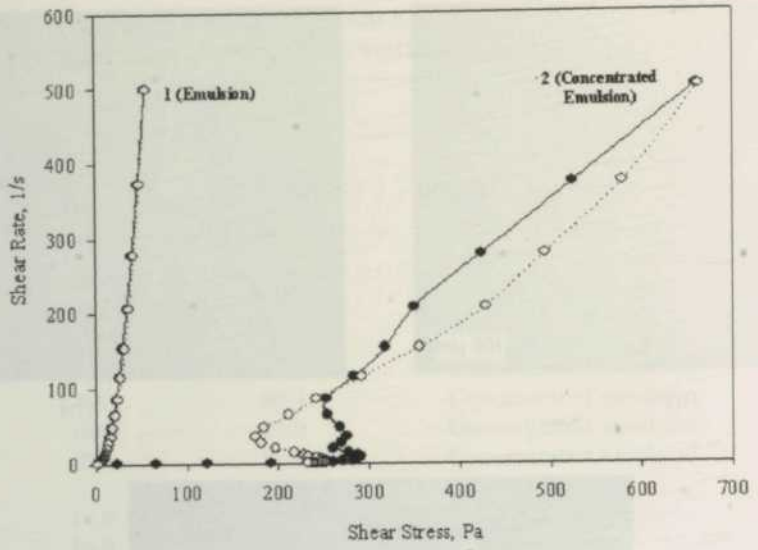

(a)

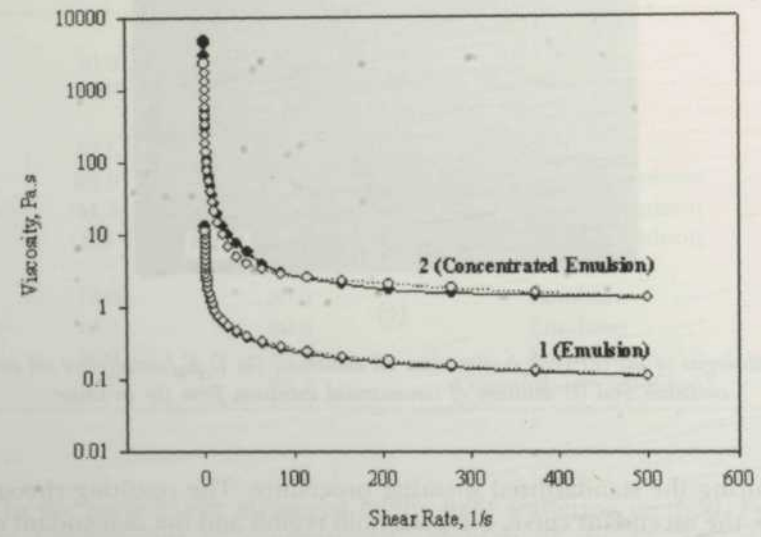

(b)

Fig. 5: (a) Flow curves of the olein oil/water/$C_{12}E_6$ emulsion (1) and olive oil/water/$C_{12}E_6$ concentrated emulsion (2) with • (closed circle) - ascendant curve and ? (open circle) – descendant curve, (b) Viscosity for emulsion of the olein oil/water/$C_{12}E_6$ system (1) and concentrated emulsion of the olive oil/water/$C_{12}E_6$ system (2) with • - descendant curve and ∘ – ascendant curve

Viscosity values provide a comparison of the resistance to structural breakdown. Both the curves in *Fig. 5(b)* decreased in viscosity as shear rate increased. This feature also indicated shear thinning behaviour. The important criteria of shear thinning materials are that: (i) the apparent viscosity decreases with increasing shear rate (or shear stress) values, and (ii) the apparent viscosity value at a given shear rate value is independent of the shear history of the sample. In curve (2), the high apparent viscosity value indicated

that the concentrated emulsion was thicker and more resistant to structure breakdown (Ribeiro *et al.*, 2003). The apparent viscosity of concentrated emulsion containing smaller droplets (1.120 μm) was significantly greater than emulsion containing larger droplets (5.987 μm).

CONCLUSIONS

Palm-based lauryl alcohol ethoxylates with an average number of 3, 6 and 100 moles of ethylene oxide were successfully synthesized. The different concentrations of oil/water/$C_{12}E_x$ determine the type of emulsion formed whether normal or concentrated. The ternary phase diagrams of oil/water/$C_{12}E_3$ consisted of only an emulsion area while the ternary phase diagrams of oil/water/$C_{12}E_6$ & oil/water/$C_{12}E_{100}$ demonstrated emulsion and concentrated emulsion phases. The particle size of concentrated emulsions was generally smaller and had a highly narrow size distribution than emulsions. Optical microscope exhibited a dense arrangement of the disperse phase in the continuous phase of the concentrated emulsions. The rheological flow curves measurement of the concentrated emulsion implied that there was structural build up instead of destruction which is an indication of high sample stability.

ACKNOWLEDGEMENTS

This project was supported by Ministry of Science, Technology and Innovation (MOSTI) through the E-Science Fund grant number 03-01-04-SF-0407.

REFERENCES

Becu, L., Grondin, P., Colin, A. and Manneville, S. (2004). How does a concentrated emulsion flow? Yielding, local rheology and wall slip. *Colloids and Surfaces A: Physicochemical and Engineering Aspects, 263*, 146-152.

Hyuk, S.Y., Mazda, O, Hyeon, Y.L., Jin, C.K., Seok, M.K., Jung, E.L., Ick, C.K., Jeong, H., Yu, S.J. and Seo, Y.J. (2006). In vivo gene therapy of type I diabetic mellitus using a cationic emulsion containing an Epstein Barr Virus (EBV) based plasmid vector. *Journal of Controlled Release, 112*, 139–144.

Kizling, J. and Kronberg, B. (2001). On the formation of concentrated stable W/O emulsions. *Advances in Colloid and Interface Sciences, 89-90*, 395-399.

Kizling, J., Kronberg, B. and Eriksson, J. C. (2006). On the formation and stability of high internal phase O/W emulsions. *Advances in Colloid and Interface Science, 123-126*, 295-302.

Latreille, B. and Paquin, P. (1990). Evaluation of emulsion stability by centrifugation with conductivity measurements. *Journal of Food Science, 55*, 1666-1668.

Niraula, B., Tan, C.K., Tham, K.C. and Misran, M. (2004). Rheology properties of glycopyranoside stabilized oil-water emulsions: Effect of alkyl chain length and bulk concentration of the surfactant. *Colloids and Surfaces A: Physicochemical and Engineering Aspects, 251*, 117-132.

Paraskevopoulou, A., Boskou, D. and Kiosseoglou, V. (2005). Stabilization of olive oil-lemon juice emulsion with polysaccharides. *Food Chemistry, 90*, 627–634.

Ravey, J.C., Stébé, M.J. and Sauvage, S. (1994). Water in fluorocarbon gel emulsions: Structures and rheology *Colloids and Surfaces A, Physicochemical and Engineering Aspects, 91*, 237-257.

Ribeiro, H. M., Morais, J. A. and Eccleston, G.M. (2004). Structure and rheology of semisolid o/w creams containing cetyl alcohol/non-ionic surfactant mixed emulsifier and different polymers. *International Journal of Cosmetic Science, 26,* 47-59.

Schramm, L.L. (2004) Emulsions: fundamentals and applications in the petroleum industry. American Chemical Society, Washington, D. C.

Semenzato, A., Bau, A., Dall'aglio, C., Nicolini, M. and Bettero, A. (1994). Stability of Vitamin A palmitate in cosmetic emulsions: influence of physical parameters. *International Journal of Cosmetic Science, 16*(4), 139–147.

Sjoblom, J. (1996). *Emulsions and Emulsion Stability. Surfactant Science Series Vol. 61.* New York: Marcel Dekker.

Solomons, N. W. and Orozco, M. (2003). Alleviation of vitamin A deficiency with palm fruit and its products. *Asia Pacific Journal of Clinical Nutrition, 12*(3), 373-384.

Strivens, T. A. (1987). An introduction to rheology. In R. Lambourne (Ed.), *Paint and Surface Coatings, Theory and Practice* (pp. 559-560). London: Ellis Horwood.

Sundram, K., Sambanthamurthi, R., Tan, Y.A. (2003). Palm fruit chemistry and nutrition. *Asia Pacific Journal of Clinical Nutrition, 12 (3),* 355-362.

Terrisse, I., Seiller, M., Rabaron, A., Gossiord, J.L. (1993). Rheology: How to characterize and to predict the evolution of W/O/W multiple emulsions. *International Journal of Cosmetic Science, 15,* 53-62.

Williams, J.M. (1991). High internal phase water-in-oil emulsions: Influence of surfactants and cosurfactants on emulsion stability and foam quality or gel-emulsions. *Langmuir,* 7, 1370-1377.

ISSN: 0128-7680
Pertanika J. Sci. & Technol. **16 (2)**: 157 - 169 (2008)

Enzymatic Saccharification of Pretreated Solid Palm Oil Mill Effluent and Oil Palm Fruit Fiber

Khaw Teik Seong, Mohd Ali Hassan and Arbakariya B. Ariff*
Department of Bioprocess Technology, Faculty of Biotechnology and Biomolecular Sciences, Universiti Putra Malaysia, 43400 UPM, Serdang, Selangor, Malaysia
**E-mail: arbarif@biotech.upm.edu.my*

ABSTRACT

The effectiveness of various chemicals pretreatment (NaOH, HCl, NH_3, HNO_3 and EDTA) on the enzymatic saccharification of solid palm oil mill effluent (POME) and oil palm fruit fibre (OPFF) was investigated. The results showed that NaOH seem to be the most suitable chemical pretreatment for enhancing sugar production and the degree of hydrolysis from saccharification of OPFF. NaOH at a concentration of 2% (w/v) appears to be optimal for alkaline pretreatment of OPFF. However, chemical pretreatment of solid POME using NaOH, NH_3, HNO_3, HCl and EDTA was found to be ineffective in enhancing the degree of hydrolysis and sugar production as compared to chemically untreated solid POME. Autoclaving OPFF at 121°C, 15 psi for 5 minutes improved the degree of hydrolysis up to 2.4 times. However, the degree of hydrolysis was not significantly affected for solid POME under the same conditions.

Keywords: Lignocellulosic materials, cellulase, fermentable sugar, palm oil mill effluent, oil palm fruit fiber

ABBREVIATIONS

OPFF	Oil palm fruit fiber
POME	Palm oil mill effluent
OPEFB	Oil palm empty fruit bunch fiber

INTRODUCTION

As the largest palm oil producer in the world, Malaysian palm oil industries have generated high export revenue because of the favorable price situation. Unfortunately, the production of palm oil from oil palm, *Elaeis guineensis,* also results to concomitant production of wastes such as palm oil mill effluent (POME) and oil palm fruit fiber (OPFF). Utilization of these palm oil wastes to generate energy sources for palm oil mills has been proposed (Ma *et al.,* 1994; Ma *et al.,* 2001). POME has been used as substrate for biohydrogen production using anaerobic contact filter (Vijayaraghavan and Ahmad, 2006) and citric acid production by *Aspergillus niger* (Jamal *et al.,* 2007). POME is also a suitable substrate for biopolymer production due to its high carbon to nitrogen ratio. Volatile fatty acids or organic acids from the anaerobic treatment of POME can be converted to polyhydroxyalkanoate (PHA) by *Rhodobacter sphaeroides* (Pandey, 2006). Industrial enzymes, such as cellulase, can also be produced using oil palm empty fruit bunch fibre as substrate (Umikalsom *et al.,* 1997).

Received : 28 November 2007
Accepted : 10 July 2008
* Corresponding Author

As lignocellulosic materials, POME and OPFF represent abundant, inexpensive and readily available sources of renewable lignocellulosic materials. These materials appear to be potential carbohydrate sources for fermentable sugars production using cellulolytic enzymes (such as cellulase). However, enzymatic hydrolysis of cellulose is hampered by the low efficiency of cellulolytic enzymes (Chahal, 1991). In general, the cellulolytic enzymes are only able to convert the cellulose portion of the lignocellulose into monomeric sugars. The low cellulose to fermentable sugar (especially glucose) conversion efficiency for lignocellulose is the result of two principle factors, the degree of crystalline nature within the cellulose and the close association between lignin-polysaccharides in plant cell walls (Cowling, 1963; Chahal, 1991). This problem is compounded by the relatively small pore sizes in untreated lignocellulose, which imposes mass transfer limitations on penetration of both microorganisms and cellulolytic enzymes (Detroy *et al.,* 1980). Therefore, structural alteration using practical pretreatment methods is needed in order to tap the cellulosic value contained in POME and OPFF for enzymatic saccharification.

This study was carried out to investigate the effect of different physical and chemical pretreatments on the performance of enzymatic saccharification of solid POME and OPFF.

MATERIALS AND METHODS

Enzymes

The enzyme employed in this study was a commercial enzyme, Celluclast 1.5 L, which is a cellulase from *Trichoderma* sp.. The enzyme in liquid form was supplied by Novo Nordisk. The activity of this cellulase was 47.4 U ml^{-1}, 66.0 U ml^{-1} and 51.1 U ml^{-1} for FPase, CMCase and β-glucosidase, respectively. The determination of the enzyme cellulase activity was according to the methods described by Wood and Bhat (1988).

Method of POME and OPFF Pretreatment

POME and OPFF were obtained from Bukit Raja Palm Oil Mill in Klang, Selangor, Malaysia. POME was centrifuged at 3000 rpm for 20 minutes to obtain solid POME and the supernatant discarded. The OPFF was reduced to an average of 2 mm fiber using Waring blender (Braun) followed by grinding using a hammer mill equipped with 2 mm round hole screens (Janke and Kunkel, IKA-Labortechnik, Staufen). The milled OPFF was collected by gravity drop after passing the particles through a 2 mm mesh. The physically treated solid POME and OPFF was preserved in a cold room at 4^0C prior to chemical treatments.

Various types of chemicals were used to study the effect of chemical pretreatment on enzymatic saccharification of solid POME and OPFF. Forty grams of either solid POME or OPFF was soaked in 400 ml of different chemical solutions (0.5% w/v) [natrium hydroxide (NaOH), hydrochoric acid (HCl), nitric acid (HNO_3), ammonia solution (NH_3) and ethylenediaminetetra acetic acid (EDTA)] at 30°C for 4 h. In the subsequent experiments, the chemically treated solid POME and OPFF were autoclaved at 121°C, 15 psi for 5 minutes. The effect of different concentrations of NaOH (0.1%, 0.5%, 1.0%, 1.5%, 2.0%, 3%, 4% and 5% w/v) on saccharification of solid POME and OPFF was also carried out using the same pretreatment method as described above. The treated solid

POME and OPFF were filtered and washed with distilled water until no trace amounts of alkali or acid could be detected. The OPFF was dried in an oven at 90°C for 48 h whereas the solid POME was centrifuged at 3000 rpm for 20 minutes to remove the water. Both solid POME and OPFF were preserved in a cold room at 4°C prior to saccharification experiments.

Saccharification Experiment

Enzymatic saccharification of solid POME and OPFF was carried out in a shaking incubator (Certomat, B Braun, Germany) at 40°C and agitated at 200 rpm. For the saccharification process, 4 g of solid POME or OPFF was filled into a 100 ml shake flask, after which 8 ml of cellulase enzyme (Celluclast 1.5L) and 72 ml of 0.05 M sodium acetate buffer (pH 5.0) were added to obtain a 5% (w/v) substrate suspension. Sodium azide (0.02% w/v) was added to the reaction mixture to avoid bacterial or fungal contamination. Samples were collected for analysis at different intervals ranging from 0 to 24 h and 0 to 120 h for solid POME and OPFF, respectively.

Analytical Procedures

Cellulose, hemicellulose and lignin contents in solid POME and OPFF were determined using the gravimetric method as described by Gorring and Van Soest (1970). The samples collected from the saccharification experiment, either using solid POME or OPFF, were centrifuged for 10 minutes at 13000 rpm. The supernatant was then used for determination of total reducing sugars and glucose. Total reducing sugars was determined using dinitrosalicylic acid (DNS) according to Miller's (1959) method. Glucose was determined using Sigma Diagnostics Glucose (Trinder) reagent. The degree of hydrolysis was calculated qualitatively according to the method described by Latif *et al.* (1994) using the following equation:

$$\text{Hydrolysis (\%)} = \frac{[\text{reducing sugar (g/l)} \times 0.9 \times 100]}{\text{substrate (g/l)} \times 0.77} \quad (1)$$

RESULTS AND DISCUSSION

Effect of Different Treatments on Chemical Composition of POME) and OPFF

The chemical composition of untreated and treated solid POME and OPFF with different chemicals is summarized in Table 1. Soaking of solid POME and OPEFB in chemical solutions without autoclaving did not produce any significant change in chemical composition as compared to the untreated form of solid POME and OPFF. However, autoclaving the OPFF at 121°C, 15 psi for 5 minutes with NaOH, NH_3 and HNO_3, showed an increase in cellulose content; and a decrease in hemicellulose and lignin content. The increase in cellulose content was dependent on the type of chemical used in the pretreatment. For example, OPFF treated with NaOH gave the highest increase in cellulose content by reducing almost 50% and 25% of the hemicellulose and lignin contents, respectively. Similar results were obtained by Umikalsom *et al.* (1997) when oil palm empty fruit bunch fiber was treated using NaOH and subsequently autoclaved at 121°C, 15 psi for 5 min. The removal of lignin and hemicellulose from OPFF was due to

the swelling effect that caused the disruption of the crystalline regions by NaOH. The swelling of lignocellulose by NaOH involves the breaking of hydrogen bonding and penetration of NaOH into the crystalline regions to solubilize the lignin-hemicellulose complex (Hannes and Leo, 1975). The degree of solubilization was further enhanced by autoclaving the lignocellulose above 100°C. Heat treatment at above 100°C also altered the physical nature of lignin by transforming the lignin into small droplets (Young *et al.,* 1985; Doppelbauer *et al.,* 1987).

About 31% and 17.6% of the hemicellulose content were removed from OPFF after treatment with HCl and EDTA followed by autoclaving, respectively. However, cellulose and lignin content were not significantly different as compared to untreated OPFF. This result is in agreement with those reported by Umikalsom *et al.* (1998) and Detroy *et al.* (1980) where cellulose content in OPEFB and wheat straw treated with 0.5% and 5% EDTA was not significantly increased. Therefore, EDTA and HCl were not suitable to treat OPFF prior to saccharification process.

In comparison to OPFF, chemically treated solid POME exhibited an entirely different response to chemical pretreatment. The cellulose content for all chemical pretreatments, except NaOH, decreased after autoclaving. The highest loss in cellulose content (11.4%) was obtained in solid POME treated with HNO_3, followed by HCl (9.6%) and EDTA (5.0%). However, solid POME treated with NH_3 showed no significant difference after autoclaving. The decrease in cellulose content after autoclaving may be due to the dissolution of cellulose in hot acid during heat treatment. Cellulose consist of a high degree of hydrogen bonding and crystalline structure, rendering it quite unreactive and insoluble in water or common solvents, but it dissolves in acids such as H_2SO_4, H_3PO_4, HCl and HNO_3 at high temperatures (Morris and Sarad, 1990). Apart from that, all of the chemical pretreatments have led to a decrease in hemicellulose and lignin contents. The highest removal of hemicellulose among the chemical pretreatments was given by HCl treated solid POME (51.6%), followed by HNO_3 (35%), NH_3 (31%), NaOH (28%) and EDTA (2.8%). Table 1 shows that the highest lignin removal (24%) was obtained in solid POME treated with HNO_3 as compared to the other chemical pretreatments such as NaOH (14.8%), HCl (14.4%), NH_3 (13.9%) and EDTA (8.5%).

Enzymatic Saccharification of Pretreated Solid POME and OPFF

Effect of Chemical Pretreatment on the Saccharification of Solid POME

The profiles of reducing sugar during saccharification of solid POME pretreated with different chemical solutions (NaOH, NH_3, HCl, HNO_3 and EDTA) are shown in *Fig. 1.* Reducing sugar was produced rapidly during the initial stage of saccharification and the rate declined gradually toward the end of the process. The concentration of reducing sugar reached a maximum value after about 8 h of the saccharification process. Generally, the maximum concentration of reducing sugar produced from saccharification of untreated solid POME (1.53 g l^{-1}) was not significantly different from that obtained in saccharification of solid POME treated with NaOH (1.59 g l^{-1}), NH_3 (1.50 g l^{-1}) and EDTA (1.48 g l^{-1}) (Table 2). However, reducing sugar produced from untreated POME was about 50% higher than that obtained in saccharification of solid POME treated with HCl and HNO_3, where the reducing sugar production was only 0.78 g l^{-1} and 0.82 g l^{-1}, respectively. The degree of hydrolysis was highest when solid POME was treated with NaOH, followed by untreated solid POME and solid POME treated with NH_3, EDTA, HNO_3 and HCl.

TABLE 1
Chemical composition of untreated and treated solid POME and OPFF with different chemical and physical treatments

Substrate	Treatment	Chemical Composition (%)				
		Cellulose	Hemicellulose	Lignin	Ash	Others
Solid palm oil mill effluent solid (Solid POME)	Untreated POME Without Autoclaving	39.3 ± 0.51	24.6 ± 0.68	22.2 ± 2.70	1.5 ± 0.20	12.5 ± 2.59
	NaOH 0.5%	39.2 ± 0.31	24.2 ± 0.51	21.2 ± 1.25	1.1 ± 0.10	14.3 ± 0.95
	NH_3 0.5%	39.0 ± 0.44	23.5 ± 0.61	20.6 ± 0.46	1.4 ± 0.10	16.1 ± 0.69
	HCl 0.5%	38.5 ± 0.87	23.6 ± 0.56	21.4 ± 0.50	1.4 ± 0.10	15.1 ± 0.84
	HNO_3 0.5%	37.4 ± 0.66	23.9 ± 0.65	20.0 ± 0.81	20 ± 0.12	16.7 ± 1.30
	EDTA 0.5%	37.7 ± 2.25	24.3 ± 0.78	23.0 ± 0.90	2.0 ± 0.13	13.1 ± 2.02
	Autoclaving					
	NaOH 0.5%	40.2 ± 0.70	17.6 ± 1.08	18.9 ± 0.45	1.2 ± 0.08	22.2 ± 1.08
	NH_3 0.5%	39.3 ± 0.71	16.9 ± 0.85	19.1 ± 0.75	1.3 ± 0.10	23.5 ± 1.45
	HCl 0.5%	35.5 ± 0.04	14.3 ± 0.80	19.0 ± 0.81	1.3 ± 0.20	29.9 ± 1.04
	HNO_3 0.5%	34.8 ± 0.06	15.9 ± 0.35	16.7 ± 1.31	2.1 ± 0.20	30.6 ± 1.16
	EDTA 0.5%	37.3 ± 0.53	23.9 ± 1.19	20.3 ± 0.53	2.1 ± 0.27	16.2 ± 0.41
	Control (autoclave without chemical)	38.7 ± 0.60	24.5 ± 0.68	21.9 ± 2.92	1.4 ± 0.14	13.5 ± 2.38
Oil palm fruit fiber (OPFF)	Untreated OPFF Without Autoclaving	48.9 ± 0.69	26.0 ± 2.22	15.7 ± 1.12	1.35 ± 0.08	8.1 ± 1.12
	NaOH 0.5%	50.2 ± 0.36	24.2 ± 0.98	14.2 ± 2.21	1.17 ± 0.28	10.2 ± 2.50
	NH_3 0.5%	48.8 ± 2.02	25.2 ± 1.91	14.5 ± 0.4	1.55 ± 0.07	9.9 ± 2.75
	HCl 0.5%	49.0 ± 0.56	24.3 ± 1.20	15.3 ± 1.71	1.11 ± 0.16	10.3 ± 1.49
	HNO_3 0.5%	48.9 ± 0.85	24.9 ± 0.91	15.0 ± 1.63	1.59 ± 0.32	9.6 ± 1.60
	EDTA 0.5%	48.8 ± 0.91	24.2 ± 0.64	15.6 ± 0.35	1.47 ± 0.07	9.9 ± 1.24
	Autoclaving					
	NaOH 0.5%	53.5 ± 0.93	13.2 ± 0.51	11.8 ± 0.70	1.13 ± 0.25	20.3 ± 1.17
	NH_3 0.5%	50.6 ± 0.70	16.6 ± 1.37	13.2 ± 0.31	1.58 ± 0.09	18.1 ± 1.56
	HCl 0.5%	49.3 ± 0.38	17.9 ± 1.36	15.0 ± 2.02	1.08 ± 0.14	16.7 ± 2.70
	HNO_3 0.5%	51.3 ± 0.47	14.9 ± 0.91	14.7 ± 1.93	1.46 ± 0.41	17.7 ± 1.68
	EDTA 0.5%	49.1 ± 1.41	21.4 ± 1.21	15.6 ± 0.46	1.47 ± 0.07	12.4 ± 2.80
	Control (autoclave without chemical)	47.6 ± 0.46	25.6 ± 1.80	15.2 ± 0.31	1.32 ± 0.03	10.3 ± 1.81

Values are means of three replicates with ± standard deviation

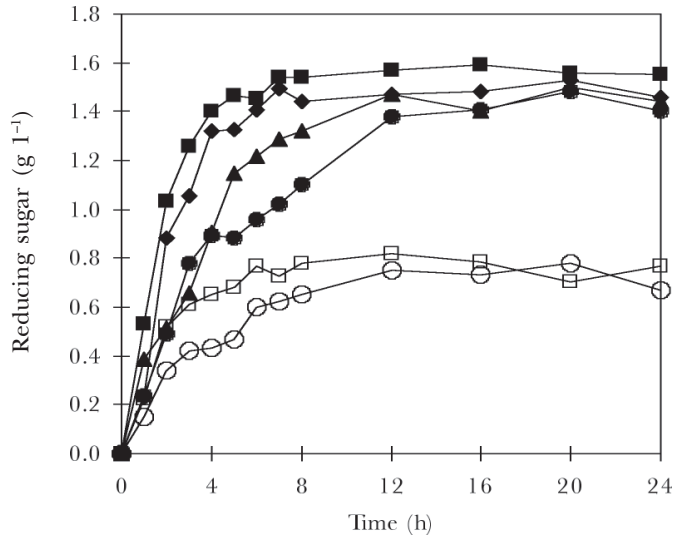

Fig. 1. Patterns of reducing sugar production during saccharification of solid POME pretreated with different chemicals. Symbols represent; (◆) Control (chemically untreated); (■) NaOH (0.5% w/v); (▲) NH_3 (0.5% w/v); (●) EDTA (0.5% w/v); (○) HCl (0.5% w/v); (□) HNO_3 (0.5% w/v)

Among the chemical pretreatment investigated, the solid POME treated with NaOH (1.03 g l^{-1}) resulted in the highest production of glucose, followed by untreated solid POME (1.01 g l^{-1}), NH_3 (0.94 g l^{-1}), EDTA (0.84 g l^{-1}), HNO_3 (0.48 g l^{-1}) and HCl (0.49 g l^{-1}). In addition, glucose yield obtained from untreated solid POME (0.25 g g^{-1}) was comparable to that obtained for Solid POME treated with either NaOH (0.26 g g^{-1}), NH_3 (0.23 g g^{-1}) or EDTA (0.21 g g^{-1}). Reduced production of reducing sugar and glucose during saccharification of solid POME treated with HCl and HNO_3 may be due to excessive loss of soluble cellulose during washing with distilled water after chemical pretreatment. Chahal (1991) reported that the use of dilute mineral, or organic acids in the pretreatment of highly crystalline lignocellulose such as cotton resulted in the formation of less susceptible products due to the removal of more readily accessible cellulose by hot acid, leaving a product of higher degree of order than the starting material. Therefore, HCl and HNO_3 are not good chemicals for pretreatment of solid POME. Additionally, the reducing sugar and glucose production from untreated solid POME was comparable to NaOH treated solid POME and even better than NH_3 and EDTA treated solid POME. Hence, for cost effectiveness, untreated solid POME was used as substrate for enzymatic saccharification in the subsequent experiment.

Effect of Chemical Pretreatment on the Saccharification of OPFF

The time courses of enzymatic saccharification of oil palm fruit fiber (OPFF) treated with NaOH, NH_3, HNO_3, HCl, EDTA and untreated OPFF are shown in *Fig. 2.* The profile of reducing sugar during saccharifiction of OPFF was almost similar to the profile of solid POME saccharification, where the reducing sugar was produced rapidly in the first 20 h and declined gradually towards the end of the process. However, chemical pretreatments appear to be more effective in enhancing saccharification of OPFF than in solid POME, as seen from higher values of the reducing sugar production in OPFF as compared to solid POME.

Among the chemical pretreatments investigated, the highest reducing sugar (10.10 g l^{-1}) was obtained from saccharification of OPFF treated with NaOH, which was almost 6-fold higher than that obtained in saccharification of untreated OPEFB (1.74 g l^{-1}) (Table 2). In addition, highest glucose production was obtained from the saccharification of OPFF treated with NaOH (3.56 g l^{-1}), followed by NH_3 (2.67 g l^{-1}), HNO_3 (1.43 g l^{-1}), HCl (1.36 g l^{-1}), EDTA (0.97 g l^{-1}) and untreated OPFF (0.68 g l^{-1}). Furthermore, the highest glucose yield, degree of hydrolysis and productivity was obtained from saccharification of OPFF treated with NaOH, which gave the values of 0.89 g g^{-1}, 88.54% and 0.14 g l^{-1} h^{-1}, respectively. Similar results were reported by Umikalsom *et al.* (1998), who found that autoclaved oil palm empty fruit bunch (OPEFB) treated with NaOH resulted in the highest rate and degree of hydrolysis as compared to other chemical pretreatments. In addition, OPEFB treated with NaOH could produce hydrolysis yield of up to 85.9%.

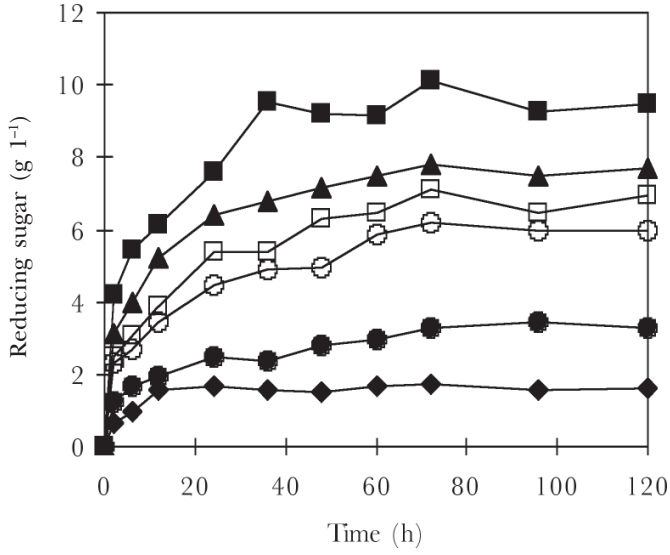

Fig. 2: The patterns of reducing sugar production during saccharification of OPFF pretreated with different chemicals. Symbols represent; (◆) Control (chemically untreated); (■) NaOH (0.5% w/v); (▲) NH_3 (0.5% w/v); (●) EDTA (0.5% w/v); (○) HCl (0.5% w/v); (□) HNO_3 (0.5% w/v)

The treatment of OPFF with NaOH seems to be the best among the chemicals used in this study for the production of reducing sugar and glucose. This may be due to the changes in the structure of OPFF caused by NaOH that led to an increase in its susceptibility to enzymatic hydrolysis. As proposed by Cowling (1963), the influence of structural features on susceptibility of lignocellulosic material to enzyme degradation involved the degree of crystallinity, degree of polymerization, lignin and hemicellulose association, and the unit cell dimensions of the crystalline present. The crystalline in lignocellulosic material can be opened up by swelling agents such as NaOH, anhydrous ammonia and certain amines (Millet *et al.,* 1976). Thus, these intracrystalline swelling agents provide a pathway toward alteration of the cellulose crystalline structure to

TABLE 2
Reducing sugar and glucose production from enzymatic saccharification of solid POME pretreated using different types of chemical

Substrate	Chemical Treatment	Reducing Sugar (g l^{-1})	Glucose (g l^{-1})	Glucose Yield (g g^{-1})	Hydrolysis (%)	Productivity (g reducing sugar l^{-1} h^{-1})
Solid Palm Oil Mill Effluent (POME)	Control	1.53	1.01	0.25	44.71	0.08
	NaOH 0.5%	1.59	1.03	0.26	46.46	0.10
	NH_3 0.5%	1.50	0.94	0.23	43.80	0.07
	HCl 0.5%	0.78	0.49	0.12	22.81	0.04
	HNO_3 0.5%	0.82	0.48	0.12	23.96	0.07
	EDTA 0.5%	1.48	0.84	0.21	43.25	0.07
Oil Palm Fruit Fiber (OPFF)	Control	1.74	0.68	0.17	30.51	0.02
	NaOH 0.5%	10.10	3.56	0.89	88.54	0.14
	NH_3 0.5%	7.78	2.67	0.67	68.20	0.11
	HCl 0.5%	6.20	1.36	0.34	54.35	0.09
	HNO_3 0.5%	6.94	1.43	0.36	62.42	0.10
	EDTA 0.5%	3.46	0.97	0.24	40.44	0.04

enhance enzymatic hydrolysis by reducing the crystalline nature, polymerization and lignin-hemicellulose association (Fox *et al.,* 1978).

The Effect of Autoclaving on Saccharification of Solid POME and OPFF

Fig. 3 shows the effect of autoclaving on the saccharification of chemically pretreated solid POME and OPFF with untreated solid POME and OPFF as control. Generally, the degree of hydrolysis for saccharification of autoclaved chemically treated solid POME did not show any significant difference as compared to non-autoclaved chemically treated solid POME. In addition, the degree of hydrolysis for autoclaved HCl and HNO_3 treated solid POME was even lower than the non-autoclaved solid POME treated with the same chemical. This result indicates that hot acid hydrolyzed the more accessible portion of solid POME during autoclaving leaving the less accessible portion, which affects the performance of enzymatic hydrolysis of solid POME to reducing sugar.

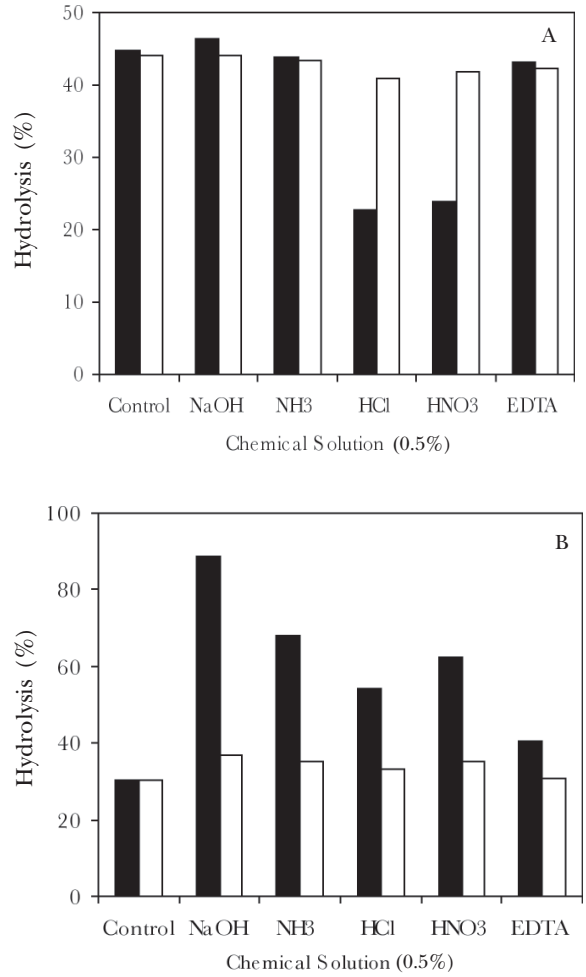

Fig. 3: Effect of autoclaving on the performance of the enzymatic saccharification of chemically treated (A) solid POME and (B) OPFF. Saccharification was carried out at 40 ^{0}C, pH 5.0, 200 rpm. (■) autoclaved; (□) non-autoclaved

On the other hand, the increase in hydrolysis for saccharification of OPFF was observed when autoclaved OPFF treated with different chemicals were used as substrate as compared to non-autoclaved OPFF. However, the effect of autoclaving on the degree of hydrolysis was dependent on the type of chemical used for pretreatment. Autoclaving the NaOH treated OPFF gave the highest response to enzymatic saccharification by increasing the degree of hydrolysis up to 2.4 times. The factors that affect autoclaving pretreatment includes residence time, temperature, particle size, moisture content and the addition of an acid catalyst such as sulphuric acid or sulfur dioxide (Sun and Cheng, 2002). However, this was not the case in our findings where the alkaline catalyst (NaOH) was more superior than the acid catalyst. The saccharification of autoclaved oil palm empty fruit bunch (OPEFB) treated with 0.5% NaOH was improved by about 3.5 times, the highest among chemical pretreatments (Umikalsom *et al.,* 1988). Therefore, the treatment of OPFF with NaOH produced the most suitable substrate for enzymatic saccharification as compared to other chemicals (NH_3, HCl, HNO_3 and EDTA). On the other hand, improvement of enzymatic hydrolysis of wood chips was obtained with steam pretreatment, at very high temperatures, of H_2SO_4-impregnated materials (Sassner, 2008). In this case, the optimal conditions were obtained at 200°C for 8-10 minutes using 0.5% (w/v) H_2SO_4.

Effect of Different NaOH Concentrations on the Saccharification of OPFF

The patterns of reducing sugar production during saccharification of OPFF treated with different NaOH concentrations (0.1%, 0.5%, 1.0%, 1.5%, 2.0%, 3.0%, 4.0% and 5.0% w/v) are shown in *Fig. 4*. In general, reducing sugar linearly increased with increasing NaOH concentration from 0.1% to 1.5% (w/v). However, the production was not significantly different for the OPFF treated with 2% and 5% (w/v) NaOH. The swelling of OPFF caused by NaOH increased with increasing NaOH concentration up to 2% (w/v). Beyond this concentration, the OPFF was fully swelled, as examined under the electron microscope (data not shown) and saturated at 2% w/v NaOH. Hence, NaOH concentration higher than 2% (w/v) did not have any effect on the swelling of OPFF, which makes the cellulose more susceptible to enzyme attack. This is a possible explanation for the increase in reducing sugar production from the saccharification of OPFF treated with concentrated NaOH.

Relationship between Cellulose and Lignin Content on Degree of Hydrolysis from Saccharification of Solid POME and OPFF

The solid POME and OPFF, subjected to different chemical pretreatments (NaOH, HCl, HNO_3, NH_3 and EDTA), yielded a wide spectrum of cellulose and lignin content (*Fig. 5*). The degree of hydrolysis from saccharification of solid POME increased slightly and almost linearly with decreasing lignin content from 21.4% to 18.9%. In addition, the degree of hydrolysis for solid POME also increased linearly with increasing cellulose content from 34.8% to 37.4%. However, the degree of hydrolysis only increased slightly from 37.7% to 40.2% for cellulase content of above 38%. This may be due to a collapse of the lignocellulose structure that shrank the availability of surface area for enzymatic attack, which is generated by the removal of the lignin seal (Fan *et al.,* 1981). In the case of OPFF, the degree of hydrolysis increased substantially with decreasing lignin content from 15.7% to 11.8%. On the other hand, the degree of hydrolysis increased but not linearly with increasing cellulose content. Similar observations were reported for enzymatic

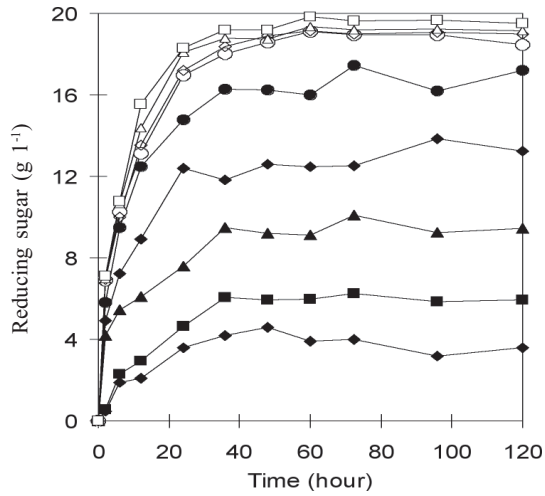

Fig. 4: Patterns of reducing sugar production from enzymatic saccharification of OPFF treated with different NaOH concentration. Symbols represent; (♦) Control; (■) NaOH (0.1% w/v); (▲) NaOH (0.5% w/v); (◆) NaOH (1.0% w/v); (●)NaOH (1.5% w/v); (○) NaOH (2.0% w/v); (◇)NaOH (3.0% w/v); (△)NaOH (4.0% w/v); (□)NaOH (5.0% w/v)

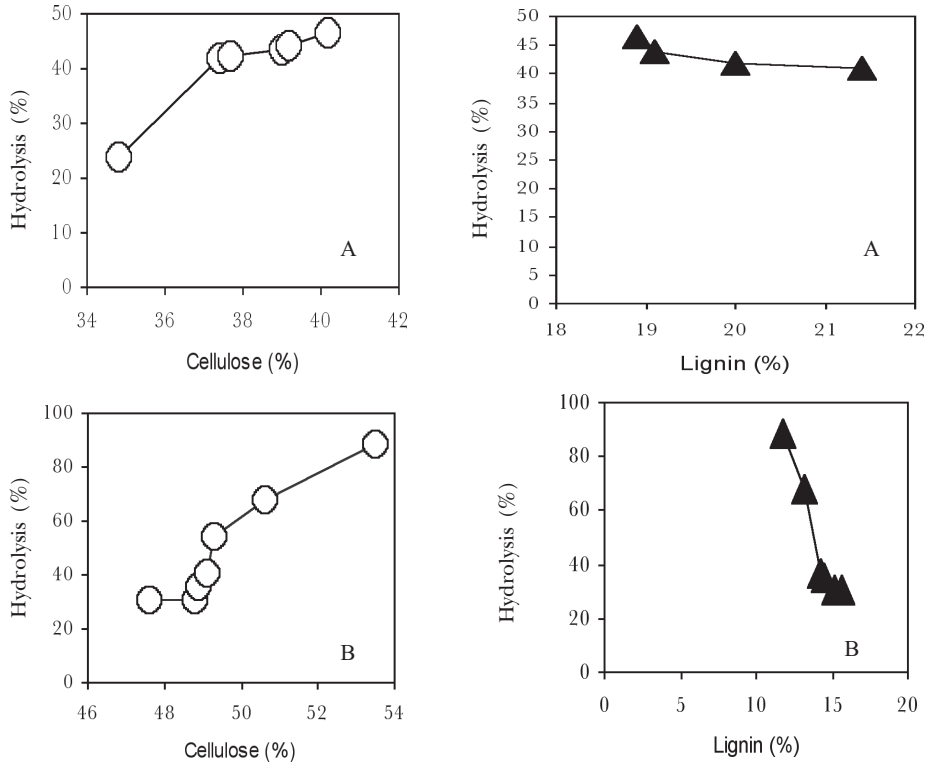

Fig. 5: Relationship between cellulose and lignin contents on the degree of hydrolysis during saccharification of (A) solid POME and (B) OPFF treated with various chemicals (NaOH, HCl, HNO_3, NH_3 and EDTA).

saccharification of oil palm empty fruit bunch treated with various types of chemicals (NaOH, HNO_3, HCl, EDA and EDTA) (Umikalsom *et al.,* 1998).

The recovery of lignin is also important in improving the economy of the process, as lignin can be utilized as a solid fuel (Wingren *et al.,* 2003). During heat and chemical pretreatments part of the lignin undergoes solubilization followed by repolymerization (Sassner *et al.,* 2008). Reactions involving lignin and sugar or sugar degradation products (furfural) also occur (Carrote *et al.,* 1999). The by-products formed in such reaction, known as pseudolignin, contribute to the amount of insoluble lignin in the pretreated materials.

CONCLUSIONS

Results from this study indicate that chemical and physical pretreatments are required for the saccharification of OPFF. Among the chemicals tested (NaOH, HCl, NH_3, HNO_3 and EDTA), the highest saccharification was obtained when OPFF was treated with 2% (w/v). In addition, autoclaving the OPFF at 121°C, 15 psi for 5 minutes also improved the degree of hydrolysis by up to 2.4 times. On the other hand, chemical pretreatment and autoclaving of solid POME did not significantly enhance the saccharification of solid POME as compared to untreated POME. The glucose yield based on the amount of substrate used for optimal enzymatic saccharification of solid POME and OPFF was 0.26 g g^{-1} and 0.89 g g^{-1}, respectively.

REFERENCES

Chahal, D.S. (1991). Pretreatment of lignocelluloses. In D.S. Chahal (Ed.), *Food, feed and fuel from biomass* (pp. 59-83). New Delhi, India: Oxford and IBH Publishing Co. Pvt Ltd.

Cowling, E.B. (1963). Structural features of cellulose that influences its susceptibility to enzymatic hydrolysis. In E.T. Reese (Ed.), *Advances in enzymatic hydrolysis of cellulose and related materials* (pp. 1-32). Macmillan, New York: Pergamon Press.

Detroy, R.W., Lindenfelser, L.A., Julian, Jr. G.S. and Orton, W.L. (1980). Saccharification of wheat straw cellulose by enzymatic hydrolysis following fermentative and chemical pretreatment. *Biotechnol. Bioeng. Symp., 10,* 135-148.

Doppelbauer, R.., Esterbauer, H., Steiner, W., Lafferty, R.M. and Steinmuller, H. (1987). The use of lignocellulosic wastes for production of cellulose by *Trichoderma reesei. Appl. Microbiol. Biotechnol., 26,* 485-494.

Fan, L.T., Gharpuray, M.M. and Yong, H.L. (1981). Evaluation of pretreatment for enzymatic conversion of agricultural residues. *Biotechnol. Bioeng. Symp., 11,* 29-45.

Fox, D.J., Gray, P.P., Dunn, N.W. and Mardsen, W.L. (1987). Factors affecting the enzymatic susceptibility of alkali and acid pretreated sugar-cane bagasse. *J. Chem. Technol. Biotechnol., 40,* 117-132.

Garrote, G., Dominguez, H. and Parajo, J.C. (1999). Hydrothermal processing of lignocellulosic materials. *Holz. Roh. Werkst., 57,* 191-202.

Gorring, H.K and Van Soest, P.J. (1970). Forage fiber analysis (Apparatus, reagents, procedures and some applications). Agricultural Handbook No. 379 (pp. 1-20). Agricultural Research Service-United States Department of Agriculture. Washington D.C.

Hannes, S. and Leo, N. (1975). The structure and properties of cellulose. In M. Bailey and T.M. Enari (Eds.), *Symposium on enzymatic hydrolysis of cellulose* (pp. 9-22). Helsinki, Finland.

Jamal, P., Alam, M.Z. and Mohamad, A. (2007). Microbial bioconversion of palm oil mill effluent to citric acid with optimum process conditions. In N.A. Ibrahim, Abu Osman, J. Usman and N.A. Kadri (Eds.), *Biomed 06, IFMBE Proceedings* (pp. 483-487). Springer-Verlag Berlin Heidelberg.

Latif, F., Rajoka, M.R. and Malik, K.A. (1994). Saccharification of *Leptochloa fusca* (Kallar Grass Straw) using thermostable cellulases. *Bioresour. Technol., 50,* 107-111.

Ma, A.N., Choo, Y.M. and Yusof, B. (1994). Renewable energy from the palm oil industry. *Elaeis, 6,* 138-146.

Ma, A.N., Chow, C.S., John, C.K., Ibrahim, A. and Isa, Z. (2001). Palm oil mill effluent – a survey. In *Proceedings of PORIM Regional Workshop on Palm Oil Mill Technology and Effluent Treatment* (pp. 233-269). Palm Oil Research Institute of Malaysia, Bangi, Malaysia.

Miller, G.L. (1959). Use of dinitrosalisylic acid reagent for determination of reducing sugars. *Anal Chem., 31,* 426-428.

Millet. M.A., Baker, A.J. and Satter, L.D. (1976). Physical and chemical pretreatment for enhancing cellulose saccharification. *Biotechnol. Bioeng. Symp., 6,* 125-153.

Morris, W. and Sarad, R.P. (1990). Wood. In J.A. Bryant and J.F. Kennedy (Eds.), *Biotechnology of biomass conversion* (pp. 41-72). Milton Keynes: Open University Press.

Pandey, A. (2006). *Concise Encyclopedia of Bioresource Technology.* Philadelphia, USA: Haworth Press Inc.

Sassner, P., Martensson, C-G., Galbe, M. and Zacchi, G. (2008). Steam pretreatment of H_2SO_4 – impregnated *Salix* for the production of bioethanol. *Bioresour. Technol., 99,* 137-145.

Sun, Y. and Cheng, J. (2002). Hydrolysis of lignocellulosic materials for ethanol production: a review. *Bioresour. Technol., 83,* 1-11.

Umikalsom, M.S., Ariff, A.B., Zulkifli, H.S., Tong, C.C., Hassan, M.A. and Karim M.I.A. (1997). The treatment of oil empty fruit bunch fiber for subsequent use as substrate for cellulase production by *Chaetomium globosum* Kunze. *Bioresour. Technol., 65,* 1-9.

Umikalsom, M.S., Ariff, A.B. and Karim, M.I.A. (1998). Saccharification of pretreated oil palm empty fruit bunch fibre using a cellulase of *Chaetomium globosum. J. Agric. Food Chem., 46,* 3359-3346.

Vijayaraghavan, K. and Ahmad, D. (2006). Biohydrogen generation from palm oil mill effluent using anaerobic contact filter. *Int. J. Hydrogen Ener., 31,* 1284-1291.

Wingren, A., Galbe, M. and Zacchi, G. (2003). A techno-economic evaluation of producing ethanol from soft wood – a comparison of SFF and SHF and identification of bottlenecks. *Biotechnol. Progr., 19,* 1109-1117.

Wood, T.M. and Bhat, K.M. (1988). Method for measuring cellulose activities. In *Methods in Enzymology,* Vol. 160, *Biomass, Part A: Cellulose and Hemicellulose* (pp. 87-112). Academic Press, Inc.

Young, R.A., Fujita, M. and River, B.H. (1985). New approaches to wood bonding: A base-activated lignin adhesive system. *Wood Sci., 19,* 368-381.

ISSN: 0128-7680
Pertanika J. Sci. & Technol. **16 (2)**: 171 - 176 (2008)

Performance of Autoregressive Order Selection Criteria: A Simulation Study

Venus Khim-Sen Liew[1], Mahendran Shitan[2*], Choong Chee Keong[3] and Hooy Chee Wooi[3]

[1]Labuan School of International Business and Finance, Universiti Malaysia Sabah, Jalan Sungai Pagar, 87000 Labuan, Malaysia

[2]Department of Mathematics/ Mathematics Research Institute, Universiti Putra Malaysia, 43400 UPM, Serdang, Selangor, Malaysia

[3]Faculty of Accountancy and Management, Universiti Tunku Abdul Rahman, Jalan Genting Kelang, 53000 Kuala Lumpur, Malaysia

ABSTRACT

Proper selection of autoregressive order plays a crucial role in econometrics modeling cycles and testing procedures. This paper compares the performance of various autoregressive order selection criteria in selecting the true order. This simulation study shows that Schwarz information criterion (SIC), final prediction error (FPE), Hannan-Qiunn criterion (HQC) and Bayesian information criterion (BIC) have considerable high performance in selecting the true autoregressive order, even if the sample size is small, whereas Akaike's information criterion (AIC) over-estimated the true order with a probability of more than two-thirds. Further, this simulation study also shows that the probability of these criteria (except AIC) in correctly estimating the true order approaches one as sample size grows. Generally, these findings show that the most commonly used AIC might yield misleading policy conclusions due to its unsatisfactory performance. We note here that out of a class of commonly used criteria, BIC performs the best for a small sample size of 25 observations.

Keywords: Autoregressive, order selection criteria, simulation

INTRODUCTION

Most econometric models are formulated based on the Autoregressive (AR) process. In particular, AR process forms the main building block of the celebrated Integrated Autoregressive Moving Average (ARIMA) model, Vector Autoregressive (VAR) model, Vector Error Correction (VEC) model, Autoregressive Distributive Lag (ARDL) model, Generalized Autoregressive Conditional Heteroscedasticity (GARCH) models, Threshold Autoregressive (TAR) model and the Smooth Transition Autoregressive (STAR) model, to name a few. A major problem with these econometric models is that the true order (p) of the AR (p) process is always unknown and the optimal order has to be determined by certain order selection criteria. Moreover, several econometric test procedures in empirical research such as the unit root tests, causality tests and cointegration tests are sensitive to the choice of autoregressive order. Thus, proper selection of autoregressive order is an important task in econometric modeling cycles and testing procedures.

The final prediction error (FPE) criterion, Schwarz information criterion (SIC), Hannan-Qiunn criterion (HQC) and Akaike's information criterion (AIC), among

Received : 14 July 2007
Accepted : 3 December 2007
* Corresponding Author

others, are commonly employed by empirical models researchers to determine the optimal autoregressive order. One interesting question that concerns many researchers is which criterion has the capability to provide the most reliable optimal order. However, there is no universally accepted solution to this question. In this study, firstly we attempt to compare via a simulation study, the performance of these criteria and second, to examine the effects of various sample sizes on the performance of these criteria in the selection of order.

We find that all selection criteria under study (except AIC) performed quite well in estimating the true order even if the sample size is small. We note that this probability is less than 0.25 for AIC even when the sample size grows to the very large value of 100,000.

AUTOREGRESSIVE ORDER SELECTION CRITERIA

There has been considerable literature published on AR order selection criteria. A brief discussion of these criteria is available in Beveridge and Oickle (1994), whereas Brockwell and Davis (1996) presented greater theoretical and practical detail and additional references for many of these criteria.

Suppose the data set $\{X_1, \ldots, X_T\}$ are in fact observations of an AR process of order p, denoted by AR(p) and defined as

$$X_t = \sum_{i=1}^{p} \phi_i X_{t-i} + \varepsilon_t \tag{1}$$

where ϕ_i, $i = 1, \ldots, p$ are autoregressive parameters to be estimated and ε_t, $t = 1, \ldots, T$ is an independent and identically distributed (iid) disturbance or error term of a zero mean and a finite variance σ^2, which can be easily calculated by $\hat{\sigma}^2 = (T - p - 1)^{-1} \sum_{t=1}^{T} \hat{\varepsilon}_t^2$, where symbol ^ stands for estimated value.

The final prediction error (FPE) criterion, which was originally proposed by Akaike (1969) for AR(p) order determination, is given by FPE = $\hat{\sigma}^2 (T - p)^{-1}(T + p)$. Having found that FPE is asymptotically inconsistent, Akaike (1973) came up with the so-called Akaike information criterion (AIC), defined as AIC=$\ln(\hat{\sigma}^2)+2p/T$. Disregarding the fact that AIC is only asymptotically unbiased (Jones, 1975) and has the tendency to pick models which are over-parameterized (Shibata, 1976), AIC is a very commonly used criterion for order selection (Basci and Zaman, 1998). Another statistics due to Akaike (1979) is the Bayesian information criterion, which is defined as BIC = $(T-p)\ln[(T-p)^{-1}T\hat{\sigma}^2]+T[1+\ln\sqrt{2\pi}]$ + $p \ln[p^{-1}(\sum_{t=1}^{T} X_t^2 - T\hat{\sigma}^2)$. There is evidence to suggest that the BIC is better than the AIC as order selection criterion (Hannan, 1980).

Schwarz (1978) derived an information criterion, known as Schwarz information criterion (SIC) defined as SIC = $\ln(\hat{\sigma}^2) + T^{-1} p \ln(T)$. SIC is also called Schwarz-Rissanen criterion as Rissanen (1978) also arrived at the same criterion independently, using different methodology. However, SIC has the advantage of being consistent over AIC (Basci and Zaman, 1998).

Hannan and Quinn (1979) and Hannan (1980) constructed the Hannan-Quinn criterion (HQC) from the law of the iterated logarithm. It provides a penalty function, which decreases as fast as possible for a strongly consistent estimator, as sample size increases. Hannan-Quinn criterion is given by $HQC = \ln \hat{\sigma}^2 + 2T^{-1}p \ln(\ln T)$. Hannan and Rissanen (1982) replaced the term $\ln(\ln T)$ by $\ln T$ to speed up the convergence of HQC. This revised version of HQ, however, was found to overestimate the model orders (Kavalieris, 1991).

SIMULATION RESULTS

To achieve our objective, we simulated the AR process with normally distributed random errors of zero mean and a finite variance σ^2. We arbitrarily set the true lag length $p = 4$ and generate ϕ_i, $i = 1, 2, 3, 4$ from a uniform distribution in the region $(-0.25, 0.25)$. The choice of this region allows us to avoid undesired nonstationary processes. Meanwhile c may take any value and is generated from an arbitrarily chosen uniform distribution in the region $(-100,100)$. We simulate data sets for various sample sizes: 25, 50, 100, 250, 500, 1000, 10000, 100000. For each sample size, we simulated 1000 independent series for the purpose of order estimation. The estimated order $\hat{p}$ can be any integer from 1 to 20. The probability of estimating the true order, denoted by $P(\hat{p} = p)$ is then determined. In addition, this study also investigated the probabilities of under- and over-estimating the true order [denoted by $P(\hat{p} > p)$ and $P(\hat{p} < p)$ respectively], in which the estimated order based on the selection criteria is less than and more than the true order, respectively. The probabilities (in percentages) of various criteria incorrectly, under- and over- estimating the true order are presented in *Figs. 1* to *3*.

The most important finding is that all selection criteria under study (except AIC) perform quite well in estimating the true order even if the sample size is small[1]. It is noteworthy that the performance of all criteria in correctly estimating the true order increases as the sample size increases. In particular, $P(\hat{p} = p)$ almost converges to 1 with a sample size of 100,000 observations for all criteria except in the case of AIC, where $P(\hat{p} = p)$ is less than 0.25 even for this extraordinary large sample size (*Fig. 1*). Taken together, these findings warrant us that the most commonly used AIC might yield misleading policy conclusions due to its unsatisfactory performance. We note here that out of a class of commonly used criteria, BIC performs the best, followed by HQC, FPE and SIC, whereas AIC shows the worst performance.

[1]Note that AR-type models (i.e. dynamic models with lagged dependent variables) are quite problematic in small samples (of less than 50 observations for instance) since both Ordinary Least Squares and Maximum Likelihood have only large small and the usual inference machinery like *t*-statistics are also only asymptotically justified in this case. However, in circumstance (for example, many economic time series hardly have more than 50 annual observations) that leaves us no choice, knowing the small sample performance of these criteria in identifying the order p become useful.

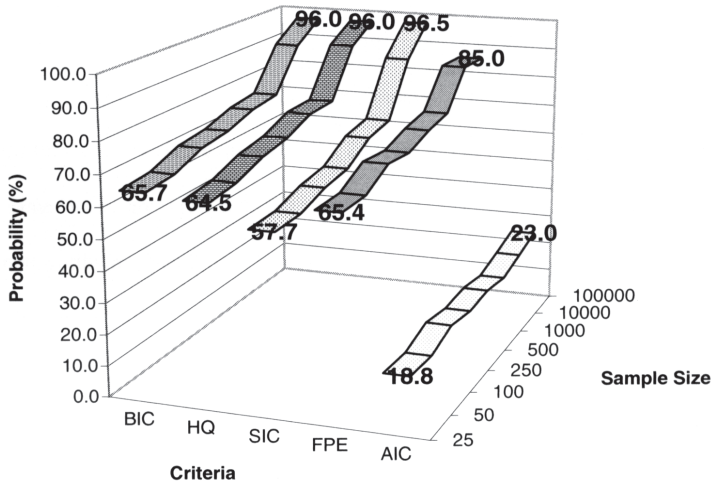

Fig. 1: Probability of correctly estimating the true order

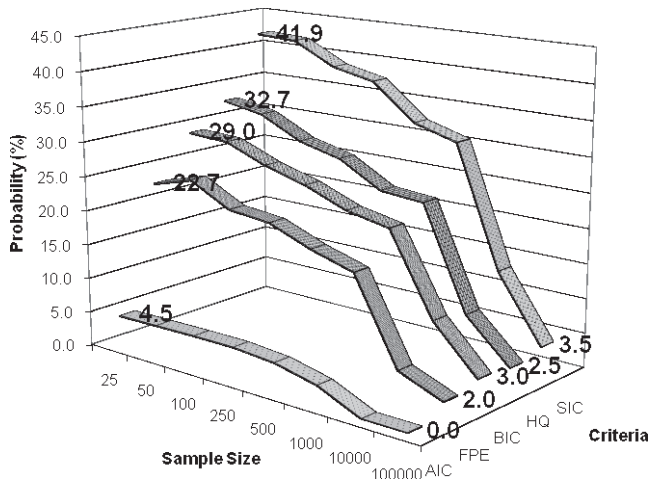

Fig. 2: Probability of under-estimating the true order

Another important finding of this study is that whenever FPE, BIC, HQC and SIC fail to estimate the true order, it is due to under-estimation rather than over-estimation. The reverse is true for AIC. For illustration, $P(\hat{p} < p)$ for these criteria are in the order, 22.7, 29.0, 32.7, 41.9 and 4.5 (*Fig. 2*), whereas $P(\hat{p} > p)$, in the same order is 11.9, 5.3, 2.0, 0.4 and 76.7 (*Fig. 3*) for a sample size of 25 observations. It is noted that in general (excluding the case of AIC), the probabilities of both under- and over-estimation reduces as sample size increases, thereby providing room for improvement in the performance of these criteria.

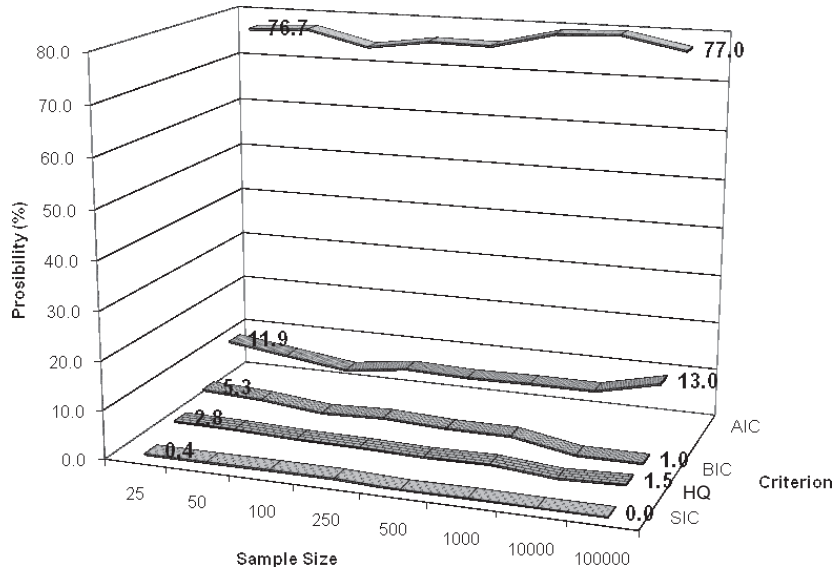

Fig. 3: Probability of over-estimating the true order

CONCLUSIONS

Econometric modeling cycles and testing procedures mostly involves the predetermination of the autoregressive order (p). In reality, the true order (p) of the autoregressive (AR) process is unknown and the best a researcher can do is to estimate it using certain commonly accepted order selection criteria. The resulting estimate is known as the optimal order. Among others, the final prediction error (FPE) criterion, Schwarz information criterion (SIC), Hannan-Qiunn criterion (HQC), Akaike's information criterion (AIC) are commonly employed in empirical study. Nonetheless, there is no consensus on which of these criteria has the capability to provide the most reliable optimal order. As these criteria have important implications on the reliability of the estimated autoregressive order and thereby the subsequent findings based on this estimation, it is important to understand their performances. In this regard, this study attempts to compare via a simulation study, the performance of these criteria. Further, the effects of various sample sizes on the performance of these criteria in the selection of order were also analyzed.

This simulation study showed that SIC, FPE, HQC and BIC display considerably good performance in picking the true autoregressive order, even if the sample size is small, whereas AIC over-estimated the true order with a probability of more than two-third. Further, this simulation study also showed that the probability of these criteria (with the exception of AIC) correctly estimating the true order approaches one as sample size grows. In general, these findings show that the most commonly used AIC might yield misleading policy conclusions due to its unsatisfactory low performance. We note here that out of a class of commonly used criteria, BIC performs the best for a small sample size of 25 observations.

ACKNOWLEDGEMENTS

The authors would like to thank the anonymous referees who have provided useful comments and suggestions on the previous version of this paper.

REFERENCES

AKAIKE, H. (1969). Fitting autoregressive models for prediction. *Annals of the Institute of Statistical Mathematics, 21,* 243–247.

AKAIKE, H. (1973). Information theory and an extension of the maximum likelihood principle. In B. N. Perron and F. Csaki (Eds.), *2nd International Symposium in Information Theory* (pp. 267–281). Budapest: Akademial Kiado.

AKAIKE, H. (1979). A Bayesian extension of the minimum AIC procedure of autoregressive model fitting. *Biometrika, 66,* 237–242.

BASCI, S. and ZAMAN, A. (1998). Effects of skewness and kurtosis on model selection criteria. *Economic Letters, 59,* 17–22.

BEVERIDGE, S. and OICKLE, C. (1994). A comparison of Box-Jenkins and objective methods for determining the order of a non-seasonal ARMA model. *Journal of Forecasting, 13,* 419 – 434.

BROCKWELL, P. J. and DAVIS, R. A. (1996). *Introduction to Time Series and Forecasting.* New York: Springer.

HANNAN, E. J. (1980). The estimation of the order of an ARMA process. *Annals of Statistics, 8,* 1071 – 1081.

HANNAN, E. J. and QUINN, B. G. (1979). The determination of the order of an autoregression. *Journal of Royal Statistical Society, 41,* 190–195.

HANNAN, E. J. and RISSANEN, J. (1982). Recursive estimation of mixed autoregressive-moving average order. *Biometrika, 69,* 81–94.

HURVICH, C. M. and TSAI, C. L. (1989). Regression and time series model selection in small samples. *Biometrika, 76,* 297–307.

JONES, R. H. (1975). Fitting autoregressions. *Journal of American Statistics Association, 70,* 590– 592.

KAVALIERIS, L. (1991). A note on estimating autoregressive-moving average order. *Biometrika, 78,* 920–922.

SCHWARZ, G. (1978). Estimating the dimension of a model. *The Annals of Statistics, 6,* 461–464.

SHIBATA, R. (1976). Selection of the order of an autoregressive model by Akaike's information criterion. *Biometrika, 63,* 117–126.

RISSANEN, J. (1978). Modelling by shortest data description. *Automatica, 14,* 467–471.

ISSN: 0128-7680
Pertanika J. Sci. & Technol. **16 (2)**: 177 - 187 (2008)

Statistical Selection Algorithm for Peer-to-Peer System

Mohamed Othman and Kweh Yeah Lun*
Department of Communication Technology and Network,
Faculty of Computer Science and Information Technology,
Universiti Putra Malaysia, 43300 UPM, Serdang, Selangor, Malaysia
**E-mail: yeahlun@yahoo.com*

ABSTRACT

Over the years, the distributed database has been developed so fast that there's a need to develop an effective selection algorithm for it. Loo *et. al.* (2002) has proposed a statistical selection algorithm with the same objective and run in multicast / broadcast environment that has been proved that it is the best among others in terms of the number of messages needed to complete the searching process. However, this algorithm has a high probability of failure. A few improvements have been done to this original algorithm. This improved algorithm is developed based on the simulation of the real multicast environment. Modifications have been added in the improved algorithm to ensure that the unique pivot that never been used before is selected every time, and to solve problem that involve rank for certain key value that occur in more than one participant. Four performance measures have been conducted for the purpose of performance analysis between original and improved algorithm. These measures include probability of failure, number of messages needed, number of rounds needed and execution time. As a result, the probability of failure for the newly improved algorithm is 3.2% while the original algorithm is 19.2% without much overhead in increasing the number of messages and number of rounds needed.

Keywords: Distributed database, multicast, performance measure, selection algorithm

INTRODUCTION

The selection algorithm has been developed to ease distributed database operations and peer-to-peer computing. It can be applied to select the closest server. Selection operations are needed in some distributed sorting algorithms (Dechter, 1986; Huang, 1990; Wegner, 1984; Loo, 1991; Loo, 1995; Loo, 1997). In these distributed sorting algorithms, it is necessary to find the n/i^{th} keys (where $i = 1, 2, \ldots, p-1$; n is size and p is the number of computers involved). A file, F, with n records which is distributed in a few sites with all records totally ordered, and design resolution algorithms which minimize the amount of communication activity rather than the amount of processing activity, has been examined (Santoro, 1989). Different solutions and bounds exist for the distributed selection problem in the point-to-point network depending on the topology of the network (Frederickson, 1983; Matsuhita, 1983; Shirira, 1983). A general selection algorithm is developed using packets and the packet complexity is shown to be a significant improvement for a large range of packet sizes over the existing bounds (Negro, 1997). It is a bit optimal in star networks. The sampling techniques are used in designing the distributed algorithms (Rajasekaran, 1997). Some distributed algorithms (Saukas, 1988;

Received : 3 March 2008
Accepted : 26 June 2008
* Corresponding Author

Santoro, 1992; Huang, 1990) were suitable for the intranet environment. These algorithms consider the availability of the broadcast / multicast communication in the system. Wei (2002) has developed an efficient selection and sorting scheme for processing large files distributed over a network.

Many other distributed selection algorithms have been developed for various purposes based on different topologies and assumptions. Most researchers work on distributed selection algorithms that run on special topologies. Rodeh (1982) presented an algorithm for the case where two computers are connected together. Shen (1991) presented his algorithm on hypercube topology and Hao (1992) presented an algorithm on mesh topology. Aggrawal (1995) presented a selection algorithm for pyramid topology. However, the topologies of this algorithm are different in the Internet / intranet environment. They need to be modified before they are applied in the Internet / intranet environment. In 2003, Wu (2003) designed a fast and scalable parallel algorithm for selection and median filtering. It is a most time efficient algorithm, especially compared to the algorithms designed by Han (2002) and Pan (1994). Alexandros (2003) presented a randomized selection algorithm whose performance is analyzed in an architecture independent way on the bulk-synchronous parallel (BSP) model of computation along with an application of this algorithm to dynamic data structures, namely parallel priority queues. Bader (2005) presented an efficient randomized high-level parallel algorithm (Fast and UltraFast) for finding the median, given a set of elements distributed across a parallel machine, which solves the general selection problem that requires the determination of the element of rank k, for an arbitrarily given integer k.

Loo (2002) analyzed the problems in database operations and presented statistical selection algorithms which are designed to select the j^{th} smallest key from a very large file distributed over many computers. The algorithm aims to minimize the frequency of communication necessary to solve the selection problem. It is assumed that all data are sorted and within a certain range in each local file (Loo, 2002). All computers that participate are equal and they have equal share of the workload. The complexity analysis based on the number of messages needed is done to compare this algorithm with the previous algorithm (Huang, 1990; Santoro, 1992).

Loo's algorithms are efficient in terms of the number of communication messages where the number of communication messages required in the statistical selection algorithm for distributed databases is lower than in any published algorithms with the same type of computer connection topologies (Loo, 2002).

Loo presented an efficient distributed multiple selection algorithm designed to select multiple keys simultaneously from different data sets which are distributed to many computers in a peer-to-peer system and aimed at reducing the number of communication messages (Loo, 2005).

This research work is based on the work by Loo (2002) which is currently the best single selection algorithm in the peer-to-peer environment. The algorithm implemented in this research is a type of statistical selection algorithm derived from improvement of an existing algorithm presented by Loo (2002). Based on the simulation that has been set up, a few problems were found. The algorithm fails at a high rate where it cannot find the key, and instead the algorithm will cause the execution to keep on looping (infinite loop) to find the key. The improvements are done based on the analysis, results and problems found in the simulation of the original algorithm. These improvements aim to reduce the probability of failure of the original algorithm and at the same time maintain the number of messages needed in the whole selection process.

SEARCH PROCESS

The following search process is based on the equations from previous work (Loo, 2002) on which the algorithm is based with modifications . First, the coordinator will calculate the initial delimiter by gathering all the information regarding the smallest key and the largest of each participant's local file by using the following equation:

$$\text{Delimiter} = m + (M - m) * i / p \quad (1)$$

where $1 \leq i \leq p - 1$ and $i = 1$
M: maximum of the key values in the global file
m: minimum of the key values in the global file
p: number of participants involved

After calculating the initial delimiter value, the coordinator sends it to all other participants. Based on this delimiter value, each participant selects a *Pivot[i]* from the key that they generated in the local file, where this key is the biggest key less than or equal to the delimiter and i is and index reference to the participant number. The rank of a key is denoted as *R[i, r]* which is the number of keys that are smaller than the pivot i for participant r. Participant i will send its pivot to other participants, so concurrently there are $p - 1$ recipients for this pivot. Each participant will compare this pivot with all the keys stored in their local file to obtain the rank for it. These ranks will be broadcasted to the other participants sequentially. Each participant will receive p-1 ranks from the other participants. These ranks are summed up to obtain the global rank for its pivot. Global rank is defined by the following equation:

$$G = \sum_{r=1}^{p} R[i,r] \quad (2)$$

If this rank is equal to target rank, j, then the process will end. Otherwise another pivot needs to be generated. At this point, the local file is split into two sub-files based on this criterion. The first sub-file contains all keys that are smaller than its pivot and the second sub-file contains all the keys that are greater than the pivot. The first sub-file is used for the following operations if the global rank, G for the pivot is less than the target rank, j. If the global rank, G for the pivot is greater than the target rank, j, then the second sub-file is used. Note that, the current pivot is not included in both sub-files. A search value is calculated using the following equation:

*New value = old pivot value + (largest key of the sub-file – smallest key of the sub-file) * offset /*

(number of keys in the sub-file) (3)

where $$offset = \frac{(j - \sum_{r=1}^{p} R[i,j])}{p} \quad (4)$$

This new search value is used as a guideline to find the next pivot in the local file. So, if the first sub-file is used, the greatest key in the remaining sub-file, which is smaller or equal to the new search value is chosen as the new pivot, else if the second sub-file

is used, the smallest key in the remaining sub-file, which is greater than or equal to the new calculated value, is identified as the new pivot. The process is repeated until the target key is found.

When the intended target key is found, the participant holding that key will notify the coordinator. Then, the coordinator will stop the search process by breaking the iteration and display the result in an output window.

MODIFICATIONS MADE TO THE ALGORITHM

Three modifications have been made to the algorithm aimed at solving the problem stated in the statement of problem.

Modification 1 placed more restriction on the key values generated by the participants. No key values can be repeated in a local file. This means that the participants cannot generate two same random numbers and store it in the local file. However, the same key value can be repeated in the global file or other participants. Number '0' is treated as a key value like other values. It does not mean nothing or null value to the system.

Modification 2 aims to solve the problem caused by the repeated key that has the same value as the target key in the global file. The second modification made to the system is with regards to finding the rank for a pivot from another participant. As stated in the assumptions, the global ranks for the repeated keys in the global file are not the same. An additional assumption needs to be made here. Let's say, there are two participants namely Client1 and Client2 who have the same key value, k in their local file. If the global rank for k in Client1 is r, then the global rank for k in Client2 is $r + 1$. Generally, for pivot k from participant p, with its global rank being r and let's say there are a few participants $p - n$, where n is a natural number and $n < p$, carrying the same key value as the pivot k, then the global rank for the key value situated in the participant closest to participant p (which means that in $p - n$, for some value n, where $p - n$ is the greatest) is $r - 1$. Now, let's say that there are a few participants $p + n$, carrying the same key value as the pivot k, then the global rank for the key value situated in the participants closest to participant p (which means that in $p + n$, for some value n, where $p + n$ is the smallest) is $r + 1$. For example, let say 104 can be found in Client1, Client3 and Client4. The global rank for 104 in Client 3 is 29, then the global rank for 104 situated in Client1 is 29 – 1 = 28 and the global rank for 104 in Client4 is 29 + 1 = 30.
The algorithm for modification 2 in the client computers is as follows:

receive pivot
check the rank of the pivot
if receiver id > sender id
then set loop to run from the first key until
the last key in the local file
if received pivot >= current test key
then increment counter for rank
increment the loop counter
else end
else
set loop to run from the first key until the last key
in the local file
if received pivot > current test key

then increment counter for rank
increment the loop counter
else end

Modification 3 ensures that a unique pivot is generated each time. A virtual buffer fixed size is used to store the previous value that has been generated. Each time before a new pivot is identified, it is compared to the values in the buffer to make sure that it is unique. The algorithm for modification 3 is as follows:

Calculate new search value based on Eqs (3) and (4)
Select smallest or greatest key that is more than or less than the new search value based on the subfile that will be use as new pivot
Set loop to run from the first key until the last key in the buffer
if new pivot == buffer[counter]
then set same = true
increase index by one
pivot = key[index]
local rank = index + 1
break
increment counter
pivot selected and saved it inside the buffer
local rank = index + 1

THE SIMULATION ENVIRONMENT

At this moment, the improved algorithm developed can only be run in the simulation environment that tries to simulate the following situations where a single broadcast channel connects all participants, a large file is physically distributed among all the participants uniformly. The keys follow a known distribution; in this case they are in uniform distribution and sorted in ascending order. Java programming language is used to implement this simulation. All keys are generated randomly based on the built-in random number generator in Java. Each Java class file represents a peer in the system. All these files are running at the same time from the beginning of the process. There is one coordinator program that coordinates the flow of the whole process. Each Java class file that acts as a peer will generate its own random number and store it in its local file. Then the delimiter and pivots are calculated based on the algorithms stated above.

Both the original and improved algorithm implemented in the simulation only focuses on finding the 30^{th} smallest key in the global file that is being distributed among participants that vary from 2 to 6. The number of participants involved in the search process does not include the coordinator. Each participant holds 30 data that have been generated randomly and sorted at the beginning of the search process. The performance and complexity analysis for both algorithms is measured based on four criteria. They are probability of failure, number of messages needed, number of rounds needed and execution time.

PERFORMANCE MEASUREMENTS

Performance measure has been conducted to compare the performance between the improved algorithm and the original algorithm in various perspectives. These perspectives

are the probability of failure, number of messages needed, and number of rounds needed. Probability of failure studies the likeliness of the algorithm to fail to find the target key in a particular search that will affect the performance of the algorithm in real applications. Number of messages needed measures how many communication messages are needed between the peers in the whole selection process. This can be used as an indicator of the cost needed when this algorithm is run in the real environment. Number of rounds needed measures how fast the algorithm can find the key and it can be used to indicate the time needed for the selection process as more rounds needed indicate that more time is needed.

Probability of Failure

The original algorithm and the improved algorithm might fail in various ways due to the problems that may come from equations like equations (3) and (4) or other factors that have already been mentioned in the previous section. To calculate the probability of failure for both algorithms, each of the algorithms is executed 50 times. The result is shown in Table 1 and *Fig. 1*.

In *Fig. 1*, it is shown that the probability of failure of the improved algorithm is lower than 0.05 compared to the probability of failure of the original algorithm which ranges from 0.1 to 0.3. The average probability of failure of the improved algorithm is 0.032 while in the original algorithm it is 0.192.

It is assumed that failure has occurred when the algorithm cannot find the target key within 20 rounds. The main factor contributing to this is the failure of equation (3). At certain points of execution, the equation may obtain the result for the new pivot that appears to be the previous pivot that has been used, then the next pivot calculated will be exactly the same as the previous pivot too, thus looping occurs and causes failure.

TABLE 1
Probability of failure

Algorithm	Number of participants				
	2	3	4	5	6
Original	0.26	0.18	0.12	0.18	0.22
Improved	0.02	0.04	0.04	0.02	0.04

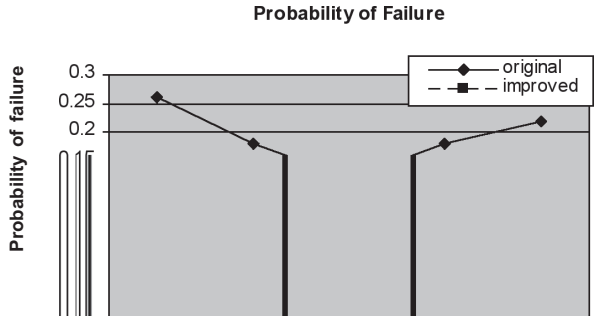

Fig. 1: Probability of failure

For the improved algorithm, the probability of failure is very low and consistent compared to the original algorithm. This improved algorithm is able to avoid the search process from looping by choose another new pivot if the current generated pivot is one that has been used before.

The Number of Messages Needed

The expected number of messages needed is also calculated based on a previous work by Loo (2002). The results are as shown in Table 2 and *Fig. 2.*

TABLE 2
Number of messages needed

Algorithm	Number of participants				
	2	3	4	5	6
Original	10.34	14.64	18.9	22.5	28.46
Improved	12.92	18.76	23.64	30.84	33.58

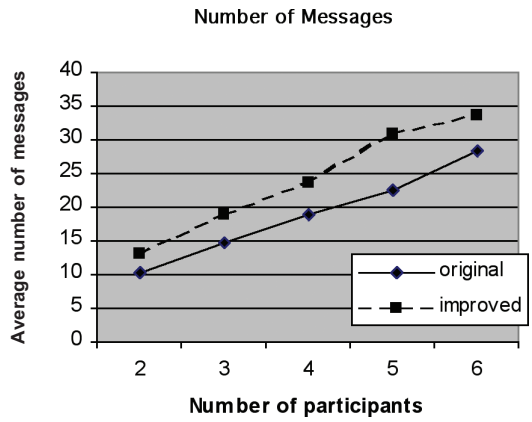

Fig. 2: Number of messages needed

For both algorithms, the number of messages increased as the number of participants increased in the system as shown in *Fig. 2.* This is because when more participants are involved, more messages are passed between them in each round and therefore more data are generated and presented in the global file. So, more pivots needed to be tested before the target key can be found. This increases the number of messages needed.

Depending on the distribution of the data to each participants, it may take more rounds to find a certain key or less than expected and thus, the number of messages needed to find the 30^{th} key is sometimes more or less, but the result is more than expectated most of the time as shown in the graph. However, as shown in the graph, the number of messages needed in the improved algorithm is more than that required in the original version by approximately 2 to 8 messages. This is because the improved algorithm can be run in most cases including cases where the data distribution is quite

complicated. For cases where the data distribution is complicated more messages are needed to find the target key.

Number of Rounds Needed

For both algorithms, the number of rounds needed for completion decreases as the number of participants increases due to the following factors. As stated in the previous section, one round is defined as the time the first participants finishes its turn, followed by the next participant and so on until the last participant. When more pivots are checked in one round, the number of rounds needed to find the target key will be less. The result is shown in Table 3 and *Fig. 3*.

The improved algorithm always utilises more number of rounds taken than the original algorithm. This is because the improved algorithm is successful in almost all types of data distributions. Different types of data distribution require different number of rounds to find the target key, so the average number of rounds taken by the improved algorithm takes into consideration all the different types of data distribution, from simple to complicated ones.

TABLE 3
Number of rounds needed

Algorithm	Number of computers				
	2	3	4	5	6
Original	3.34	3.12	3.04	2.98	2.88
Improved	3.92	3.72	3.46	3.34	3.18

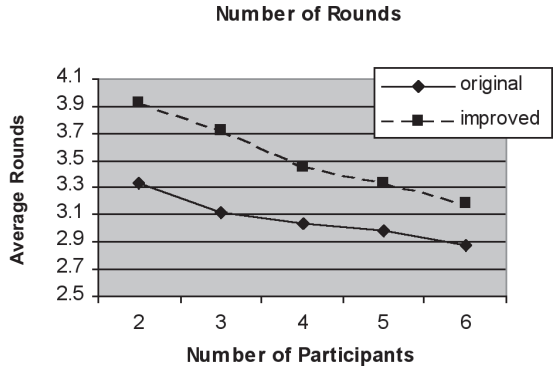

Fig. 3: Number of rounds needed

DISCUSSION ABOUT MODIFICATIONS

In modification 1, no repeated key is allowed in the same local file but it is allowed in the global file. This is because in a distributed system environment especially the distributed database system, the repeated keys are quite common in the whole system where each database system at different sites may have the same keys (data) for the

purpose of data redundancy and reliability. However, there is no point in having the repeated keys in the same local file (database) as the keys in the database should each be unique.

In modification 2, the global ranks for repeated keys in different peers must be unique so that the selection process can be made simple without much execution time wasted in determining which peer is carrying the repeated key to be selected if all repeated keys have the same global rank. Modification 2 aimed to solve this problem by placing each peer in sequence where the global rank of the repeated key in the local file of the peer in lower sequence is smaller than the global rank of the repeated key in the local file of the peer in higher sequence.

In modification 3, when the file is broken up into two sub-files after finding that the pivot is not the target key, the keys in the second sub-file will include the pivot itself while the first sub-file does not include this pivot. In the modification, both sub-files will not contain the current pivot. This is to avoid the problem of selecting the same pivot as the next pivot. As stated in the methodology section, for both the original and improved algorithms, the criteria to find the next pivot depends on which sub-file is going to be used. If the first sub-file is used, then the greatest pivot that is smaller or equal to the search value is chosen, else if the second sub-file is used, then the smallest pivot that is greater or equal to the search value is chosen. This is in contrast with the original methodology provided by Loo (2002), which stated that the smallest key that is greater or equal to the search value is selected as the new pivot for both sub-files. The reason that these changes are made is to ensure that the newly selected pivot comes from the sub-file that is going to be used. The original methodology will lead to a situation where the next pivot selected is the same as the previous pivot.

To eliminate the looping problem, a buffer of size 10 is used. This buffer records the pivot that has already been used. After the new pivot has been selected from the sub-file, it is compared to the values stored in the buffer, if it is the same as one of the previous pivots, then a new value is selected by adding one to the index of the current pivot, and thus the next pivot selected is one that is greater and next in sequence to the current pivot. This will ensure that the pivots selected will always be unique and different.

However, this modification does have some limitations to the system. The modification that has been made in the improved algorithm takes up more space in the memory and requires longer execution time. If the search process takes up more than 10 rounds, then the pivot in the first index of the buffer is overwritten by the next pivot that is going to be recorded in 11^{th} round. Thus, the looping problem still cannot be totally avoided. In this case, the pivot recorded in the first index will be lost and the pivot selected in the future may be equal to the pivot that has been erased from the buffer.

CONCLUSIONS AND FUTURE STUDIES

The improved algorithm has decreased the probability of failure present in the original algorithm. However, some of the added new features in the improved algorithm consume more messages than the original algorithm and some of the cases require more rounds to be complete to find the target key. Although the number of messages and the number of rounds needed has been increased in the improved algorithm, the execution time for both algorithms is almost the same and falls within a certain range for all cases with a different number of participants in the system.

Future studies include further modification of the algorithm to reduce the probability of failure to zero, and select other k^{th} smallest key to compare their performance.

REFERENCES

AGGRAWAL, C., JAIN, N. and GUPTA, P. (1995). An efficient selection algorithm on the pyramid. *Journal of Information Processing Letters, 53,* 37-47.

ALEXANDROS, V., GERBESSIOTIS, CONSTANTINOS and SINIOLAKIS, J. (2003). Architecture independent parallel selection with applications to parallel priority queues, *Theoretical Computer Science, 301,* 119 – 142.

BADER, D. (2004). An improved, randomized algorithm for parallel selection with an experimental study. *Journal of Parallel and Distributed Computing, 64,* 1051-1059.

DECHTER, R. and KLEINROCK, L. (1986). Broad communications and distributed algorithms, *Journal of IEEE Transactions on Computers, C-35*(3), 123-128.

FREDERICKSON, G.N. (1983). Tradeoffs for selection in distributed networks. In *Proceedings of 2nd ACM Symposium Principles Distributed Computing* (pp. 154-160). Montreal, Quebec, Canada.

HAN, Y., PAN, Y. and SHEN, H. (2002). Sublogarithmic deterministic selection on arrays with a reconfigurable optical bus. *IEEE Transaction on Computers, 51*(6), 702 – 707.

HAO, M., MACKENZIE, P. and STOUT, Q. (1992). Selection on the reconfigurable mesh. In *Proceedings of 4th Symposium on the Frontiers of Massively Parallel Computation* (pp. 38-45). McLean, Virginia, USA.

HUANG, J.H. and KLEINROCK, L. (1990). Distributed selectsort sorting algorithms on broadcast communication networks, *Journal of Parallel Computing, 16*(2/3), 183-190.

LOO, A. (2005). Distributed multiple selection algorithm for peer-to-peer systems. *The Journal of Systems and Software, 78,* 234 – 248.

LOO, A., BLOOR, C. and GREY, D. (1997). Complexity analysis of distributed database algorithm. *Proceedings of High Performance Computing in Engineering 97,* Gran Canaria, Spain.

LOO, A. and CHOI, Y.K. (2002). A peer-to-peer distributed selection algorithm for the internet. *Journal of Internet Research: Electronic Networking Applications and Policy, 12*(1), 16-30.

LOO, A., CHUNG, C., FU, R. and LO, J. (1995). Efficiency measurement of distributed statistical sorting algorithms. *Proceeding of Applications of High Performance Computing in Engineering,* Milan, Italy.

LOO, A. and NG, J. (1991). Distributed statistical sorting algorithm. *Proceeding of IEEE Singapore International Conference on Networks(SICON)* (pp. 222-225). Singapore.

MATSUHITA, T.A. (1983). Distributed algorithms for election (Master Thesis, Department of Computer Science, University of Illinois, Urbana, Illinois, USA, 1983).

NEGRO, A and SANTORO, N. (1997). Efficient distributed selection with bounded messages. *Journal of IEEE Transactions on Parallel and Distributed Systems, 8*(4), 397-401.

PAN, Y. (1994). Order statistics on optically interconnected multiprocessor systems. *Proceeding of First International Workshop Massively Parallel Processing Using Optical Interconnections* (pp. 162 – 169).

RAJASEKARAN, S. and WEI, D.S.L. (1997). Designing efficient distributed algorithms using sampling techniques. *Proceedings of 11th International Parallel Processing Symposium (IPPS'97)* (pp. 397-401). Geneva, Switzerland.

RODEH, M. (1982). Finding the median distributively. *Journal of Computer and System Science, 24*(2), 162-167.

SANTORO, N., SIDNEY, J.B. and SIDNEY, S.J. (1992). A distributed selection algorithm and its expected communication complexity. *Journal of Theoretical Computer Science, 100,* 185-204.

SANTORO, N. and SUEN, E. (1989). Reduction techniques for selection in distributed files. *Journal of IEEE Transactions on Computers, 38*(6), 891-896.

SAUKAS, E. and SONG, S. (1988). Efficient selection algorithms on distributed memory computers. *Proceedings of High Performance Networking and Computing,* Orlando, Florida, USA.

SHEN, H. (1991). A universal algorithm for parallel k-selection in hypercubes. *Journal of Parallel Computing, 18,* 139-145.

SHIRIRA, L., FRANCEZ, N. and RODEH, M. (1983). Distributed k-selection: from a sequential to a distributed algorithm. *Proceedings of 2nd ACM Symposium Principles of Distributed Computing* (pp. 143-153). Montreal, Quebec, Canada.

WEGNER, L.M. (1984). Sorting a distributed file in a network. *Journal of Computer Networks, 8,* 451-461.

WEI, D.S.L., RAJASEKARAN, S., CHENG, Z. and NAIK, K. (2002). Efficient selection and sorting schemes using coteries for processing large distributed files. *Journal of Parallel and Distributed Computing, 62,* 1295 – 1313.

WU, C.H. and HORNG, S.J. (2003). Fast and scalable selection algorithms with applications to median filtering. *IEEE Transaction on Parallel and Distributed Systems, 14*(10), 983 – 992.

ISSN: 0128-7680
Pertanika J. Sci. & Technol. **16 (2)**: 189 - 199 (2008)

Molecular Characterization of an Unknown Protein (Acc. No. EU795363) from the ESTs of Oil Palm (*Elaeis guineensis* Jacq.) Cell Suspension Culture

Le Vinh Thuc[1], Huynh Ky[1], Siew-Eng Ooi[2], Suhaimi Napis[1], Zamzuri Ishak[2] and Parameswari Namasivayam[1*]

[1]Department of Cell and Molecular Biology, Faculty of Biotechnology and Biomolecular Sciences, Universiti Putra Malaysia, 43400 UPM, Serdang, Selangor, Malaysia

[2]Malaysian Palm Oil Board, 6 Persiaran Institusi, Bandar Baru Bangi, 43000 Kajang, Selangor, Malaysia

**E-mail: parameswari@biotech.upm.edu.my*

ABSTRACT

A large quantity of ESTs is available from various cDNA libraries of oil palm. The information from oil palm EST databases has been utilized to identify several interesting sequences for molecular characterization. In this study, we report molecular characterization of clone 583 (Acc. No. EU795363) isolated from cell suspension culture of oil palm. This clone is predicted to encode a single major open reading frame for a polypeptide of 177 amino acids with a predicted molecular mass of 19.6 kDa. The predicted amino acid sequence does not contain any signal peptide and transmembrane region. Based on Kyte-Doolittle hydropathy profile, this protein is predicted to be a soluble protein. The predicted ORF of clone 583 was 59% identical to an amino acid sequence of an unknown protein from *Oryza sativa* (Acc. BAD25663). Southern analysis showed that this clone might be a member of a multigene family in the oil palm genome. Gene expression study by real time quantitative RT-PCR showed that transcripts of clone 583 might be present in low abundance.

Keywords: Molecular characterization, unknown protein, oil palm, *Elaeis guineensis*

INTRODUCTION

Oil palm is an economically important plant as it is the second largest source of edible oil in the world. The priority of Malaysia at present is to ensure that the yearly surplus of palm oil is exported to satisfy the growing market demand of oils and fats worldwide which is expected to rise to about 58 million tonnes by 2020 (Yusof and Chan, 2004). The area planted with oil palm in this country increased from 0.06 million hectares in 1960 to 3.5 million hectares in 2001 and is predicted to increase to up to 4.72 million hectares in 2010. With the expansion of the oil palm cultivation areas, palm oil production rose from 91,793 tonnes in 1960 to 11.80 million tonnes in 2001 and is expected to reach 18.81 million tonnes in 2020 (MPOB, 2001). Although there has been an increase in production with the expansion of planted areas, the national yield of oil per hectare does not reflect the technological and scientific advances made in the oil palm industry, especially in breeding, agronomy and other estate management practices (Jalani *et al.* 2002). As the breeding cycle of the oil palm is very long and the progeny of crosses shows

Received : 3 March 2008
Accepted : 13 June 2008
* Corresponding Author

large variations in yield, the palm oil industry has invested in the development of new techniques for multiplying superior parents for seed production and elite progeny palms for commercial planting (Basri *et al.,* 2005). Clonal propagation of oil palm has been studied for many years as a potential way to develop high-yielding collections while circumventing the long generation time required with traditional breeding techniques. The oil palm, *Elaeis guineensis* Jacq., is amenable for vegetative propagation by means of somatic embryogenesis. Cell suspension cultures, initiated at an early stage in embryo development, have been extensively utilized in oil palm micropropagation (Gorret *et al.* 2004; Tarmizi *et al.,* 2004). Tissue culture of oil palm has resulted in the production of elite palms that are uniform with desirable traits and optimum yield. Nevertheless, *in vitro* propagation of oil palm frequently induces a somaclonal variant called the 'mantled' abnormality (Syed-Alwee *et al.,* 2006) which is observed only in palms produced by tissue culture (Jouannic *et al.,* 2005). In addition, the rate of callogenesis from oil palm explants remains low, at about 19% (Corley and Tinker, 2003), while the average rate of embryogenesis from proliferating callus cultures has been reported to be only 6% (Wooi, 1995). To alleviate these problems, markers could be developed at the molecular level to detect callogenesis, embryogenesis and abnormality, making large-scale propagation viable (Low *et al.,* 2006). In this aspect, a large quantity of Expressed Sequence Tags (ESTs) would be an effective first step towards gene discovery and the characterisation of transcription patterns. The EST databases from oil palm projects will facilitate the identification of many important genes. However, there are many unknown genes involved in the regulation of various developmental processes. Unknown genes can represent a significant portion of ESTs, for example, Cooke *et al.* (1996) estimated that only a third of the 5000 non-redundant ESTs corresponded to unknown proteins. In any case, ESTs may be an important means of discovering new biochemical and regulatory pathways (Fristensky *et al.,* 1999). Thus, the aim of this study is to characterize an unknown protein from the ESTs of oil palm cell suspension cultures which may have implications in the tissue culture processes of oil palm.

MATERIALS AND METHODS

Materials

The EST clone 583 was previously isolated from oil palm cell suspension cultures (Ho *et al.*, 2007). The GenBank accession number for this sequence is EU795363. The *in vitro* cultures of oil palm and clone 583 were kindly provided by the Malaysian Palm Oil Board (MPOB). Chemicals used in all experiments were generally obtained from Sigma, Biosciences and MERCK. Primer synthesis and sequencing of DNA were done by First Base Laboratories Sdn. Bhd., Kuala Lumpur, Malaysia.

Sequence Analysis

Sequence analysis was carried out using BLAST 2.0 (Altschul *et al.,* 1997), accessible from the internet (http://www.ncbi.nlm.nih.gov.BLAST). A homology search using the BLASTX algorithm, at the protein level, was carried out by comparing the translated protein sequence with other protein sequences available in the databases. Alignment of the protein sequence with several closely related genes was carried out using the CLUSTAL W (Thompson *et al.,* 1994). Other sequence analyses were conducted using Biology Workbench version 3.2 available at http://biowb.sdsc.edu/CGI/BW.cgi to compute

predicted molecular weight (MW) and isoelectric point (pI) while prediction of transmembrane topology was done using Localizome (Lee *et al.*, 2006). A phylogenetic tree was constructed using the neighbour joining method via MEGA4 package (Tamura et al. 2007). The reliability of the neighbour joining tree was estimated by bootstrap analysis of 1000 replicates.

Southern Blot

Genomic DNA was extracted from young leaves according to the cetyltrimethylammonium bromide method (Murray and Thompson, 1980) and digested with 4 restriction endonucleases, *Hin*dIII, *Not*I, *Eco*RI and *Taq*I (Fermentas), in respective optimal reactions. Digested genomic DNA (30 µg/lane) was separated on 0.7% (w/v) agarose gel in 1 × Tris-borate buffer and then transferred onto a positive-charged nylon membrane Hybond N^+ (Amersham Biosciences) by capillary blotting with 0.4 M NaOH and hybridized overnight with DNA probe. The radioactive DNA probe was prepared using the High Prime reaction mix (Roche), purified 3'UTR PCR product as a template, forward primer (5'-AGAATCTAATCAAGCACCGGCTAC-3') and reverse primer (5'-CCTACCCAGAAA GGAACCGTTTTTA-3') according to the manufacturer's instructions. The hybridization protocol used for Southern analysis was based on the method by Church and Gilbert (1984). The pre-hybridization and hybridization temperature was set at 60°C and hybridizations were carried out for 20 hours. Stringency washes were performed twice in 40mM sodium phosphate buffer (pH 7.4), 1% (w/v) SDS for 5 minutes each at room temperature. The blots were then washed in 40mM sodium phosphate buffer (pH 7.4), 5% (w/v) SDS at the hybridization temperature for 15-20 minutes. The blots were exposed to an imaging plate (FujiFilm) and scanned using a PhosphorImager (FujiFilm FLA5100).

Real Time RT- PCR

Total RNA was extracted from all tissues sampled (leaves, meristems, roots, female flowers, suspension cultures, non-embryogenic calli and embryogenic calli) according to the SDS-phenol/LiCl method (Shizadegan *et al.,* 1991). Two micrograms of total RNA was used for reverse transcription into first-strand cDNA using the Quantitect Reverse Transcription Kit (Qiagen) according to the manufacturer's instructions. All oligonucleotides for TaqMan were designed by Sigma-Proligo (Sigma-Genosys, Sigma-Aldrich Co.). The primer sequences are given in Table 1. All reactions were carried out in three replicates using the ABI Prism 7900 Sequence Detection System and software (PE Applied Biosystems, USA). The PCRs were performed under the following conditions: 2 min at 50°C, 10 min at 95°C, and 40 cycles of 15 sec at 95°C and 1 min at 57°C in 384-well optical reaction plates (Applied Biosystems, USA). A validation graph was generated and PCR efficiency was estimated for each primer pair by using a serial dilution of reverse transcription products and plasmid DNA. The quantity of gene expression in every experimental tissue is expressed relative to the calibrator, suspension culture. PCR reactions contained all components: 100 nM forward and reverse primers, 250 nM TaqMan probe (Table 1), TaqMan Universal PCR Master Mix (Applied Biosystems, USA), in a final volume of 20 µl. The quantification of the relative transcript levels was performed using the comparative C_T method (Livak and Schmittgen, 2001). The transcript levels of the target genes were normalized against the GAPDH gene, an endogenous control, as described in the ABI PRISM 7700 Sequence Detection System user Bulletin #2 (Applied Biosystems).

TABLE 1
Primers and probe sequences for real time RT-PCR

Name	Sequences 5'-3'
GAPDH For	5' - GCCAGCTTTAACATCATTCCTAGC-3'
GAPDH Rev	5' - AGCTTTCCATTTAAGGCAGGAAG-3'
GAPDH PRO	5'-(Tet)CAACAGCCTTGGCAGCACCAGTGC(Tamra)
Clone 583 For	5'-GTTCTTGTGCTTCTTCCGATTGC- 3'
Clone 583 Rev	5'-TGTTAGTAGGGGGAACCGTTAAGG- 3'
Clone 583 PRO	5'-(6-Fam)AGCAGCAGCAGCAAACCCCCAGC(Tamra)

Notes: For: Forward primer, Rev: Reverse primer; PRO: probe

RESULTS AND DISCUSSION

Sequence Analysis

The full sequence of clone 583 is 833 bp in length. This sequence was translated into six possible frames, and the longest ORF was a start codon at position $A_{57}TG$ and a stop codon at position $T_{588}AG$ as shown in *Fig. 1,* which encodes 177-aa (amino acids, aa) protein. The statistics based on amino acid abundance of the predicted protein of clone 583 showed that it consists of lysine (11.79%), serine (11.67%), leucine (9.47%), arginine (8.34%), asparagine (7.29%), phenylalanine (6.64%), glutamine (6.66%), proline (6.44%), glycine (6.29%), threonine (6.60%) and tyrosine (5.08%). The deduced polypeptide had a predicted molecular mass of 19.6 kDa and a theoretical isoelectric point of 7.6. Four potential functional sites are present in this sequence (*Fig. 1*). These are Protein kinase C phosphorylation site, N-myristoylation site, cAMP-and cGMP-dependent protein kinase phosphorylation site and Casein kinase II phosphorylation site. The presence of the potential site for casein kinase II phosphorylation which has a role in the regulation of transcription factor activity is noteworthy (Lin and Hiscott, 1999). The casein kinase II phosphorylation is probably involved in the regulation of metabolic pathways and in the process of cell division and proliferation (Meisner and Czech, 1991). The activities of casein kinase II protein require cAMP-dependent protein kinase as a substrate and a frequent feature of casein kinase II protein phosphorylations is that they are apparently 'silent' as they do not promote any sharp and obvious change of activity (Pinna, 1990).

The results from BLASTX showed that the amino acid sequence of clone 583 is 59% (55/93) identical to an amino acid sequence of an unknown protein (BAD25663), 46% (54/116) identical to a cold induced protein-like (BAB55503) from *Oryza sativa* and 49% (44/89) identical to an unknown cold induced protein from *Deschampsia antarctica* (AAM11916) (*Fig. 2*).

Conserved domain database (CDD, NCBI) search recognized a SIN3 domain from the deduced amino acid sequence of clone 583 (*Fig. 3*). The SIN3 domain is located towards the N'- terminus of the amino acid sequence i.e. from amino acids 43 to 70. SIN3 domain functions as a global transcriptional regulator for a diverse and ever growing set of cellular processes (Silverstein and Ekwall, 2005). It also behaves as a platform for multiple protein complexes that acts as a transcription silencer (Kurita *et al.,* 2007). In yeast, the SIN3 gene encodes a global regulatory factor that has been shown to affect expression of numerous unrelated genes (Slekar and Henry, 1995). In Arabidopsis, a

```
3     CAC GAG AGG CTC CAT ATC CTT CAT CTC TTA GGT TCC AAA GAC CAG   47
48    AAA CCA GGC ATG GGT GAA GAT CTC AGC CAG AGG TTT CAT GGG ATC   92
                  M   G   E   D   L   S   Q   R   F   H   G   I    12
93    CTA CCT TGT GAC GAG GAT GAT GAT GAG CGA CGA GAA TCT TCC TCC   137
13    L   P   C   D   E   D   D   D   E   R   R   E   S   S   S    27
138   TTC TCC GGC GAC TCC GAA GAC GAA GAT TTC AGG GAG GAG GAA ACT   182
28    F   S   G   D   S   E   D   E   D   F   R   E   E   E   T    42
183   TAT TCT CCA AAA TTT CCA CCA CCT TTG GAC AAA ACA ACC TCC TTG   227
43    Y   S   P   K   F   P   P   P   L   D   K   T   T   S   L    57
228   CCA TCA AAA TTC GAT GCA ACT GGG CCT CTC TAC GAT TTA TCC TCC   272
58    P   S   K   F   D   A   T   G   P   L   Y   D   L   S   S    72
273   CTC ACG GCG CAA CTT CCT AGC AAG AGG GGG CTA TCA AAG TAC TAT   317
73    L   T   A   Q   L   P   S   K   R   G   L   S   K   Y   Y    87
318   CAA GGG AAG TCC CAG TCC TTC ACC TCC CTG TCC GAT GTG AGG TGC   362
88    Q   G   K   S   Q   S   F   T   S   L   S   D   V   R   C   102
363   CTC CAG GAT CTG CCT AAG AAA GAG ACT CCC TTC AGA AGG AAG ATG   407
103   L   Q   D   L   P   K   K   E   T   P   F   R   R   K   M   117
408   AAG TCA TGC AAG AGC TAT GCA GGA GGT CTA GAT GGA AGC ACA GAA   452
118   K   S   C   K   S   Y   A   G   G   L   D   G   S   T   E   132
453   TCT AAT CAA GCA CCG GCT ACT TCC AGG AAG ACC AGA TCA AAG AAG   497
133   S   N   Q   A   P   A   T   S   R   K   T   R   S   K   K   147
498   GCG TCA AGA GGT TCT TGT GCT TCT TCC GAT TGC AAG CAG CAG CAG   542
148   A   S   R   G   S   C   A   S   S   D   C   K   Q   Q   Q   162
543   CAA ACC CCC AGC TAT TCC TGT ACG AAA GGG ATT TTT GTC TCC ACT   587
163   Q   T   P   S   Y   S   C   T   K   G   I   F   V   S   T   177
588   TAA ATT TCA TGG ACA TAA AAA AGC CCT TAA CGG TTC CCC CTA CTA   632
      *
633   ACA TTA TAT TTT AGG ATT TTT AAA AGA AGA AGA AAG CCG GGG AGG   677
678   GAT GCA TGG TGG TCC GAG GTT TTC CTT TTG TAA TTC GGT GGG CCA   722
723   ATC CTT TAT TTA AAA ACG GTT CCT TTC TGG GTA GGG GTA AAA AAA   767
768   AAA AAA AAA ATT TTT TGG GGG GGG AAA GGT TTT TTC CAA GGC CAA   812
813   AAA AAA AAA AAA AAA AAA AAA   833
```

Fig. 1: The nucleotide and deduced amino acid sequences of clone 583. Predicted start and stop codons are in bold. Putative functional sites are indicated by underlines/italics and box: Protein kinase C phosphorylation site (aa6-8, aa44-46, aa79-81, aa119-121, aa139-141, aa140-142, aa145-147), N-myristoylation site (aa11-16, aa125-130, aa126-131, aa129-134, aa151-156, aa172-177), cAMP-and cGMP-dependent protein kinase phosphorylation sites (aa22-25, aa108-111, aa146-149), Casein kinase II phosphorylation site (aa32-35, aa59-62, aa96-99). The polyadenylation signal is shaded

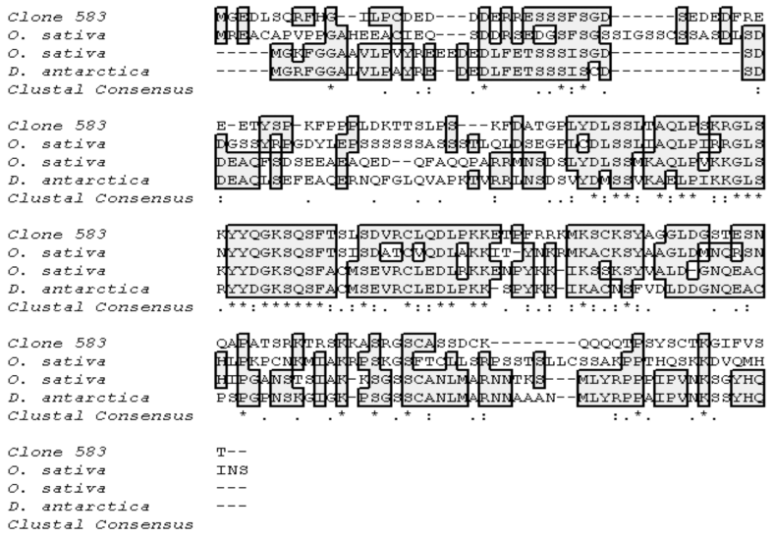

Fig. 2: Amino acid sequence alignment of clone 583 with an unknown protein (BAD25663; second sequence from top), a cold induced protein-like (BAB55503; third sequence) from O.sativa *and an unknown cold induced protein (AAM11916) from* D. antarctica. *Dashed lines are gaps introduced to maximize alignments. The conserved residues are highlighted. * represent those that are highly conserved*

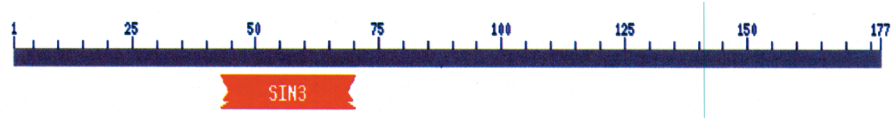

Fig. 3: Location of SIN3 domain (from amino acids 43 to 70) that was recognized based on deduced amino acid sequence of clone 583 using NCBI-CDD program

Sin3-like protein was indicated to effect on a transcription factor which may be a part of a transcriptional repressor complex (Song *et al.*, 2005).

The Localizome program predicts the deduced protein of clone 583 to be an extracellular protein (*Fig. 4a*). According to Bishop-Hurley *et al.* (2003) some extracellular proteins may be involved in the process of initiation and termination of cell wall expansion that occurs during somatic embryogenesis. The Kyte Doolitle hydropathy profile for clone 583 showed that it was predicted to be a soluble protein (*Fig. 4b*). Most of the soluble proteins found in carrot suspension culture were suggested to play important roles in regulating gene expression during somatic embryogenesis (Nomura and Komamine, 1986).

A neighbour-joining tree consisting of clone 583 and similar members identified from Genbank with scores above 80 is shown in *Fig. 5*. This predicted protein is clustered with the OsI006314 protein which was predicted to be involved in cell adhesion but bootstrap value was not determined. According to Doyle and Gaut (2000), a bootstrap value of 70-80% is often taken to indicate strong support for a cluster of sequences. This

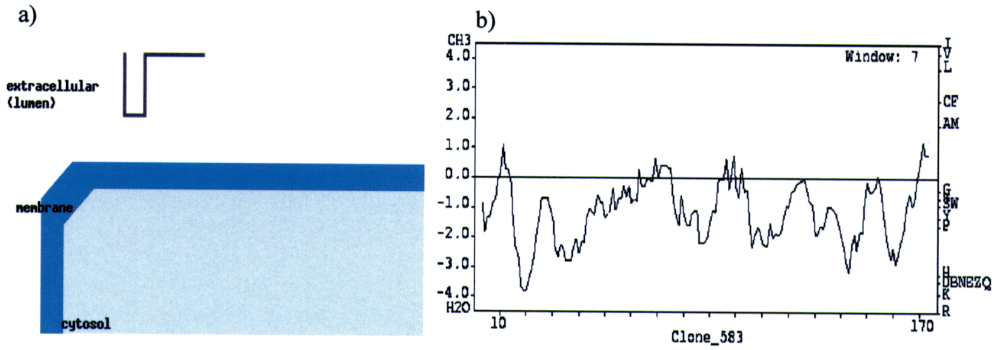

Fig. 4: a) Prediction of transmembrane topologies of clone 583 using Localizome b) Kyte Doolittle hydropathy profile of clone 583

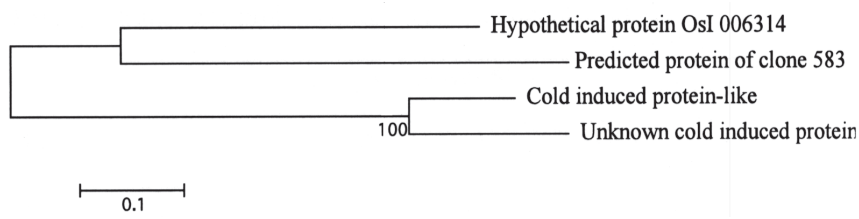

Fig. 5: A neighbour-joining tree displaying the phylogenetic relationship of predicted protein of clone 583 to hypothetical protein OsI006314 (EAY85081) and cold induced protein-like (BAB55503) from O. sativa *and unknown cold induced protein (AAM11916) from* D. antarctica. *Bootstrap values are indicated for each branch divergence of 1,000 replicates. Undermined bootstrap values are not shown*

gene is not the same cluster as cold induced protein-like from rice and unknown cold induced protein from *D. antarctica.*

Southern Hybridization

To examine the genomic organization of clone 583 gene in oil palm, genomic DNA blot analysis was performed using a 310 bp fragment at 3'UTR region as probe. Genomic DNA was isolated from oil palm leaves and digested with four restriction enzymes. These restriction sites were not found within the probe sequence, therefore, the expected results were one fragment hybridizing to the probe, should it be a single copy gene. However, there were two fragments each from *Taq*I-digestion and *Eco*RI-digestion that hybridized to the probe (*Fig. 6a*). These extra bands could be due to the presence of introns. To confirm that there is no intron within the 3'-UTR region, this region was amplified using oil palm genomic DNA as the template. The PCR product (*Fig. 6b*) and sequencing result (data not shown) verified that there is no intron within the 3'-UTR used as the probe for Southern hybridization. Therefore, the additional bands hybridizing to the probe were possibly due to the presence of multiple copies of clone 583 in the oil palm genome.

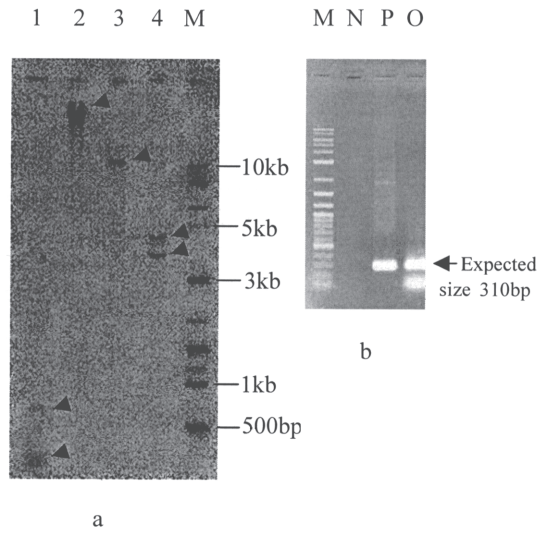

Fig. 6: a) Southern blot analysis with 3'UTR region of clone 583 as probe on oil palm genomic DNA digested with TaqI (1), NotI (2), HindIII (3) and EcoRI (4), M: 2-log marker; b) PCR analysis of 3'UTR of clone 583 using cDNA (P) and oil palm genomic DNA (O) as templates, N: negative control

Real Time Quantitative RT-PCR

The results from *Fig. 7a* show that the housekeeping gene, GAPDH, was amplified with nearly 100% amplification efficiency (slope = - 3.35, R^2=0.99). These results indicated that the tested sample used in this experiment was qualified. However, using the same sample (first strand cDNA of cell suspension culture), amplification of clone 583 was not detected, although amplification of the target from the plasmid DNA of clone 583 showed nearly 100% amplification efficiency (slope = - 3.33, R^2=0.99) (*Fig. 7b*). Even though this cDNA was isolated from cell suspension cultures, the qPCR results suggested that the transcripts of clone 583 might be produced at other stages of cell suspension culture than the suspension culture used in this qPCR experiment or was present at levels too low to be detected. Most genes involved in the regulation of developmental pathways are normally expressed at very low abundance levels in the cells, such as DcSERK. DcSERK was found to be expressed at low levels during carrot embryogenesis with expression ceasing after the globular stage (Schmidt *et al.* 1997).

Gene expression studies by real time quantitative RT-PCR suggested that expression levels of clone 583 were either too low to be detected or absent in all samples tested (Table 2). Hence, this gene may be a low abundant gene in oil palm or requires a specific induction signal for expression. According to Zhang (2003) plant regulatory factors are mainly responsible for selectivity in gene regulation, and are often expressed in a tissue-specific, developmental-stage-specific or stimulus-dependent manner. This could be the scenario for clone 583 transcripts.

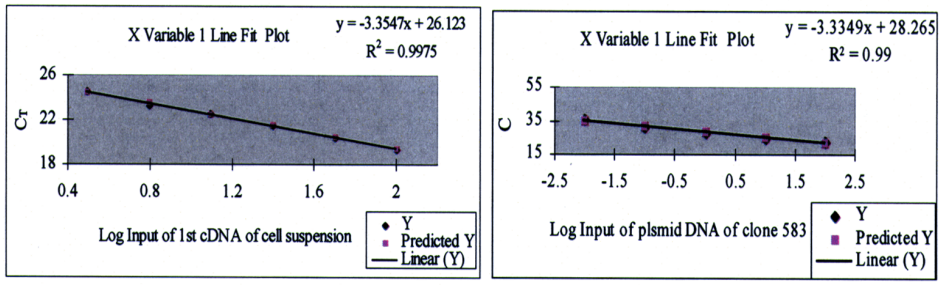

Fig. 7: Real time PCR results indicating the PCR efficiencies of: (a) the housekeeping GAPDH primers in a dilution series of first strand cDNA of cell suspension culture and (b) the target 583 primers in a dilution series of plasmid DNA of clone 583

TABLE 2
C_T values of GAPDH and target 583 gene on different tissues

Tissues	C_T values	
	GAPDH	Target gene
E	19.99557 ± 0.097	Undetermined
L	19.82735 ± 0.150	Undetermined
FF	19.61802 ± 0.147	Undetermined
M	20.10332 ± 0.108	Undetermined
N	19.77532 ± 0.091	Undetermined
SC	19.45607 ± 0.139	Undetermined
R	20.00530 ± 0.102	Undetermined

Notes: E: embryogenic calli, L: leaves, FF: female flowers, M: meristem, N: non-embryogenic calli, SC: suspension culture and R: roots

CONCLUSIONS

In this study, we report the characterization of a novel protein of clone 583, which is highly similar to an unknown protein from rice. Clone 583 might be a transcription factor involved in gene regulation in cell suspension cultures of oil palm. This gene may be a member of a multigene family in the oil palm genome. In future, the functional study of clone 583 should be conducted to understand the role of this gene in the cell suspension process.

ACKNOWLEDGEMENTS

This work was supported by the Ministry of Science, Technology and Innovation (MOSTI) under the Intensified Research for Priority Areas (IRPA), Grant No. 01-02-04-0387-PR0015/07-02.

REFERENCES

Altschul, S.P., Madden, T.L., Schaffer, A.A., Zhang, J., Zhang, Z., Miller, W. and Lipman, D.J. (1997). Gapped BLAST and PSI-BLAST: a new generation of protein database search programs. *Nucleic Acids Research, 25,* 3389-33402.

Basri, M.W., Siti Nor Akmar, A. and Henson, I.E. (2005). Oil palm-achievements and potential. *Plant Prod. Sci., 8,* 288-297.

Bishop-Hurley, S.L., Gardner, R.C. and Walter, C. (2003). Isolation and molecular characterization of genes expressed during somatic embryo development in Pinus radiate. *Plant Cell, Tissue and Organ Culture, 74,* 267-281.

Church, G.M. and Gilbert, W. (1984). Genomic sequencing. *Proceedings of the National Academy of Sciences USA, 81,* 1991-1995.

Cooke, R., Raynal M., Laudie, M., Grellef, F. and Delseny, M. et al. (1996). Further progress towards a catalogue of all Arabidopsis genes analysis of a set of 5000 non-redundant ESTs. *Plant Journal, 9,* 101-124.

Corley, R.H.V. and Tinker, P.B. (2003). Vegetative propagation and biotechnology. In (4th eds) *The Oil Palm* (p. 201-215). Oxford: Blackwell Science Ltd.

Doyle, J.J. and Gaut, B.S. (2000). Evolution of genes and taxa: A primer. *Plant Molecular Biology, 42,* 1-23.

Fristensky, B., Balcerzak, M., He, D. and Zhang, P. (1999). Expressed sequence tags from defense response of *Brassica napus to Leptosphaeria maculans. Molecular Plant Pathology Online* www.bspp.org.uk/mppol/1999/0301FRISTENSKY.

Gorret, N., bin Rosli, S.K., Oppenheim, S.F., Willis, L.B., Lessard, P.A., Rha, C. and Sinskey, A.J. (2004). Bioreactor culture of oil palm (*Elaeis guineensis*) and effects of nitrogen source, inoculum size, and conditioned medium on biomass production. *Journal of Biotechnology, 108,* 253-263.

Ho, C.L., Kwan, Y.Y., Choi, M.C., Tee, S.S. and Ng, W.H. et al. (2007). Analysis and functional annotation of expressed sequence tags (ESTs) from multiple tissues of oil palm (*Elaeis guineensis* Jacq.) *BMC Genomics, 8,* 381.

Jalani, B.S., Yusof, B., Ariffin, D., Chan, K.W. and Rajanaidu, N. (2002). Prospects of elevating national oil palm productivity: a Malaysian perspective. *Oil Palm Industry Economic Journal, 2,* 1-9.

Jouannic, S., Argout, X., Lechauve, F., Fizames, C., Borgel, A., Morcillo, F., Aberlenc-Bertossi, F., Duval, Y. and Tregear, J. (2005). Analysis of expressed sequence tags from oil palm (*Elaeis guineensis*). *FEBS Letters, 579,* 2709-2714.

Kurita, M., Suzuki, H., Kawano, Y., Aiso, S. and Matsuoka, M. (2007). CR/periphilin is a transcriptional co-repressor involved in cell cycle progression. *Biochemical and Biophysical Research Communications, 364,* 930-936.

Lee, S., Lee, B., Jang, I., Kim, S. and Bhak, J. (2006). Localizome: a server for identifying transmembrane topologies and TM helices of eukaryotic proteins utilizing domain information. *Nucleic Acids Res., 34,* 99-103.

Lin, R. and Hiscott, J. (1999). A role for casein kinase II phosphorylation in the regulation of IRF-1 transcriptional activity. *Mol. Cell Biochem., 191,* 169-180.

Livak, K.J. and Schmittgen, T.D. (2001). Analysis of relative gene expression data using real-time quantitative PCR and the 2(-Delta Delta $C_{(T)}$) Method. *Methods, 25,* 402-408.

Low, E.T.L, Tan, J.S, Chan, P.L, Boon, S.H. and Wong, Y.L. et al. (2006). Developments toward the application of DNA chip technology in oil palm tissue culture. *Journal of Oil Palm Res.,* 87-98.

Meisner, H. and Czech, M.P. (1991). Phosphorylation of transcriptional factors and cell-cycle-dependent proteins by casein kinase Il. *Curr. Opin. Cell Biol., 3,* 474-483.

MPOB. (2001). *Oil Palm Statistics* (21st edn). Bangi: MPOB Press.

Murray, M.G. and Thompson, W.F. (1980). Rapid isolation of high molecular weight plant DNA. *Nucleic Acids Res., 8,* 4321-4325.

Nomura, K. and Komamine, A. (1986). Somatic embryogenesis in cultured carrot cells. *Develop. Growth and Differ., 28,* 511-517.

Pinna, L.A. (1990). Casein kinase 2: an 'eminence grise' in cellular regulation? Biochim. *Biophys. Acta, 1054,* 267-284.

Schmidt, E.D.L., Guzzo, F., Toonen, M.A.J. and de Vries, S.C. (1997). A leucine-rich repeat containing receptor-like kinase marks somatic plant cells competent to form embryos. *Development, 124,* 2049-2062.

Shizadegan, M., Christie, P. and Seemann, J.R. (1991). An efficient method for isolation of RNA from tissue cultured plant cells. *Nucleic Acids Res., 19,* 6055.

Silverstein, R.A. and Ekwall, K. (2005). Sin3: a flexible regulator of global gene expression and genome stability. *Curr. Genet., 47,* 1-17.

Slekar, K.H. and Henry, S.A. (1995). SIN3 works through two different promoter elements to regulate INOl gene expressionin yeast. *Nucleic Acids Res., 23,* 1964-1999.

Syed-Alwee, S., Van der Linden, C.G., Van der Schoot, J., de Folter, S. Angenent, G.C., Cheah, S.C. and Smulders, M.J.M. (2006). Characterization of oil palm MADS box genes in relation to the mantled flower abnormality. *Plant Cell, Tissue and Organ Culture, 85,* 331-344.

Tamura, K., Dudley, J., Nei, M. and Kumar, S. (2007). MEGA4: Molecular Evolutionary Genetics Analysis (MEGA) software version 4.0. *Molecular Biology and Evolution, 24,* 1596-1599

Tarmizi, A.H., Norjihan, M.A., Zaiton, R. (2004). Multiplication of oil palm suspension cultures in a bench-top (2-litre) bioreactor. *Journal of Oil Palm Research, 16,* 44-49.

Thompson, J.D., Higgin, D.G. and Gibson, T.J. (1994). CLUSTAL W: improving the sensitive of progressive multiple sequence alignment through sequence weighting, position specific gap penalties and weight matrix choice. *Nucleic Acids Research, 22,* 4673-4680.

Wooi, K.C. (1995). Oil palm tissue culture - current practice and constraints. In Rao, V., Henson, I.E. and Rajanaidu, N. (Eds), *Recent Developments in Oil Palm Tissue Culture and Biotechnology* (p. 21-32). Bangi: MPOB Press.

Yusof, B. and Chan, K.W. (2004). The oil palm and its sustainability. *Journal of Oil Palm Research, 16,* 1-10.

Zhang, J.Z. (2003). Overexpression analysis of plant transcription factors. *Curr. Opin. in Plant Biology, 6,* 430-440.

Song, C.P., Agarwal, M., Ohta, M., Guo, Y., Halfter, U., Wang, P. and Zhua, J.K. (2005). Role of an arabidopsis AP2/EREBP-Type transcriptional repressor in abscisic acid and drought stress responses. *The Plant Cell, 17,* 2384-2396.

ISSN: 0128-7680
Pertanika J. Sci. & Technol. **16 (2)**: 201-212 (2008)

Cold Flow Binary Fluidization of Oil Palm Residues Mixture in a Gas-Solid Fluidized Bed System

Fauziah, M.[1*], Norazah, A.R.[1], Nornizar, A.[1], Azil Bahari, A.[1] and Tajuddin, M.J.[2]
[1]Faculty of Chemical Engineering, Universiti Teknologi MARA,
40450 Shah Alam, Selangor, Malaysia
[2]Faculty of Mechanical Engineering, Universiti Teknologi MARA,
40450 Shah Alam, Selangor, Malaysia
**E-mail: fauziah176@salam.uitm.edu.my*

ABSTRACT

Fluidized bed gasification of biomass is a promising technology. However, significant development work is required before large-scale implementation can be realized. In this work, binary mixture fluidization of silica sand and oil palm residues were accomplished to visualize the fluidization behavior of the mixture in a cold rig. The most critical characteristics for biomass gasifier operation, the minimum (U_{mf}) and complete (U_{cf}) fluidization velocity of the mixtures were determined. The mixtures were prepared by adding 70%$^{w/w}$, 75%$^{w/w}$, 80%$^{w/w}$, 85%$^{w/w}$, 90%$^{w/w}$ and 95%$^{w/w}$ of silica sand to palm kernel shell and/or palm pressed fiber. Experiments were performed in a 0.15 m diameter by 1.0 m height cylindrical column gas-solid fluidized bed system, at a constant 3 kg bed weight. The mixture was pre-mixed before being fed in to the column. The U_{cf}/U_{mf} ratio was found to decrease with increasing weight percentage of palm kernel shell in the mixture while the ratio increased as the weight percentage of palm pressed fibre increased in the mixture. It was also observed that segregation was reduced when the content of silica sand was increased in the binary mixture.

Keywords: Binary mixture, minimum fluidization velocity, complete fluidization velocity, segregation

INTRODUCTION

Fluidization is the principal process that governs gasification technology. The fluidization characteristics of biomass materials are very important for the modelling and design of the reactors (Sun *et al.*, 2005). However, reported values of fluidization hydrodynamics for biomass are scarce (Gomez and Lora, 1995). As stated by Sadaka *et al.* (2002), most works done on biomass gasification did not include the hydrodynamic parameters.

The most important aspects in fluidization hydrodynamics are minimum fluidization velocity and pressure drop across the bed. The minimum fluidization velocity of biomass particles is important for the preliminary sizing in designing the biomass gasifier. As an example, the gasifier diameter can be calculated by using an estimation of the superficial gas velocity which is often related to the minimum fluidization velocity of the bed (Enden and Lora, 2004).

Oil palm residues are wastes that can be turned into gold when appropriate process is applied to extract energy. Looking at the prospects, gasification of oil palm residues

Received : 3 March 2008
Accepted : 8 April 2008
* Corresponding Author

is the most suitable and promising technology which can be exploited in Malaysia. It is a common practice in gasification process where silica sand is used as a starting 'burning' material, in which the heated fluidizing silica sand is used to gasify the biomass supplied to the reactor. Hence, the purpose of this study is to investigate the fluidization behaviour of oil palm residues when fluidized with silica sand in order to understand and predict the gasification process.

THEORY

Pressure Drop Across the Bed

According to Geldart (1986), pressure drop across the bed is the only parameter that can be predicted accurately. Then, a dimensionless index for fluidization was adopted (Marring *et al.,* 1994), where ratio between experimental and theoretical pressure drop was calculated. The Fluidization Index, FI, is defined as:

$$FI = \frac{\Delta PA}{0.1M_B} \quad [1]$$

where M_B is mass of solid in bed, ΔP is pressure drop across the bed and A is the cross-sectional area of the bed.

Definitions of Minimum and Complete Fluidization Velocity for Mixture

Determination of minimum fluidization velocity, U_{mf}, is a complex process when binary mixtures are involved in the fluidization process. Peculiarities in sizes, shapes and densities of biomass particles are the main contributors for this complexity.

There are numerous discussions on determination of the minimum and complete fluidization of binary mixtures. For a monodisperse system, U_{mf} is defined as the superficial velocity at which the packed bed becomes a fluidized bed. According to Chiba *et al.* (1971) (Nienow and Chiba, 1985) fluidization of a binary particles system can be divided into three categories; (a) perfect segregation; (b) partial mixing; (c) perfect mixing; as illustrated in *Fig. 1(i)*. Binary mixtures involve two components with the same or different properties. Component 1 will have a lower Umf compared to component 2. Components 1 and 2 will fluidize at U_F and U_P respectively. F and P refer to more and less fluidizable components. When the mixture is fluidized at U>>Up, and then U is reduced at a steady rate to zero (the defluidizing procedure), the settled bed will generally have one of the three mixing-segregation states. When more fluidizable particles are in large proportion in the mixture, superficial gas velocity will be close to U_F (Delebarre *et al.*, 1994).

For mixtures with small difference in size and equal density components, a good mixture may be obtained throughout the bed regardless of the defluidizing procedure. $\Delta P/\Delta P_{fluidized}$ against superficial gas velocity, U provides a unique measure of minimum fluidization velocity, U_M.

If one component is bigger and more dense than the other, the system remains completely segregated independent of the defluidizing procedure as illustrated in *Fig. 1(i)(a)*. In this case, $\Delta P/\Delta P_{fluidized}$ plotted against U will be the sum of contributions from the pure components (*Fig. 1(ii)(a)*). However, in order to obtain U_{mf} value, some special definition must be adopted, since at $U_F<U<U_P$, the upper part of the bed is well fluidized

while the bottom is packed. The U_{mf} is obtained from the velocity at the intersection of the two extrapolated linear portions of the plot corresponding to the regions where the whole bed is first, fluidized ($U>U_P$) and second, packed ($U<U_F$). This apparent minimum fluidization velocity is shown as U_S.

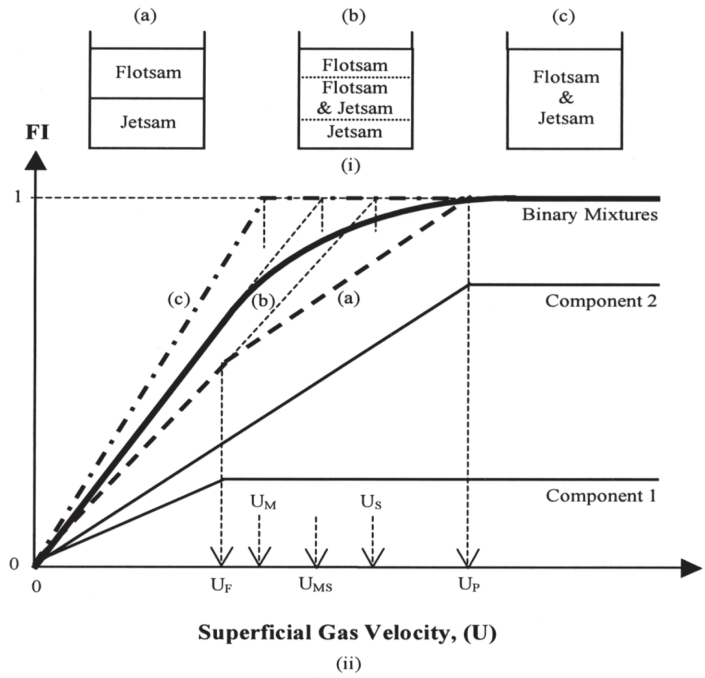

Fig. 1: Relationship between bed pressure drop and gas velocity for fluidization of binary particles system

Generally, the upper part of the bed is flotsam-rich, the lower jetsam-rich and there is a mixed region in the middle as shown in *Fig. 1(i)(b)*. Ongoing from U_P to U_F, a steadily decreasing amount of the bed will be fluidized, but as long as at least some of it is still fluidized, particle rearrangement can occur. If defluidization is slow and the species differ in density, *Fig.1(i)(b)* will tend towards *Fig. 1(i)(a)*. If the species only differ in size and defluidization is rapid, *Fig. 1(i)(b)* will tend towards *Fig. 1(i)(c)*. In each case, FI versus U will in general be as shown in *Fig. 1(ii)(b)* with U_{MS} being a function of the defluidization procedure.

The common graphical representation for minimum fluidization velocity, U_{mf} in ΔP versus U curve is defined as corresponding to the intersection of the fully fixed and fully fluidized straight lines. Formisani (1991) suggests obtaining the value of the minimum fluidization velocity at increasing velocities for a perfect mixed initial state rather than during defluidization when segregation may occur. Work from Pilar Aznar *et al.* (1992) observed U_{mf} as common graphical presentation and U_{cf} by observation at which the entire bed (biomass and second solid) is in motion, independently of where this velocity starts or whether or not all the biomass is segregated in the upper or lower part of the bed, or the movement of the biomass is different (small plugs, for example) from the movement of the second fluidizing solid. Rao and Bheemarasetti (2001) obtained the

minimum fluidization velocity from the intersecting point of the defluidization curve with the constant pressure line. Patil *et al.* (2005) determined U_{mf} at the point where the pressure drop across the fluidizing bed became constant.

MATERIALS AND METHODS

Sample Pre-treatment

Biomass sample was dried using a MEMMERT GmbH universal oven model g604.0435 to achieve biomass moisture content to be below 10-20% for gasification (Cummer and Brown, 2002). The oven-drying was performed according to technical specification CEN TC335 Solid Biofuels (Samuelsson *et al.*, 2006). The temperature of the oven was set to 1050C and left to be dried for 24 hours. Moisture content in the biomass sample was measured by using Precisa moisture analyzer, model XM 60 before and after oven-drying. Oil palm biomass was then ground to particle size by using the Retsch cutting mill model SM 100 with a bottom sieve of perforation size of 2 mm. Silica sand used in the experiment was sieved and separated. The mean particle size of the sand used in this work was 287.5 μm. This size range was chosen as the most suitable for the pilot plant gasifier as proven in the work done by Pilal Aznar *et al.* (1992). Table 1 shows the properties of materials used as the feed to the fluidized bed and *Fig. 2* exhibits photos of oil palm residue when received and after pre-treatment processes.

FLUIDIZATION

Fig. 3 shows the experimental set-up of the fluidized bed and the apparatus comprises of a 150 mm diameter Perspex tube 1000mm in height. The distributor was made from PVC with 36 holes, 8mm in diameter each. A layer of gauze cloth was placed over the distributor. The top end of the Perspex tube was covered with filtration material to prevent the particles from elutriating out. A transparent scale was attached on the bed wall to provide direct bed expansion measurement. Air at ambient temperature and with a relative humidity of 50% was used as the fluidizing agent and was supplied from a 0.5hp blower.

TABLE 1
Properties of materials used in the experiment

Material	Mean Diameter (μm)	Bulk Density, ρ_b (kg/m^3)	Particle Density, ρ_p (kg/m^3)	Voidage, ε_{mf}	Geldart's Classification
Palm Kernel Shell	1425	150	398.7	0.62	B
Palm Pressed Fibre	675	73*	407.4*	0.82	A
Silica Sand	287.5	554	1086.8	0.49	B

*Values taken from Abdullah *et al.* (2003)

(a)

(b)

Fig. 2: (a) Palm kernel shell as received; (b) Palm pressed fibre as received

Oil palm residues used in this experiment were taken on weight basis and the mixture studied contains 5, 10, 15, 20, 25 and 30 weight percent of oil palm residues. The total weight of oil palm residues and silica sand in the bed was kept constant at 3 kg in all experiments. Sand and oil palm residues were weighed according to their respective percentage. Random mixture method is chosen in this work where a Z-blade mixer was used to randomly mix the pre-weighed oil palm residues and silica sand for a period of 10 minutes to ensure uniformity for all the mixtures prior to feeding into the Perspex tube. Air was passed to the bed increasingly from zero to fluidization stage (when all

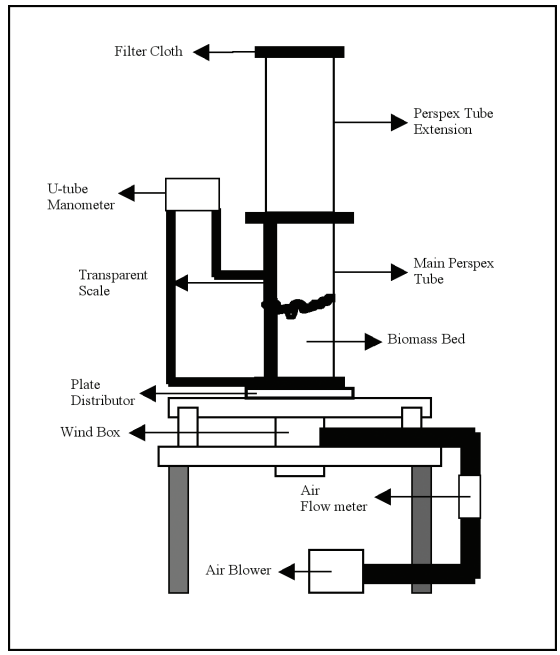

Fig. 3: Schematic diagram of fluidized bed apparatus

particles in the bed move vigorously). Two ranges of air velocity were set; 0-19 cm/s and 0-29 cm/s for mixtures of palm kernel shell or palm pressed fibres with silica sand respectively. Then, the gas flow rate was gradually decreased (defluidization stage). At each gas flow rate, either in fluidization or defluidization stage, the pressure loss across the bed and the bed height was recorded. The important parameters, minimum fluidization velocity, U_{mf} and complete fluidization velocity, U_{cf} were observed and recorded. All of the experiments were repeated at least three times to ensure reproducibility.

RESULTS AND DISCUSSION

Fluidization Behaviour

Palm pressed fibre is considered as polydisperse material which has wide particle size distributions. Each of the fractions has their own U_{mf} (Reina *et al.*, 2000). When fluidized with silica sand (jetsam), palm pressed fibre (flotsam) will move to the upper bed. At $U_{mf}<U<U_{cf}$, fraction of smaller flotsam will elutriate out from the bed and some of it will stick to the wall of the Perspex tube extension. However, most of the particles will circulate back into the bed since the fluidization column is covered with a filter cloth. These fractions of particles fluidize vigorously in their own region at the upper part of the bed without any mixing with silica sand. Larger fraction of flotsam is observed to mix and segregate simultaneously.

Figs. 4 and *5* display the profile of the dependency of pressure drop across the bed to superficial gas velocity of the mixture of 85% silica sand and 15% palm pressed fibre

and palm kernel shell respectively. From the graphs, the mixture of palm pressed fibre and silica sand show that complete fluidization occurs at FI value of 1.3, which is higher than FI indicated in complete fluidization for mixture of palm kernel shell and silica sand (FI = 1.2). This is probably due to high interparticle forces in palm pressed fibre particles where a higher pressure drop and superficial gas velocity are noticeable for the mixtures to reach complete fluidization. It was observed that the palm pressed fibre has high tendency to stick to the column wall which indicates the presence of high electrostatic charge. The charges build-up resulting in particle agglomeration causing stagnant spots in the bed, which later increase the value of U_{mf} and subsequently U_{cf}. These charges were generated as a result of repeated particle contact and separation, supplemented by the friction of particles rubbing against each other and the column wall (Mehrani *et al.*, 2007). High electrostatic charge also was suspected to contribute to the limitation of fluidization capabilities of palm pressed fibre mixture where the bed can only be fluidized if the fibre content is less than 20 weight percent of the total bed weight. Fluidizing mixture of palm pressed fibre with higher than 20 weight percent results in the formation of channels across the bed, and later the formation of vertical rat hole from the bottom to the surface of the bed. The rat hole became bigger as U increased and the palm pressed fibre starts to be blown out of the column. As for the fluidization of the palm kernel shell and sand mixture, segregation is observed to be more visible. This is probably due to its free-flowing nature of ground palm kernel shell, where fluidization occurs up to 30 weight percent of residues in the bed.

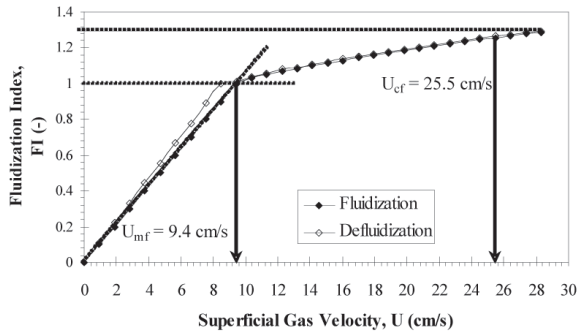

Fig. 4: Fluidization index versus superficial gas velocity for mixture of 85% silica sand and 15% palm pressed fibre

According to Cheung *et al.* (1974), segregation through percolation occurs if packing arrangements that allow the smaller spheres to pass through the other particles are between $\frac{d_s}{d_B}$= 0.417 for the loosest packing and $\frac{d_s}{d_B}$= 0.154 for closest packing. In this experiment, binary mixtures of silica sand and palm kernel shell and silica sand and palm pressed fibre have $\frac{d_s}{d_B}$ values of 0.201 and 0.426 respectively. In both cases, segregation is visually observed to be more severe when silica sand content is reduced in the mixture. However, no indicative measurement was done to investigate the mixing/segregation phenomena in this work.

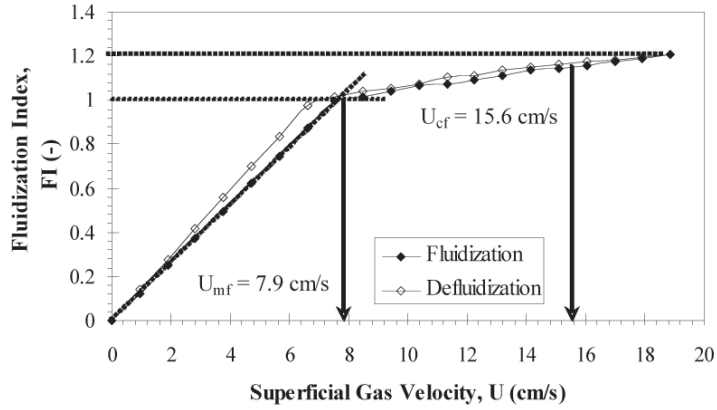

Fig. 5: Fluidization index versus superficial gas velocity for mixture of 85% silica sand and 15% palm kernel shell

Determination of U_{mf} and U_{cf}

Figs. 4 and *5* are typical plots of fluidization and defluidization curves for mixtures of oil palm residue and silica sand. As shown in both figures, U_{mf} values are taken at the intersection of fluidization curve from point 0 and FI equals to 1. During this time, the upward drag force exerted by the gas on the particles is equal to the apparent weight of particles in the bed. Theoretically, the particles will be lifted up by the gas, the separation of the particles increases and bed becomes fluidized. This is observed by the commencing of bubbles or expansion of the bed according to their respective group of powders classified prior to the experiment. U_{cf} is determined when all the particles in the bed are observed to move (Pilar Aznar *et al.*, 1992; Patil *et al.*, 2005). Both the U_{mf} and U_{cf} values for fluidization of the palm kernel shell mixture were found to be smaller than for the palm pressed fibre. This result is as expected as both the U_{mf} and U_{cf} are heavily affected by physical characteristics of the fluidizing materials used. As discussed in section 4.2, the palm kernel shell behaves as free-flowing particles and hence contributes to less particle-particle interactions in the bed, which results in smaller U_{mf} and U_{cf}. Meanwhile, physical characteristics of palm pressed fibre results in higher velocity needed to break the interparticle forces of the fibrous materials (Fauziah *et al.*, 2006).

As can be seen in *Fig. 4*, the defluidization curve is almost the same as the fluidization curve when $U_{mf}<U<U_{cf}$. A dynamic equilibrium state may have been reached where mixing and segregation occurs simultaneously. Furthermore, a large amount of sand was used in the mixture and it belongs to free-flowing group B particles; hence, it is expected that the fludization - defludization profile of this bed mixture does not show much difference between one other in that specified region. However, the defluidization curve for both types of mixtures is slightly higher than the fluidization plot especially after passing U_{mf} values. This is because the bed is less permeable in the defluidization stage due to segregation, as well as due to the effect of flotsam and jetsam of particles with different densities and shape.

Ratio of U_{cf}/U_{mf}

As exhibited in *Fig. 6,* the ratio of U_{cf}/U_{mf} decreases as the percentage of palm kernel shell mixture increases. Meanwhile, a different pattern is observed for the mixture of

palm pressed fibre and silica sand. As the percentage of the palm pressed fibre in the mixture increases, the ratio of U_{cf}/U_{mf} also increases sharply as displayed on *Fig. 7*. However, as can be seen in Table 2, the U_{cf} and U_{mf} trends for both mixtures (palm kernel shell/palm fibre with silica sand) only demonstrate increment pattern with increasing percentages of residue in the mixtures. A large difference in superficial gas velocity between U_{mf} and U_{cf} in every weight fraction is noticed in Table 2(b) and these explained the sharp increment of the U_{cf}/U_{mf} ratio for mixtures of palm pressed fibre and silica sand. The trend dissimilarity in U_{cf}/U_{mf} ratio for both mixtures is probably due to the physical characteristic of this residue material where palm pressed fibre is physically light weighted, sustained rod shape after grinding and have a very high voidage. The interparticle forces are known to be very high as explained in previous section. Therefore, higher velocity is needed to fluidize all the particles in the bed vigorously.

From *Figs. 6* and *7*, it is clear that U_{cf}/U_{mf} ratio of palm kernel shell and silica sand is much lower than mixtures of palm pressed fibre. This is due to the physical characteristics of the palm kernel shell which has lower voidage and retains a more free-flowing nature in comparison to fibrous palm pressed fibre. Mixture of palm kernel shell and silica sand is also observed to start fluidizing at a lower gas velocity.

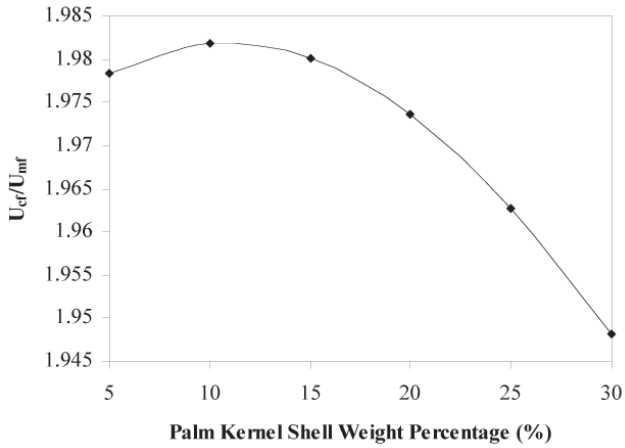

Fig. 6: U_{cf}/U_{mf} ratio for mixture of silica sand and palm kernel shell

TABLE 2(a)
U_{mf} and U_{cf} for different mixtures for palm kernel shell with silica sand

Palm Kernel Shell Weight Percentage (%)	U_{mf} (cm/s)	U_{cf} (cm/s)
5	7.4	14.6
10	7.6	15.1
15	7.9	15.6
20	8.1	16.0
25	8.4	16.5
30	8.7	17.0

TABLE 2(b)
U_{mf} and U_{cf} for different mixtures for palm pressed fibre with silica sand

Palm Pressed Fibre Weight Percentage (%)	U_{mf} (cm/s)	U_{cf} (cm/s)
5	7.6	17.0
10	8.5	20.8
15	9.4	25.5
20	11.5	32.1

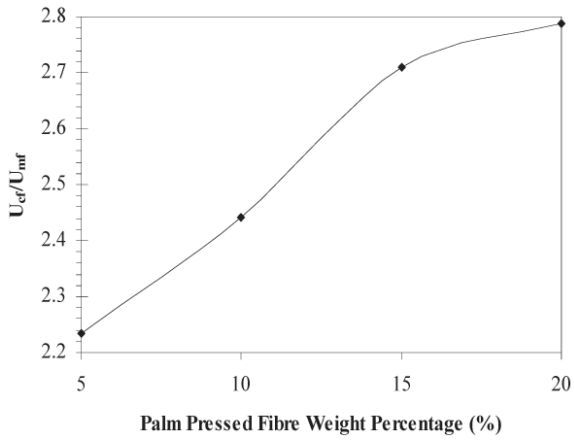

Fig. 7: U_{cf}/U_{mf} ratio for mixture of silica sand and palm pressed fibre

CONCLUSIONS

Ratio of U_{cf}/U_{mf} of binary fluidization of oil palm residues with silica sand shows a totally different pattern for different types of residues used. Increment pattern is observed in the mixture of palm pressed fibre and silica sand while a decreasing pattern is obtained in the fluidization of palm kernel shell and silica sand, which is contributed by the physical characteristics of the materials used. The inequality of patterns is determined by the amount of superficial gas velocity necessary for the particle to reach complete fluidization from minimum fluidization velocity at the initial stage. It is also observed by visual observation that segregation is reduced when the content of oil palm residues used in the mixture is in small amounts.

ACKNOWLEDGEMENTS

The authors gratefully acknowledge the Institute of Research, Development and Commercialization (IRDC) of Universiti Teknologi MARA for the financial support for this work.

REFERENCES

Aznar, M.P., Gracia-Gorria, F.A. and Corella, J. (1992a). Minimum and maximum velocities for fluidization for mixtures of agricultural and forest residues with second fluidized solid. I. Preliminary data and results with sand-sawdust mixtures. *International Chemical Engineering, 32,* 95-102.

Aznar, M.P., Gracia-Gorria, F.A. and Corella, J. (1992b). Minimum and maximum velocities for fluidization for mixtures of agricultural and forest residues with second fluidized solid. II. Experimental results for different mixtures. *International Chemical Engineering, 32*(1), 103-113.

Cheung, L., Nienow, A.W. and Rowe, P. N. (1974). Minimum fluidisation velocity of a binary mixture of different sized particles. *Chemical Engineering Science, 29,* 1301-1303.

Cummer, K.R. and Brown, R.C. (2002). Ancillary equipment for biomass gasification. *Biomass & Bioenergy, 23*, 113-128.

Delebarre, A.B., Pavinato, A. and Leroy, J.C. (1994). Fluidization and mixing of solids distributed in size and density. *Powder Technology, 80*(3), 227-233.

Enden, P. J. v. d. and Lora, E.S. (2004). Design approach for biomass fed fluidized bed gasifier using the simulation software CSFB. *Biomass & Bioenergy, 26,* 281-287.

Fauziah, M., Norazah, A.R. and Nornizar, A. (2006). Fluidization of oil palm residues in binary particle system. Paper presented at the Symposium of Malaysian Chemical Engineers (SomChE), Universiti Teknologi MARA.

Formisani, B. (1991). Packing and fluidization properties of binary mixtures of spherical particles. *Powder Technology, 66*(3), 259-264.

Geldart, D. (1986). *Gas Fluidization Technology*. Wiley.

Gomez, E.O. and Lora, E.S. (1995). Constructive features, operation and sizing of fluidized-bed gasifiers for biomass. *Energy for Sustainable Development, 2*(4), 52-57.

Marring, E., Hoffmann, A.C. and Janssen, L.P.B.M. (1994). The effect of vibration on the fluidization behaviour of some cohesive powders. *Powder Technology, 79*(1), 1-10.

Nienow, A.W. and Chiba, T. (1985). Fluidization of dissimilar materials. In J. F. Davidson, R. Clift and D. Harrison (Eds.), *Fluidization* (2nd ed.). London: Academic Press.

Mehrani, P., Bi, H.T. and Grace, J.R. (2007). Bench-scale tests to determine mechanisms of charge generation due to particle-particle and particle-wall contact in binary systems of fine and coarse particles. *Powder Technology, 173*(2), 73-81.

Patil, K.N., Bowser, T.J., Bellmer, D.D. and Huhnke, R.L. (2005). Fluidization characteristics of sand and chopped switchgrass-sand mixtures. *Agricultural Engineering International: The CIGR Ejournal, VII,* 1-9.

Rao, T.R. and Bheemarasetti, J.V.R. (2001). Minimum fluidization velocities of mixtures of biomass and sands. *Energy, 26*(6), 633-644.

Reina, J., Velo, E. and Puigjaner, L. (2000). Predicting the minimum fluidization velocity of polydisperse mixtures of scrap-wood particles. *Powder Technology, 111*(3), 245-251.

Sadaka, S.S., Ghaly, A.E. and Sabbah, M.A. (2002). Two phase biomass air-steam gasification model for fluidized bed reactors: Part I - model development. *Biomass & Bioenergy, 22,* 439-462.

SAMUELSSON, R., BURVALL, J. and JIRJIS, R. (2006). Comparison of different methods for the determination of moisture content in biomass. *Biomass & Bioenergy, 30,* 929-934.

SUN, Q., LU, H., LIU, W., HE, Y., YANG, L. and GIDASPOW, D. (2005). Simulation and experiment of segregating/mixing of rice husk-sand mixture in a bubbling fluidized bed. *Fuel, 84,* 1739-1748.

ISSN: 0128-7680
Pertanika J. Sci. & Technol. **16 (2)**: 213 - 223 (2008)

Equilibrium and Kinetic Studies of Pb (II) Ions Biosorption by Immobilized Cells of *Pycnoporus sanguineus*

Mashitah Mat Don*, Yus Azila Yahaya and Subhash Bhatia
School of Chemical Engineering, Engineering Campus, Universiti Sains Malaysia, 14300 Nibong Tebal, Seberang Prai Selatan, Pulau Pinang, Malaysia
**E-mail: chmashitah@eng.usm.my*

ABSTRACT

The biosorption of Pb (II) ions from aqueous solution onto immobilized cells of *Pycnoporus sanguineus* (*P. sanguineus*) was investigated by considering the effect of pH, initial lead (II) concentration and biomass loading at 150 rpm for 2 hr. Results showed that the uptake of Pb (II) ions increased with the increase of initial Pb (II) concentration and pH. The optimum pH for Pb (II) biosorption was at pH 4 with initial Pb (II) concentration of 3.12 mg/g. Langmuir, Freundlich and Redlich-Peterson isotherm models fitted the data well with correlation coefficients R^2> 0.90. The change in biosorption capacity with time was found to fit the pseudo-second order followed by intraparticle diffusion equation at different temperatures.

Keywords: **Biosorption, equilibrium, kinetics, lead, *Pycnoporus sanguineus*, immobilized cells, fungus, heavy metals**

ABBREVIATIONS

a_{rp}	Redlich-Peterson isotherm constant	$(dm^3/mg)^{\beta}$
β	Redlich-Peterson isotherm constant	
C_e	equilibrium concentration	(mg/L);
C_i	initial concentration	(mg/L)
C_f	final or equilibrium concentration	(mg/L)
k_1	rate constant of first-order biosorption	(1/min)
k_2	rate constant of second-order biosorption	(g/mg min)
K_b	Langmuir equilibrium constant	(dm^3/mg)
K_f	Freundlich constant	
K_{rp}	Redlich-Peterson isotherm constant	(dm^3/mg)
n	Freundlich constant	
q	metal ions biosorbed per g of biomass	(mg/g)
q_{max}	maximum specific uptake corresponding to the site's saturation	(mg/g)
q_e	amount of metal ions uptake at equilibrium	(mg/g)
q_t	amounts of adsorbed Pb(II) ions on the biosorbent at time t	(mg/g)
V	volume of metal solution in the flask	(L)
W	weight of biosorbent	(g)

Received : 3 March 2008
Accepted : 8 April 2008
* Corresponding Author

INTRODUCTION

The presence of lead (Pb (II)) in the environment such as in soil and water poses serious problems to members of the ecological system, including humans. It may come from various industrial sources e.g. battery manufacturing, textile, mining and metal finishing (Tunali *et al.*, 2006). Removal of the Pb (II) ions from water and industrial wastewater have become a challenge to researchers as it has been classified the premier environmental poison among the toxic metals existing in the world (Rai and Amit, 2002). Exposure to this metal at high levels can damage the reproductive system, kidneys, nervous system and cause mental retardation (Sheng *et al.*, 2004). Conventional methods used to remove metal ions from industrial effluents, e.g. chemical precipitation, membrane separation, activated carbon adsorption and ion exchange (Beszedits, 1983; Metcalf and Eddy, 1991), may not be usable for removing lead due to inefficiencies, high operational costs at low concentrations of the metal ion in the treated water (Arica *et al*, 2001) and difficulties in disposing of the metal sludge (Malkoc and Nuhoglu, 2005).

In the past few decades, biosorption has become an alternative method used to remove heavy metals from wastewater (Kim *et al.*, 2003). Biosorption may involve several chemical processes including adsorption, covalent binding and ion-exchange (Tobin *et al.*, 1994). Heavy metals biosorption that utilizes microorganisms as a biosorbent has received great attention due to its capability to remove metal ions from wastewater treatment or contaminated wastewater (Aksu and Acikel, 2000). Metal binding by microorganisms can be classified as extracellular accumulation, cell surface sorption and intracellular accumulation (Ahalya *et al.*, 2003; Veglio and Beolchini, 1997).

Fungi have been used as a biosorbent of heavy metals for years (Tunali *et al.*, 2006). Cell walls of fungi consists of three major biopolymers including polysaccharides, protein and nucleic acids (Aloysius *et al.*, 1999). These biopolymers carry many functional groups such as carboxylate, hydroxyl, amino groups and phosphate which provide active binding sites for metals biosorption to occur (Aloysius *et al.*, 1999; Tunali *et al.*, 2006). Both living and dead fungal cells can take up metal ions (Brady and Tobin, 1994). Although, several fungal biosorbents (*Aspergillus niger, Cephalosporium aphidicola, Pycnoporus sanguineus and Trametes versicolor*) have been evaluated as potential biosorbents for the removal of heavy metals from aqueous solutions (Bayramoglu *et al.*, 2003; Kapoor and Viraraghavan, 1997; Mashitah *et al.*, 1999; Tunali *et al.*, 2006), less studies were reported on Pb (II) biosorption by live immobilized cell system of *P. sanguineus* in a batch mode. Immobilized cell concept offers additional advantages over free cells including regeneration and reuse of the biosorbent, easier solid liquid separation, enhanced mechanical strength of microbials and minimal clogging problems in continuous operations (Ting and Sun, 2000; Arica *et al.*, 2001; Bayramoglu *et al.*, 2003; Annadurai *et al.*, 2007; Vijayaraghavan and Yan, 2007).

Hence, the main objective of this study was to determine the potential of immobilized living cells of *P. sanguineus* to adsorb Pb (II) ions in shake flask culture. Adsorption isotherms and kinetic models were also evaluated.

MATERIAL AND METHODS

Microorganism and Production Medium

P. sanguineus capable of adsorbing heavy metals was obtained from the Forest Research Institute of Malaysia (FRIM), Kepong, Selangor (Mashitah *et al.*, 1999). It was maintained

by weekly transfer on malt extract agar slants incubated at 30°C for 6 days, after which the slants were stored at 4°C until required. The composition of the production medium comprised of (g/L): glucose 20, yeast extract 10 and malt extract 10. The pH of the medium was adjusted to 9.0 prior to autoclaving at 121°C (1.5 bar) for 15 minutes.

Immobilized Cell Preparation

A cell suspension was prepared by inoculating a stock culture of *P. sanguineus* onto malt extract agar plates and incubating them at 30°C for 6 days. The mycelial mat formed was scraped off by using a sterile blade and mixed with 10 ml sterile Tween 20 solution prior putting it into a sterile sampling bottle (100 ml). The sampling bottle was vortexed for 3 minutes so that the mycelium was evenly distributed in the liquid.

Fifteen ml of the cell suspension was inoculated into an Erlenmeyer flask containing 135 ml of the production medium. The flask was incubated on a rotary shaker at 30°C, 150 rpm for 66 hr. The harvested sample was centrifuged at 3500 rpm for 4 minutes at 25°C and known as free cells of *P. sanguineus*. Immobilized cells of *P. sanguineus* beads were prepared by dropping a mixture of 1.5 % (w/v) sodium alginate solution and *P. sanguineus* mycelium into a 2% (w/v) $CaCl_2$ solution stirred slowly at room temperature, 25$\pm$ 3.0°C. The beads were stirred slowly for 30 minutes, then collected by filtration, washed three times with sterile deionized water and stored in Tris-HCl buffer (pH 7) at 4°C until used.

Preparation of Metal Ions

Metal solutions were prepared by diluting 1000 mg/L of Pb $(NO_3)_2$ (Mallinckrodt) solutions with deionized water to a desired range of 50 to 300 mg/L. For each solution, the initial metal concentrations and the concentrations in the samples after biosorption treatment were determined using an Atomic Absorption Spectrophotometer (Model Shimadzu AA 6650).

Batch Biosorption Procedures

The biosorption of Pb (II) ions by the immobilized *P. sanguineus* from aqueous solution was evaluated in batch biosorption equilibrium experiments. Effects of initial Pb (II) ion concentration, pH, biomass loading and temperature on the biosorption rate and capacity were examined.

The effect of solution pH between 2 and 4 on the biosorption of Pb (II) by the immobilized *P. sanguineus* preparation was evaluated in cultures kept at 150 rpm, 30°C for 2 hr. For initial Pb (II) concentration, the biosorption studies were conducted at pH 4 as described above, but the concentration of Pb (II) varied from 58 to 300 mg/L. The effect of biomass loading was evaluated at 1 to 6 g with other procedures as described previously. For the equilibrium study, the initial Pb (II) concentration was 100 mg/L and the working pH was 4. The contact time varied from 15 to 120 min at 30°C (303 K), 35°C (308 K) and 40°C (313 K), respectively.

The amount of Pb (II) bound by the biosorbent was calculated as:

$$q = \frac{V(C_i - C_f)}{W} \quad (1)$$

where q is mg of metal biosorbed per g of biomass (mg/g), C_i (mg/L) is the initial concentration, C_f (mg/L) is the final or equilibrium concentration, V (L) is the volume of metal solution in the flask and W (g) is the weight of the biosorbent. Each experiment was repeated three times and the results given are average values. Samples taken after the desired incubation period were measured with an Atomic Absorption Spectrophotometer (Model Shimadzu AA 6650).

Kinetics experiments were carried out at known Pb (II) concentrations with various biosorbent loadings and shaking at 150 rpm. At pre-determined interval times, samples were withdrawn, filtered and the Pb (II) concentration measured with an Atomic Absorption Spectrophotometer (Model Shimadzu AA 6650).

Equilibrium Isotherm and Kinetics Studies

i. Equilibrium isotherm models

Langmuir, Freundlich and Redlich-Peterson models have all been used to determine the sorption equilibrium between a solid biosorbent and metal ions. The Langmuir model assumes that a monomolecular layer is formed when biosorption occurs and that the adsorbed molecules do not interact with one another (Langmuir, 1916; Malkoc and Nuhoglu, 2003).

The Langmuir equation is:

$$q_e = \frac{q_{\max} K_b C_e}{1 + K_b C_e} \tag{2}$$

where q_{max} is the maximum specific uptake corresponding to the site saturation, K_b is an equilibrium constant (dm^3/mg) and both parameters can be determined from a linearised form of Eq. (3) as followed:

$$\frac{C_e}{q_e} = \frac{1}{q_{\max} K_b} + \frac{C_e}{q_{\max}} \tag{3}$$

where C_e is the equilibrium concentration (mg/L); q_e is the amount of metal ion uptake at equilibrium (mg/g), q_{max} is q_e for a complete monolayer (mg/g) and K_b is the equilibrium constant (dm^3/mg).

The Freundlich isotherm model (Freundlich, 1906) is

$$q_e = K_f C_e^n \tag{4}$$

and the equation may be linearised and described as:

$$\ln q_e = \frac{1}{n} \ln C_e + \ln K_f \tag{5}$$

where q_e is the amount of metal ion uptake (mg/g); C_e is the equilibrium concentration (mg/L); K_f and n are Freundlich constants and can be determined by plotting $ln\ q_e$ versus $ln\ C_e$.

The Redlich-Peterson isotherm (Redlich and Peterson, 1959) has three parameters and incorporates features from both the Langmuir and the Freundlich isotherms. It can be described as:

$$q_e = \frac{K_{rp} C_e}{1 + a_{rp} C_e^{\beta}} \tag{6}$$

where K_{rp}, a_{rp} and β ($0 < \beta < 1$) are the Redlich-Peterson isotherm constants. These isotherms can be evaluated from a linear plot of

$$\ln(K_{rp}\frac{C_e}{q_e} - 1) = \beta \ln(C_e) + \ln a_{rp} \tag{7}$$

using a nonlinear regression method.

ii. Kinetic modeling

Kinetic models such as pseudo first-order, pseudo second-order and intraparticle diffusion equations have been used to evaluate the mechanisms of biosorption and potential rate controlling steps such as mass transport and chemical reaction processes. The first-order rate expression of Lagergren (Lagergren, 1898) based on solid capacity was used:

$$\log(q_e - q_t) = log(q_e) - \frac{k_1}{2.303} t \tag{8}$$

where q_e and q_t are the amounts of Pb(II) ions adsorbed at equilibrium and at time t (respectively mg/g), and k_1, is the rate constant of first-order biosorption (min^{-1}).

The pseudo second-order equation is also based on the sorption capacity of the solid phase and can be obtained from (Arica et al., 2001):

$$\frac{t}{q_t} = \frac{1}{k_2 q_e^2} + \frac{1}{q_e^2} t \tag{9}$$

where k_2 is the rate constant of second-order biosorption (g/mg min) and q_e is the biosorption capacity calculated by the pseudo-second order kinetic model (mg/g).

The intraparticle diffusion equation was introduced to indicate the behaviour of intraparticle diffusion as the rate limiting step in the biosorption (Sharma and Foster, 1994). The equation is given as:

$$R = K_s t^b \tag{10}$$

where R is the percent metal adsorbed, t is the contact time (min), b is the gradient of linear plots and K_s is the intraparticle diffusion constant.

RESULTS AND DISCUSSION

Effect of Initial Pb (II) Ions Concentrations

The effect of initial Pb (II) ion concentration on Pb (II) uptake was studied in a range from 58 to 300 mg/L (*Fig. 1*). Increasing the initial Pb (II) concentration increased the amount of Pb (II) taken up. The increase in initial Pb (II) concentration could increase the mass transfer driving force of the ions between the aqueous and solid phases (Aksu, 2002; Fawzi and Sameer, 2000; Malkoc and Nuhoglu, 2005). However, at a higher concentration the percentage of Pb (II) ions removed decrease. For an initial Pb (II) ion concentration of 58 mg/L, 96% of the ions were removed within 2 hours, whereas only 39% of the ions were removed from a 300 mg/L solution in the same time period. Thus, at higher metal concentrations, the available sites at which the biosorption process occurs are limited and the biosorption yield decline (Malkoc and Nuhoglu, 2005).

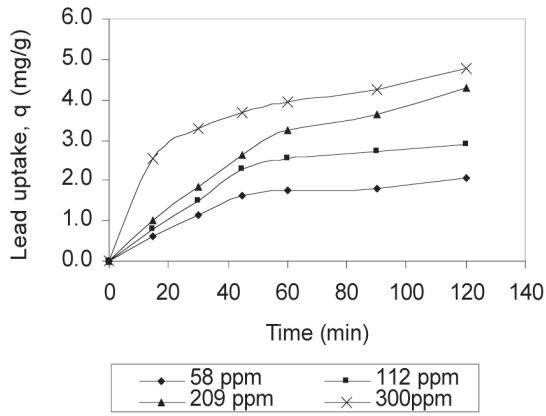

Fig. 1: Effect of initial metal concentration on the biosorption of Pb (II) ions by immobilized cells of P. sanguineus *(Condition: pH 4.0; biomass loading 3 g; agitation 150 rpm)*

Effect of pH

Heavy metals biosorption was found to be significantly dependent on pH (Malkoc and Nuhoglu, 2005). To determine the effect of pH on Pb (II) removal by immobilized cells of *P. sanguineus*, biosorption studies were carried out at pH 2.0, 3.0 and 4.0. Previous studies stated that at lower pH, the surface charge on the cells became positive and that metal cations and protons compete for binding sites on cell walls, which results in lower Pb (II) uptake from the medium (Malkoc and Nuhoglu, 2005). At pH above the isoelectric point, the surface charges are negative and the ionic state of ligands such as amino groups, carboxyls and phosphates promote reactions with the Pb (II) ions, resulting in rapid efficient binding (Arica *et al.*, 2001). In most of Pb (II) ion removal studies, the optimum pH for Pb (II) ions biosorption was in the range pH 3.0 to 7.0 as presented in Table 1. In this study, the percent removal of Pb (II) by immobilized cells of *P. sanguineus* was more than 90% within 2 h at pH 4. No experiments were conducted at pH above 4 as the Pb (II) ions precipitate.

TABLE 1
pH for Pb (II) ions biosorption by different biosorbent

Biosorbent material	pH	Reference
Streptomyces noursei	6.1	(Mattuschka and Straube, 1993)
Pennicillium chrysogenum	4.5	(Niu *et al.*, 1993)
Rhizopus arrhizus	5.0-7.0	(Sag and Kutsal, 2000)
Rhizopus arrhizus	4.0-5.0	(Fourest and Roux, 1992)
Zoogloea ramigera	4.0-5.0	(Sag and Kutsal, 2000)
Saccharomyces cerevisiae	5.0	(Cabuk *et al.*, 2007)
Phanerochaete chrysosporium	6.0	(Say *et al.*, 2001)
Cephalosporium aphidicola.	5.0	(Tunali *et al.*, 2006)
Aspergillus niger	4.0	(Dursun, 2005)
Trametes versicolor	4.0-6.0	(Bayramoglu *et al.*, 2003)
Pycnoporus sanguineus	4.0	This study

Effect of Biosorbent Loading

The biosorption capacity for Pb (II) ions varies with the biosorbent loading (*Fig. 2*). Pb (II) ion removal increased from 23% to 99% when the amount of immobilized cells of *P. sanguineus* increased from 1.0 to 6.0 g. This increase could be attributed to the presence of more binding sites for binding the Pb (II) ions (Malkoc and Nuhoglu, 2005). However, the Pb (II) uptake decreased from 2.89 to 1.95 mg/g as the biosorbent dosage increased. The maximum metal uptake capacity occurred at 3.0 g of immobilized cells (*Fig. 2*). The high biosorbent loading may produce a 'screen' effect on the cell wall, protecting the binding sites and thus lowering the Pb (II) uptake (Malkoc and Nuhoglu, 2005; Mashitah *et al.*, 1999; Pons and Futse, 1993).

Equilibrium Isotherms

The linearised Langmuir, Freundlich and Redlich-Peterson equilibrium isotherm constants for Pb (II) ion biosorption were obtained at 30°C (303 K), 35°C (308 K) and 40°C (313 K) (Table 2). Biosorption of the metals by the immobilized cells of *P. sanguineus* could

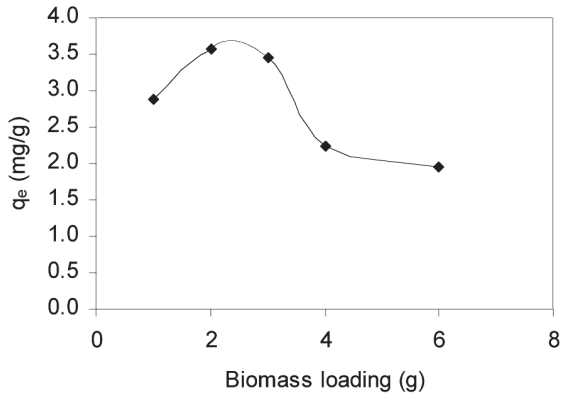

Fig. 2: Effect of biomass loading on the uptake of Pb (II) ions by immobilized cells of P. sanguineus *(Condition: pH 4.0; 100 mg/L Pb (II) ions; agitation 150 rpm)*

be represented well by any of the three isotherm models, as all had a correlation coefficient (R^2) of approximately 1. The Langmuir constants K_b and q_{max} were determined using Eq. (3). The equilibrium sorption capacity, q_{max} increased from 3.62 to 4.43 mg/g when the temperature increased from 30 to 40°C. The higher the K_b value, the higher the affinity for binding metal ions. The highest K_b occurred at 313 K. The increase in K_b with temperature shows that a chemical interaction occurs between the metal ions and the biosorbent (Malkoc and Nuhoglu, 2005).

TABLE 2
Biosorption equilibrium constant obtained from Langmuir, Freundlich and Redlich-Peterson isotherms for the biosorption of Pb (II) ions onto immobilized cells of *P. sanguineus*

T	Langmuir	Freundlich					Redlich-Peterson			
(°C)	q_{max} (mg/g)	K_b (dm^3/mg)	R^2	K_f	n	R^2	K_{rp} (dm^3/mg)	a_{rp} $(dm3/mg)^{\beta}$	β	R^2
30	3.62	1.341	1.000	1.553	4.713	0.933	3.928	1.075	1.000	1.000
35	4.00	1.416	0.999	1.840	5.025	0.962	9.955	2.630	0.990	0.999
40	4.43	1.569	0.999	2.179	5.313	0.949	25.234	7.059	0.950	0.999

The K_f values for the Freundlich isotherms also increased with increase in temperature (Table 2). Since the n values obtained were > 1.0, the Pb (II) ions were favorably adsorbed by the biosorbent at all temperatures studied (Dursun, 2005). For the Redlich-Peterson constant K_{rp}, the values also increased with reaction temperature and most values of β were between 0.95-1.0.

Biosorption Kinetics Modeling

To evaluate the biosorption kinetics of Pb (II) ions, the pseudo-first order, pseudo-second order and intraparticle diffusion equations were applied to the experimental data. The corresponding constants for all three models obtained are presented in Table 3. The pseudo-second order model fitted the experimental data better than the intraparticle diffusion and pseudo-first order models with correlation coefficients (R^2) of approximately 1.

TABLE 3
Kinetic constants of pseudo first, pseudo second-order and intraparticle diffusion models for the biosorption of Pb (II) ions onto immobilized cells of *P.sanguineus* at different temperatures

T (°C)	First-order kinetic model		Second-order kinetic model		Intraparticle diffusion	
	k_1 (min^{-1})	R^2	k_2 (g/mg min)	R^2	K_s	R^2
30	0.039	0.988	0.147	0.947	1.515	0.916
35	0.035	0.979	0.198	0.972	1.556	0.907
40	0.008	0.768	0.333	0.990	1.717	0.873

CONCLUSIONS

Live immobilized cells of *Pycnoporus sanguineus* revealed a potential as a biosorbent for the removal of Pb (II) ions from an aqueous solution. The ability of immobilized cells of *P. sanguineus* to adsorb Pb (II) ions from aqueous solution was evaluated in batch studies. The initial Pb (II) concentration, pH and biomass loading all affected Pb (II) biosorption. The Langmuir, Freundlich and Redlich-Peterson isotherms fitted well with the experimental data at $R^2 \geq 0.90$. The kinetics of Pb (II) ions sorption at different temperatures was best described with a pseudo second order model.

ACKNOWLEDGEMENTS

This work was supported by a short term grant from Universiti Sains Malaysia (6035132).

REFERENCES

Ahalya, N., Ramachandra, T.V. and Kanamadi, R.D. (2003). Biosorption of heavy metals. *Research Journal of Chemistry and Environment, 7*, 71-79.

Aksu, Z. (2002). Determination of the equilibrium, kinetic and thermodynamic parameters of the batch biosorption of nickel (II) ions onto *Chlorella vulgaris. Process Biochem., 38*, 89-99.

Aksu, Z. and Acikel, U. (2000). Modelling of a single-staged bioseparation process for simultaneous removal of iron (II) and chromium (VI) by using *Chlorella vulgaris. Biochem. Eng. J., 4*, 229-238.

Aloysius, R., Karim, M.I.A. and Ariff, A.B. (1999). The mechamism of a cadmium removal from aqueous solution by nonmetabolizing free and immobilized live biomass of *Rhizopus oligosporus. World J. Microbiol. Biotechnol., 15*, 571-578.

Annadurai, G., Ling, L.Y. and Lee, J.F. (2007). Biodegradation of phenol by *Pseudomonas pictorum* on immobilized with chitin. *African J. Biotechnol., 6*, 296-303.

Arica, M.Y., Kacar, Y. and Genc, O. (2001). Entrapment of white-rot fungus *Trametes versicolor* in Ca-alginate beads; preparation and biosorption kinetics analysis for cadmium removal from an aqueous solution. *Biores. Technol., 80*, 121-129.

Baklashova, T.G., Koshcheenko, K.A. and Skryabin, G.K. (1984). Hydroxylation of indolyl-3-acetic acid by immobilized medium of *A. niger. Appl. Microbiol. Biotechnol., 19*, 217-223.

Bayramoglu, G., Bektas, S. and Arica, M.Y. (2003). Biosorption of heavy metal ions on immobilized white-rot fungus *Trametes versicolor. J. Hazard Mater., B101*, 285-300.

Brady, J.M. and Tobin, J.M. (1994). Adsorption of metal ions by *Rhizopus arrhizus* biomass: characterization studies. *Enzyme Microbiol. Technol., 6*, 671-675.

Beszedits, S. (1983). Heavy metals removal from wastewaters. *Engineering Digest,* 18-25.

Cabuk, A., Akar, T., Tunali, S. and Gedikli, S. (2007). Biosorption of Pb (II) by industrial strain of *Saccharomyces cerevisiae* immobilized on the biomatrix of cone biomass of pinus nigra: Equilibrium and mechanism analysis. *Chem. Eng. J., 131*, 293-300.

Dursun, A.Y. (2005). A comparative study on determination of the equilibrium, kinetic and thermodynamic parameters of biosorption of copper (II) and lead (II) ions onto pretreated *Aspergillus niger. Biochem. Eng. J., 28*, 187-195.

Fawzi, A. and Sameer, A.A. (2000). Biosorption of phenol by chicken feathers. *Environ. Eng. Policy, 2*, 85-90.

Federici, F., Miller, M.W. and Petruccioli, M. (1987). Glucoamylase production by immobilized *Aureobasidium pullulans* in sequential batch processes. *Annali di Microbiologia e Enzimologia, 37*, 17-24.

Federico, F., Petruccioli, M. and Millar, M.W. (1990). Enhancement and stabilization of the production of Glucoamylase by immobilized cells of *Aureobasidium pullulans* in a fluidized bed reactor. *Appl. Microbiol. Biotechnol., 33*, 407-409.

Federici, F. (1993). Potential applications of viable, immobilized fungal cell systems. *World J. Microbiol. Biotechnol., 9*, 495-502.

Fourest, E. and Roux, J.C. (1992). Heavy metal biosorption by fungal mycelial by-products: mechanism and influence of pH. *Appl. Microbiol. Biotechnol., 37*, 399-403.

Freundlich, H.M.F. (1906). Uber die adsorption in losungen. *J. Physical Chemistry, 57A*, 385-470.

Kapoor, A. and Viraraghavan, T. (1997). Heavy metal biosorption sites in *Aspergillus niger. Biores. Technol., 61*, 21-28.

Kim, S.K., Park, C.B., Koo, Y.M. and Yun, H.S. (2003). Biosorption of cadmium and copper ions by *Trichoderma reesei* RUT C30. *J. Ind. Eng. Chem., 9*, 403-406.

Kopp, B. and Rehm, H.J. (1984). Semicontinuous cultivation of immobilized *Claviceps purpurea. Appl Microbiol Biotechnol, 19*, 141-145.

Lagergren, S. (1898). Zur theorie der sogenannten adsorption gel oster stoffe. Kungliga Svenska Vetenskapsakademiens, *Handlingar, 24*, 1–39.

Langmuir, I. (1916). The constitution and fundamental properties of solids and liquids. *J. American Chem Society, 38*, 2221-95.

Li, G.X., Linko, Y.Y. and Linko, P. (1984). Glucoamylase and ?-amylase production by immobilized *A. niger. Biotechnol. Lett., 6*, 645-650.

Malkoc, E. and Nuhoglu, Y. (2005). Investigations of nickel (II) removal from aqueous solutions using tea factory waste. *J. Hazard Mater., B127*, 120-128.

Mashitah, M.D., Zulfadhly, Z. and Bhatia, S. (1999). Ability of *Pycnoporus sanguineus* to remove copper ions from aqueous solution. *Artificial Cells, Blood Substitutes and Immobilization Biotechnol., 27*, 429-433.

Mattuschka, B. and Straube, G. (1993). Biosorption of metals by a waste biomass. *J. Chem. Technol. Biotechnol., 58*, 57-63.

Metcalf and Eddy. (1991). *Wastewater Engineering: Treatment, Disposal, and Reuse* (3d ed., pp. 68-88). Singapore: McGraw-Hill, Inc.

Niu, H., Xu, X.S., Wang, J.H. and Volesky, B. (1993). Communication to the Editor: Removal of lead from aqueous solutions by *Penicillium* biomass. *Biotechnol. Bioeng., 42*, 785-787.

Pons, M.P. and Futse, C.M. (1993). Uranium uptake by immobilized cells *Pseudomonas strain* EPS 5028. *Appl. Microbiol. Biotechnol., 39*, 661-665.

Puranik, P.R. and Paknikar, K.M. (1997). Biosorption of lead and zinc from solutions using *Streptoverticillum cinnamoneum* waste biomass. *J. Biotechnol., 55*, 113-124.

Rai, U.N. and Amit, P. (2002). Health hazards of heavy metals. *Internacional Society of Environmental Botanists, 8*, 1-4.

Redlich, O. and Peterson, D.L. (1959). A useful adsorption isotherm. *J. Physical Chem., 63*, 1024.

SAG, Y. and KUTSAL, T. (2000). Determination of the biosorption heats of heavy metal ions on *Zoogloea ramigera* and *Rhizopus arrhizus*. *Biochem. Eng. J., 6*, 145-151.

SAY, R., DENIZLI, A. and ARICA, M.Y. (2001). Biosorption of cadmium (II), lead (II) and copper (II) with the filamentous fungus *Phanerochaete chrysosporium*. *Biores. Technol., 76*, 67-70.

SHARMA, D.C. and FOSTER, C.F. (1994). A preliminary examination into the adsorption of hexavalent chromium using low-cost adsorbents. *Biores. Technol., 47*, 257-264.

SHENG, P. X., TING, Y. P., CHEN, J. P. and HONG, L. (2004). Sorption of lead, copper, cadmium, zinc and nickel by marine algal biomass: characterization of biosorptive capacity and investigation of mechanism. *J. Colloid. Int. Sci, 275*, 131-141.

TING, Y.P. and SUN, G. (2000). Use of polyvinyl alcohol as a cell entrapment matrix for copper biosorption by yeast cells. *J. Chem. Technol. Biotechnol., 75,* 541-546.

TOBIN, J.M., WHITE, C. and GADD, G.M. (1994). Metal accumulation by fungi: applications in environmental biotechnology. *J. Ind. Microbiol, 13*, 126-130.

TSEZOS, M. (1984). Recover of uranium from biological adsorbent-desorption equilibrium. *Biotechnol Bioeng, 26*, 773-781.

TUNALI, S., AKAR, T., SAFA OZCAN, A., KIRAN, I. and OZCAN, A. (2006). Equilibrium and kinetics of biosorption of lead (II) from aqueous solutions by *Cephalosporium aphidicola*. *Sep. Purif. Technol., 47*, 105-112.

VEGLIO, F. and BEOLCHINI, F. (1997). Removal of metals by biosorption: A review. *Hydrometallurgy, 44*, 301-316.

VIJAYARAGHAVAN, K. and YUN, Y.S. (2007). Chemical modification and immobilization of *Corynebacterium glutamicum* for biosorption of reactive black 5 from aqueous solution. *Ind. Eng. Chem. Res, 46*, 608-617.

ISSN: 0128-7680
Pertanika J. Sci. & Technol. **16 (2)**: 225 - 229 (2008)

Rheological and Textural Characteristic of Restructured Fruit Puree

Noraziah Muda[1] and Mostafa Barigou[2]
[1] Department of Process and Food Engineering, Faculty of Engineering, Universiti Putra Malaysia, 43400 UPM, Serdang, Selangor, Malaysia
[2]School of Chemical Engineering, University of Birmingham, Edgbaston, Birmingham, B15 2TT, England, United Kingdom
**E-mail: nxm280@bham.ac.uk*

ABSTRACT

Sago starch is a cheap form of starch which is isolated from sago palm (Metroxylon spp.) and is available in abundance in South East Asian countries. Given its low cost, Sago starch has great potential to be used as a substitute for other forms of starch. The objectives of this work were to study the effects of paste concentration on the rheological behaviour of sago starch paste, their texture properties and their freeze thaw stability compared to other types of starch. The rheological properties of sago starch were investigated at different paste concentrations (3-8 wt %). The textural properties of the samples were investigated by examining the gel strength of the samples. The percent syneresis of sago starch was also studied to examine the freeze-thaw stability of the material. The freeze thaw stability of sago starch with the addition of certain biopolymers were also characterized.

Keywords: Freeze-thaw, rheology, starch concentration, texture analysis

INTRODUCTION

The use of starch has continued to grow over the years. Starch has been used in a wide range of products, either as raw material or as an additive, and thus, starch plays an important role in many industries such as food, pharmaceuticals, textiles and even biodegradable polymers. The choice of starch for the production of food ingredients would depend on factors such as availability, cost, efficiency of processing and quality of the final product. Sago starch is a cheap source of starch that is available in abundance in South East Asian countries. It may be used as a thickener in food and can replace more expensive sources of starch. There is lack of literature on sago starch especially on its rheological characterization. Any improvement in this area will lead to better utilization of sago starch and eventual cost savings. This study will also increase the economic value of sago and provide more choices for food manufacturers when selecting their food ingredients.

Sago starch is a form of starch isolated from sago palm (Metroxylon spp.). Sago starch is extracted from the sago palm trunk. The tall heavy trunks with pinnate leaves accumulate starch, and just before flowering is initiated, the entire trunk is cut, and prepared for the extraction of sago.

Received : 3 March 2008
Accepted : 8 April 2008
* Corresponding Author

MATERIALS AND METHODS

Sample Preparation

Starch paste was prepared by dispersing a required amount of dry starch in distilled water in a magnetic stirrer plate for 10 minutes at room temperature. The starch dispersions were brought up to 90°C in a water bath and stirred for 15 minutes to achieve complete gelatinization. The beaker was then weighed again and the volume corrected for any evaporation loss on heating using hot distilled water.

Rheological Measurement

The rheological studies were performed on the Bohlin CV0 controlled stress rheometer. The rheological studies were performed using cone and plate geometry with roughened surface to eliminate wall slip. Solvent trap was applied to eliminate moisture loss. All experiments were replicated thrice. Steady shear flow properties were measured by subjecting samples to increasing shear stress and measuring the corresponding shear rate in the range of 0.001 to 1000s-1. For dynamic rheological properties, samples were subjected to a stress sweep (0.01 to 100 Pa) at 0.01 and 10 Hz to determine the linear viscoelastic region. Frequency sweep experiments were carried out within the linear viscoelastic region and the viscoelastic parameters (G', G") were measured.

Textural Measurements

Gel strength of samples was determined by registering resistance to puncture in a Stable Micro Texture Analyzer fitted with 5 kg load cell. A 10 mm diameter delrin plunger penetrated the samples at 0.5 mm/s to a depth of 8 mm. Gel strength was measured as the penetration force required to broke gels. Measurements were made on three different fresh surfaces in recently opened 100 ml jars (55mm❑) of each sample.

Freeze-thaw Analysis

20 g (accurate weight) of the starch paste was added into each pre-weighted 15 mL centrifuged tubes, and allowed to cool to 30°C. Then these starch paste samples were frozen at -18°C in a freezer for 20 hours. After 20 hours, all tubes were removed from the freezer and thawed at room temperature for 4 hours. Thawed samples were centrifuged at 3000 rpm for 15 minutes. The clear liquid was decanted, and the residue weighed. The percentage syneresis was then calculated as

RESULTS AND DISCUSSION

Rheological Characterisation

Fig. 1 shows that sago starch paste exhibits very shear-thinning behaviour with a presence of a Newtonian plateau region at low shear rate values and were well described by a modified Cross model, wherein the infinite shear viscosity in the original Cross model was considered negligible. From non-linear regression analysis (using Sigma plot 7.0), the magnitude of zero shear viscosity increased as the concentration increased (Table 1).

Fig. 2 shows the frequency spectra of sago starch at different concentrations. Sago starch at lower concentration (3%) shows a G'-frequency dependence with G' increasing

as frequency increased. In contrast, samples with higher concentration (8%) exhibits a more gel like behaviour with G' almost independent of frequency.

Textural Characterisation

Fig. 3 shows that gel strength of sago starch increased exponentially as the concentration of starch increased. The regression model resulted in a gel strength constant of 11.73 N, an exponential constant of 0.5561 and the coefficient of regression (R^2) was 0.992.

Freeze-thaw Stability

As depicted in *Fig. 4*, sago starch shows poor resistance to freeze thaw cycles, where even after 1 cycle, the % syneresis was almost 50% and increased to more than 55% after 5 cycles. Starch gel becomes spongy after the first cycle. The freeze thaw stability of sago starch can be improved by adding a certain amount of biopolymers.

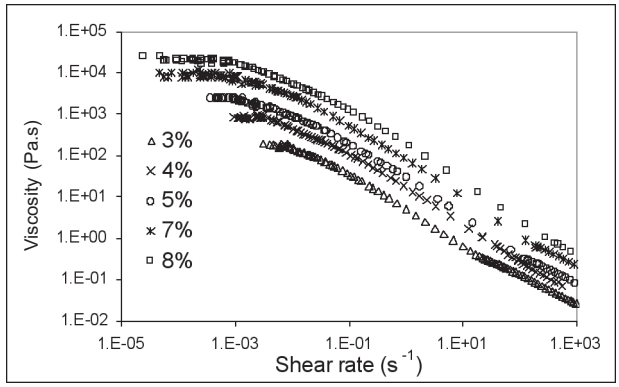

Fig. 1: Shear profile of sago starch at different concentrations (2-8% w/v)

TABLE 1
Regression coefficient based on cross model for sago starch paste at different concentrations

Conc. w/v (%)	η_o (Pa.s)	K	N	R^2
3.00	331.12	56.04	0.863	0.993
4.00	850.14	76.94	0.943	0.984
5.00	2178.56	126.84	0.814	1.000
6.00	4926.33	174.91	0.906	0.988
7.00	9584.70	279.26	0.940	1.000
8.00	22124.86	330.40	0.940	1.000

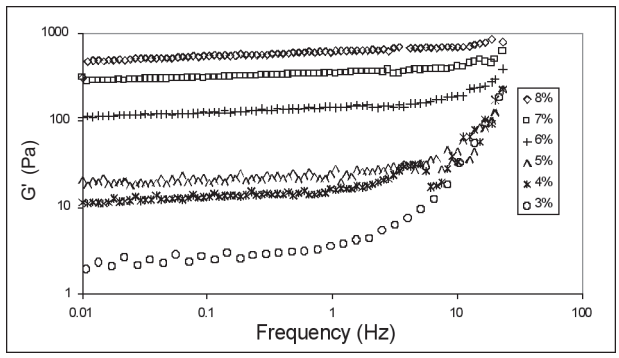

Fig. 2: Comparisons of storage modulus of sago starch at different concentrations

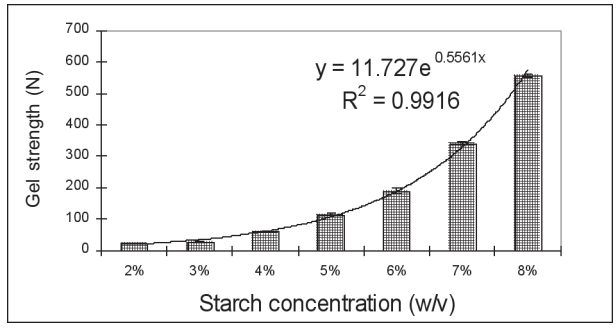

Fig. 3: Gel strength of sago starch at various concentrations

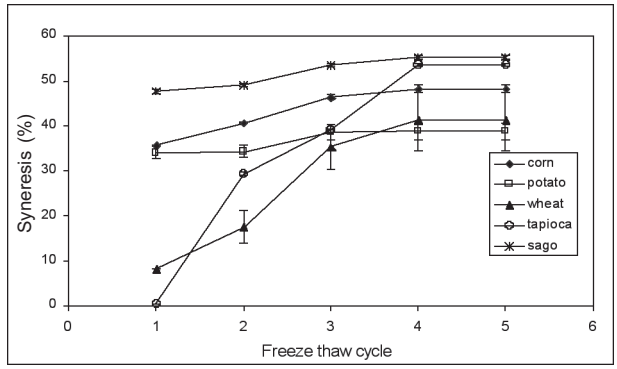

Fig. 4: Syneresis of 4% sago starch compared to other starch with repeated freeze thaw cycle

Fig. 5 shows that the freeze-thaw stability of sago starch increases with the addition of carrageenan, gellan, xanthan and whey protein, but decreases with the addition of alginate and locust bean gum. Mixture of starch and carrageenan gives the best resistance towards freeze-thaw treatments.

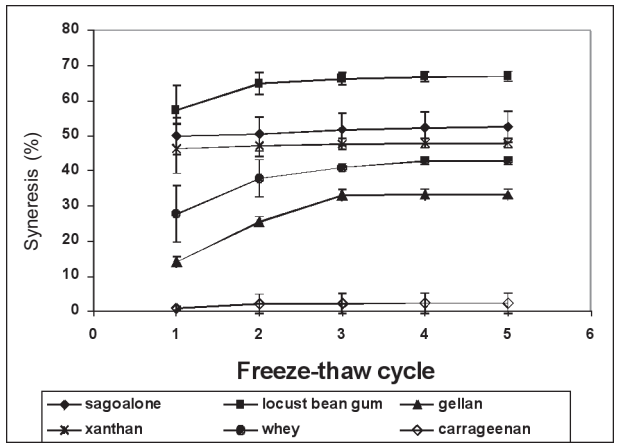

Fig. 5: Syneresis of 4 %(w/v) sago starch with 0.5% biopolymers with repeated freeze thaw cycle

CONCLUSIONS

Sago starch paste exhibits a shear thinning behaviour that can be well predicted by the Cross model. The higher the concentration of starch in the sample, the higher the magnitude of zero viscosity, more gel like behaviour and the better the strength of the gel. Freeze thaw stability of sago starch can be improved by adding a small amount of biopolymer. This can still be economical considering the low price of sago starch.

REFERENCES

DIEGO, B. GENOVESE and RAO, M. A. (2003). Role of starch granule characteristics on the rheology of starch dispersion with or without amylase. *Cereal Chemistry, 80*(3), 350-355.

SHARMA, S. K., MULVANEY, S.J. and RIZVI, S.S.H. (2000). Rheology of liquid and semisolid foods. In *Food process engineering: Theory and laboratory experiments* (pp. 51-67). New York: John Wiley and Sons Inc.

ISSN: 0128-7680
Pertanika J. Sci. & Technol. **16 (2)**: 231 - 237 (2008)

Detection of Hazardous Volatile Organic Compound by Using Semiconductor Based Catalytic Pellet

Mohamad Zailani Abu Bakar*, Ahmad Zuhairi Abdullah, Lau Ee Lian and Jusliha Juhari
School of Chemical Engineering, Engineering Campus, Universiti Sains Malaysia, Seri Ampangan, 14300 Nibong Tebal, Pulau Pinang, Malaysia
**E-mail: chmohdz@eng.usm.my*

ABSTRACT

Catalytic pellets that comprise of various compositions of titanium oxide (TiO_2) and tin oxide (SnO_2) as a substrate have been developed for detection of volatile organic compound (VOC). The pellets were tested for gas-sensing properties in the experimental rig at temperature ranges between 100°C to 400°C. The morphological and structural characteristics of the catalytic pellets were investigated by means of a Scanning Electron Microscope (SEM) and X-ray Diffraction (XRD). The results showed that the sensitivity of the pellet decreased at higher compositions of TiO_2. The structural analysis revealed the appearance of $Ti_{0.1}Sn_{0.9}O_2$ phase, rather than TiO_2 phase in the TiO_2-SnO_2 catalytic pellets. The surface morphology of the pellets indicated that the average grain size decreased with the addition of TiO_2.

Keywords: **Catalytic pellet, ethanol vapour sensor, VOCs, semiconductor based sensor, titanium oxide, tin oxide**

ABBREVIATIONS

S	sensitivity	% (percent)
R_{air}	electrical resistance in air	Ω (ohm)
$R_{ethanol}$	electrical resistance in ethanol vapour	Ω (ohm)

INTRODUCTION

One of the major environmental pollutants in the atmosphere is volatile organic compounds (VOC). Among the various types of VOCs benzene, toluene and xylene are confirmed human carcinogens and could cause diversiform cancers (Brickus *et al.*, 1998). VOCs may be released into the environment through industrial activities where they may have been used as raw materials or solvents in the manufacturing or separating process. Due to its effect on humans, the detection and control of VOCs is deemed necessary. The detection becomes more important especially in the indoor environment, because an average person spends more than 80% of daytime in the indoor environment either in the home or in the work place (Srivastava *et al.*, 2000).

Low concentrations of VOCs often cannot be detected by smell, and are usually well below the detection limit of common sensors. Thus, many researches have been carried out to develop VOC gas sensors, especially with the use of tin oxide (SnO_2) as the sensing

Received : 3 March 2008
Accepted : 8 April 2008
* Corresponding Author

medium. SnO_2 is proven to be one of the most attractive materials for gas sensor application due to its high sensitivity to gas as well as high chemical stability (Senguttuvan *et al.*, 2007). SnO_2 is an n-type semiconductor material, which at typical working temperatures of between 200°C and 450°C, adsorbs oxygen from the surrounding atmosphere to form an electron-depleted zone. Its electrical resistance decreases in the presence of a reducing gas, which reacts with the adsorbed oxygen leading to an increase in the electronic concentration. The measured change in the resistive value of the sensor due to the chemical reaction serves as the sensing signal (Lin *et al.*, 1997).

Lack of selectivity is one of the main drawbacks of the SnO_2 gas sensor. In order to enhance the gas sensing properties, the use of metal catalysts such as Ag, Pt, and Pd has been intensively studied (Yamazoe *et al.*, 1983). In addition, composite type sensors using a mixture of n-type and p-type semiconductors such as ZnO(n)/SnO_2(n) (Yu *et al.*, 1999), and CuO(p)/ZnO(n)/SnO_2(n) (Yu *et al.*, 2001) have been proposed in order to obtain stable interfaces. Among other metal oxides the TiO_2 is well known for its high sensitivity to changes in the surrounding gas composition. Furthermore, the applicability of a gas sensor based on composites of TiO_2-SnO_2 has been demonstrated for catalytic photodegradation of organic contaminants assisted by UV light (Zakrzewska *et al.*, 2007). In the present work, catalytic pellets that comprise of various compositions of titanium oxide (TiO_2) and tin oxide (SnO_2) have been developed for detection of volatile organic compounds (VOC). Ethanol was used as the volatile organic compound. The pellets were tested for their gas-sensing properties in the experiment rig at temperatures ranging between 100°C to 400°C. The morphological and structural characteristics of the catalytic pellets were investigated by mean of Scanning Electron Microscope (SEM) and X-ray Diffraction (XRD).

MATERIALS AND METHODS

Pellet Preparation

An appropriate amount of SnO_2 powder (Acros Organics, 99.9%) and TiO_2 powder (Acros Organics, 99+%) were milled in ethanol for 7 hours by using a ball-mill. The mixture was then dried and pressed into pellets (20 mm diameter and 2 mm thickness) using a hydraulic press machine at 10kPa. The pellets were sintered at 650∞C for 3h in air and cooled to room temperature.

Pellet Characterization

The morphological and structural characteristics of the catalytic pellets were investigated by means of a Scanning electron microscope, SEM (Leo Supra 50VP) and X-ray diffraction, XRD (Philip PW 1710 with Cu Ka radiation).

Sensing Performance

Each catalytic pellet was sandwiched between two copper electrodes in a quartz tube to measure the electrical conductivity and sensing behavior in the presence of ethanol vapour as shown in *Fig. 1*. The two copper electrodes were connected to an I-V electronic circuit to measure I-V characteristics. Firstly, the pellet was heated to 150°C in dry air for 10 minutes in order to exclude the moisture effect in the measurement. The electrical conductivity was measured after equilibrating the pellet in dry air for 30 minutes. The

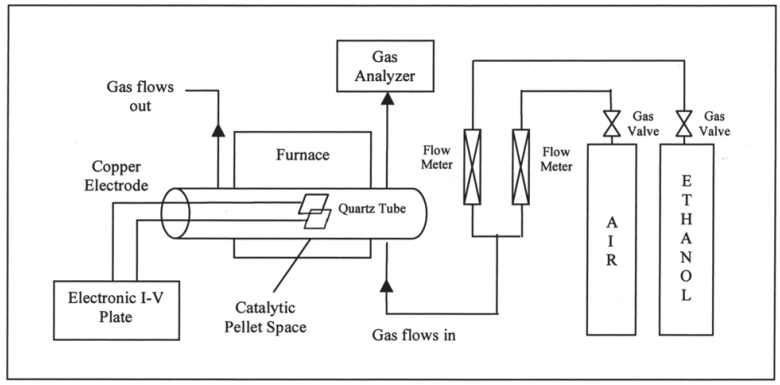

Fig. 1: Experimental rig setup

applied voltage was varied from 15 to 25 V and the resulting current was measured 2 seconds after applying the voltage. The pellet was then kept in dry air for 15 minutes before changing the measurement temperature from 50°C to 300°C. The electrical measurements were repeated after flowing 500 ppm of ethanol vapour in air for 5 minutes. For both sets of measurements, the total gas flow rate was set at 45 cm^3/min. The sensitivity of the sensor pellet to ethanol vapour is defined as;

$$S = \frac{R_{air-R_{ethanol}}}{R_{air}} \times 100\% \quad (1)$$

where S is the sensitivity (%), R_{air} and $R_{ethanol}$ are the electrical resistance of the pellet in air (ohm) and in ethanol vapour (ohm) respectively. The pellets' variations in sensitivity against temperature were performed.

RESULTS AND DISCUSSION

Surface Morphology

Figs. 2(a) and *2(b)* show the surface morphologies of pure SnO_2 and SnO_2 with 5 % TiO_2, respectively. It is obvious that the grains in *Fig. 2(a)* are of relatively uniform size, while there are two sizes of grains present in *Fig. 2(b)*. The larger sizes are the SnO_2 grains and the smaller size grains are those of TiO_2. It can also be observed that the grain size decreased when 5wt% of TiO_2 was added. It seems that by adding TiO_2 grain growth was hindered. Zhu *et al.* (2006) made similar observations in ZnO-based varistor. When TiO_2 was added more grains clogged together. It seems that TiO_2 not only reacts with SnO_2 to form another phase along the grain boundaries but also diffuses into the bulk grain.

In order to identify the phases of the sample, XRD was used and the diffraction patterns obtained as shown in *Fig. 3* for the sample that was sintered at 650^0C for 2 h. It was found that the sample has a spinel structure which is the $Ti_{0.1}Sn_{0.9}O_2$ (blue colour) phase. In addition to $Ti_{0.1}Sn_{0.9}O_2$, only the SnO_2 phase (red colour) is detected. It can be concluded that the SnO_2 nanoparticle reacts with TiO_2 at sintering conditions to form the composite.

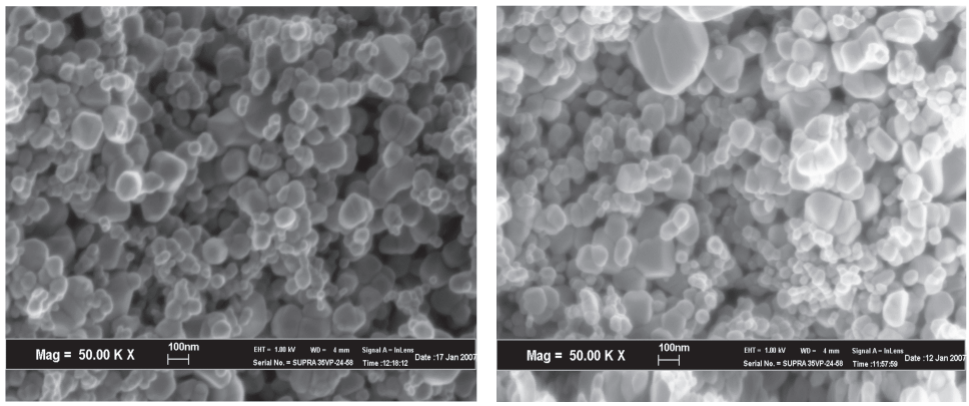

(a) (b)

Fig. 2: Surface morphology of catalytic pellet: (a) pure SnO_2, (b) SnO_2-5% TiO_2

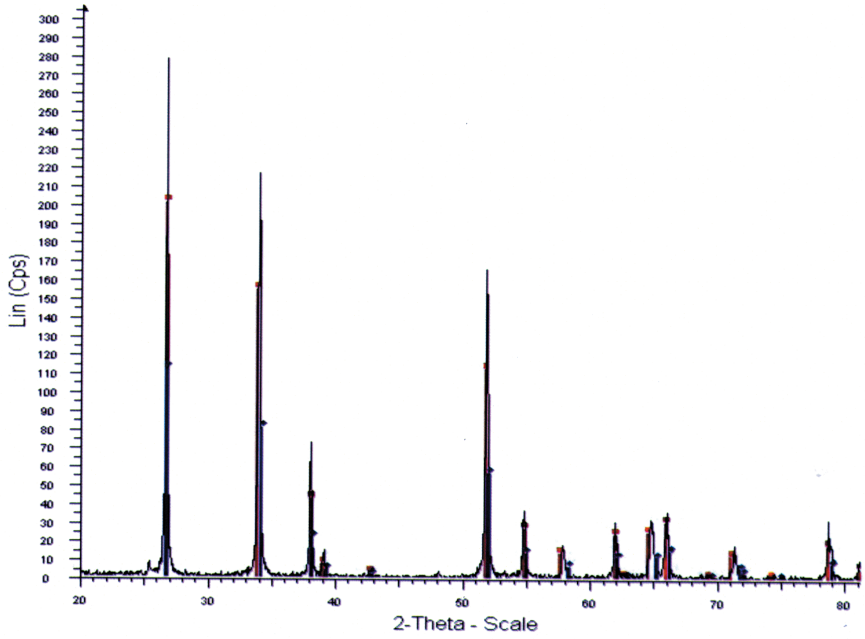

Fig. 3: X-ray diffraction patterns of 5 wt% TiO_2-SnO_2 catalytic pellet sintered at 650°C for 2 h

Fig. 4 shows the X-ray diffraction pattern of SnO_2 catalytic pellets that have 1, 5 and 10 wt% of TiO_2. It can be observed that there are sharp diffraction peaks which indicate the samples have a high degree of crystallization.

Ethanol Sensitivity

The effect of TiO_2 addition on SnO_2 catalytic pellets on gas sensitivity to ethanol vapour was studied in this work. The sensitivity of the catalytic pellets to ethanol vapour is shown

in *Fig. 5*. It was observed that the catalytic pellet of 1wt% TiO_2-SnO_2 has the highest sensitivity. The optimum detection temperature is about 250∞C. *Fig. 5* also shows that sensitivity increases with temperature before it reaches its maximum value. The increase in sensitivity with operating temperature can be attributed to the fact that the thermal energy obtained was high enough to overcome the activation energy barrier of the reaction, while the reduction in sensitivity was due to the difficulty in exothermic vapor adsorption (Chang *et al.*, 2002).

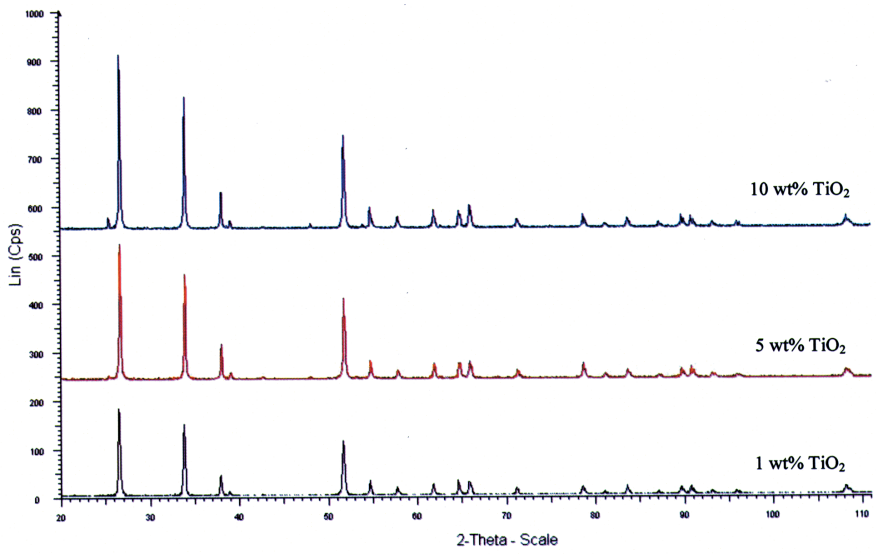

Fig. 4: X-ray diffraction patterns of the catalytic pellet with different TiO_2 contents sintered at 650°C for 2 h

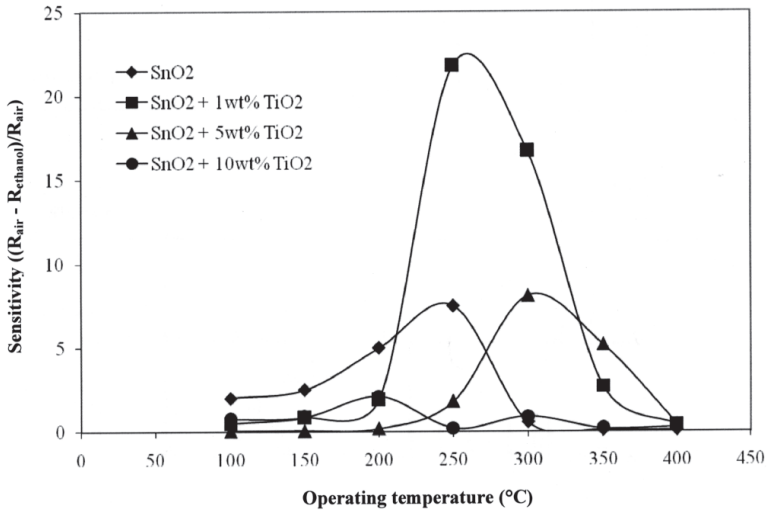

Fig. 5: Sensitivity of ethanol detection at various temperatures

The resistance change is controlled by the species and amount of chemisorbed oxygen on the surface thus the gas sensing mechanism of SnO_2 based sensors belong to the surface controlled type. It is proposed that the the oxidation of ethanol takes place via two routes, one the dehydrogenation to acetaldehyde as shown in Eq. (2) and the other, the dehydration to ethylene as given by Eq. (2) in which [O] represents the surface oxygen ions.

$$[O] + C_2H_5OH\ (gas) \rightarrow CH_3\,CHO + H_2O \quad (2)$$

and

$$[O] + C_2H_5OH\ (gas) \rightarrow C_2H_4 + H_2O \quad (3)$$

The oxidative hydrogenation reaction is mainly catalysed on the basic sites and dehydration is favored on the acidic sites. It is known that the first one has more sensitivity than the latter. The intermediate products, acetaldehyde and ethylene are subsequently oxidized to carbon dioxide and water (Vaishnav *et al.*, 2005).

As mentioned earlier, the addition of a small amount of TiO_2 altered the structure of the SnO_2 catalytic pellet and enhanced the chemisorption of oxygen on the surface. However, this behaviour only occurs at low amounts of TiO_2. When the percentage of TiO_2 was increased to 5% and 10%, the sensitivity reduced remarkably. This could be due to the reduction of pellet porosity, which may retard the adsorption of oxygen.

CONCLUSIONS

Catalytic pellets that comprise of various compositions of titanium oxide (TiO_2) and tin oxide (SnO_2) have been developed for detection of VOC. Surface morphology showed that the catalytic pellet has a porous structure. The results also showed that the sensitivity of the catalytic pellet to ethanol vapour increases when 1 wt% of TiO_2 was added.

ACKNOWLEDGEMENTS

The authors are thankful to the Malaysian Ministry of Science, Technology and Innovation (MOSTI) for providing the Long-term Science Fund (6013303) research grant.

REFERENCES

Brickus, S.R.L., Cardoso, J.N. and Feda, N. (1998). *Science and Technology, 32*, 3485.

Chang, J.F., Kuo, H.H., Leu, I.C. and Hon, M.H. (2002). The effects of thickness and operation temperature on ZnO:Al thin film CO gas sensor. *Sensors and Actuators B, 84*(2-3), 258-264.

Lin, H.M., Keng, C.H. and Tung, C.Y. (1997). Gas-sensing properties of nanocrystalline TiO_2. *Nanostructured Materials, 9*(1-8), 747.

Senguttuvan, T.D., Rai, R. and Lakshmikumar, S.T. (2007). Gas sensing properties of lead doped tin oxide thick films. *Materials Letters, 61*, 582-584.

Srivastava, U.P.K., Pandit, G.G., Sharma, S. and Mohan Rao, A.M. (2000). Volatile organic compounds in indoor environments in Mumbai, India. *The Science of The Total Environment, 255*(1-3), 161.

VAISHNAV, V.S., PATEL, P.D. and PATEL, N.G. (2005). Indium tin oxide thin film gas sensors for detection of ethanol vapours. *Thin Solid Films, 490*, 94-100.

YAMAZOE, N., KUROKAWA, Y. and SEIYAMA, T. (1983). Effects of addition on semiconductor gas sensor. *Sensors and Actuators B, 4*, 283-289.

YU, J.H. and CHOI, G.M. (1999). Electrical and CO-sensing properties of ZnO/ SnO_2 hetero-contact. *Sensors and Actuators B, 61*(1-3), 59-67.

YU, J.H. and CHOI, G.M. (2001). Selective CO detection of CuO- and ZnO-doped SnO_2 gas sensor. *Sensors and Actuators B, 75* (1-2), 56-61.

ZAKRZEWSKA, K. and RADECKA, M. (2007). TiO_2-SnO_2 system for gas sensing-photodegradation of organic contaminants. *Thin Solid Films, 515*, 8332–8338.

ZHU, B.L., XIE, C.S., WU, J., ZENG, D.W., WANG, A.H. and ZHAO, X.Z. (2006). Influence of Sb, In and Bi dopants on the response of ZnO thick films to VOCs. *Materials Chemistry and Physics, 96*(2-3), 459-465.

ISSN: 0128-7680
Pertanika J. Sci. & Technol. **16 (2)**: 239 - 247 (2008)

Bread Crust Thickness Estimation Using *L a b* Colour System

Y.M. Mohd. Jusoh[1], N.L. Chin[1*], Y.A. Yusof[1] and R. Abd. Rahman[2]
[1]Department of Process and Food Engineering, Faculty of Engineering,
[2]Department of Food Technology, Faculty of Food Science and Technology,
Universiti Putra Malaysia, 43400 UPM,
Serdang, Selangor, Malaysia
**E-mail: chinnl@eng.upm.edu.my*

ABSTRACT

The crust formation of bread is imperative as it contributes to aroma, flavour and texture of the product. The extent of surface browning during formation of crust is suspected to correspond to the thickness of crust and gradually affects the quality of the bread produced. A method to distinguish the crust and crumb was developed using the *L a b* colour system. Commercial breads of different categories, sandwich, open and standing breads, were used as samples to set up the colour range for crust and crumb. In general, *L* is always higher in the crumb compared to crust. However, *a* and *b* values in crust are consistently higher than crumb which indicates the browning effect. The xE between crust and crumb in sandwich, open and standing breads were 30.98, 29.86 and 25.96, respectively. Bread crust is identified as the brown region with *L* value lower than 66, *a* value higher than 2.4 and *b* value higher than 22.3. Baking temperatures in the range of 175 to 200°C and baking times from 30 to 50 minutes were used to bake open loaves with different crust colours and thickness. Higher baking temperature and time are proven to produce bread with intense surface colour and thicker crust. The correlation between crust colour and its thickness shows good linear relationships indicating the possibility of predicting crust thickness using its surface colour.

Keywords: Bread crust, surface browning, *L a b* colour system, DE

INTRODUCTION

The study on crust is a challenging new area in bread research. Previous studies on bread mainly focus on bread crumb, thus the important functions of the crust on bread have not been thoroughly investigated. Bread crust has many effects on bread properties. Lu Zhang *et al.* (2007) showed that the formation of crust affects bread volume, density and porosity. It also acts as a natural protective layer that prevents moisture evaporation as reported by Walhby and Skjoldebrand (2002).

Crust as interpreted by Jefferson *et al.* (2005) is the surface of bread which has higher density than crumb. Crust coloration and thickening occurs simultaneously during the baking process. Therthai *et al.* (2002) highlighted that crust colour and bread qualities e.g. moisture content, crumb firmness and shelf-life are affected by baking conditions. Furthermore, high baking conditions may cause excessive evaporation that leads to dryer crumb in the finished product. Patel *et al.* (2005) reported that higher heating rate

Received : 3 March 2008
Accepted : 8 April 2008
* Corresponding Author

application also causes higher degree of firmness in crumb since heat affects the starch properties and subsequently influences the storage quality of bread. Gil *et al.* (1997) shows that higher moisture in bread can retard staling process since it helps to reduce crumb firmness. The relationship between colour and moisture content in bread during baking was reported by Purlis and Salvadori (2007). The findings justify the importance of investigating crust colour since it can be associated with ingredients, processing factors, quality and shelf-life of produced breads.

The first objectives of this study were to develop a method to distinguish the crust from its crumb through the application of *L a b* colour system and to find the correlation between crust thickness and its colour for estimation of crust thickness.

MATERIALS AND METHODS

Crust and Crumb Measurement

Three categories of breads, sandwich (SW), open (OP) and standing (ST) breads were chosen for this study. Each category was represented by three different loaves. The Colour Reader (CR-10, Konica Minolta, Japan) (*Fig. 1*) was used to measure the level of lightness of material, (*L*), redness, (*a*), and yellowness, (*b*), of the samples. The total colour variation or difference, (ΔE), was calculated using Equation [1].

$$\Delta E = \sqrt{\Delta L^2 + \Delta a^2 + \Delta b^2} \qquad [1]$$

Fig. 1: Colour reader (CR-10, Konica Minolta, Japan)

The locations for crust and crumb colour measurements are shown in *Fig. 2.* The colour of the crust was measured by pointing the colour reader directly to the top surface of the crust. The *L, a,* and *b* values were indicated after the scanning process. The colours of crumb were measured and recorded at five locations, from 1 to 5 cm from the crust. The crumb of the bread was divided into five layers where the first layer was 1 cm from the crust surface while the second layer was 1 cm from the first layer and so on.

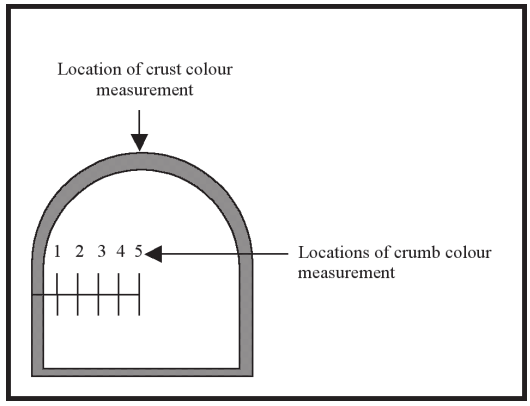

Fig. 2: Locations for measuring crust and crumb

Crust Thickness Determination

The thickness of crust was measured using a digital vernier caliper (500-196-20, Mitutoyo, Japan) (*Fig. 3*). In measuring the thickness, a simple colour guide drawn from the results obtained from Section 2.1 was used. The crust is defined as the brown region with $L < 66$, $a > 2.4$, $b > 22.3$ while the crumb is the white region with values below or above the *L a b* ranges that have been set for the crust.

Crust Colour and Thickness Investigation

The relationship between the crust colour and its thickness was investigated by conducting a factorial design experiment for standard baking tests in AACC 10-10 (1976). Three levels of baking temperatures (175, 185 and 200°C) and three levels of baking time (30, 40 and 50 minutes) were varied in triplicate. Table 1 shows the formulation used in the baking test. The colour and thickness of the bread crust were measured after resting for two hours using the crust colour and thickness methods mentioned earlier.

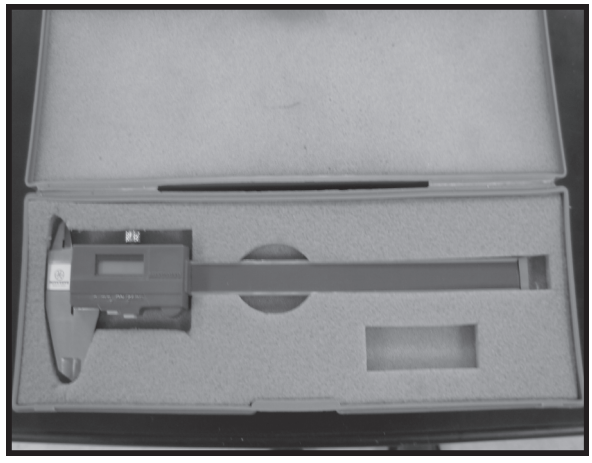

Fig. 3: Digital vernier caliper (500-196-20, Mitutoyo, Japan)

TABLE 1
Formulation of bread for baking tests

Ingredients	% (based on 500 g flour loading)
Flour	100
Water	63
Sugar	5
Yeast	3
Salt	1

RESULTS AND DISCUSSION

Crust and Crumb Colour Range

Figs. 4 to *6* show the average *L a* b values of crust and crumb for all three commercial bread samples. The *L* values of crumb for all samples were always higher than that for the crust showing that the crumb is always lighter than the crust. This is true for baked goods as the crust becomes darker due to direct heat penetration during the baking process. The bread crumb maintains a lighter colour because it is protected from direct heating. The major difference in *L* values between the crust and crumb was found in the sandwich and open bread samples. The difference in *L* values between the crust and crumb for standing breads were less significant. This may be due to the less dense crumb structure of the standing bread compared to the sandwich and open breads. The high porosity crumb surface may be the cause of insufficient reflection of brightness, thus resulting in lower *L* crumb values.

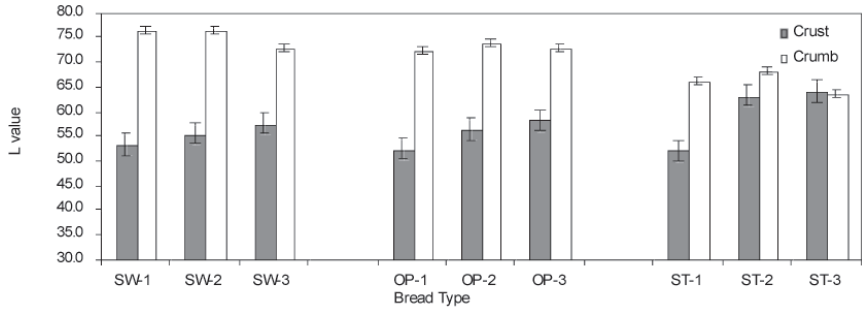

Fig. 4: L value for crust and crumb of commercial SW, OP and ST breads

The values of *a* and *b* are always higher in the crust compared to the crumb. This condition may be related to caramelization and Maillard reaction during crust formation. These two prominent processes during baking are responsible for transforming reducing sugars to other components and changing the colours of material with the existence of heat. The difference of *a* values between crust and crumb is more vivid than *b* values. The open bread in general has higher *a* and *b* values in the crust region compared to

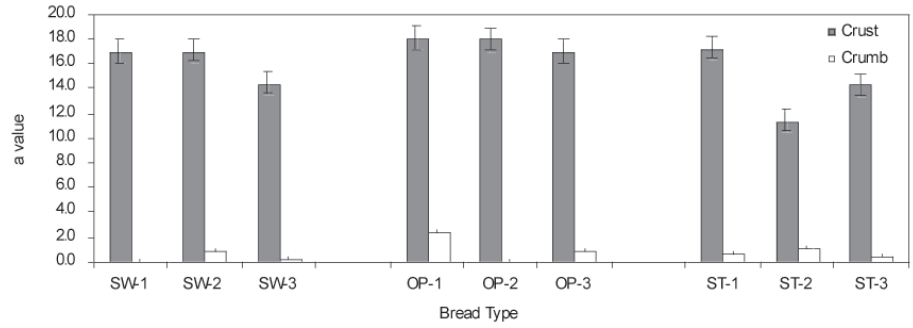

Fig. 5: a value for crust and crumb of commercial SW, OP and ST breads

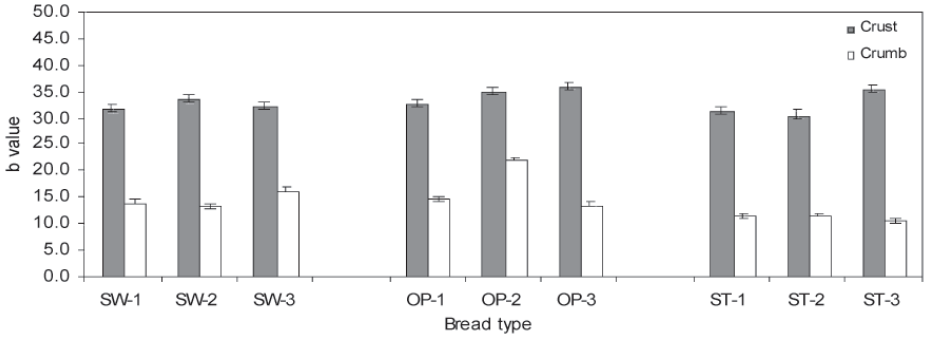

Fig. 6: b value for crust and crumb of commercial SW, OP and ST breads

the sandwich and standing breads. This is highly associated with its baking operations as the open bread is exposed to higher heat surface areas and thus possesses a significant browning effect. Baking temperature is one of the main factors that cause browning effect. Martin *et al.* (2001) emphasized that caramelization and Maillard browning were governed by baking temperature and time. Extensive modeling for bread baking and browning kinetics of bread surface have been conducted by Zanoni *et al.* (1993, 1994, 1995) and Purlis and Salvadori (2007).

Effect of Baking Conditions on Crust Colour

The baking tests conducted by varying the baking temperatures and times show that these conditions have a significant impact on the surface colour and thickness of the top crust. *Fig. 7* illustrates the effect of temperature and time on *L* value of crust. Both factors were inversely proportional with the *L* value. Bread baked at lower temperature and time has higher *L* value. The other colour components, *a* and *b,* however, reacted differently from *L*. *Fig. 8* and *9* show that the *a* and *b* values are directly proportional to baking temperature and time. Lower baking temperature and time produced breads of lower *a* and *b* values indicating lower redness and yellowness intensity. Variation in baking conditions has significant impact on crust colour ($p<0.05$).

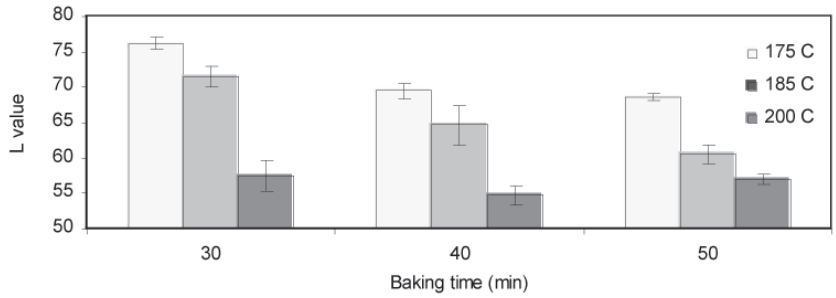

Fig. 7: Effect of baking temperature and time on L value of open bread top crust

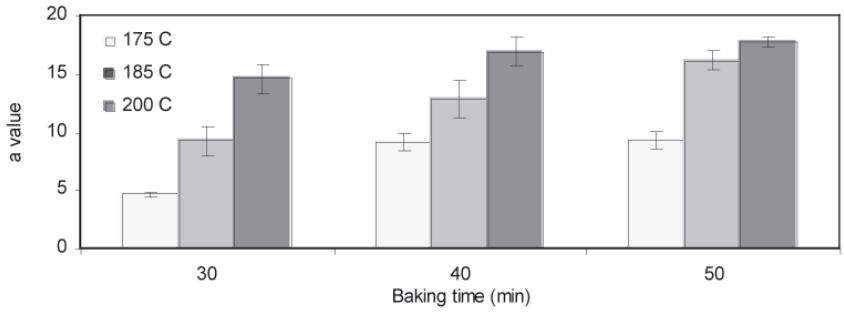

Fig. 8: Effect of baking temperature and time on a value of open bread top crust

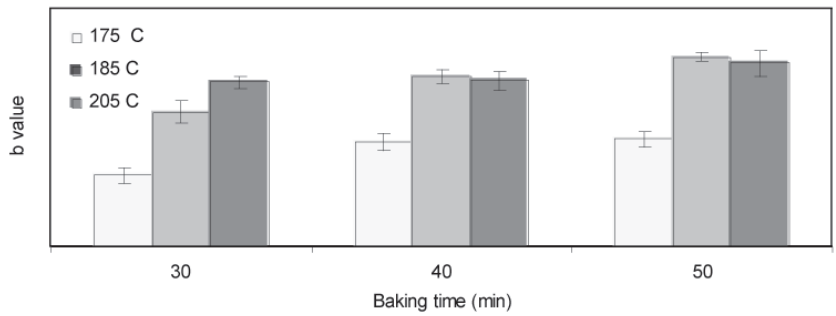

Fig. 9: Effect of baking temperature and time on b value of open bread top crust

Correlations between Baking Conditions and Crust Thickness

Besides bread crust colour, the baking conditions also affected the formation of crust. Zanoni *et al.* (1993) suggested that the formation of the two separate regions, crust and crumb, is due to the progressive advance of heat into inner bread as a result of the evaporation front phenomena. *Fig. 10* shows the correlation between baking conditions and crust thickness. Crust thickness increases as baking temperature and time increase. The increment in crust thickness was more pronounced for bread baked at 200°C compared to bread baked at lower temperatures as indicated by the steep slope value of

0.0465. The reason for this condition is probably due to the high temperature gradient between the surface of the crust and the inner bread. Excessive heat made the crust dry and forced inner moisture to evaporate from crumb. This excessive evaporation caused the bread structure at the surface to collapse and become dense. As a result, thicker and darker crust was formed. On the other hand, only slight increment in thickness was observed in bread baked at 175°C suggesting that increasing baking time at this temperature does not significantly affect crust thickness.

Correlations between Crust Colour and Thickness

As baking conditions directly affected the colour and thickness of the crust, thus the correlations between the colour and crust thickness of bread were also investigated. These correlations are important as they allow prediction of crust colour when thickness is known or vice versa. These correlations are presented in *Figs. 11(a)-(c). Fig. 11(a)* shows a negative relationship between the *L* value and the crust thickness. As the crust thickness

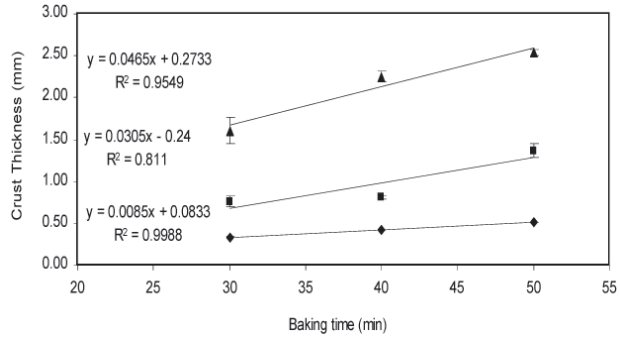

Fig. 10: Correlation between baking time and top crust thickness for baking temperatures at 175°C (◆), 185°C (■) and 200°C (▲)

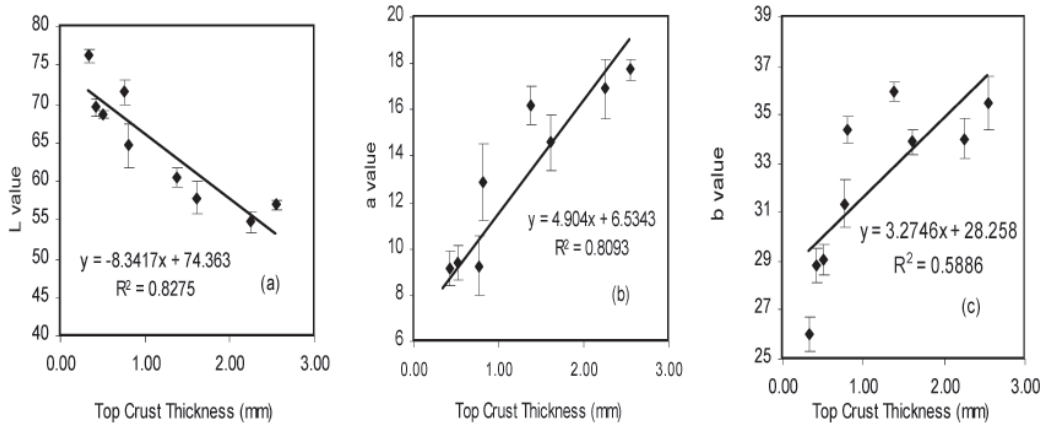

Fig. 11: Correlations between colour components of L (a), a (b) and b (c) with thickness of top crust

increases, the lightness of the crust surface decreases. In order to make the crust thicker, the bread surface must be exposed to higher baking temperature and time which in the end results in darker bread surface (*Fig. 10*). The values of *a* and *b* behave otherwise. The correlations between crust thickness with *a* and *b* values result in positive straight lines as shown in *Fig. 11(b)* and *(c)*. These relationships indicate that the thicker the crust, the higher the *a* and *b* values or in other words the redness and yellowness of the crust increases as the crust becomes thicker. Heat supplied causes intense browning effect on the bread surface resulting from the caramelization and Maillard process.

CONCLUSIONS

A method to distinguish bread crust and crumb using *L a b* colour system was successfully developed. The bread crust is identified as the brown region with *L* value lower than 66, *a* value higher than 2.4 and *b* value higher than 22.3. Different types of breads give different values of *L a b*. These differences occur due to the processing factors, *e.g.* method of heat exposure to bread during baking (whether direct or indirect) and/or baking times. The correlation study between crust colour and its thickness shows good linear relationships indicating the possibility of predicting crust thickness via its surface colour.

ACKNOWLEDGEMENTS

The authors are grateful to the Ministry of Higher Education of Malaysia for funding of this project, 01-01-07-214FR.

REFERENCES

AACC. (1976). Approved methods of the American Association of Cereal Chemists: method 10-10. First approved 13/4/61. American Association of Cereal Chemists

Jefferson, D.R., Lacey, A.A. and Sadd, P.A. (2005). Crust density in bread baking: Mathematical modeling and numerical solutions. *Applied Mathematical Modelling.*

Therthai, N., Zhou, W. and Adamczak, T. (2002). Optimization of temperature profile in bread baking. *Journal of Food Engineering, 55,* 41-48.

Gil, M.J., Callejo, M.J. and Rodriguez, G. (1997). Effect of water content and storage time on white pan quality: instrumental evaluation. *Z. Lebensm. Unters Forch A., 205,* 268-273.

Lu Zhang, Lucas, T., Doursat, C., Flick, D. and Wagner, M. (2007) Effects of crust constraints on bread expansion and CO2 release. *Journal of Food Engineering 80,*1302-1311.

Patel, B.K., Waniska, R.D. and Seetharaman, K. (2005). Impact of different baking processes on bread firmness and starch properties in breadcrumb. *Journal of Cereal Science, 42,* 173-184.

Purlis, E. and Salvadori, V.O. (2007). Bread browning kinetics during baking. *Journal of Food Engineering, 80,* 1107-1115.

Martins, S.I.F.S., Jongen, W.M.F. and Van Boekel, M.A.J.S. (2001). A review in Maillard reaction in food and implications in kinetics modelling. *Trends in Food Science and Technology.*

Wahlby, U. and Skjoldebrand, C. (2002). Reheating characteristics on crust formed on buns and crust formation. *Journal of Food Engineering, 53,* 177-184.

Zanoni, B., Peri, C. and Pierucci, S. (1993). A study of bread-baking process I. phenomenological model. *Journal of Food Engineering, 23,* 321-336.

ZANONI, B., PERI, C. AND PIERUCCI, S. (1994). A study of bread-baking process II. A mathematical modelling. *Journal of Food Engineering, 19,* 389-398.

ZANONI, B., PERI, C. and BRUNO, D. (1995). Modelling of browning kinetics of bread crust during baking. *Lebensm.-Wiss u.-Technology, 28,* 604-609.

ISSN: 0128-7680
Pertanika J. Sci. & Technol. **16 (2)**: 249 - 258 (2008)

Modelling of Methylene Blue Adsorption via Activated Carbon Derived from Indigenous Agricultural Solid Waste

Azam Taufik Mohd Din*, Bassim H. Hameed and Abdul Latif Ahmad
School of Chemical Engineering, Universiti Sains Malaysia, Engineering Campus, 14300 Nibong Tebal, Seberang Prai Selatan, Penang
**E-mail: chazam@eng.usm.my*

ABSTRACT

Conversion of indigenous agricultural solid waste into high quality activated carbon was a multi-fold strategy to counteract two major environmental problems; pollutant agricultural solid waste open burning and a partial solution for high-cost coloured industry effluents treatment, particularly in textiles and food processing plants by offering low-cost activated carbon. In this study, coconut shells were physiochemically treated at high temperature (850°C) in the presence of potassium hydroxide (KOH) with 1:1 impregnation weight ratio and carbon dioxide (CO_2) which acted as an oxidizing gas during activation stage. In order to evaluate the adsorption performance of prepared activated carbon (CS850A), a series of batch adsorption experiments were conducted at controlled parameters with initial concentrations of methylene blue ranging from 100 - 500 mg l^{-1}, temperature 30 ± 0.5°C, adsorbent loading 2.0 g and agitation speed of 100 RPM. It was found that the methylene blue adsorption on coconut shell-based activated carbon conformed to the Langmuir isotherm. The kinetic studies were well characterized by pseudo second order kinetic model. A suggestion has been made that the adsorption was favourable and was driven by a combination of physical and chemical adsorption forces. The monolayer adsorption capacity, Q_0 was found to be 222.0 mg g^{-1}.

Keywords: Activated carbon, methylene blue, batch adsorption, Langmuir, Freundlich

NOMENCLATURE

C_0	Initial adsorbate concentration	(mg l^{-1})
C_e	Equilibrium adsorbate concentration	(mg l^{-1})
C_t	Adsorbate concentration at time t	(mg l^{-1})
k_1	Rate constant of pseudo-first-order adsorption	(h^{-1})
k_2	Rate constant of pseudo-second-order adsorption	(g $(h.mg)^{-1}$)
K_L	Langmuir isotherm constant	(l g^{-1})
a_L	Langmuir isotherm constant	(l mg^{-1})
K_F	Freundlich isotherm constant	((mg g^{-1}) (l $mg^{-1})^{1/n}$)
$1/n$	Heterogeneity factor, dimensionless	
q_e	Amount of adsorbate adsorbed at equilibrium	(mg g^{-1})
q_t	Amount of adsorbate adsorbed at time t	(mg g^{-1})
R_L	Langmuir separation factor, dimensionless	
Q_0	Maximum adsorption capacity at monolayer	(mg g^{-1})
V	Volume of solution	(l)
w	Mass of adsorbent	(g)

Received : 3 March 2008
Accepted : 7 April 2008
* Corresponding Author

INTRODUCTION

Dyes have been regarded as major water pollutants since ages ago. Nowadays, dyes are widely used in textiles, food, rubber, paper, plastic and cosmetics industries (Lorenc-Grabowska and Gryglewicz, 2007). The presence of dyes in fresh water streams, even at low concentration can be easily detected through colour changes. Pollutant dyes discharged into fresh water stream may create unpleasant surroundings and decrease the esthetical value of the affected area. Besides, dyes can be very harmful to some aquatic life and reduce the light penetration into water thus affecting the photosynthesis capability of submerged green plants (Pearce *et al.*, 2003). In particular, methylene blue causes eye burns, inhalation difficulties, nausea, vomiting and methemoglobinemia (Ghosh and Bhattacharyya, 2002; Avom *et al.*, 1997). Therefore, the treatment of effluent containing such dye is necessary.

Adsorption techniques using activated carbon as adsorbent is the most popular approach to treat wastewater. The adsorption process is effective, cheap and flexible which makes it feasible in many wastewater treatment applications. Activated carbon is preferable due to its large surface area, high adsorption capacity, porous structure, selective adsorption and high purity standards (Ucer *et al.*, 2006). Most commercial activated carbons are produced from various types of coals; non-renewable material with limited source. In addition, the price of activated carbon has been increasing due to overwhelming demand. So, it is reasonable to seek a new activated carbon starting material which is cheap, renewable and a guaranteed steady supply throughout the year. The use of agricultural solid waste such coconut shell is rising in this context. Coconut trees are widely planted across Malaysia's coastal line for its oil, coconut milk and copra. It is estimated that 142,000 hectares of land was planted with coconut in 2006 (Agrolink, 2006). This huge planted area has resulted in higher harvest which apparently generates millions of tonnes of agricultural solid waste consistently. Typically, the shell is used as burning fuel or just being left to rot gradually. Coconut shell is very suitable to be converted into activated carbon due to its hardness and abrasion resistance. Further, the chemical composition of coconut shell is akin to hard wood which mainly composes of lignin and cellulose (Rodriguez and Pinto, 2007).

This research investigated the adsorption properties of activated carbon prepared from coconut shell by using methylene blue as a model solute. Consequently, this paper reports adsorption equilibriums and isotherms, and kinetic modeling studies of the particular batch adsorption system.

MATERIALS AND METHODS

Preparation of Activated Carbon

The coconut shell used in this research was collected from local wet markets within the Kerian district in the state of Perak, Malaysia. As received, the material was washed, sun dried, and crushed to particle size of 1-2 mm. The shell was then carbonized at 700 °C under the influence of nitrogen flow (150 cm^3 min^{-1}) for 1 hour. An accurate weight of produced char then was impregnated with equivalent weight of potassium hydroxide at impregnation ratio of 1:1. The mixture was dehydrated in a drying oven at 110 °C overnight. The dried solid mixture was placed in a stainless steel vertical tubular reactor and pyrolysed in a vertical tube furnace under high purity nitrogen (99.995%) with flow

rate of 150 cm^3 min^{-1} till it reached the desired temperature of 850°C. The gas was subsequently switched to carbon dioxide and the activation was continued for 2 hours. The activated char was then cooled to room temperature under nitrogen influence and washed a few times with hot deionized water and hydrochloric acid (0.01 M) to unclog the pores from tar and other chemical residues. The washed activated carbon, named CS850A was finally dried and kept in air tight closed containers. Table 1 presents the physical properties of the prepared activated carbon from coconut shell.

TABLE 1
Surface area and pore volume properties of CS850A

Properties	
Total surface area (m^2 g^{-1})	1026.0
Micropore area (m^2 g^{-1})	943.2
Mesopore area (m^2 g^{-1})	82.5
Total pore volume (cm^3 g^{-1})	0.5768
Average pore diameter (nm)	2.249

Batch Adsorption Modelling

The stock solution of methylene blue was prepared by diluting 1 gram of the respective adsorbate with 1000 ml deionized water in a volumetric flask. The stock solution then was diluted to the desired initial concentrations ranging from 100–500 mg l^{-1}. An amount of 0.2 gram adsorbent was added into 250 ml conical flasks filled with 200 ml of adsorbates solution of known initial concentrations. The conical flasks were then covered with glass stoppers and placed inside the water bath shaker at room temperature, 30 ±1°C and shaking speed of 125 rpm for 48 hours. The solution pH was adjusted by adding either a few drops of hydrochloric acid or sodium hydroxide (0.01 M). The samples were then withdrawn at appropriate time intervals using a glass syringe to determine the residual concentration of the adsorbate. The concentration of methylene blue in the aqueous solution was determined using a double beam UV spectrophotometer (Shidmadzu UV-1601, Japan) at wavelength 668 nm.

The amount of adsorbate adsorbed at time, q_t (mg g^{-1}) and at equilibrium condition, q_e (mg g^{-1}) was calculated according to the following equations:

$$q_t = \frac{V(C_0 - C_t)}{w} \tag{1}$$

$$q_e = \frac{V(C_0 - C_e)}{w} \text{z} \tag{2}$$

where C_0 and C_e are initial and equilibrium adsorbate concentrations (mg l^{-1}), respectively. C_t is adsorbate concentration at time (mg l^{-1}). V is volume of solution (l) and W is mass of adsorbent (g).

RESULTS AND DISCUSSION

Equilibrium

Dye removal is depends highly on concentration. The methylene blue uptake increased with increasing methylene blue initial concentrations. The trend is clearly elucidated in *Fig. 1.* This is due to a high driving force for mass transfer resulting from changes in concentration gradient within the solid-liquid bulk phase of the particular adsorption system. The equilibrium time was recorded after 5 hours for all ranges of initial concentrations. A steep slope in the first 3 hours indicates a rapid adsorption process. After a time lapse, the adsorption process got slower; the slope becomes less steep and eventually forming a plateau line; which is evidence that the whole adsorption system has achieved equilibrium state. The adsorption capacity at equilibrium increases from 99.38 to 227.0 mg g^{-1} with an increase in initial dye concentration from 100 – 500 mg l^{-1}. It is evident that the activated carbon prepared from coconut shell is efficient at adsorbing methylene blue dye from aqueous solution. The adsorption of methylene blue dye may follow four sequential steps. First, the migration of dye from bulk solution to the surface of activated carbon. Second, the diffusion of dye through the boundary layer to the surface of activated carbon. Third, the attachment of dye on the active site at activated carbon surface and finally, the intra-particle diffusion of dye into the interior pores of activated carbon matrix (Kannan and Sundaram, 2001).

Isotherms

The adsorption isotherms depict the distribution of solute molecule between liquid-solid phases at equilibrium. *Fig. 2* shows the adsorption isotherm of methylene blue on coconut shell-based activated carbon, CS850A. The isotherm was a typical L-type in which describes a favourable adsorption process. The L or Langmuir isotherm shape means no strong competition between the solvent (water) and the adsorbate (methylene blue) to occupy the adsorbent sites. In this case, the longitudinal axes of the adsorbed molecules are parallel to the adsorbent surface (Giles *et al.*, 1960).

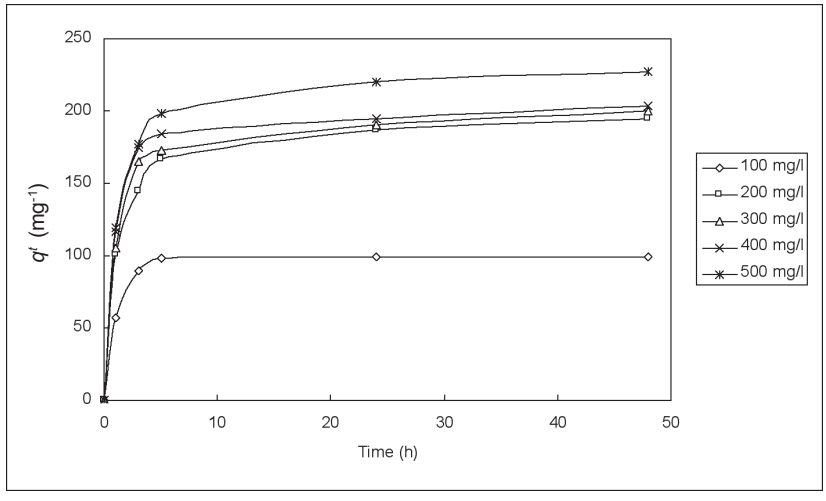

Fig. 1: Adsorption profiles of methylene blue-CS850A batch adsorption system

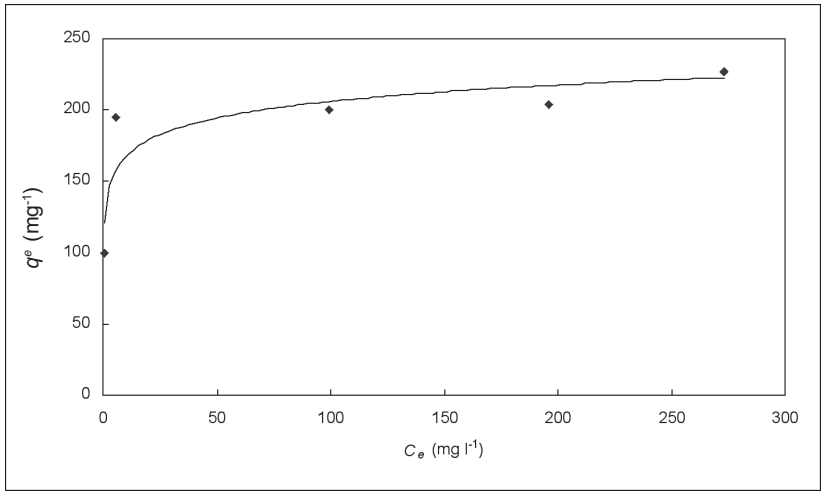

Fig. 2: Adsorption isotherm of methylene blue by CS850A

The analysis of the isotherm data by fitting them to different isotherm models is a crucial step to find the suitable model that can be used for design purpose (El-Guendi, 1991). Langmuir isotherm assumes monolayer formation of solute on the adsorption sites with homogenous energy distribution whereas; Freundlich isotherm assumes heterogenous energy distribution. Equations 3 and 4 represent Langmuir and Freundlich isotherm model, accordingly.

$$\frac{C_e}{q_e} = \frac{1}{K_L} + \frac{a_L}{K_L} C_e \tag{3}$$

$$\log q_e = \log K_F + \frac{1}{n} \log C_e \tag{4}$$

where q_e is amount of adsorbate adsorbed at equilibrium (mg g^{-1}), C_e is equilibrium concentration of the adsorbate (mg l^{-1}). K_L and a_L are Langmuir isotherm constants (l g^{-1}) and (l mg^{-1}), respectively. For Langmuir, plots of C_e/q_e versus C_e gives a straight line of slope a_L/K_L and intercept $1/K_L$, where K_L/a_L gives the Langmuir constant related to maximum adsorption capacity at monolayer, Q_0 (mg g^{-1}). As for Freundlich, a plot of log q_e versus log C_e enables the determination of constant K_F and exponent $1/n$. K_F is Freundlich constant, (mg g^{-1})(l mg^{-1})$^{1/n}$ and $1/n$ is dimensionless heterogeneity factor. The Langmuir separation factor, R_L is defined as Equation 5.

$$R_L = \frac{1}{(1 + a_L C_0)} \tag{5}$$

where C_0 is the maximum initial concentration (mg l^{-1}). The adsorption is favourable if the value of R_L lies within 0 to 1.

Figs. 3 and *4* illustrate the methylene blue adsorption isotherm plots of Langmuir and Freundlich, respectively. The coefficient values for both Langmuir and Freundlich isotherm models are shown in Table 2. The linear correlation coefficient, R^2 for Langmuir and Freundlich were 0.994 and 0.762, respectively. Hence, it is evident that methylene blue adsorption onto coconut shell-based activated carbon used in this study is well-fitted to Langmuir isotherm model. Therefore, it can be concluded that the methylene blue adsorption was characterized by monolayer surface coverage. The monolayer adsorption capacity, Q_0 was found to be 221.96 mg g^{-1}; an encouraging finding. High surface area of CS850A activated carbon (1026.0 m^2 g^{-1}) provides ample adsorption sites for dye molecule to attach on it; thus maximizing the uptakes. The average pore diameter (2.249 nm) is slightly larger than size of methylene blue dye molecule (≈ 1.5 nm), which simplifies the molecule to traverse beyond the internal pores. The adsorption process was favourable in nature as indicated by the R_L value.

Kinetics

Linear forms of pseudo-first and pseudo-second order kinetic equations are given in Equations 6 and 7, respectively.

$$\mathrm{In}(q_e - q_t) = \mathrm{In}\ q_e - k_1 t \tag{6}$$

$$\frac{t}{q_t} = \frac{1}{k_2 q_e^2} + \frac{1}{q_e} t \tag{7}$$

where q_t is the amount of solute adsorbed per unit weight (mg g^{-1}) of adsorbent per time, k_1 is rate constant of pseudo-first order sorption (h^{-1}) and k_2 is rate constant of pseudo-second order sorption (g (h mg)$^{-1}$). Linear plots of pseudo-first and second order kinetic model for methylene blue adsorption onto CS850A are given in *Figs. 5* and *6*, respectively. The applicability of the models is verified through the sum of error squares (SSE). The mathematical equation of SSE is given in Equation 8.

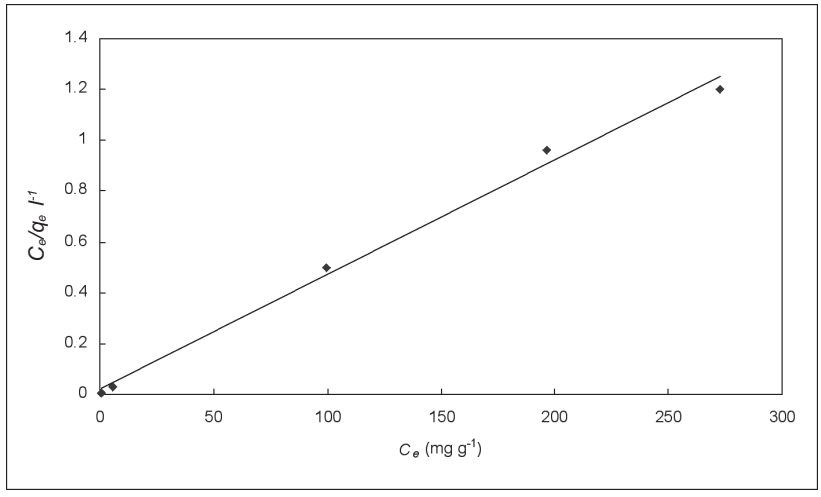

Fig. 3: Langmuir adsorption isotherm of methylene blue onto CS850 at 30°C

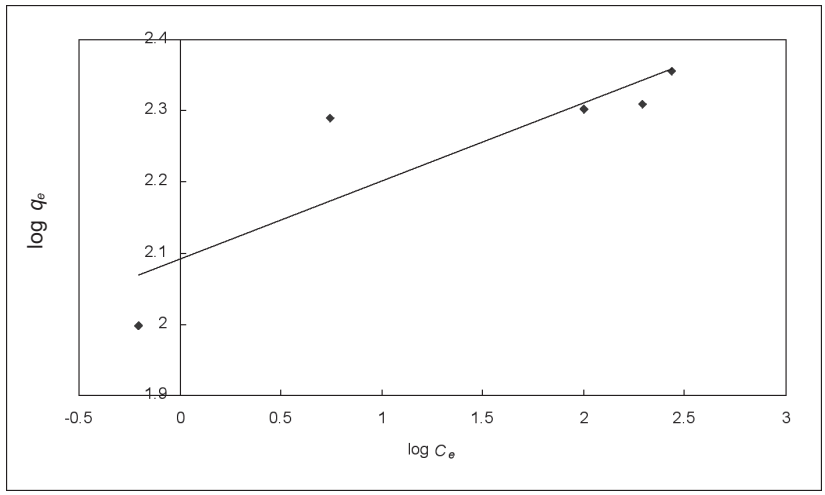

Fig. 4: Freundlich adsorption isotherm of methylene blue onto CS850 at 30°C

TABLE 2
Langmuir and Freundlich coefficients for methylene blue-CS850A batch adsorption system

	Langmuir isotherm parameters				Freundlich isotherm parameters			
Adsorbent	Q_O (mg g^{-1})	K_L (l g^{-1})	a_L (l mg^{-1})	R_L	R_2	K_F (mg g^{-1}) (l mg^{-1})$^{1/n}$	n	R_2
CS850A	221.96	49.505	0.223	0.009	0.994	123.34	9.107	0.762

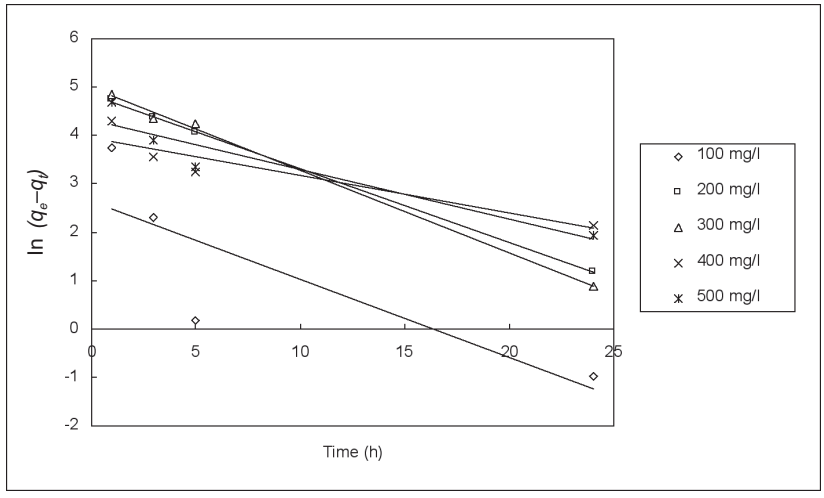

Fig. 5: Plots of Pseudo-first order kinetic model of methylene blue adsorption onto CS850A

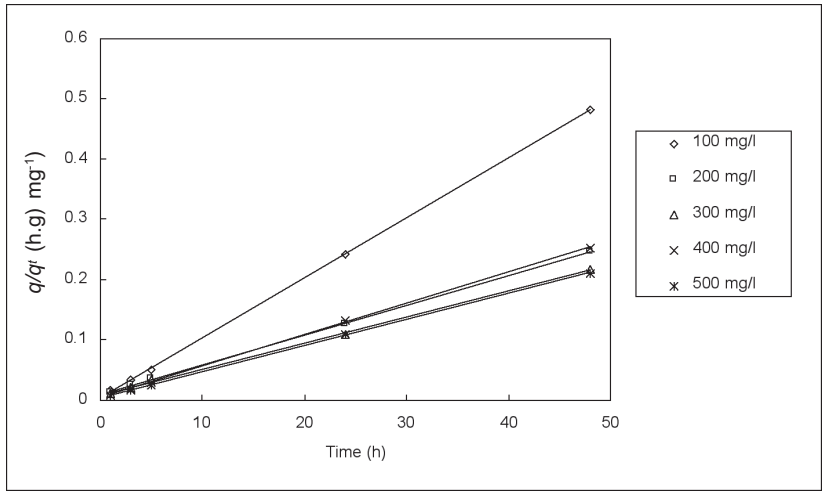

Fig. 6: Plots of Pseudo-second order kinetic model of methylene blue adsorption onto CS850A

$$SSE,\% = \sqrt{\frac{\sum (q_{e,exp} - q_{e_{calc}})^2}{N}} \tag{8}$$

where N is number of data points, $q_{e,exp}$ is amount of adsorbate adsorbed at equilibrium obtained from experiment (mg g^{-1}) and $q_{e,calc}$ is amount of adsorbate adsorbed at equilibrium obtained from the models (mg g^{-1}).

Figs. 5 and *6* elucidate the plots of pseudo- first and pseudo-second order kinetic models for methylene blue adsorption onto CS850A, respectively. It is a proof that the methylene blue adsorption onto CS850A is well-agreed to pseudo-second order kinetic model; indicating chemical reaction as a rate controlling parameter. The R^2 values are near unity.The model applicability was validated by small SSE values (< 5.6%) throughout various ranges of initial dye concentration. The coefficient values for both kinetic models are given in Tables 3 and 4, accordingly. No strong agreement was shown by the pseudo-first order kinetic model due to poor R^2 values and higher SSE values.

TABLE 3
Pseudo-first order kinetic constants for methylene blue-CS850A batch adsorption system

Concentration (mg l^{-1})	k_1 (h^{-1})	$q_{e,cal}$ (mg g^{-1})	R^2	SSE (%)
100	0.163	14.9	0.6691	42.24
200	0.154	128.3	0.9996	33.10
300	0.171	145.4	0.9972	37.99
400	0.078	52.4	0.8696	68.78
500	0.102	75.2	0.8902	75.92

TABLE 4
Pseudo-second order kinetic constants for methylene blue-CS850A batch adsorption system

Concentration (mg l^{-1})	k_2 (g $(h.mg)^{-1}$)	$q_{e,cal}$ (mg g^{-1})	R^2	SSE (%)
100	2.439	100.0	0.9999	0.31
200	0.500	200.0	0.9995	2.70
300	0.551	232.6	0.9994	5.58
400	1.182	192.3	0.9997	1.15
500	1.049	232.6	0.9999	2.78

CONCLUSIONS

Coconut shell based-activated carbon can be effectively used as a high performance adsorbent for removal of methylene blue dye from aqueous solution. The adsorption isotherm is well-fitted to Langmuir isotherm indicating the formation of monolayer solute coverage on the adsorbent surface. A conformation to pseudo-second order kinetic model signifies chemical reaction as a rate controlling parameter. It is suggested that the adsorption was favourable in nature and was driven by a combination of physical and chemical adsorption forces. The monolayer adsorption capacity, Q_o (221.96 mg g^{-1}) is encouraging.

ACKNOWLEDGEMENTS

The authors acknowledge the research grant provided by Ministry of Science, Technology and Innovation (MOSTI), Malaysia under long term IRPA grant (Project no: 08-02-05-1021 EA001) for this study.

REFERENCES

Avom, J., Mbadcam, J.K., Noubactep, C. and Germain, P. (1997) Adsorption of methylene blue from an aqueous solution onto activated carbon from palm-tree cobs. *Carbon, 35,* 365-369.

El-Guendi, M. (1991). Homogenous surface diffusion model of basic dyestuffs onto natural clay in batch adsorbers. *Adsorption Science and Technology, 8,* 217-225.

Ghosh, D. and Bhattacharyya, K.G. (2002). Adsorption of methylene blue on kaolinite. *Applied Clay Science, 20,* 295-300.

Giles, C.H., MacEwan, T.H., Nakhwa, S.N. and Smith, D. (1960). Studies in adsorption. Part XI. A system of classification of solution adsorption isotherms, and its use in diagnosis of adsorption mechanisms and in measurements of specific surface areas of solids. *Journal of Chemistry Society, 10,* 3973-3993.

Kannan, N. and Sundaram, M.M. (2001). Kinetics and mechanism of removal of methylene blue by adsorption on various carbons – a comparative study. *Dyes and Pigments, 51,* 25-40.

Lorenc-Grabowska, E. and Gryglewicz, G. (2007). Adsorption characteristics of congo red on coal-based mesoporous activated carbon. *Dyes and Pigments, 74,* 34-40.

Ministry of Agriculture and Agro-based industry Malaysia. (2006). Keluasan bertanam bagi tanaman terpilih. Retrieved from http://agrolink.moa.my/moa/images/stories/bpsa/data%20statistik/data%20utama%20pertanian/2.5.pdf, agrolink.moa.my, Putrajaya, Malaysia (accessed on 23 May 2007).

Pearce, C.I., Lloyd, J.R. and Guthrie, J.T. (2003). The removal of colour from textile wastewater using whole bacteria cells: A review. *Dyes and Pigments, 58,* 179-196.

Rodriguez, S. and Pinto, G.A.S. (2007). Ultrasound extraction of phenolic compounds from coconut (*Cocos nucifera*) shell powder. *J. of Food Engineering, 80,* 869-872.

Ucer, A., Uyanik, A. and Aygun, S.F. (2006). Adsorption of Cu(II), Cd(II), Zn(II), Mn(II) and Fe(III) ions by tannic acid immobilised activated carbon. *Separation and Purification Technology, 47,* 113-118.

ISSN: 0128-7680
Pertanika J. Sci. & Technol. **16 (2)**: 259 - 263 (2008)

Addition of Co_3O_4 to Introduce Pinning Centre in Bi-Sr-Ca-Cu-O/Ag Tapes

Mohd Mustafa Awang Kechik[1], Mohd Faisal Mohd Aris[1], Abdul Halim Shaari[1]*, Chen Soo Kien[1] and Roslan Abd Shukor[2]

[1]Department of Physics, Faculty of Science, Universiti Putra Malaysia
43400 UPM, Serdang, Selangor, Malaysia
[2]School of Applied Physics, Universiti Kebangsaan Malaysia
43600 UKM, Bangi, Selangor, Malaysia
**E-mail: ahalim@fsas.upm.edu.my*

ABSTRACT

This study investigated the flux pinning capability of Co_3O_4 in Bi-Sr-Ca-Cu-O superconductor tapes. The Bi-Sr-Ca-Cu-O powders were prepared by using the co-precipitation technique with the addition of Co_3O_4 as pinning centre to enhance the transport critical current density (J_c) of the system. The Ag sheathed $(Bi,Pb)_2Sr_2Ca_2Cu_3O_{10}$ (2223) and $(Bi,Pb)_2Sr_2Ca_2Cu_3O_{10}$-$(Co_3O_4)_{0.01}$ high temperature superconductor tapes were fabricated using the powder in tube method. The effects of Co_3O_4 addition on the microstructure, critical temperature and critical current density were studied. The J_c value of the Co_3O_4 added tapes increased to ~4500 A/cm_2. This tape showed the highest J_c and Tc when heated at 845°C for 50 hours. XRD diffraction pattern showed that the addition of Co_3O_4 inhibits the 2223 phase formation. This study shows that magnetic particles can act as effective pinning centres leading to the enhancement of J_c in the system.

Keywords: Superconductivity, flux pinning, Co_3O_4 addition

INTRODUCTION

Bi-2223/Ag superconductor tape is one of the most promising materials for tape or wire applications. Its poor performance under magnetic fields, which arises from the weak pinning of flux lines, limits its applications (Van Bael *et al.,* 2001) High critical current density J_c is required to meet practical applications. The strong increase of the critical current density J_c, up to the theoretical limit can be achieved when the flux lines are pinned and their movement completely prevented (Aloysius *et al.,* 2005). The flux lines in the solid state could be pinned by introducing effective artificial pinning centers so as to sustain the current density at higher fields and higher temperatures. These studies introduce ferromagnetic impurities as the pinning centers. Magnetic dots are successfully used as artificial pinning arrays in superconducting film covering the dots (Jia *et al.*, 2000).

MATERIALS AND METHODS

Samples with nominal composition $Bi_{1.6}Pb_{0.4}Sr_2Ca_2Cu_3O_\delta$ (BPSCCO) were prepared using the metal acetates of bismuth, strontium, lead, calcium and cooper (purity ≥ 99.99%), oxalic acid, deionized water and 2-propanol. The coprecipitation method was used in this

Received : 11 January 2008
Accepted : 8 April 2008
* Corresponding Author

system due to advantages such as good homogeneity, low reaction temperature, and fine and uniform particle size. The co-precipitation precursors were prepared by pouring the solution containing the metal ions into another containing 0.5 M oxalic acid dissolved in deionized water:2-propanol (1:1.5) and uniform, stable, blue suspension was obtained. The slurry was filtered after 5 minutes of reaction time followed by a drying stage at temperatures of 80˚C for 12 hour. The blue precipitate powders were heated up to 730˚C in air to remove remaining volatile materials. The calcined powders were reground and heated again at 845˚C in air for 24 hours followed by cooling at 2˚C /min. After the sintering process Co_3O_4 (300-400 nm) ultrafine particles were added to the composition with $Bi_{1.6}\ Pb_{0.4}\ Sr_2Ca_2Cu_3O_\delta$-$(Co_3O_4)_x$ where x = 0.00 and 0.01. The powders were ground and combined with 0.01 wt% Co_3O_4 before being packed into Ag tube with outer diameter of 6.12 mm and inner diameter of 4.43 mm. This wt% was chosen based on our previous study on bulk 2223 samples where 0.01 wt% of Co_3O_4 optimized the superconducting properties of the system (Kilic *et al.*,1998).

The tube was groove rolled, drawn into wire and then flat rolled into tape form. All deformations processed were carried out using a rolling cylinder 20 mm in diameter and rolling speed of about 0.6 m/min. The tapes were cut into 2 cm long sections and divided into six groups. Each group was sintered for 50 hours at different sintering temperatures. The FC 201 sample was sintered at 840°C, FC 111 at 845°C and FC 121 at 850°C sintered for 50 hours. FN 101, FN 111 and FN 121 are tapes without Co_3O_4 addition sintered at various temperatures for 50 hours as summarized in Table 1.

TABLE 1
Sintering temperature, J_c and T_c for tapes samples

Samples	Sintering Temperature (°C)	J_c at 77K A/cm^2	T_c (K)
$Bi_{1.6}\ Pb_{0.4}\ Sr_2Ca_2Cu_3O_\delta$			
FN 101	840	2455	78
FN 111	845	3090	78
FN 121	850	2182	80
$Bi_{1.6}\ Pb_{0.4}\ Sr_2Ca_2Cu_3O_\delta$-$(Co_3O_4)_{0.01}$			
FC 101	840	3308	88
FC 111	845	4507	93
FC 121	850	2308	97

The transition temperature was determined using the standard four-point probe method contact in conjunction with a closed cycle refrigerator. Transport critical current measurements were done at 77 K using four probe methods with the 1μVcm^{-1} criterion. In this criterion as the current is varied, the voltage (V) across the bar shape sample is measured and the distance between the voltage probes divided. Phase analysis of the samples was done using an XRD (Philips PW 3040/60 X'pert Pro) equipped with a monochromator at the diffracted beam side.

RESULTS AND DISCUSSION

Table 1 shows J_c for different sintering temperatures. It is clearly seen that J_c is strongly correlated with the sintering temperature with optimum value at 845°C.

Fig. 1 displays the effect of sintering temperature on the temperature dependence of critical current density J_c to non addition and addition of Co_3O_4 tape. At low temperature (30 K), J_c values are higher due to thermal activated flux motion becoming zero instead of being pronounced at higher temperature (77 K). It was found that J_c is enhanced in added tape as the size of the grains is decreased. This is an indication that the energy losses are higher in samples having large grains than in samples with small grains (Dou *et al.,* 1993).

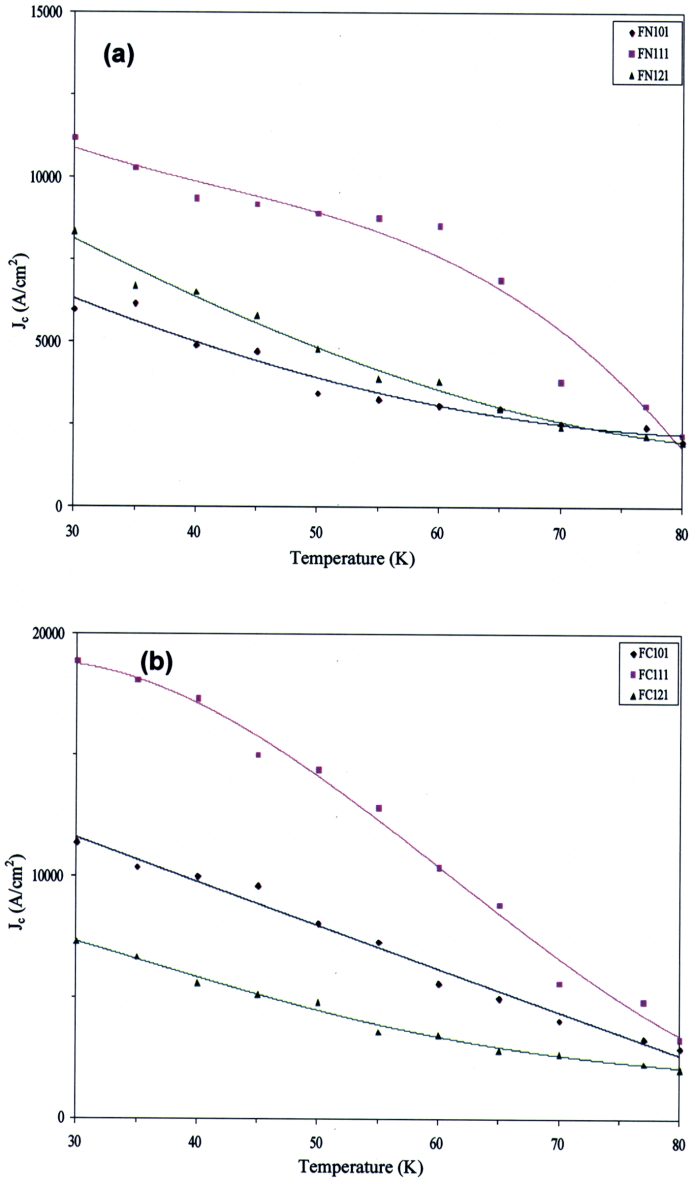

Fig. 1: Critical current density J_c vs. temperature with different temperature dependences for (a) Bi-2223 tape (b) after Co_3O_4 added

Fig. 2 shows the effect of temperature and sintering time duration on XRD spectrum to $(Bi,Pb)_2Sr_2Ca_2Cu_3O_{10}$, and $(Bi,Pb)_2Sr_2Ca_2Cu_3O_{10}$-$(Co_3O_4)_{0.01}$ tape core in Ag sheet. Sintering temperature from 840°C to 845°C reduced 2201 and 2212 phase peaks. 115 L, 0111 L and 0110 L peaks reduced when the sintering temperature increased. Number of peaks in 2223 phase domination shown in *Fig. 2(b)* where 200 H maximum peak in FC 111 sample. *Fig. 2* clearly shows the sample shift from 2212 phase to 2223 phase. This study shows that the addition of Co_3O_4 inhibits 2223 phase formation.

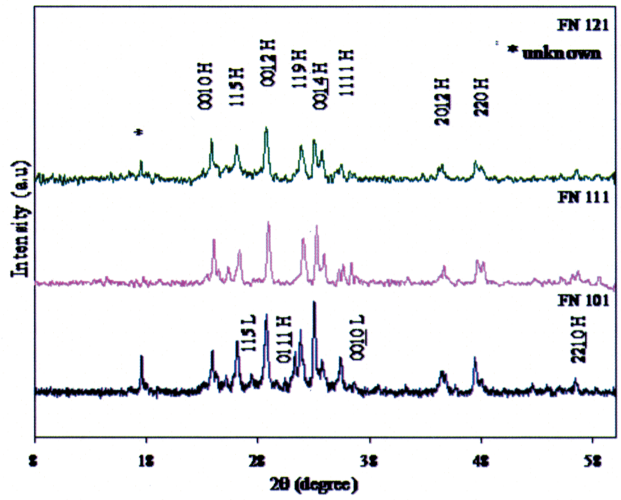

(a)

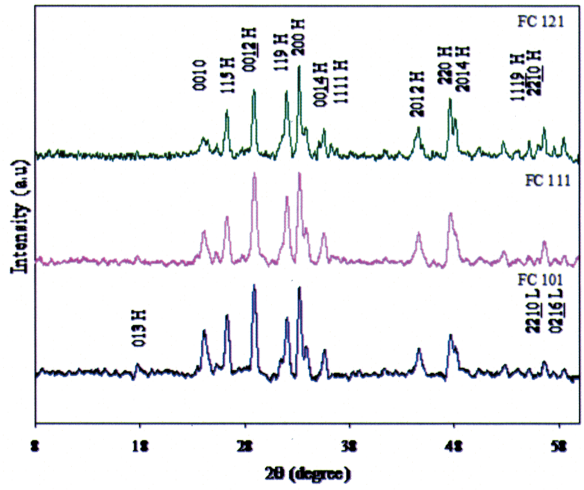

(b)

Fig. 2: XRD spectrum for (a)$(Bi,Pb)_2Sr_2Ca_2Cu_3O_{10}$, 840°C (FN101), 845°C (FN111) and 850°C (FN121) (b)$(Bi,Pb)_2Sr_2Ca_2Cu_3O_{10}$-$(Co_3O_4)_{0.01}$, 840°C (FC101), 845°C (FC111) and 850°C (FC121), sintered for 50 hour

CONCLUSIONS

This study found that the addition of Co_3O_4 increases the pinning strength in Ag-sheathed $(Bi,Pb)_2Sr_2Ca_2Cu_3O_{10}$ tapes. Magnetic impurities generally suppress conductivity. However, our results show that Co_3O_4 can be employed to enhance the flux pinning capability of Ag-sheathed $(Bi,Pb)_2Sr_2Ca_2Cu_3O_{10}$ tapes leading to enhancement of J_c in the system. The various sintering temperatures show that the 2223 phase formation increases at higher temperatures. It also happens when Co_3O_4 is added.

REFERENCES

A.Killic and Kilic, K. J. (1998). Grain size dependence of the current-voltage characteristics and critical current density in the self-field approximation. *Applied Physics, 84,* 3254-3262.

Dou, S.X. and Liu, H.K. (1993). Ag-Sheathed Bi(Pb)SrCaCuO superconducting tapes. *Supercond. Sci. Technol., 6,* 297-314.

M. J. Van Bael, Van Look, L., Lange, M., Temst, K., Guntherodt, G., Moshchalkov, V. V. and Bruynseraede, Y. (2001). Vortex self-organization in the presence of magnetic pinning arrays. *J. of Superconductivity: Incorporating Novel Magnetism, 14*(2), 355-364.

Aloysius, R. P., Guruswamy, P. and Syamaprasad, U. (2005). Highly enhance critical current density in Pr added (BiPb)-2212 superconductor. *J. Supercond. Sci. Technol., 18,* L23-L28.

Jia, Z.Y., Tang, H., Yang, Z.Q., Wang, Y.T. and Qiao, G.W. (2000). Effects of nano-ZrO2 particles on the superconductivity of Pb-doped BSCCO. *Physica C, 337,* 130-132.

ISSN: 0128-7680
Pertanika J. Sci. & Technol. **16 (2)**: 265 - 273 (2008)

Thermal Diffusivity Measurement of SnO_2-CuO Ceramic at Room Temperature

Aiza M.M.*, Zaidan A.W., Wan Mahmood M.Y. and Norfarezah H.E.
Applied Optics Laboratory, Department of Physics, Faculty of Science, Universiti Putra Malaysia, 43400 UPM, Serdang, Selangor, Malaysia
**E-mail: masya197@yahoo.com.sg*

ABSTRACT

Thermal diffusivity is a measure of rapidity of heat propagation through a material. The property is important in the understanding of gas sensor performance. Photoflash technique was used to determine thermal diffusivity of SnO_2-based materials with varying amount of CuO ranging from 10 to 50 mol%, at room temperature. The samples were made disc-shaped, 10 mm in diameter with thickness ranging from 2.4 to 2.8 mm. We found that the thermal diffusivity values of SnO_2-CuO samples ranging from 6.21 to 7.51×10^{-2} cm^2s^{-1} were better than the reported thermal diffusivity value of pure SnO_2 sample (1.45×10^{-2} cm^2s^{-1}). The thermal diffusivity behaviour was supported by results from XRD and SEM.

Keywords: Photoflash technique, SnO_2-CuO, thermal diffusivity

INTRODUCTION

Atmospheric pollution and safety requirements for industry have led to research and development of a variety of gas sensors using different materials and technologies particularly for better sensor performance (Chang *et al.*, 2002). An n-type semiconducting oxide such as tin dioxide (SnO_2) is one of the most important and extensively used materials for the detection of a number of toxic gases (Saadeddin *et. al.*, 2006, Vasiliev *et al.*, 1998). It is well established that the SnO_2-based gas sensors offer desirable attributes of cheapness, simplicity and high sensitivity (Kocemba *et al.*, 2001). However, there are some limitations to the wide use of semiconductor gas sensors i.e. lack of selectivity, long term drift and sensitivity to air humidity. The improvement of sensor properties of these materials can be achieved by the addition of adequate dopants.

Thermal diffusivity, α, is a measure of rapidity of the heat propagation through a material. The higher the value of thermal diffusivity of a material, the faster will be the heat propagation. For gas sensor application, it is important to first heat up the sensor to its operating temperature in order to activate the gas sensing property. For the sensor to be immediately used, we need the sensor to reach its operating temperature in a short time. So, sensors with higher thermal diffusivity material will give faster initialization time than sensors with lower thermal diffusivity. In this study, copper oxide, CuO was added to SnO_2 as the dopant to see its effects on the thermal diffusivity.

Nowadays, several different techniques for the determination of the thermal diffusivity may be found in the literatures. The proper method is usually selected by considering the

Received : 11 January 2008
Accepted : 8 April 2008
* Corresponding Author

specimen size, shape, temperature characteristics and temperature range. The photoflash technique which has been developed by Parker *et al.* (1961) has been widely used due to the ease of sample preparation, less material requirements and fast measurements. One typically obtains accuracy within ± 5% when implementing careful measurement techniques.

MATERIALS AND METHODS

SnO_2-CuO ceramic was prepared using solid state route (Moon *et al.*, 2001). The raw materials used were SnO_2 (99.9%, Alfa Aesar) and CuO (extra pure, Scharlau). The details of the samples composition are shown in Table 1.

TABLE 1
Samples composition

Sample Name	Composition (mol%)	
	SnO_2	CuO
SC1	90	10
SC2	80	20
SC3	70	30
SC4	60	40
SC5	50	50

All the powders were weighed according to their compositions, wet mixed and stirred for 24 hours. The slurry was dried in an oven at 120°C for 10 hours. The mixtures were pre-sintered at 850°C for 2 hours at the heating and cooling rate of 3°Cmin^{-1}. The samples were sieved using 75 μm sieve. The green bodies were pressed into pellets of 10 mm in diameter with thickness ranging from 2.4 to 2.8 mm, at the pressure of 20 kN. Samples were then sintered at 1000°C for 3 hours.

The X-ray diffraction analysis was carried out for all samples using a Philip model 7602 EA Almelo X-ray Diffractometer (CuKα, λ=1.5418 Å) at range of 20 to 80 degree. The data was collected and analyzed with a Philips X'Pert Data Collector (Version 1.2d) software. The microstructure of the samples was observed by using a JEOL model 6400 Scanning Electron Microscope (SEM). To protect samples from charging by the electron beam during observation, the samples were coated with a thin gold film. Each sample was scanned at 10 kV accelerating voltage.

An important property of any material is its density. Measuring sample's density is one way to investigate the porosity of the sample. The increase of density for the sample could be due to the sufficient space or vacancies for an effective transportation of metal ions and the decrease of density could indicate the increased number and size of pores trapped within the grains. All sintered samples had their dimensions measured and were dry weighed. The geometrical density calculation is defined as:

$$D = \frac{m}{\pi\left(\frac{d}{2}\right)^2 L} \quad (1)$$

where *m*, *d* and *L* are the mass, diameter and thickness of the pellet sample, respectively. The theoretical density of the samples was calculated using the equation;

$$\rho_{theo} = \frac{m_s}{(V_{SnO_2} + V_{CuO})} \tag{2}$$

where ρ_{theo} , m_s , V_{SnO2} and V_{CuO} are the theoretical density, the mass of the mixture of sample, the volume fraction of SnO_2 and the volume fraction of CuO, respectively.
Thermal diffusivity of SnO_2-CuO ceramics was measured by using the photoflash technique at room temperature. The sample was polished using abrasive silicone carbide sandpaper to obtain a flat surface and also to get rid of impurities. Calibration was performed using standard Aluminium sample before starting the experiment. The schematic diagram of this technique is shown in *Fig. 1*. The front surface of the sample was exposed to a short burst of radiant energy from photoflash. The transient temperature curve of the rear surface of the sample was then measured with a thermocouple.

For photoflash technique, two ways of determining thermal diffusivity have been deduced by Parker *et al.* (1961) from the equation below.

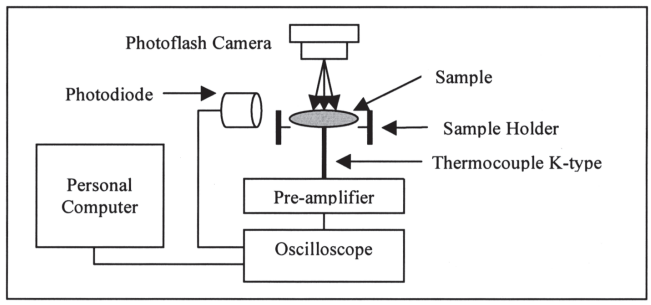

Fig. 1: Schematic diagram of the photoflash technique

$$V = 1 + 2\sum_{n=1}^{\infty}(-1)^n exp(-n^2 w) \tag{3}$$

When V is equal to 0.5, ω is equal to 1.37, so

$$\alpha = 1.37\frac{L^2}{\pi^2 t_{1/2}} \tag{4}$$

where $t_{1/2}$ is the time required for the back surface to reach half of the maximum temperature rise. Alternatively, t_x, the tangent to the temperature-time curve at the point of maximum gradient can be extrapolated to the time axis where the intercept, occur at ω = 0.48 from which

$$\alpha = 0.48\frac{L^2}{\pi^2 t_x} \tag{5}$$

where t_x is the time axis intercept versus time curve. Actually we may also use any percentage rise as the reference point for the calculation of thermal diffusivity as given below:

$$\alpha = k_x \frac{L^2}{t_x} \tag{6}$$

where K_x is a constant corresponding to an x percentage rise of temperature at the rear surface of slab and t_x is the elapsed time to an x percentage rise.

In the calculation of thermal diffusivity, it is advisable to rely on a single point from the whole curve, as in the case with expression [4]. Expression [6] permits the use of the portion of the response curve, which has been least affected by interferences. The use of expression [6] is therefore strongly recommended.

The characteristics rise time is important in order to quantify whether the corrections for finite pulse effect should be applied to the measurement. For the finite pulse time effect considerations, the pulse duration, τ (5ms) of the photoflash was compared with the characteristic rise time, t_c of the sample. The finite pulse effect in this study was always less than 1 ($\tau/t_c \ll 1$), so the finite pulse time correction is negligible (Maglic *et al.* 1992).

Heat loss usually occurs in the flash method. Radiation heat loss corrections can be done based on Clark and Taylor (1975) rise-curve data by employing the ratio technique. For the $t_{0.75}$ / $t_{0.25}$ ratio i.e, the time to reach 75% of the maximum divided by the time to reach 25% of the maximum, the ideal value of the ratio is 2.272. This ratio must be determined from the experimental data. Then the correction factor, K_R can be calculated from the equation

$$K_R = -0.3461467 + 0.361578\left(\frac{t_{0.75}}{t_{0.25}}\right) - 0.06520543\left(\frac{t_{0.75}}{t_{0.25}}\right)^2 \tag{7}$$

The corrected value of thermal diffusivity at the half time will be

$$\alpha_{corrected} \frac{\alpha_{0.5} K_R}{0.13885} \tag{8}$$

Besides that, corrections by using many other ratios can also be used if the constants for calculating the correction factor are provided.

RESULTS AND DISCUSSION

The phase composition analyzed by XRD, showed that there were no impurity phases in SnO_2-CuO system, *Fig. 2.* All peaks are presented by SnO_2 and CuO (Zhang and Liu, 2000). The absence of CuO peaks in the SC1 sample may be due to the smaller X-ray scattering power of CuO than SnO_2. The CuO peak was observed for SC_2, but the intensity of CuO peak remains low, suggesting that the concentration of CuO phase in SnO_2–CuO is small. Strong peaks of CuO (-111, 111) were observed in SC3 (at 2θ = 35.57°, 38.77°, respectively).The intensity of peaks corresponding to the CuO phases

increased slightly from SC3 to SC5 while SnO_2 peaks (110, 101, 211) at 2θ = 26.60°, 33.89° and 51.80°, respectively were gradually decreased when the concentration of CuO phase in SnO_2–CuO were increased.

Fig. 3 shows one of the thermograms obtained from the thermal diffusivity measurements. The rest of the data obtained in this study are presented in Table 2 which show the characteristic rise time and corrected thermal diffusivity, α_c value at different composition of CuO mixed with SnO_2. *Fig. 4* shows the relationship between thermal diffusivity and SnO_2–CuO system.

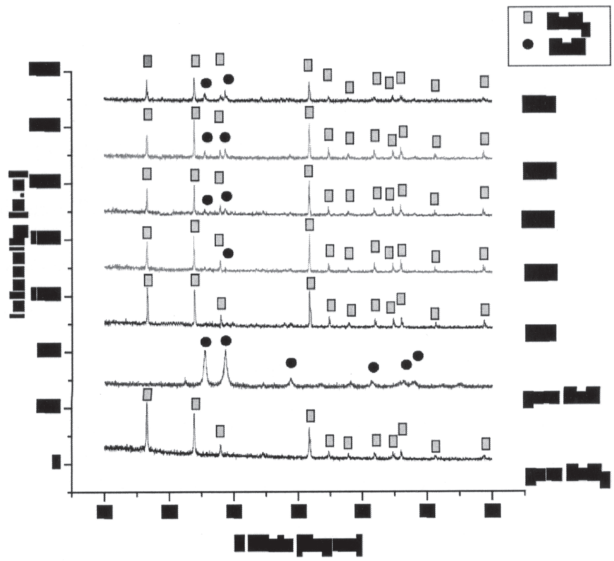

Fig. 2: XRD patterns of SnO2-CuO samples

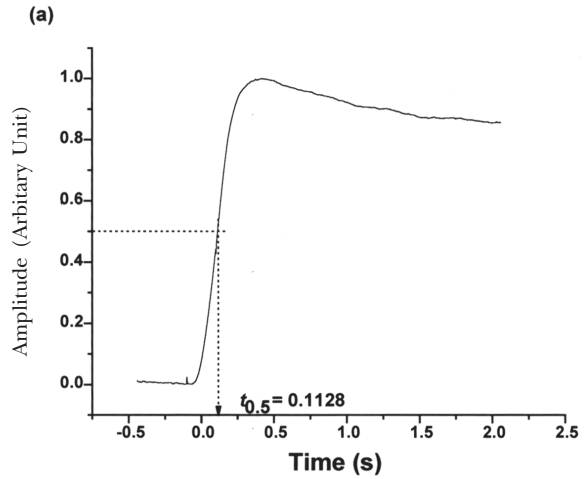

Fig. 3: Thermogram of SC1 sample (thickness, L=0.2354 cm)

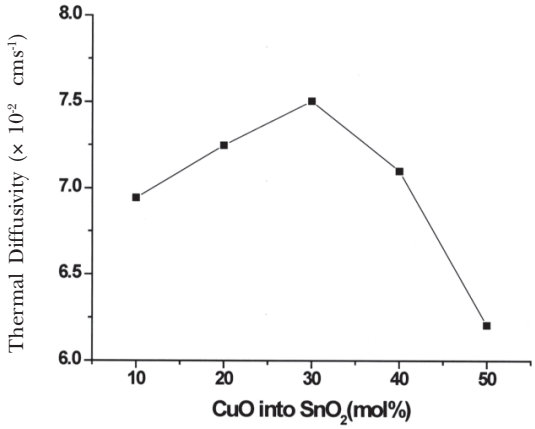

Fig. 4: Thermal diffusivity of SnO_2-CuO at different composition

TABLE 2
Characteristic rise time and the corrected thermal diffusivity value of SnO_2-CuO at different composition

Sample	Thickness (cm)	Half rise time $t_{0.5}$ (s)	Characteristic rise time, $t_c = L^2/\alpha\pi^2$ (s)	τ / t_c (s)	Corrected thermal diffusivity, α_c ($\times 10^{-2}$ cm^2s^{-1})
SC1	0.2354	0.1128	0.0818	0.0611	6.9436
SC2	0.2325	0.1100	0.0803	0.0623	7.2468
SC3	0.2719	0.1484	0.1083	0.0462	7.5048
SC4	0.2722	0.1554	0.1132	0.0442	7.0995
SC5	0.2782	0.1758	0.1283	0.0390	6.2059

Thermal diffusivity of pure SnO_2 has been reported to be 1.45×10^{-2} cm^2s^{-1} (Rosyaini, 2004). The introduction of CuO (10-50 mol %) into the ceramic system, resulted in thermal diffusivity range of 6.21 to 7.51×10^{-2} cm^2 s^{-1}. The addition of CuO up to 30 mol% increased the thermal diffusivity value from 1.45×10^{-2} cm^2s^{-1} (pure SnO_2) to 7.51×10^{-2} cm^2 s^{-1} (SC3). However, further addition of CuO beyond 30 mol% decreases thermal diffusivity value to 6.21×10^{-2} cm^2 s^{-1}.

The influence of CuO on the sintered samples densities, theoretical densities, relative densities and porosities is shown in Table 3 while *Fig. 5* shows the relative density as a function of mole percentage of CuO addition. *Fig. 6* shows the porosity percentage as a function of mole percentage of CuO addition.

Based on the density measurement, the density of the sintered sample decreases gradually as CuO was increased (10-50 mol%). The highest density (ρ = 5.87 gcm^{-3}), was obtained for the SC1 sample where its relative density was about 85% of the theoretical density, while SC5 gave the lowest density (ρ = 5.39 gcm-3) where its relative density was about 80% of the theoretical density. This indicates that more pores were present in this sample as more CuO was introduced.

It is well understood that heat propagation will be retarded as they encounter grain boundaries. Every grain boundary is a potential site for phonon scattering. For heat

TABLE 3
Influence of CuO on the sintered samples densities, theoretical densities, relative densities and porosities

Sample	Sintered Density (gcm^{-3})	Theoretical Density (gcm^{-3})	Relative Density (%)	Porosity (%)
SC1	5.87	6.92	84.86	15.14
SC2	5.72	6.89	83.04	16.96
SC3	5.63	6.85	82.09	17.91
SC4	5.46	6.81	80.07	19.93
SC5	5.39	6.77	79.63	20.37

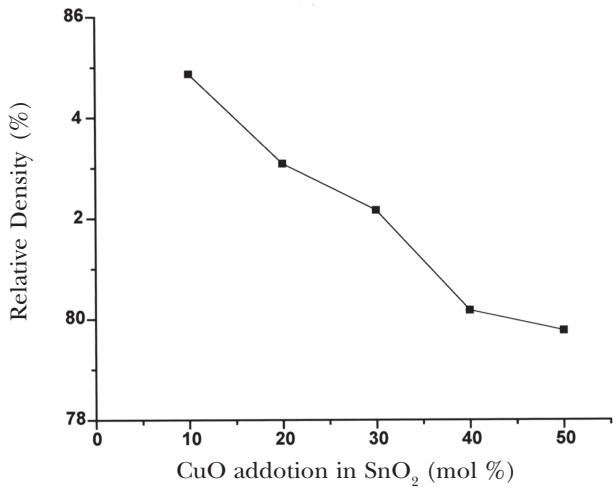

Fig. 5: Influence of CuO addition to relative density

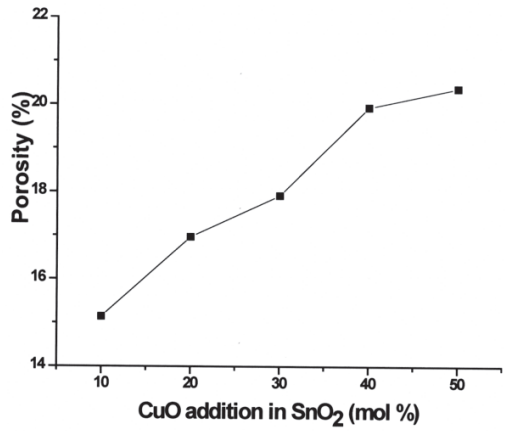

Fig. 6: Influence of CuO addition to porosity

propagation in two samples with two different grain sizes at a same micrometer distance, the one with bigger grain size will have less grain boundaries for the heat propagation to encounter than the other sample with smaller grain size which has more grain boundaries to be encountered. Hence, phonon scattering will be less in the sample with bigger grain size; thus will show higher thermal diffusivity value. This is in agreement with the SEM micrographs in *Fig. 7. Fig. 7(a), (b)* and *(c)* represent 10 mol%, 20 mol% and 30 mol% CuO mixed with SnO_2 respectively. It shows that the particle size of these compositions was getting slightly bigger as we increased CuO from 10-30 mol% in SnO_2 samples. Therefore the addition of CuO (10-30 mol%) had contributed to the increase in the thermal diffusivity values. However, the thermal diffusivity values keep decreasing as more CuO (40-50 mol%) were doped into SnO_2 samples. The decrease in density and an increase in porosity as evidenced in SEM micrograph in *Fig. 7(d)* and *(e)*, resulted in the decrease in thermal diffusivity of the sample with more than 40 mol% CuO.

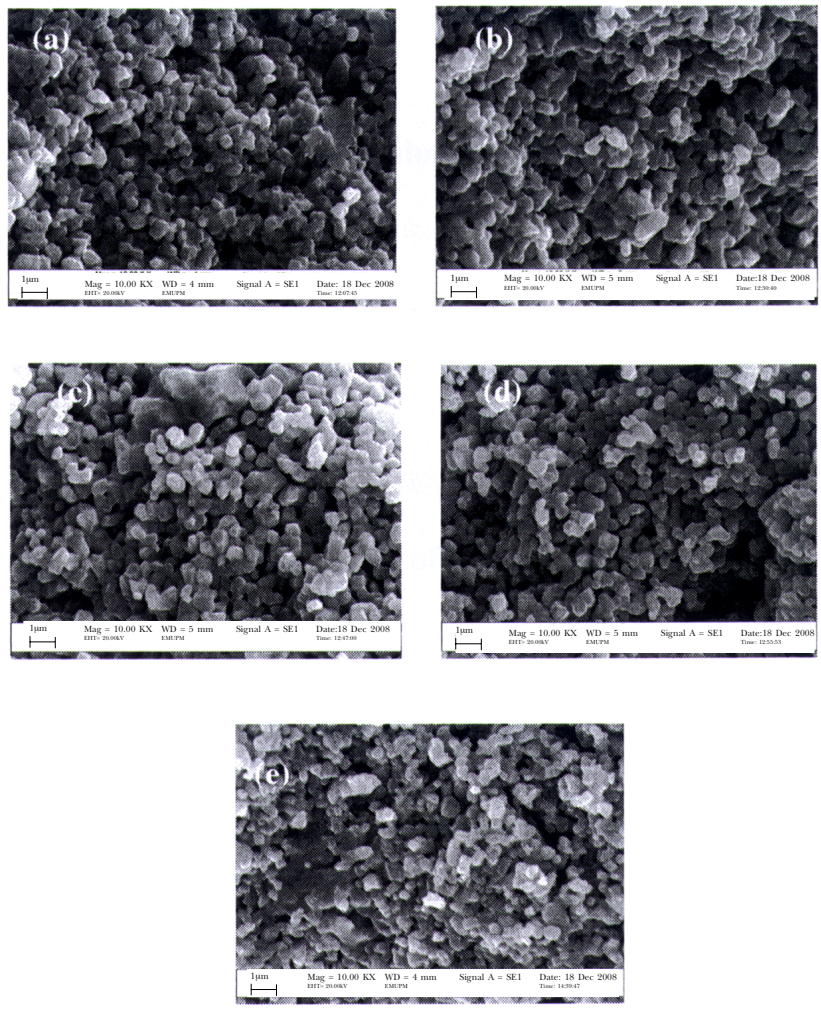

Fig. 7: SEM micrograph of fractured SnO2-CuO samples at different composition (a)10 mol% CuO (b) 20 mol% CuO (c) 30 mol% CuO (d) 40 mol% CuO (e) 50 mol% CuO, at 10,000 magnification

CONCLUSIONS

The influence of CuO used as additive (10-50 mol%) on the thermal and micro-structural properties of the SnO_2-based ceramics were studied. The phase composition analyzed by XRD, showed that there was no impurity phases in SnO_2-CuO system. We found that thermal diffusivity values of SnO_2-CuO samples ranging from 6.21 to 7.51 × 10-2 cm^2 s^{-1} which is better from the reported thermal diffusivity value of pure SnO_2 i.e 1.45 × 10^{-2} cm^2 s^{-1}. So, better performance of SnO_2 gas sensor in terms of thermal diffusivity, can be achieved by introducing 30 mol% CuO into SnO_2. The thermal diffusivity behavior was explained based on the crystallite aspect and density-porosity effect and it was supported by SEM micrographs.

ACKNOWLEDGEMENTS

All the facilities and support provided by the Department of Physics, Faculty of Science, Universiti Putra Malaysia are gratefully acknowledged.

REFERENCES

Chang, J.F. et al. (2002). The effects of thickness and operation temperature on ZnO:Al thin film CO gas sensor. *Sensors and Actuators B, 84,* 258-264.

Clark, L.M. and Taylor, R.E. (1975). Radiation loss in the flash method for thermal diffusivity. *Journal of Applied Physics, 46,* 714-719.

Kocemba, I. et al. (2001). The properties of strongly pressed tin oxide-based gas sensors. *Sensors and Actuators B, 79,* 28-32.

Maglic, K.D. et al. (1992). *Compendium of Thermophysical Property Measurement Methods.* Plenum Press.

Moon, W.J. et al. (2001). Selective CO gas detection of SnO_2-Zn_2SnO_4, *Sensors and Actuators B, 80,* 21-27.

Parker, W.J. et al. (1961). Flash method of determining thermal diffusivity, heat capacity and thermal conductivity. *J. Appl. Phys., 32.*

Rosyaini, A.Z. (2004). Sensor characteristic studies and thermal diffusivity measurement of tin (IV) oxide-based ceramic gas sensors (MSc. Thesis, Universiti Putra Malaysia, 2004).

Saadeddin et al. (2006). Simultaneous doping of Zn and Sb in SnO2 ceramics: enhancement of electrical conductivity. *Solid State Sciences, 8,* 7-13.

Vasiliev et al. (1998). CuO/SnO2 thin film heterostructures as chemical sensors to H2S. *Sensors and Actuators B, 50,* 186-193.

Zhang, G., and Liu, M. (2000). Effect of particle size and dopants on properties of SnO2 based gas sensor. *Sensors and Actuators B, 69,* 144-152.

ISSN: 0128-7680
Pertanika J. Sci. & Technol. **16 (2)**: 275 - 280 (2008)

Photopyroelectric Spectrum of MNO_2 Doped Bi_2O_3 - TiO_2 - ZnO Ceramic Combination

Zahid Rizwan[1], Azmi Zakaria[2]*, W. Mahmood Mat Yunus[2], Mansor Hashim[2] and Abdul Halim Shaari[2]

[1]National Textile University, Sheikhupura road, Faisalabad (37610), Pakistan
[2]Department of Physics, Faculty of Science, Universiti Putra Malaysia, 43400 UPM, Serdang, Selangor, Malaysia
**E-mail: azmizak@fsas.upm.edu.my*

ABSTRACT

Photopyroelectric spectroscopy is used to study the energy band-gap of the ceramic (ZnO + 0.25 Bi_2O_3 +0.25 TiO_2 + x MnO_2), x = 0 - 1.3 mol%, sintered at isothermal temperature 1190 and 1270°C for 2 hours in air. The wavelength of incident light, modulated at 9 Hz, is kept in the range of 300 to 800 nm and the photopyroelectric spectrum with reference to the doping level is discussed. The energy band-gap is estimated from the plot $(phv)^2$ vs hv and is 2.80 eV for the samples without MnO_2 at both sintering temperatures. It decreases to 2.08 eV with a further increase of MnO_2. The phase constitution is determined by XRD analysis. Microstructure and compositional analysis of the selected areas are analyzed using SEM and EDX. The maximum relative density, 91.4 %, and the grain size, 47 μm, were observed in this ceramics combination.

Keywords: Photopyroelectric, band gap, zinc oxide

INTRODUCTION

A white polycrystalline solid material Zinc Oxide (ZnO) crystallizes into a wurtzite structure. It is a n-type semiconductor material with a wide energy band-gap 3.2 eV (Gupta, 1990). It is widely used in the manufacturing of paints, rubber products, cosmetics, pharmaceuticals, floor covering, plastics, textiles, ointments, inks, soap, batteries, and also in electrical components such as piezoelectric transducers, phosphors, solar cell electrodes, blue laser diodes, gas sensors and varistors (Lin *et al.*, 1998; Look, 2001).

The exact role of many additives in the electronic structure of ZnO varistors is uncertain. ZnO based varistor is formed with small amounts of metal oxides such as Bi_2O_3, Co_3O_4, Cr_2O_3 MnO, Sb_2O_3 and others. These additives are the main tools that are used to improve the non-linear response and the stability of ZnO varistor (Eda, 1989). It is necessary to get information of optical absorption of the ceramic ZnO doped with different metal oxides. This paper reports the use of photopyroelectric (PPE) spectrometer, a powerful non-radiative tool (Mandelis, 1984) to study optical properties and a discussion on the PPE spectroscopy of ZnO doped with xMnO_2 in the presence of 0.25 Bi_2O_3, 0.25 TiO_2.

Received : 11 January 2008
Accepted : 8 April 2008
* Corresponding Author

MATERIALS AND METHODS

ZnO (99.9 % purity) was doped with 0.25 Bi_2O_3, 0.25 TiO_2, and xMnO_2 where x = 0 - 1.3 mol%. Pre-sintered powders at 760°C in air for 2 hours were pressed at 800 kg cm^{-2} to form disk shape samples. Disks were sintered at 1190 and 1270°C for 2 hours in air at the heating and cooling rate of 2.5°C min^{-1}. The density was measured by geometrical method. The mirror like polished samples were thermally etched for the microstructure analysis. Average grain size was determined by the grain boundary-crossing method. The disks of each sample were ground to make a fine powder for the PPE spectroscopic and XRD analysis. The XRD data were analyzed by using X'Pert High Score software for the identification of the crystalline phases. The measurement of PPE signal amplitude using the PPE spectrometer system to produce a PPE spectrum has been described elsewhere (Mandelis, 1984). In the present system, light beam was a 1 kW Xenon arc lamp that was kept in the range of 300 to 800 nm, mechanically chopped at 9 Hz, and scanned at 2 nm step size. The true PPE spectrum of the sample was obtained by normalizing PPE spectrum of sample with that of carbon black. Prior the PPE measurement, fine powder sample was ground in deionised water and a few drops of each mixture were dropped on 1.5 cm^2 aluminium foil and dried in air to form a thin sample layer about 12 μm thick on foil. The foil was placed in contact with PPE transducer (Tam and Coufal, 1983) using a very thin-layer of silver conductive grease. In determining the energy band-gap (E_g), it was assumed that the fundamental absorption edge of doped ZnO is due to the direct allowed transition. The optical absorption coefficient β varies with the excitation light energy $h\upsilon$ (Toyoda *et al.*, 1985) and is given by the expression, $(\beta h\upsilon)^2 = C\ (h\upsilon - E_g)$ near the band gap, where $h\upsilon$ is the photon energy, C is the constant independent of photon energy, and E_g is the direct allowed energy band-gap. The PPE signal intensity ρ is directly proportional to β, hence $(\rho h\upsilon)^2$ is related to $h\upsilon$ linearly. From the plot of $(\rho h\upsilon)^2$ versus $h\upsilon$, E_g is obtained by extrapolating the linear fitted region that crosses photon energy axis.

RESULTS AND DISCUSSION

The XRD analysis, *Fig. 1*, of the ceramic shows that the major phase is hexagonal ZnO and the secondary phase is $Bi_4Ti_3O_{12}$ (ref. code 00-12-0213) developed in all samples at all doping levels and temperatures. Few peaks of Bi_2O_3 (ref. code 00-018-0244), Mn_2TiO_4 (ref. code 00-016-0241) were also observed in the pattern. Relative density increases from 88.7, 89.3% to 91.4, 90.6% with the increased of MnO_2 for 1190 and 1270 °C sintering temperatures, respectively, *Fig. 2*. It is slightly higher at lower sintering temperature. Grain size increased from 22.5, 24.8 to 46.3, 47.1 μm with the increase of MnO_2 for the sintering temperature 1190, 1270 °C, respectively, as depicted in *Fig. 3*. This indicates that the MnO_2 acts as a grain enhancer even in the presence of the other grain enhancers 0.25 Bi_2O_3 and 0.25 TiO_2 which are present in the ceramic.

From SEM and EDX, *Fig. 5*, it shows that Bi_2O_3 is segregated at grain boundaries as well as at triple point junctions. Some patches of the Zn, Ti, Mn additives were found on the grain surface of the grains. These are due to the in-homogeneous mixture of the ceramics. The energy band-gap (E_g) of the ceramics is reduced from 3.2 eV (pure ZnO) to 2.80 ± 0.01 eV at the 0 mol% of MnO_2 for 1190 and 1270°C sintering temperatures, *Fig. 4*. The reduction of 0.40 ± 0.01 eV is due to the interface states produced by the combined effect of Bi_2O_3 and TiO_2 additives at the two sintering temperatures. The energy band-gap is drastically decreased down to 2.24, 2.22 eV for sintering temperatures

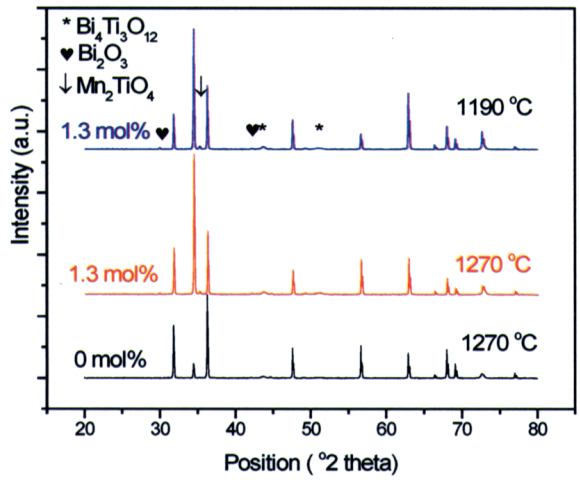

Fig. 1: XRD pattern at different doping level of MnO_2

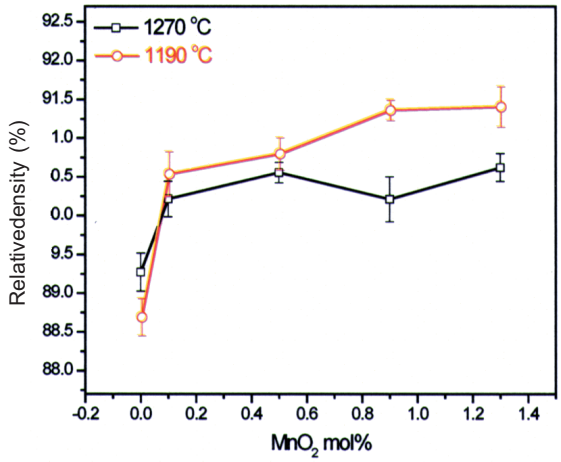

Fig. 2: Variation of density with MnO_2

1190, 1270 °C, respectively, at 0.1 mol% of MnO_2. This rapid decrease is about 0.58 eV which is due to the growth of interface states in the grain interior and also in the grain boundaries. With further amount of MnO_2 addition into the ceramic, E_g is found continuously decreasing down to 2.08 eV at 1.3 mol% of MnO_2 at both sintering temperatures. This small decrease, about 0.14 eV, is due to the growth of interface states with the addition of MnO_2 (Toyoda and Shimamoto, 1998). The overall value of E_g is slightly lower at the higher sintering temperature at all doping levels. This indicates that the increase in the sintering temperature is not effective at decreasing the value of E_g. It is observed that the decrease in the E_g due to the combined effect of the 0.25 Bi_2O_3 and 0.25 TiO_2 additives at both sintering temperatures is about 0.40 eV but the decrease in

E_g is about 0.58 eV only at 0.1 mol% MnO_2. Ionic radius of Mn ion (0.53 Å) is smaller than the ionic radius of Zn (0.74 Å) (Yoshikazu *et al.*, 2002; Dow and Redfield, 1972; Urbach, 1953) so Mn ions substitutes the Zn ions and contributes to further increase of interface states hence further decrease of E_g.

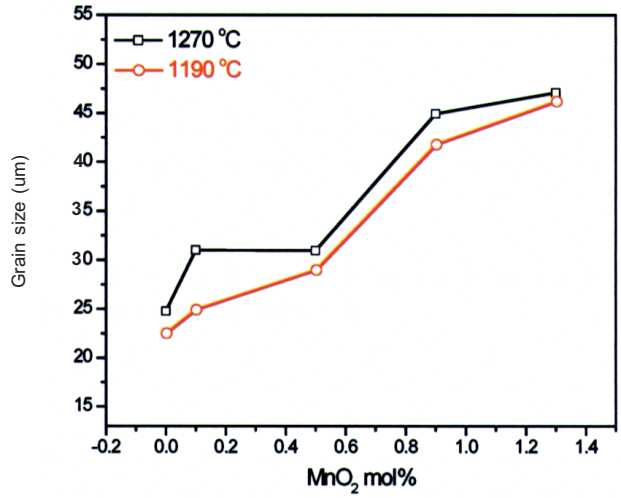

Fig. 3: Variation of grain size with MnO_2

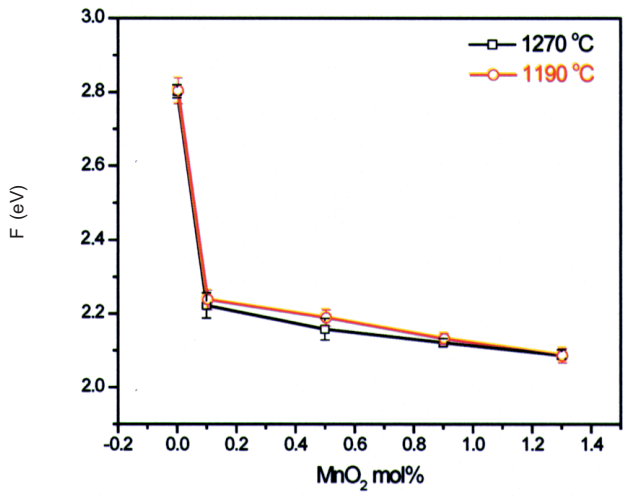

Fig. 4: Dependence of E_g on MnO_2

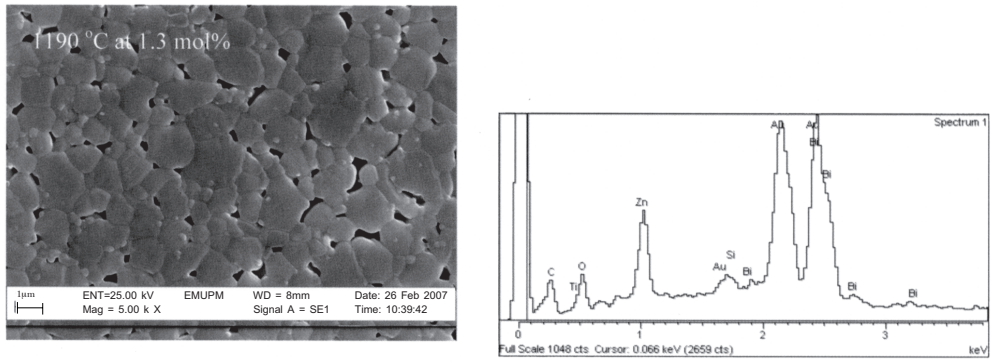

Fig. 5: SEM micrograph for 1.3 mol% and EDX spectrum at the grain boundary for 0.1 mol% MnO_2 at 1190 °C sintering temperature

CONCLUSIONS

Spectroscopic results are discussed with the doping of MnO_2 and found that the MnO_2 acts as a grain enhancer. Both Bi_2O_3 and TiO_2 reduce the energy band-gap but MnO_2 does contribute more prominently.

ACKNOWLEDGEMENTS

Thanks to MOSTI for the financial assistance (Grant FRGS No. 01-01-07-139FR) for this research.

REFERENCES

Dow, J.D. and Redfield, D. (1972). Towards a unified theory of Urbach's rule and exponential absorption edge. *Phys. Rev., B5,* 594.

Eda, K. (1989). Zinc oxide varistors. *IEEE Elect. Insul. Mag., 5,* 28-41.

Gupta, T.K. (1990). Application of zinc oxide varistors. *J. Am. Ceram. Soc., 73*(7), 1817-40.

Lin, H.M., Tzeng, S.J., Hsiau, P.J. and Tsai, W.L. (1998). Electrode effects on gas sensing properties of nanocrystalline zinc oxide. *Nanostruct. Mater., 12,* 465- 77.

Look, D.C. (2001). Recent advances in ZnO materials and devices. *Mat. Sci. Eng. B, 80,* 383-87.

Mandelis, A. (1984). Frequency-domain photopyroelectric spectroscopy of condensed phases (PPES): A new, simple and powerful spectroscopic technique. *Chem. Phys. Lett., 108,* 388-92.

Tam, A.C. and Coufal, H. (1983). Photoacoustic generation and detection of 10-ns acoustic pulses in solids. *Appl. Phys. Lett., 42,* 33-5.

Toyoda, T., Nakanishi, H., Endo, S., and Irie, T. (1985). Fundamental absorption edge in semiconductor $CdInGaS_4$ at high temperatures. *J. Phys. D Appl. Phys., 18,* 747-51.

Toyoda, T. and Shimamoto, S. (1998). Effect of Bi_2O_3 impurities in ceramic ZnO on photoacoustic spectra and current-voltage spectra. *Jpn. J. Appl. Phys., 37,* 2827-31.

YOSHIKAZU, S., YASUHIRO, O., TOSHIO, K. and JUN, M. (2002). Evaluation of Sb_2O_3-doped ZnO varistors by photoacoustic spectroscopy. *Jpn. J. Appl. Phys., 41,* 3379-82.

URBACH, F. (1953). The long-wavelength edge of photographic sensitivity end of the electronic absorption of solids. *Phys. Rev., 92,* 1324.

ISSN: 0128-7680
Pertanika J. Sci. & Technol. **16 (2)**: 281 - 289 (2008)

Catch Per Unit Effort of Estuarine Push Net with Emphasis on Occurrence and Abundance of *Acetes* Shrimps in the Coastal Waters of Malacca, Peninsular Malaysia

S. M. Nurul Amin*, Aziz Arshad, Sarikha binti Shamsudin, Japar Sidik Bujang and Siti Shapor Siraj
Department of Biology, Faculty of Science, Universiti Putra Malaysia, 43400 UPM, Serdang, Selangor, Malaysia
**E-mail: smnabd02@yahoo.com*

ABSTRACT

Catch per unit effort (CPUE) of estuarine push net (EPN) and abundance of *Acetes* shrimps in the coastal waters of Klebang Besar, Malacca were investigated based on the catch data from April 2006 to March 2007. The average monthly CPUE of the EPN observed was 3.53 (± 3.99) kg/fisherman/hour. The total catch comprised of three major categories namely: *Acetes* shrimps (90%), fish juveniles (9%) and other shrimps (1%). Amongst the *Acetes* shrimps, three species (*A. indicus*, 87%, *A. japonicus,* 12% and *A. intermedius*, 1%) were recorded from the investigated area. The peak catches were observed during the months of September, November and December. There was no significant correlation ($p > 0.05$) between monthly catches and environmental parameters (temperature, dissolved oxygen, salinity and pH).

Keywords: CPUE, estuarine push net, *Acetes* shrimps, Peninsular Malaysia

INTRODUCTION

The Estuarine Push Net (EPN) is locally known as Suongkor (*Fig. 1*) in the coastal region of Malacca, Peninsular Malaysia. It is a triangular shape and the mesh size decreases from 3.2 cm at anterior section to 0.5 cm at the cod end. It is used intensively all along the coast and estuaries of Malacca to collect *Acetes* shrimps (Udang geragau). Fishing is done normally during day time by pushing the net against the flow of tide (Omori, 1975). The EPN catches the species of shrimps that drift with current or do not swim fast enough. There is a large population which is depending on the income from this fishery in the coastal region of Malacca. However, little is known about the fishery of *Acetes*. The fishery statistics are particularly inadequate, because the shrimps are mainly consumed locally. Observation on the commercial fishing, sampling and examination of specimens landed was made in various localities in Japan, Taiwan, Hong Kong, South Vietnam, Thailand, Malaysia, Singapore, Indonesia and India (Omori, 1975). The EPN has been used for decades but the catch per unit effort (CPUE) and temporal variation of catches are unknown. It is assumed that the small mesh size net used may lead to an overexploitation of the shrimps living in the estuarine area. Therefore, an attempt was made to study the CPUE of estuarine push net fishery and the temporal distribution of *Acetes* shrimps in the coastal waters of Malacca, Peninsular Malaysia.

Received : 11 January 2008
Accepted : 8 April 2008
* Corresponding Author

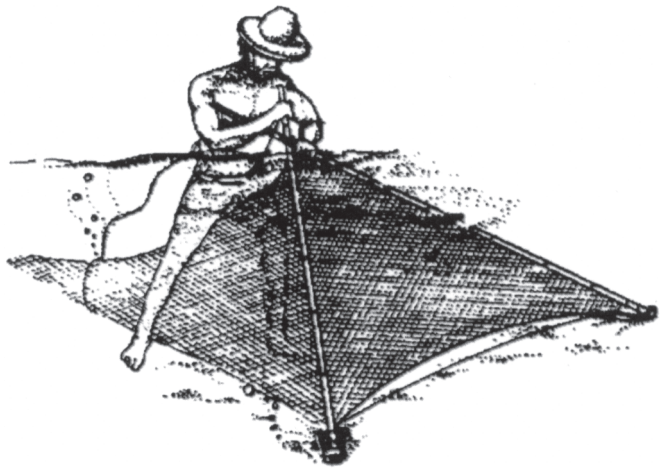

Fig. 1: Estuarine push net (EPN) which is used to catch Acetes shrimps along the coast of Malacca, Malaysia

(Source: www.fao.org)

MATERIALS AND METHODS

Samplings were done fortnightly between April 2006 and March 2007 from Klebang Besar (N $02^0$13.009′ & E 102^0 11.921′) in the Malacca coastal waters, Straits of Malacca (*Fig. 2*). The estuarine push net was operated between the depth of 1 m and 1.5 m. The fishing effort was one man per hour and the towing length was approximately 1000 m along the coast of Klebang Besar, Malacca. After collection, samples of total catches were immediately preserved in 10% formalin in the field and transported to the laboratory for further analysis. The specimens were identified in the laboratory using a Nikon dissecting microscope (Nikon-122764, Japan). For species composition, 20 gm sub-sample of *Acetes* was taken randomly from the total catch after separation of fish juveniles and other shrimps. Annual percent composition and temporal distribution of *Acetes* shrimps were calculated from monthly sub-sample data. The identification of *Acetes* shrimps was based on the work of Hansen (1919) and Omori (1975). Physico-chemical parameters such as water temperature, salinity, dissolved oxygen and pH were measured fortnightly (April 2006 to March 2007) using a calibrated Hydro Lab (Model: Surveyor 4A, Hydrolab Corporation, USA).

RESULTS AND DISCUSSION

Environmental Variables

The average subsurface water temperature recorded from the Klebang Besar during the study period was 30.13 ± 1.23°C (mean ± SD). The lowest temperature (28.09°C) was found in February, while the highest temperature (32.95°C) was recorded during September (*Fig.3*). The mean value of salinity recorded was 26.23 ± 4.82 ppt. The lowest value of salinity recorded was 19.50 ppt in October, while the highest was 33.82 ppt in March (*Fig. 3*). The mean value of dissolved oxygen recorded was 5.10 ± 1.12 mg L^{-1}. The

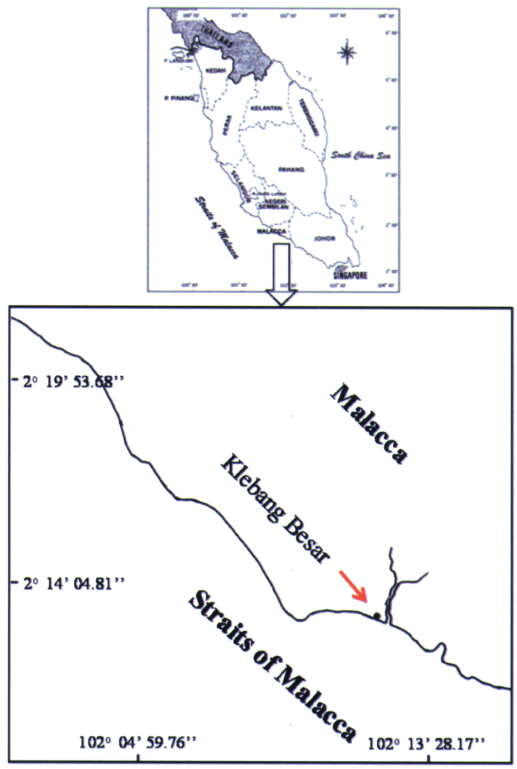

Fig. 2. Geographical location of the sampling area in the coastal waters of Malacca

lowest dissolved oxygen recorded was 3.24 mg L^{-1} in October, while the highest value was 6.97 mg L^{-1} in May (*Fig. 4*). The fluctuation of pH during the study period was low between 7.37 and 8.37 (*Fig.4*) with a mean of 7.91 ± 0.30.

Estuarine Push Net Fishery

There were three (3) major groups of the species observed from the catches of EPN in the coastal waters of Malacca (*Fig. 5*). The dominant group was *Acetes* shrimps (90%), followed by fish juveniles (9%), and other shrimps (1%). The monthly average total CPUE of EPN was found to be 3.53 (± 3.99) kg/fisherman/hr. The highest catch (15.10 kg/fisherman/hr) was observed in December and the lowest (0.3 kg/fisherman/hr) was observed in the month of January (*Fig. 6*). It is noted that in the inshore coastal areas of Malacca, estuarine push net is commonly used to catch the *Acetes* shrimps. The catching capabilities of the EPN depend on the strength of the operator, his experience on the ground and the season (Tham, 1954). There is no published report regarding the CPUE of EPN fishery except the report by Tham (1954) which stated that the highest catches are observed during the north-east monsoon in Singapore. The present study revealed that the highest catches observed in the coastal waters of Malacca are in the months of November and December, the beginning of the north-east monsoon season. In the study area, *Acetes* are caught two times each month during the neap tide, between new moon and full moon. The average fishing days per month were 6 ± 3.52. Fishermen

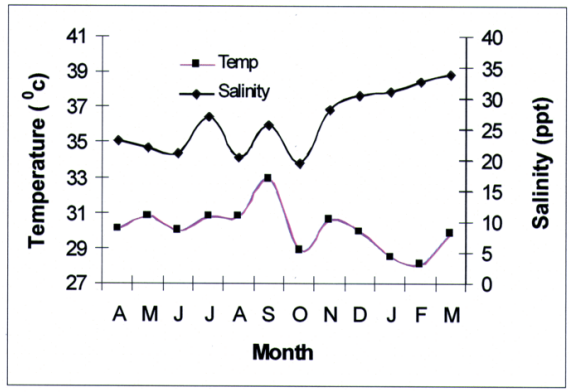

Fig. 3: Monthly variation of temperature and salinity in the coastal waters of Malacca, Malaysia

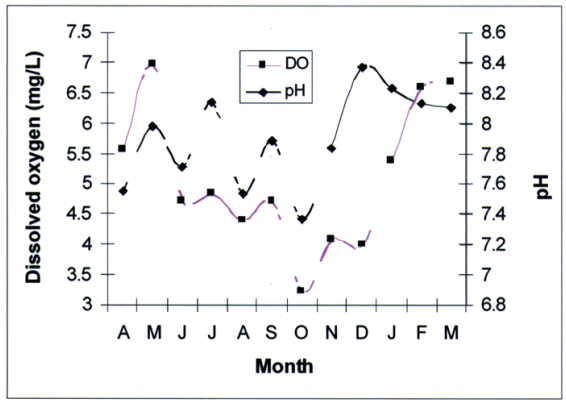

Fig. 4: Monthly variation of dissolved oxygen and pH in the coastal waters of Malacca

sell *Acetes* shrimps near the beach or road side directly to the consumer or to middlemen. Most of *Acetes* shrimps are sold in wet condition (95%) and the rest (5%) in dry condition. The average price of wet *Acetes* was at RM 3.00 in the coastal region of Malacca. The mean monthly CPUE showed a moderate positive correlation with temperature ($r = 0.29$, $p > 0.05$), salinity ($r = 0.22$, $p > 0.05$) (*Fig. 7*) and pH ($r = 0.37$, $p > 0.05$). However, the mean monthly CPUE showed negative correlation with dissolved oxygen ($r = - 0.47$, $p > 0.05$) (*Fig. 8*).

Occurrence and Abundance of Acetes *Shrimps*

The planktonic shrimps of the genus *Acetes* were observed in the area throughout the study period. There were three species of *Acetes* (*Acetes indicus, Acetes japonicus* and *A. intermedius*) found in the coastal waters of Malacca. The annual percent compositions of *A. indicus, A. japonicus* and *A. intermedius* were 87%, 12% and 1%, respectively (*Fig. 9*).

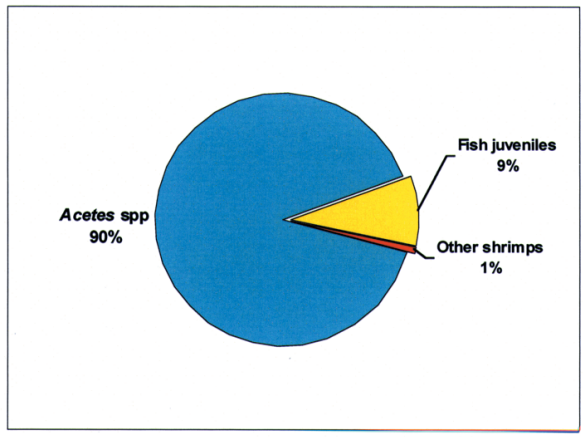

Fig. 5: Annual major catches categories of EPN along the coast of Malacca, Malaysia

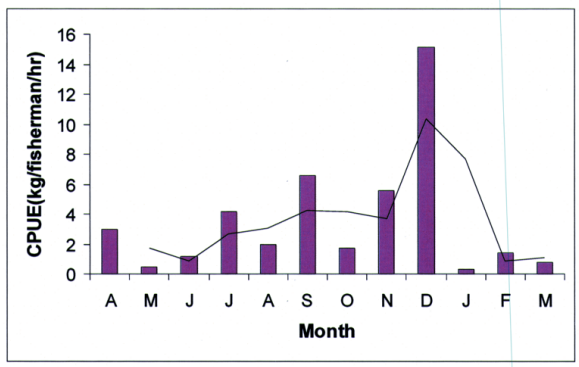

Fig. 6: Monthly average catches (Kg/fisherman/hr) of EPN along the coast of Malacca, Malaysia

Acetes indicus

Highest densities (more than 70%) of *A. indicus* were recorded almost every month (*Fig. 10*) in the study area. Bhattacharya (1988) reported that the temperature for *A. indicus* ranged from 13°C to 35°C. In the coastal waters of Klebang Besar, temperature varied from 28.09°C to 32.95°C and *A. indicus* was found in comparatively lower density from January to May and peak in June – December months (*Fig. 10*). Bhattacharya (1988) also mentioned that a large number of *A. indicus* occurred when salinity varied from 26.50 ppt to 35.00 ppt. In the coastal waters of Malacca, this species was recorded with the salinity from 19.50 ppt to 33.82 ppt. But there was no significant correlation ($p > 0.05$) between the abundance of *A. indicus* and the salinity in the study area. *Acetes indicus* occurs in the central part of the Indo-West Pacific, from South China Sea through the Gulf of Thailand (Omori, 1975; Chaitiamvong, 1980; Chaitiamvongse and Yoodee, 1982) and the Bay of Bengal, Bangladesh (Mahmood *et al.*, 1978, Zafar and Alam, 1997), Straits of Malacca (Pathansali, 1966) and Andaman Sea to the entire east and west coasts of India

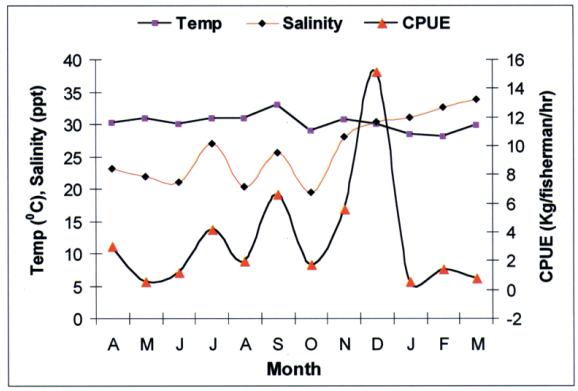

Fig. 7: Monthly variation of CPEU with temperature and salinity in the coastal wateres of Malacca, Malaysia

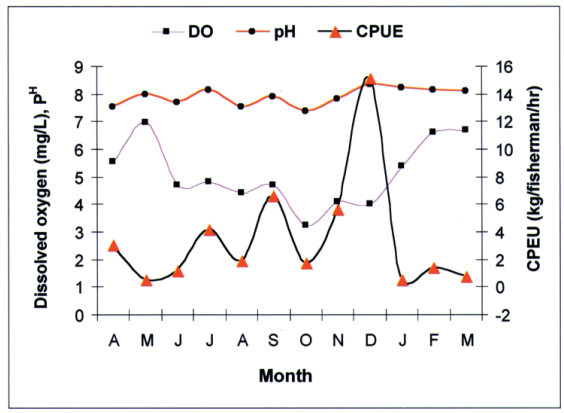

Fig. 8: Monthly variation of CPEU with dissolved oxygen and pH in the coastal wateres of Malacca, Malaysia

(Ravindranath, 1980). This species is the most common shrimp along the Moharashtra coast in northwestern India, especially at Bombay (Aravindakshan *et. al.*, 1985) and in Galle Harbour of Sri Lanka and Manora Channel near Karachi, Pakistan (Tirmizi and Ghani, 1982).

Acetes japonicus

The occurrence of *A. japonicus* was observed all year round but the number was negligible from June to December (*Fig. 10*). The maximum density (35.35%) of *A. japonicus* was in March and the minimum (1.23%) in September (*Fig. 10*). The monthly percent of abundance of *A. japonicus* showed positive correlation with dissolved oxygen ($r = 0.83$; $p < 0.05$) and salinity ($r = 0.43$; $p > 0.05$). No significant correlation ($p > 0.05$) was found between the monthly abundance of *A. japonicus* and the two variables (Temperature and pH). *Acetes japonicus* is distributed along the coastal areas of the Yellow Sea, South China Sea (Wang, 1987; Lei, 1988), Gulf of Thailand (Omori, 1975), Java Sea and Straits of Malacca (Pathansali, 1966; Omori, 1975). It has also been reported from the southwest coast of India (Achuthankutty *et al.*, 1973), Bangladesh (Mahmood *et al.*, 1978) and

Manora channel near Karachi of Pakistan (Tirmizi and Ghani, 1982). In Japan, the species is found in neritic waters around the Islands of Kyushu and the western part of Honshu (Harada, 1968) and is commercially fished in the Ariake Sea (Omori, 1975). Great swarms of this species can occur in Suruga Bay usually in July and August (Omori, 1975). The species is also recorded in Vietnam (Omori, 1975) and along the coast of Pakistan and in Kuwait Bay of the Gulf of Arabia (Enomoto, 1971).

Acetes intermedius

The occurrence of *A. intermedius* was observed in February and March during the investigation (*Fig. 10*). The occurrence of *A. intermedius* was absent in the 20 gm sub sample in the other months during the study period. The abundance of *A. intermedius* showed positive significant correlation with salinity ($r = 0.91$, $p < 0.05$). Higher degree positive correlation was also found with conductivity ($r = 0.87$, $p > 0.05$) and moderately correlated with TSS ($r = 0.62$). The occurrence of *A. intermedius* was in February and March during the investigation. It is well known that *A. intermedius* is a highly migratory species. It migrates from estuaries to offshore waters and performs a diel vertical

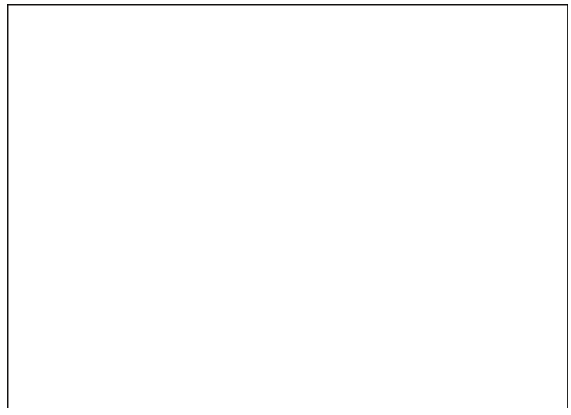

Fig. 9: Annual species composition of Acetes shrimps *in the coastal waters of Malacca, Malaysia*

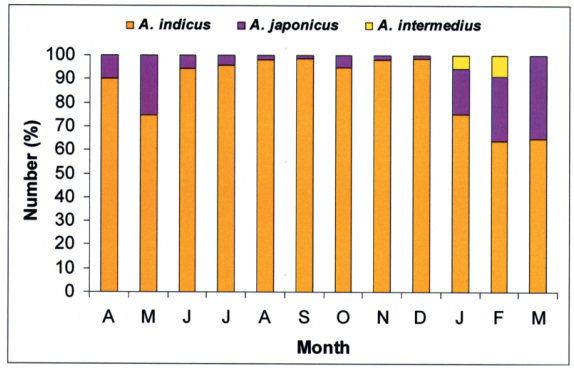

Fig. 10: Monthly abundance of three Acetes shrimps in the coastal waters of Malacca, Malaysia

migration in the coastal waters of south-western Taiwan during the period from June to October (Chiou *et al.*, 2000). May be due to its migratory character, the species could not be found in other months except February and March in the study area. It is one of the most important commercial shrimp resources and is also an important component of the marine ecosystem in the coastal waters of south-west Taiwan (Chiou *et al.,* 2000). The species *A. intermedius* is previously reported from Bangladesh (Zafar, 2000); Taiwan, Philippines and south coast of Java, Indonesia (Omori, 1975) and now in the coast of the Straits of Malacca, Peninsular Malaysia.

CONCLUSIONS

The major component in the EPN catches were *Acetes* shrimps (90%). The percentage compositions of *A. indicus, A. japonicus* and *A. intermedius* were 87%, 12% and 1%, respectively. The average catch was 3.54 kg/fisherman/hr and the highest catch was observed in the months of November and December. There was no significant correlation ($p > 0.05$) between monthly CPUE of total catch and environmental parameters (temperature, salinity, dissolved oxygen and pH). It could be concluded from the study that estuarine push net is the effective fishing gear for *Acetes* fishery since the dominant component in the EPN catches are *Acetes* shrimps (90%). However, further studies are needed to find out the composition of juvenile fishes and their commercial value to evaluate the effectiveness of the estuarine push net.

ACKNOWLEDGEMENTS

This work is part of a PhD thesis funded by the Ministry of Science, Technology and Innovation (MOSTI), Malaysia (Grant No. 5450247). The authors would like to thank MOSTI for providing financial support to carry out this research work. Special thanks to Universiti Putra Malaysia for providing Graduate Research Fellowship (GRF) during the study period. We are also indebted to Laboratory of Marine Science and Aquaculture, Institute of Bioscience, Universiti Putra Malaysia for providing the facilities to carry out this study.

REFERENCES

Achuthankutty, C.T., Nair, K.K.C. and Purushan, K.S. (1973). A shoal of sergestid shrimp *Acetes* in association with a swarm of gammarid amphipods in the southwest coast of India. *Current Science, 42,* 840.

Aravindakshan, M., Ramamurthy, S. and Karbhari, J.P. (1985). On the occurrence of *Acetes johni* Nataraj and *A. japonicus* Kishinouye in Bombay waters. *Journal of the Marine Biological Association of India, 27,* 191-193.

Bhattacharya, S. S. (1988). Effect of salinity and temperature on the distribution of the shrimp *Acetes indicus* H. Milne Edwards. In M. M. Joseph (Ed.), *Proceedings of the First Indian Fisheries Forum Mangalore: Asian Fisheries Society* (pp. 309-312). Indian Branch.

Chaitiamvong, S. (1980). *Biological studies on planktonic shrimp and shrimp-like in the Gulf of Thailand.* Annual Report of the Invertebrate Fisheries Unit of Marine Fisheries Division, 18pp. Bangkok. (In Thai with English abstract).

Chaitiamvongse, S. and Yoodee, K. (1982). The fisheries of planktonic shrimp and shrimp-like in the Gulf of Thailand. *Thai Fisheries Gazette, 35,* 67-88. (In Thai with English abstract).

Chiou, W.D, Wu, C.C. and Cheng, L.Z. (2000). Spatio-temperal distribution of sergistid shrimp *Acetes intermedius* in the coastal waters of southwestern Taiwan. *Fisheries Science, 66,* 1014-1025.

Enomoto, Y. (1971). Oceanography and biological study of shrimps in the waters adjacent to the eastern coasts of the state of Kuwait. *Bulletin of the Tokai Regional Fisheries Research Laboratory, 66,* 1-74.

Hansen, H.J. (1919). The Sergestidae of the Siboga Expedition, Siboga-Expeditie. Monographe 38 of Uitkomsten op Zoologishch, Botanisch, Oceanographisch en Geologisch Gebied, 65 pp.

Harada, E. (1968). Ecology and biological production of Lake Naka-umi and adjacent regions: Seasonal changes in distribution and abundance of some decapod crustaceans. Special Publications. *Seto Marine Biological Laboratory, 2,* 75-103.

Lei, M. (1988). Studies in the biology of *Acetes japonicus* Kishinouye in the eastern coastal waters of Guangdong Province, China. In *Selected Oceanic Works in China* (p. 234-243). Bejing: Ocean Press.

Mahmood, N., Khan, Y.S.A. and Hussain, M. (1978). Shrimp fishery: records of three sergistid shrimps in Bangladesh. In *Proceedings of the Zoological Society of Bangladesh* (pp. 204-214). Dhaka, Bangladesh.

Omori, M. (1975). The systematics, biogeography and fishery of epipelagic shrimps of the genus *Acetes* (Crustacea, Decapoda, Sergistidae). *Bulletin of the Ocean Research Institute, 7,* 1-91.University of Tokyo.

Pathansali, D. (1966). *Acetes* (Sergistidae) from the Malay Peninsula. *Bulletin of the National Museum Singapore, 33,* 59-63.

Ravindranath, K. (1980). Shrimps of the genus *Acetes* H. Milne Edwards (Crutacea, Decapoda, Sergistidae) from the estuarine system of river Krishna. Proceedings of the Indian Academy of Sciences. *Animal Sciences, 89,* 253-273.

Tham, A.K. (1954). The shrimp industry of Singapore. *Proceedings of Indo-Pacific Fisheries Council, 5*(2), 145-155.

Tirmizi, N.M. and Ghani, N.A. (1982). New distributional records for three species of *Acetes* (Decapoda, Sergistidae). *Crustaceana, 42,* 44-53.

Wang, Y.H. (1987). Notes on the shrimp and lobster fauna of the Zhoushan Islands. *Oceanologia et Limnologia Sinica, 18,* 48-54 (In Chinese).

Zafar, M. (2000). Study on Sergestid shrimp *Acetes* in the vicinity of Mathamuhuri river confluence, Bangladesh (PhD Thesis, University of Chittagong, Bangladesh, 223 pp, 2000).

Zafar, M. and Alam, M.D. (1997). Occurrence and abundance of *Acetes* shrimps in the Kutubdia channel of Bangladesh coastal water. *Bangladesh Journal of Fisheries Research, 1*(2), 91-96.

Pertanika Journal of Science & Technology

Subject Index for Volume 16 Nos. 1 & 2 2008

Pertanika Journal of Science & Technology

Author Index for Volume 16 Nos. 1 & 2 2008

REFEREES FOR THE PERTANIKA JOURNAL OF SCIENCE AND TECHNOLOGY (JST)

January – July 2008

The Editorial Board of the Journal of Science and Technology wish to thank the following for acting as referees for manuscripts submitted to JST between January and July 2008.

Abdul Halim Mohd Yatim
AHM Rahmatullah Imon
Ali Selamat
Ammar Mohd Akhir
Anton Abdulbasah Kamil
Azah Mohamed
Chan Lai Keng
Farah Saleena Taip
Faridah Qamaruz Zaman
Hasimah Mohamed
K Ramar
Kaida Khalid
KS Rama Rao
Ling Tau Chuan
Luqman Chuah Abdullah
Mahiran Basri
Maizah Hura Ahmad
Michael Khoo Boon Chong
Mohamad Deraman
Mohd Amran Mohd Salleh
Mohd Azmi Ambak
Mohd Hamiruce Marhaban
Mohd Hekarl Uzir
Mohd Marzuki Mustafa
Mohd Zobir Hussein
Nor Aripin Shamaan
Norashikin Ab Aziz
Norhani Abdullah
Noriah Bidin
Raha Abdul Rahim
Richard Ahsley
Rosnita A Talib
Salmiaton Ali
Shafreeza Sobri
Siti Aslina Hussain
Siti Khalijah Daud
Siti Mazlina Mustapa Kamal
Thomas Choong, SY
Umi Kalsom Md. Shah
Yus Aniza Yusof
Zainal Abidin Talib
Zurina Zainal Abidin

While every effort has been made to include a complete list of referees for the period stated above, however if any name(s) have been omitted unintentionally or spelt incorrectly, please notify the Executive Editor, *Pertanika* Journals at ndeeps@admin.upm.edu.my.

Any inclusion or exclusion of name(s) on this page does not commit the Pertanika Editorial Office, nor the UPM Press or the University to provide any liability for whatsoever reason.

Pertanika

Our goal is to bring high quality research to the widest possible audience

Pertanika is Indexed in Scopus & EBSCO

Pertanika is an international peer-reviewed leading journal in Malaysia which began publication in 1978. The journal publishes in three different areas — Journal of Tropical Agricultural Science (JTAS); Journal of Science and Technology (JST); and Journal of Social Sciences and Humanities (JSSH).

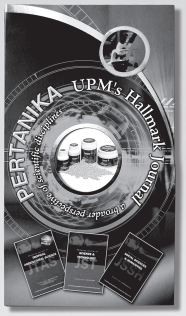

JTAS is devoted to the publication of original papers that serves as a forum for practical approaches to improving quality in issues pertaining to tropical agricultural research or related fields of study. It is published twice a year in **February** and **August**.

JST caters for science and engineering research or related fields of study. It is published twice a year in **January** and **July**.

JSSH deals in research or theories in social sciences and humanities research with a focus on emerging issues pertaining to the social and behavioural sciences as well as the humanities, particularly in the Asia Pacific region. It is published twice a year in **March** and **September**.

Call for Papers

Pertanika invites you to explore frontiers from all fields of science and technology to social sciences and humanities. You may contribute your scientific work for publishing in UPM's hallmark journals either as a ***regular article***, ***short communications***, or a ***review article*** in our forthcoming issues. Papers submitted to this journal must contain original results and must not be submitted elsewhere while being evaluated for the Pertanika Journals.

Submissions in English should be accompanied by an abstract not exceeding 300 words. Your manuscript should be no more than 6,000 words or 10-12 printed pages, including notes and abstract. Submissions should conform to the Pertanika style, which is available at www.rmc.upm.edu.my/pertanika or by mail or email upon request.

Papers should be double-spaced 12 point type (Times New Roman fonts preferred). The first page should include the title of the article but no author information. Page 2 should repeat the title of the article together with the names and contact information of the corresponding author as well as all the other authors. Page 3 should contain the abstract only. Page 4 and subsequent pages to have the text - Acknowledgments - References - Tables - Legends to figures – Figures, etc.

Questions regarding submissions should only be directed to the Executive Editor, Pertanika Journals.

Remember, ***Pertanika is the resource to support you in strengthening research and research management capacity***.

Why should you publish in Pertanika Journals?

Benefits to Authors

PROFILE: our journals are circulated in large numbers all over Malaysia, and beyond, in Southeast Asia. Recently, we have widened our circulation to other overseas countries as well. We will ensure that your work reaches the widest possible audience in print and online, through our wide publicity campaigns held frequently, and through our constantly developing electronic initiatives through e-pertanika and Pertanika Online.

QUALITY: Our double-blind peer refereeing procedures are fair and open, and we aim to help authors develop and improve their work. Pertanika JTAS is now over 30 years old; this accumulated knowledge has resulted in Pertanika JTAS being indexed by Scopus (Elsevier).

AUTHOR SERVICES: we provide a rapid response service to all our authors, with dedicated support staff for each journal, and a point of contact throughout the refereeing and production processes. Our aim is to ensure that the production process is as smooth as possible, is borne out by the high number of authors who publish with us again and again.

LAG TIME & REJECTION RATE: the elapsed time from submission to publication for the articles in Pertanika averages 6-8 months. A decision of acceptance of a manuscript is reached in 1 to 3 months (average 7 weeks).

Our journals have a 30% rejection rate of its submitted manuscripts, many of the papers fail on account of their substandard presentation and language (frustrating the peer reviewers).

An Award Winning International-Malaysian Journal

FEB. 2008

Mail your submissions to:

The Executive Editor
Pertanika Journals
Research Management Centre (RMC)
Publication Division
4th Floor, Administration Building
Universiti Putra Malaysia
43400 UPM, Serdang, Selangor, Malaysia

Tel: +603-8946 6192
ndeeps@admin.upm.edu.my
www.rmc.upm.edu.my/pertanika

Pertanika

Our goal is to bring high quality research to the widest possible audience

INSTRUCTIONS TO AUTHORS

(Manuscript Preparation & Submission Guidelines)

Revised May 2007

We aim for excellence, sustained by a responsible and professional approach to journal publishing. We value and support our authors in the research community.

Please read the guidelines and follow these instructions carefully; doing so will ensure that the publication of your manuscript is as rapid and efficient as possible. The Editorial Board reserves the right to return manuscripts that are not prepared in accordance with these guidelines.

Guidelines for Authors

Publication policies

Pertanika policy prohibits an author from submitting the same manuscript for concurrent consideration by two or more publications. It prohibits as well publication of any manuscript that has already been published either in whole or substantial part elsewhere.

Editorial process

Authors are notified on receipt of a manuscript and upon the editorial decision regarding publication.

Manuscript review: Manuscripts deemed suitable for publication are sent to the Editorial Advisory Board members and/or other reviewers. We encourage authors to suggest the names of possible reviewers. Notification of the editorial decision is usually provided within to six weeks from the receipt of manuscript. Publication of solicited manuscripts is not guaranteed. In most cases, manuscripts are accepted conditionally, pending an author's revision of the material.

Author approval: Authors are responsible for all statements in articles, including changes made by editors. The liaison author must be available for consultation with an editor of The *Journal to answer* questions during the editorial process and to approve the edited copy. Authors receive edited typescript (not galley proofs) for final approval. Changes cannot be made to the copy after the edited version has been approved.

Please direct all inquiries, manuscripts, and related correspondence to:

Executive Editor
Research Management Centre (RMC)
4th Floor, Administration Building
Universiti Putra Malaysia
43400 UPM, Serdang, Selangor
Malaysia
Phone: + (603) 8946 6192
Fax: + (603) 8947 2075
ndeeps@admin.upm.edu.my

Manuscript preparation

Pertanika accepts submission of mainly four types of manuscripts. Each manuscript is classified as **regular** or **original** articles, **short communications**, **reviews**, and proposals for **special issues**. Articles must be in **English** and they must be competently written and argued in clear and concise grammatical English. Acceptable English usage and syntax are expected. Do not use slang, jargon, or obscure abbreviations or phrasing. Metric measurement is preferred; equivalent English measurement may be included in parentheses. Always provide the complete form of an acronym/abbreviation the first time it is presented in the text. Contributors are strongly recommended to have the manuscript checked by a colleague with ample experience in writing English manuscripts or an English language editor. Lingually hopeless manuscripts will be rejected straightaway (e.g., when the language is so poor that one cannot be sure of what the authors really mean). This process, taken by authors before submission, will greatly facilitate reviewing, and thus publication if the content is acceptable.

The instructions for authors must be followed. Manuscripts not adhering to the instructions will be returned for revision without review. Authors should prepare manuscripts according to the guidelines of Pertanika.

1. Regular article

Definition: Full-length original empirical investigations, consisting of introduction, materials and methods, results and discussion, conclusions. Original work must provide references and an explanation on research findings that contain new and significant findings.

Size: Should not exceed 5000 words or 8-10 printed pages (excluding the abstract, references, tables and/or figures). One printed page is roughly equivalent to 3 type-written pages.

2. Short communications

Definition: Significant new information to readers of the Journal in a short but complete form. It is suitable for the publication of technical advance, bioinformatics or insightful findings of science and engineering development and function.

Size: Should not exceed 2000 words or 4 printed pages, is intended for rapid publication. They are not intended for publishing preliminary results or to be a reduced version of Regular Papers or Rapid Papers.

3. Review article

Definition: Critical evaluation of materials about current research that had already been published by organizing, integrating, and evaluating previously published materials. Re-analyses as meta-analysis and systemic reviews are encouraged. Review articles should aim to provide systemic overviews, evaluations and interpretations of research in a given field.

Size: Should not exceed 4000 words or 7-8 printed pages.

4. Special issues
Definition: Usually papers from research presented at a conference, seminar, congress or a symposium.

Size: Should not exceed 5000 words or 8-10 printed pages.

5. Others
Definition: Brief reports, case studies, comments, Letters to the Editor, and replies on previously published articles may be considered.

Size: Should not exceed 2000 words or up to 4 printed pages.

With few exceptions, original manuscripts should not exceed the recommended length of 6 printed pages (about 18 typed pages, double-spaced and in 12-point font, tables and figures included). Printing is expensive, and, for the Journal, postage doubles when an issue exceeds 80 pages. You can understand then that there is little room for flexibility.

Long articles reduce the Journal's possibility to accept other high-quality contributions because of its 80-page restriction. We would like to publish as many good studies as possible, not only a few lengthy ones. (And, who reads overly long articles anyway?) Therefore, in our competition, short and concise manuscripts have a definite advantage.

Format

The paper should be formatted in one column format with the figures at the end. A maximum of eight keywords should be indicated below the abstract to describe the contents of the manuscript. Leave a blank line between each paragraph and between each entry in the list of bibliographic references. Tables should preferably be placed in the same electronic file as the text. Authors should consult a recent issue of the Journal for table layout. There is no need to spend time formatting your article so that the printout is visually attractive (e.g. by making headings bold or creating a page layout with figures), as most formatting instructions will be removed upon processing.

Manuscripts should be typewritten, typed on one side of the ISO A4 paper with at least 4cm margins and double spacing throughout. Every page of the manuscript, including the title page, references, tables, etc. should be numbered. However, no reference should be made to page numbers in the text; if necessary, one may refer to sections. Underline words that should be in italics, and do not underline any other words.

Authors are advised to use Times New Roman 12-point font. Be especially careful when you are inserting special characters, as those inserted in different fonts may be replaced by different characters when converted to PDF files. It is well known that 'μ' will be replaced by other characters when fonts such as 'Symbol' or 'Mincho' are used.

We recommend that authors prepare the text as a Microsoft Word file.

1. Manuscripts in general should be organised in the following order:
   - **Page 1: Running title.** Not to exceed 50 characters, counting letters and spaces.
     Corresponding author. Street address, telephone number (including extension), fax number and e-mail address for editorial correspondence.
     Subject areas. Most relevant to the study. Select one or two subject areas from (*refer to Referral Form A–**attachment***).
     Number of black and white figures, colour figures and tables. Figures submitted in color will be printed in colour at the authors' expense. See *"6. Figures & Photographs"* for details of cost.
   - *Authors of Short Communications should state the total number of words (including the Abstract)
   - **Page 2: Authors.** Full names, institutions and addresses
     Abbreviations. Define alphabetically, other than abbreviations that can be used without definition. Words or phrases that are abbreviated in the introduction and following text should be written out in full the first time that they appear in the text, with each abbreviated form in parenthesis.
     Footnotes. Current addresses of authors if different from heading.
   - **Page 3: Abstract.** Less than 250 words for a Regular Paper, and up to 100 words for a Short Communication.
     For papers submitted to Pertanika Journal of Tropical Agricultural Science (JTAS) and Pertanika Journal of Science and Technology (JST), submissions should be made in English. Pertanika Journal of Social Sciences and Humanities (JSSH) accepts submissions in both English and *Bahasa Melayu*. However, if the paper is submitted in *Bahasa Melayu*, an abstract in English should be provided by the author submitting the paper.
     Keywords. Not more than eight in alphabetical order. Include the common name or scientific name, or both, of plant materials, etc.
   - **Page 4 and subsequent pages:** Text - Acknowledgments - References - Tables - Legends to figures - Figures.

2. **Authors' addresses.** Multiple authors with different addresses must indicate their respective addresses separately by superscript numbers:
   George Swan[1] and Nayan Kanwal[2]
   [1]Department of Biology, Faculty of Science, Duke University, Durham, North Carolina, USA.
   [2]Research Management Centre, Universiti Putra Malaysia, Serdang, Malaysia.

3. **Text.** Regular Papers should be prepared with the headings **Introduction, Materials and Methods, Results and Discussion, Conclusions** in this order. Short Communications should be prepared according to *"9. Short Communications."* below.

4. **Tables.** All tables should be prepared in a form consistent with recent issues of Pertanika and should be numbered consecutively with Arabic numerals. Explanatory material should be given in the table legends and footnotes. Each table should be prepared on a separate page. (Note that when a manuscript is accepted for publication, tables must be submitted as data - .doc, .rtf, Excel or PowerPoint file- because tables submitted as image data cannot be edited for publication.)

5. **Equations and Formulae.** These must be set up clearly and should be typed triple spaced. Numbers identifying equations should be in square brackets and placed on the right margin of the text.

6. **Figures & Photographs.** Submit an original figure or photograph. Line drawings must be clear, with high black and white contrast. Each figure or photograph should be prepared on a separate sheet and numbered consecutively with Arabic numerals. Appropriate sized numbers, letters and symbols should be used, no smaller than 2 mm in size after reduction to single column width (85 mm), 1.5-column width (120 mm) or full 2-column width (175 mm). Failure to comply with these specifications will require new figures and delay in publication. For electronic figures, create your figures using applications that are capable of

preparing high resolution TIFF files acceptable for publication. In general, we require 300 dpi or higher resolution for coloured and half-tone artwork and 1200 dpi or higher for line drawings. For review, you may attach low-resolution figures, which are still clear enough for reviewing, to keep the file of the manuscript under 5 MB. Illustrations will be produced at extra cost in colour at the discretion of the Publisher; the author will be charged Malaysian Ringgit 50 for each colour page.

7. **References.** Literature citations in the text should be made by name(s) of author(s) and year. For references with more than two authors, the name of the first author followed by 'et al.' should be used.

   Swan and Kanwal (2007) reported that …
   The results have been interpreted (Kanwal et al. 2006).
   - References should be listed in alphabetical order, by the authors' last names. For the same author, or for the same set of authors, references should be arranged chronologically. If there is more than one publication in the same year for the same author(s), the letters 'a', 'b', etc., should be added to the year.
   - When the authors are more than 11, list 5 authors and then et al.
   - Do not use indentations in typing References. Use one line of space to separate each reference. For example:
     - Jalaludin, S. (1997a). Metabolizable energy of some local feeding stuff. *Tumbuh*, 1, 21-24.
     - Jalaludin, S. (1997b). The use of different vegetable oil in chicken ration. *Mal. Agriculturist*, 11, 29-31.
     - Tan, S.G., Omar, M.Y., Mahani, K.W., Rahani, M., Selvaraj, O.S. (1994). Biochemical genetic studies on wild populations of three species of green leafhoppers *Nephotettix* from Peninsular Malaysia. *Biochemical Genetics*, 32, 415 - 422.
   - In case of citing an author(s) who has published more than one paper in the same year, the papers should be distinguished by addition of a small letter as shown above, e.g. Jalaludin (1997a); Jalaludin (1997b).
   - Unpublished data and personal communications should not be cited as literature citations, but given in the text in parentheses. 'In press' articles that have been accepted for publication may be cited in References. Include in the citation the journal in which the 'in press' article will appear and the publication date, if a date is available.

8. **Examples of other reference citations:**
   Monographs: Turner, H.N. and Yong, S.S.Y. (2006). *Quantitative Genetics in Sheep Breeding*. Ithaca: Cornell University Press.

   Chapter in Book: Kanwal, N.D.S. (1992). Role of plantation crops in Papua New Guinea economy. In Angela R. McLean (Eds.), *Introduction of livestock in the Enga province PNG* (p. 221-250). United Kingdom: Oxford Press.

   Proceedings: Kanwal, N.D.S. (2001). Assessing the visual impact of degraded land management with landscape design software. In N.D.S. Kanwal and P. Lecoustre (Eds.), *International forum for Urban Landscape Technologies* (p. 117-127). Lullier, Geneva, Switzerland: CIRAD Press.

9. **Short Communications** should include **Introduction, Materials and Methods, Results and Discussion, Conclusions** in this order. Headings should only be inserted for Materials and Methods. The abstract should be up to 100 words, as stated above. Short Communications must be 5 printed pages or less, including all references, figures and tables. References should be less than 30. A 5 page paper is usually approximately 3000 words plus four figures or tables (if each figure or table is less than 1/4 page).

   *Authors should state the total number of words (including the Abstract) in the cover letter. Manuscripts that do not fulfill these criteria will be rejected as Short Communications without review.

STYLE OF THE MANUSCRIPT

Manuscripts should follow the style of the latest version of the Publication Manual of the American Psychological Association (APA). The journal uses British spelling and authors should therefore follow the latest edition of the Oxford Advanced Learner's Dictionary.

SUBMISSION OF MANUSCRIPTS

All articles submitted to the journal must comply with these instructions. Failure to do so will result in return of the manuscript and possible delay in publication.

The original manuscript and one copy, four copies of photographic figures, as well as a disk with the **electronic copy** (including text and figures) and a **declaration form** and **referral form A**, together with a **cover letter** need to be enclosed. They are available from the Pertanika's home page or from the Executive Editor's office. Please do **not** submit manuscripts directly to the editor-in-chief or to the UPM Press. All manuscripts should be submitted through the executive editor's office to be properly acknowledged and rapidly processed:

Dr. Nayan Kanwal
Executive Editor
Research Management Centre (RMC)
4th Floor, Administration Building
Universiti Putra Malaysia
43400 UPM, Serdang, Selangor, Malaysia
email: ndeeps@admin.upm.edu.my
tel: +603-8946 6192
fax: +603 8947 2075.

Laser quality print is essential. Authors should retain copies of submitted manuscripts and correspondence, as materials can not be returned.

Cover letter

All submissions must be accompanied by a cover letter detailing what you are submitting. Papers are accepted for publication in the journal on the understanding that the article is original and the content has not been published or submitted for publication elsewhere. This must be stated in the cover letter.

The cover letter must also contain an acknowledgement that all authors have contributed significantly, and that all authors are in agreement with the content of the manuscript.

The cover letter of the paper should contain (i) the title; (ii) the full names of the authors; (iii) the addresses of the institutions at which the work was carried out together with (iv) the full postal and email address, plus facsimile and telephone numbers of the author to whom correspondence about the manuscript should be sent. The present address of any author, if different from that where the work was carried out, should be supplied in a footnote.

As articles are double-blind reviewed, material that might identify authorship of the paper should be placed on a cover sheet.

Note When your manuscript is received at Pertanika it is considered to be in its final form. Therefore, you need to check your manuscript carefully before submitting it to the executive editor (see also **English language editing** below).

Electronic copy

For preparation of manuscripts on disk, articles prepared using any one of the more popular word-processing packages are acceptable. Submissions should be made on a double-density or high-density 3.5" disk but a CD or DVD is preferable. The format, word-processor format, file name(s) and the title and authors of the article must be indicated on the disk/CD. The disk must always be accompanied by a hard-copy version of the article, and the content of the two must be identical. The disk text must be the same as that of the final refereed, revised manuscript. Disks formatted for IBM PC compatibles are preferred, though those formatted for Apple Macintosh are acceptable. The article must be saved in the native format of the word processor used, e.g. Microsoft Word (office version), etc. Although most popular word processor file formats are acceptable, we cannot guarantee the usability of all formats. If the electronic copy proves to be unusable, we will publish your article from the hard copy. Please do not send ASCII files, as relevant data may be lost. Leave a blank line between each paragraph and between each entry in the list of bibliographic references. Tables should be placed in the same electronic file as the text. Authors should consult a recent issue of the Journal for table layout.

Peer review

In the peer-review process, three referees independently evaluate the scientific quality of the submitted manuscripts. The Journal uses a double-blind peer-review system. Authors are encouraged to indicate in **referral form A** the names of three potential reviewers, but the editors will make the final choice. The editors are not, however, bound by these suggestions.

Manuscripts should be written so that they are intelligible to the professional reader who is not a specialist in the particular field. They should be written in a clear, concise, direct style. Where contributions are judged as acceptable for publication on the basis of content, the Editor or the Publisher reserves the right to modify the typescripts to eliminate ambiguity and repetition and improve communication between author and reader. If extensive alterations are required, the manuscript will be returned to the author for revision.

The editorial review process

What happens to a manuscript once it is submitted to Pertanika? Typically, there are seven steps to the editorial review process:

1. The executive editor and the editorial board examine the paper to determine whether it is appropriate for the journal and should be reviewed. If not appropriate, the manuscript is rejected outright.

2. The executive editor sends the article-identifying information having been removed to three, reviewers. Typically, one of these is from the Journal's editorial board. Others are specialists in the subject matter represented by the article. The executive editor asks them to complete the review in three weeks and encloses two forms: (a) referral form B and (b) reviewer's comment form. Comments to authors are about the appropriateness and adequacy of the theoretical or conceptual framework, literature review, method, results and discussion, and conclusions. Reviewers often include suggestions for strengthening of the manuscript. Comments to the editor are in the nature of the significance of the work and its potential contribution to the literature.

3. The executive editor, in consultation with the editor-in-chief, examines the reviews and decides whether to reject the manuscript, invite the author(s) to revise and resubmit the manuscript, or seek additional reviews. Final acceptance or rejection rests with the Editorial Board, who reserves the right to refuse any material for publication. In rare instances, the manuscript is accepted with almost no revision. Almost without exception, reviewers' comments (to the author) are forwarded to the author. If a revision is indicated, the editor provides guidelines for attending to the reviewers' suggestions and perhaps additional advice about revising the manuscript.

4. The authors decide whether and how to address the reviewers' comments and criticisms and the editor's concerns. The authors submit a revised version of the paper to the executive editor along with specific information describing how they have answered' the concerns of the reviewers and the editor.

5. The executive editor sends the revised paper out for review. Typically, at least one of the original reviewers will be asked to examine the article.

6. When the reviewers have completed their work, the executive editor and the editor-in-chief examine their comments and decide whether the paper is ready to be published, needs another round of revisions, or should be rejected.

7. If the decision is to accept, the paper is in press and the article should appear in print in approximately three to four months. The Publisher ensures that the paper adheres to the correct style (in-text citations, the reference list, and tables are typical areas of concern, clarity, and grammar). The authors are asked to respond to any queries by the Publisher. Following these corrections, page proofs are mailed to the corresponding authors for their final approval. At this point, only essential changes are accepted. Finally, the article appears in the pages of the Journal and is posted on-line.

English language editing

Authors are responsible for the linguistic accuracy of their manuscripts. Authors not fully conversant with the English language should seek advice from subject specialists with a sound knowledge of English. The cost will be borne by the author, and a copy of the certificate issued by the service should be attached to the cover letter.

Author material archive policy

Authors who require the return of any submitted material that is rejected for publication in the journal should indicate on the cover letter. If no indication is given, that author's material should be returned, the Editorial Office will dispose of all hardcopy and electronic material.

Copyright

Authors publishing the Journal will be asked to sign a declaration form. In signing the form, it is assumed that authors have obtained permission to use any copyrighted or previously published material. All authors must read and agree to the conditions outlined in the form, and must sign the form or agree that the corresponding author can sign on their behalf. Articles cannot be published until a signed form has been received.

Lag time

The elapsed time from submission to publication for the articles averages 6-8 months. A decision of acceptance of a manuscript is reached in 1 to 3 months (average 7 weeks).

Back issues

Single issues from current and recent volumes are available at the current single issue price from UPM Press. Earlier issues may also be obtained from UPM Press at a special discounted price. Please contact UPM Press at penerbit@putra.upm.edu.my or you may write for further details at the following address:

UPM Press
Universiti Putra Malaysia
43400 UPM, Serdang
Selangor Darul Ehsan
Malaysia.

Selected Papers from the World Engineering Congress 2007
Guest Editors: *(Siti Mazlina Mustapa Kamal, Farah Saleena Taip and Siti Aslina Hussain)*

Selected Papers from the Science Seminar 2007
Guest Editorial Board: *(W. Mahmood Mat Yunus, Nor' Aini Mohd Fadzillah, Abdul Halim Abdullah, Hishamuddin Zainuddin, Mahendran a/I Shitan and Shamarina Shohaimi)*

Pertanika Journal of Science & Technology
Volume 16 (2) Jul. 2008

Contents

Regular Articles

Research Management Centre (RMC)
4th Floor, Administration Building
Universiti Putra Malaysia
43400 UPM Serdang
Selangor Darul Ehsan
Malaysia

http://www.rmc.upm.edu.my
E-mail : pertanika@rmc.upm.edu.my
Tel : +603 8946 6185/ 6192
Fax : +603 8947 2075

UPM Press
Universiti Putra Malaysia
43400 UPM Serdang
Selangor Darul Ehsan
Malaysia

http://penerbit.upm.edu.my
E-mail : penerbit@putra.upm.edu.my
Tel : +603 8946 8855/8854
Fax : +603 8941 6172

ISSN 0128-7680
07
9 770128 768083